MICROWAVE ELECTRONICS

INVESTIGATIONS ON WIDEBAND SCS's & OTHER PERIODIC STRUCTURES FOR RCS REDUCTION TECHNIQUES

A THESIS SUBMITTED BY

SAJI STEPHEN D.

IN PARTIAL FULFILMENT OF THE REQUIREMENTS

FOR THE DEGREE OF

DOCTOR OF PHILOSOPHY

DEPARTMENT OF ELECTRONICS

FACULTY OF TECHNOLOGY

COCHIN UNIVERSITY OF SCIENCE AND TECHNOLOGY

KOCHI-682 022, INDIA

MARCH 1996

CERTIFICATE

This is to certify that the thesis entitled "INVESTIGATIONS ON WIDEBAND SCS's & OTHER PERIODIC STRUCTURES FOR RCS REDUCTION TECHNIQUES" is a bonafide record of the research work carried out by Mr.Saji Stephen. D. under my supervision in the Department of Electronics, Cochin University of Science & Technology. The results embodied in this thesis or part of it have not been presented for any other degree.

Dr.K.G.Nair
(Supervising Teacher)
Professor Emeritus
Dept. of Electronics
Cochin University of
Science & Technology

Kochi 22
11th March 1996

INVESTIGATIONS ON WIDEBAND SCS's & OTHER PERIODIC STRUCTURES FOR RCS REDUCTION TECHNIQUES

CONTENTS

Chapter 1

INTRODUCTION

The laws governing the behaviour of electromagnetic waves were established by the year 1900 by the pioneering efforts of great men like Hertz, Faraday, Ampere, Coulomb and Maxwell. Each one made his own contribution, but it was James Clerk Maxwell who assembled the results of these experiments and formulated the basis of modern electromagnetic theory.

Electromagnetic waves are oscillatory waves. They can have various frequencies. The difference from one wave to another is its frequency of oscillation. E.M.waves ranges from electrical disturbances, radio waves, infrared, light, ultraviolet, X-rays, γ-rays and cosmic rays in the spectrum from long wavelengths to shorter ones.

Radar echo mechanism is strictly an electromagnetic phenomenon. Although the development of radar as a full-fledged technology did not occur until world war II, the basic principle of radar detection has been almost as old as the subject of electromagnetism itself. Heinrich Hertz in 1886, experimentally tested the theories of Maxwell and demonstrated the similarity between radio and light waves. Hertz showed that radiowaves could be reflected by metallic and dielectric bodies. Marconi recognised that short waves can be used for radio detection and he strongly urged their use in radio detection. Radar was developed independently and simultaneously in several countries just prior to world war-II.

Radar is an electromagnetic system for detection and location of objects. It operates by transmitting a waveform and detecting the nature of the echo signal. An elementary form of radar consists of a transmitting antenna emitting electromagnetic radiation generated by an oscillator of some sort, a receiving antenna, and an energy detecting device or receiver. A portion of the transmitted signal is intercepted by a target and is reradiated in all directions. The energy reradiated in the backward direction is of prime interest to the radar. The receiving antenna collects the returned energy and delivers it to the receiver, where it is processed to detect the presence of the target and to determine its location and its relative velocity.

Improvements in radar technology have been enormous since the world war II. In the transmitter side, the development of high power TWT, millimeter wave power tubes and solid state microwave sources have been important. In the receiver system, solid state technology has improved mixers and allowed development of LNA. In the antenna section large scale phased arrays have become practical. In signal processing system, the advent of the small, fast digital computer has made much development in radar techniques. The modern radar would not have come to reality had there not been such developments in these various systems.

A bistatic radar is one in which the transmitting and receiving antennas are separated by a considerable distance. A radar is called monostatic when a common antenna is used for both transmitting and receiving. The principle of bistatic radar was known and demonstrated many years before the development of practical monostatic radar. These early radars were known as wave interference equipment. These are the same as "bistatic radar". The early experiments with bistatic radar led to the development of monostatic radar. Separating the transmitter and receiver in the bistatic radar results in considerable different radar characteristics than those obtained with the monostatic radar. A CW radar requires considerable isolation between the transmitter and the receiver to prevent the transmitted signal from leaking into the receiver. Isolation is obtained in the bistatic radar because of the inherent separation between the transmitter and the receiver. It is difficult to make a precise comparison between bistatic and monostatic radars because of the dissimilarity in their geometries. The coverage of a monostatic radar is basically hemispherical, while the coverage of the bistatic radar is more or less planar.

When an electromagnetic wave is incident on a target, the target intercepts a portion of the incident power and reradiates it in various directions. The measure of the amount of incident power intercepted by the target and reradiated back in the direction of the radar is denoted as the radar cross section (RCS) 'σ'. RCS is a characteristic of the particular target and is a measure of its size as seen by the radar. It is a measure of the power that is returned or scattered in a given direction, normalized with respect to the power density of the incident field. RCS is a function of target configuration, frequency, incident polarization, receiver polarization and the angular orientation of the target with respect to the incident field. The basis for the design and operation of dynamic RCS test ranges is the radar range equation. The radar range equation shows how the received power is influenced by the RCS of the target characteristics and other parameters.

The prediction of RCS of bodies is a difficult electromagnetic problem that has challenged scientists and engineers since the development of the radar. Although the principles, of electromagnetic theory are remarkably well developed, the application of these principles for predicting radar echo strengths often leads to complex and incredibly extensive computations. There is always the need to test the theory or verify the predictions, and this can usually be accomplished only by means of measurements made on the test range. A practical justification for RCS measurements is that it is an incentive to develop products that satisfy RCS requirements in addition to the more usual requirements of mission, range and payload. RCS measurements are necessary to verify anticipated performance as well as to evaluate design approaches. In addition, measurements are required for the evaluation of absorbers. The study of Radar Cross Section and its reduction is of great importance in modern communications, electronic warfare and defence applications.

Reduction of Radar Cross Section is a method for increasing survivability by reducing detectability of objects of strategic importance like aeroplanes, rockets, missiles etc. There are four basic techniques for reducing radar cross section. They are "shaping", "use of radar absorbing materials"," passive cancellation" and "active cancellation". Each of these techniques adopts different philosophic approaches and exploits different aspects of the encounter between the radar and the object.

In the shaping technique, it must be assured that the radar beam appears within a definable and limited cone of direction. The objective of shaping is to orient the target surfaces and edges so as to deflect the energy in directions away from the radar. This cannot be done for all viewing angles within the entire field of view. However, this is virtually impossible to do with a particular target which has a definite shape and size.

Radar absorbing materials reduce the energy reflected back to the radar by means of absorption. In order to absorb energy materials must be found out in which the induced current is in phase with the incident field. Most of the absorbing materials contain carbon and the dissipation of energy takes place by the conversion of electro magnetic energy into heat. There are dielectric materials whose indices of refraction, which includes magnetic as well as electrical effects, are complex numbers and it is the imaginary part that gives rise to the loss. The molecules in the material are small dipoles that try to orient themselves along the incident field. If the field changes too fast, or if the dipoles lag the impressed field variations, torque is exerted and energy is deposited in the material. The dipoles experience a kind of molecular friction as they try to follow the oscillations in the field. Magnetic absorbers are widely used for operational systems. The loss mechanism in this case is due to a magnetic dipole moment, and compounds of iron are its basic ingredients. Magnetic materials offer the advantage of compactness because they are a fraction of the thickness of dielectric absorbers. At the same time magnetic absorbers are heavy because of their iron content. The desirable magnetic properties of these materials fade away when the frequency becomes too high, and their effectiveness virtually disappears when the ambient temperature rises above the curie point.

Passive cancellation, (also known as impedance loading) is severely limited. The basic concept is to introduce an echo source whose amplitude and phase can be adjusted so as to cancel another echo source. This can be accomplished for relatively simple objects provided that a loading point can be identified on the body. A port can be machined in the body and the size and shape of the interior cavity can be designed to present an optimum impedance at the aperture. Even for simple bodies it is extremely difficult to generate the required frequency dependence for this built-in impedance and the reduction obtained for one frequency in the spectrum rapidly disappears as the frequency is changed.

In active cancellation (also known as active loading) the target must emit radiation whose amplitude and phase cancels the reflected energy. This implies that the target must be smart enough to know its own echo characteristics for that particular wave; the angle of arrival, intensity, frequency and waveform of the incident wave; and fast enough to generate the proper waveform and frequency; and versatile enough to adjust and radiate a pulse of the proper amplitude and phase in the proper direction. The cost of designing and building active cancellation systems with the required characteristics is probably high enough that more conventional methods will remain attractive despite their shortcomings.

One way of eliminating reflections from a plane metallic surface is by making corrugations on it. Using the principle of Bragg scattering it is possible to eliminate specular reflections from plane metallic surfaces employing corrugations. Periodic metallic strips etched on a dielectric substrate with a ground plane shows similar properties of corrugated surfaces and are called "Simulated Corrugated Surfaces" (SCS) [70]. An important advantage of Simulated Corrugated Surfaces over corrugations is in the fabrication technique. The photolithographic and etching technique are very much helpful for its accurate design and fabrication. Geometry of a Simulated Corrugated Surface is shown in figure 1.1.

A plane wave incident on a periodic surface excites a discrete spectrum of scattered plane waves. For maximum constructive interference from adjacent cells spaced 'd', the angle of diffraction for the n^{th} spectral order θ_n is related to the angle of incidence θ_i from the normal to the surface by

$$kd(Sin\theta_n - Sin\theta_i) = 2\pi n$$

$$Sin\theta_n = Sin\theta_i + \frac{n\lambda}{d} \qquad \ldots\ldots\ (1)$$

$$n = 0, \pm 1, \ldots\ldots$$

where $k = 2\pi/\lambda$ is the free space propagation constant and λ is the wavelength.

Forward scatter [$0 \leq \theta_n \leq \pi/2$] from a surface will be reduced by increasing backscatter

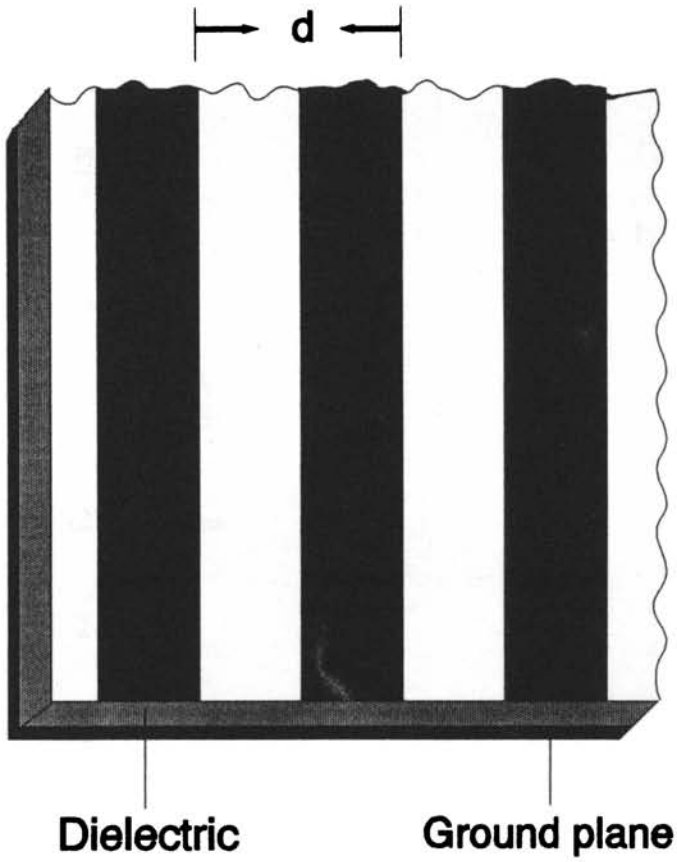

(a)

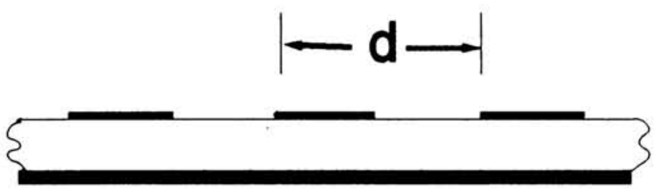

(b)

Fig.1.1 Simulated Corrugated Surface

(a) Front view
(b) Side view

$[-\pi/2 \leq \theta_n \leq 0]$.

Maximum constructive interference in the direction of backscatter, i.e back in the direction of incidence occurs for

$$kd Sin\theta_i = m\pi$$

$$Sin\theta_i = \frac{m\lambda}{2d} \qquad \ldots\ldots\ldots (2)$$

$$m = 1, 2, \ldots\ldots$$

which in equation (1) gives

$$Sin\theta_n = \left(n + \frac{m}{2}\right)\frac{\lambda}{d} \qquad \ldots\ldots\ldots (3)$$

If m = 1, equation (2) becomes

$$Sin\theta_i = \frac{\lambda}{2d} \qquad \ldots\ldots\ldots (4)$$

which is called Bragg condition.

Then equation (3) is

$$Sin\theta_n = \left(n + \frac{1}{2}\right)\frac{\lambda}{d} \qquad \ldots\ldots\ldots (5)$$

and for periods in the range $[\lambda/2 < d < 3\lambda/2]$ the only real solutions to equation (5) are θ_0 and θ_{-1} and from equation (4) & (5)

$$\theta_{-1} = -\theta_i$$

Specular reflection (n = 0) and backscatter (n = -1) alone occur and any increase in backscatter produces a corresponding decrease in specular reflection. In this way specular reflection from an infinite perfectly conducting periodic surface may be completely eliminated. For periods $[d < \lambda/2]$ the surface behaves as a plane conductor. For large periods specular reflection is reduced by scatter into other spectral orders, some of which may also cause multipath interference. Specular reflection is never completely eliminated whenever more than two spectral orders are excited. Therefore the proper choice of period lies in the range [$\lambda/2 < d < 3\lambda/2$].

It is possible to reduce the RCS to a considerable extent by covering the planar reflecting surface with a strip grating. When the period of the grating satisfies the Bragg condition and the dielectric thickness is of proper choice, the specularly reflected power is completely eliminated and a non-reflecting conducting surface is obtained. So it is useful for the design of efficient radar targets. The shaping technique to reduce the RCS of a target is limited in many ways like the aerodynamical problems in aircrafts and missiles. Strip gratings does not offer any air resistance because thin strips are in the same plane as the dielectric sheet. Multipath interference from building surfaces is a problem familiar to urban TV reception. It is a serious problem for air-traffic control systems at airports due to the interference from hanger walls near airport runways. An approach to avoid this is to design the dressing of hanger walls with these surfaces to eliminate specular reflection. The diffraction grating has potential applications as polarizers, frequency multiplexers and scanners in addition to multipath interference suppression and reduction of RCS of targets.

The angular range and frequency range over which effective reduction in specular reflection occurs is usually important in the design of reflection free surfaces. The main disadvantage of strip gratings developed earlier is that elimination of specular reflection is effective only for limited frequency range and limited angular range. Scattering properties of a self complementary strip grating compared to that of a planar reflecting surface of the same dimensions is shown in figures 1.2 and 1.3.

From the figure 1.2 it is clear that specular reflection is eliminated only for a particular angle of incidence. Figure 1.3 shows that frequency bandwidth for the elimination of specular reflection is very low. But there is need for application of Simulated Corrugated Surfaces with the existence of the behaviour of suppression of specular reflection for wider frequency range and wider angular range.

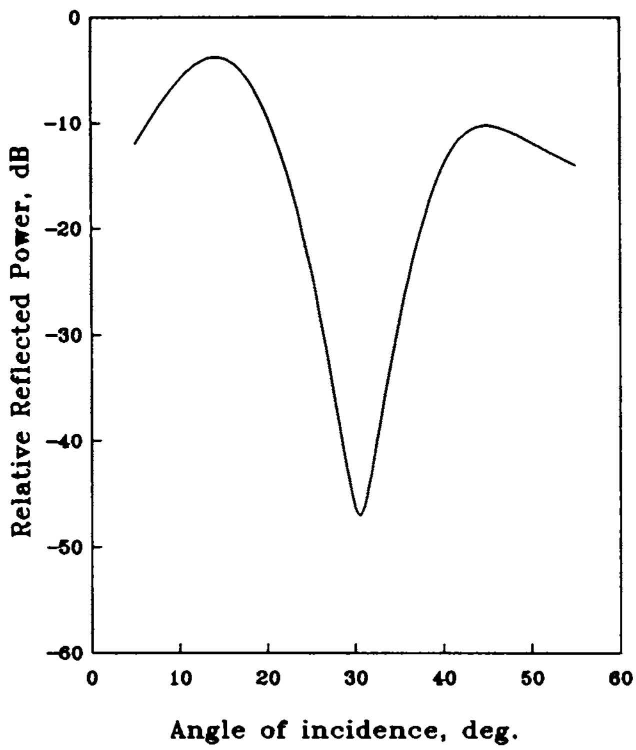

Fig.1.2 Variation of relative reflected power with angle of incidence

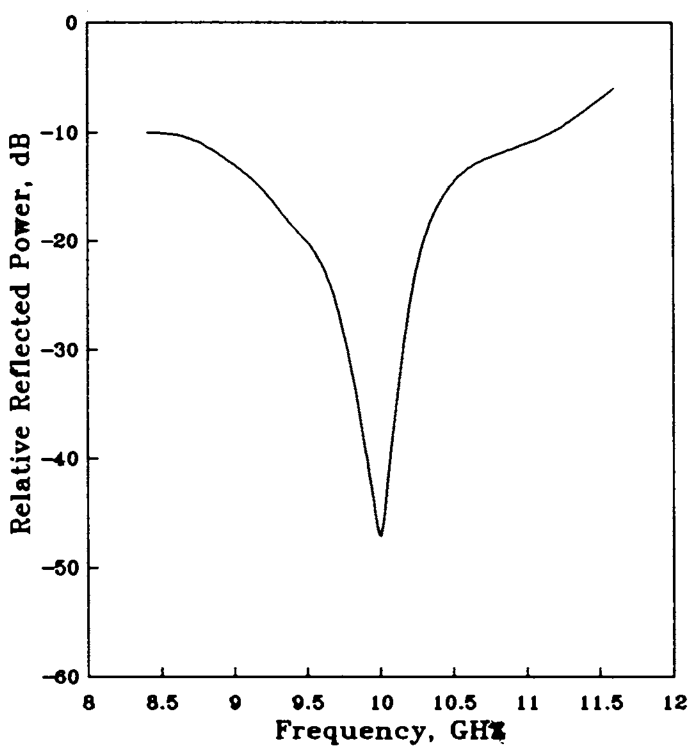

Fig.1.3 Variation of relative reflected power with frequency

This thesis presents the results of an investigation conducted for improvement of Simulated Corrugated Surfaces for wide band applications. It has been observed that the frequency bandwidth and angular range increases considerably by modifying the geometry of the structure. A schematic presentation of the work is given below.

A review of the past work done in the field of Radar Cross Section reduction is presented in chapter 2. Both experimental and theoretical works on grating structures are reviewed in this chapter.

The methodology adopted and experimental techniques for the investigation is given in chapter 3.

Chapter 4 highlights the experimental results of the investigation. A number of adjustable parameters are available for the SCS to reduce RCS to a minimum. The work carried out is to optimise these parameters and new parameters are added for further improvement in RCS reduction for wider angular range and frequency range.

5th chapter presents the theoretical analysis used to explain the experimental results. Comparison between the experimental and theoretical results is also presented in this chapter.

Conclusions drawn from the investigation are given in chapter 6. The advantages of the developed system is discussed along with the scope for further investigations in the field.

The experimental results of the investigations done in related fields are presented as Appendix. The application of Simulated Corrugated Surfaces on corner reflectors and development of a broadband microstrip reflectarray are included in it.

Chapter

REVIEW OF THE PAST WORK IN THE FIELD

2

Radar cross section and its reduction has been studied by many researchers over the past few decades. One of the methods used for reduction of radar cross section is by using strip grating technique. A chronological review of the past work done on the scattering properties of periodic strip grating structures, both theoretical and experimental, is presented in this chapter.

Many works on RCS and its measurements are available in open literature [1-5]

Edward and Joseph [6] worked out the effect of resistivity of wire gratings in the amplitude of the reflection coefficient and phase of the transmission coefficient.

Using a method based on the calculus of residues, Hurd [7] investigated the propagation of an electromagnetic wave along an infinite corrugated surface.

Robin [8] presented theoretical and experimental results for reflection and transmission of a uniform plane e.m.wave normally incident on an ideal strip grating.

Using physical optics method Senior [9] determined the scattering coefficients of a plane wave incident on a perfectly conducting sheet having sinusoidal corrugations.

Bachman et al. [10-12] have presented an analysis of low RCS measurement techniques and the important problems incurred in realizing the sensitivities for long distances. They listed different types of radar cross section ranges and each type was evaluated quantitatively in terms of the salient problems.

Senior [13] reviewed the analytical techniques available for estimating the backscattering cross section of metallic targets. The cross sections were classified according to the dimension - to - wavelength ranges and attempts were made to interpret them in the light of the scattering processes.

A review of the history of cross section measurements was presented by Blacksmith et al. [14]. They discussed major measurement problems and gave some details of measurement systems.

Kell and Pedeson [15] compared RCS measurements in narrow band continuous wave system and on short pulse system. They also presented data for one model target.

In order to determine analytical formulations suitable for the estimation of radar cross section Ross [16] investigated the scattering from flat plates. He used geometrical diffraction theory for the estimation of RCS. A method for deriving the diffraction coefficient was also presented by him.

A rigorous electromagnetic theory of diffraction of light by blazed lamellar gratings was developed by Armand and Roger [17].

Jacobsen [18] conducted and described an analytical, numerical and experimental investigation of a practical two - dimensional periodically modulated slow wave structure. The structure used was a dielectric slab with a perfectly conducting ground plane on one side and perfectly conducting thin strips perpendicular to the direction of propagation on the other side.

The integral equation for the currents induced on an infinite perfectly conducting grating by a plane wave is presented by Green [19]. An equivalent problem of reflection inside the terminated waveguide was also considered. This showed good agreement between theory and experiment.

Chao - chun chen [20] formulated a general solution to the problem of determining the aperture field distribution and the transmission and reflection coefficients of an infinite planar conducting sheet perforated periodically with apertures.

Kalhor and Neureuther [21] showed how a general numerical integral equation technique could be used to analyze diffraction gratings of arbitrary groove shape. The method consists of formulating the integral equation over one cell and then solving numerically by the method of moments to find the surface fields from which the energies in the radiating orders can finally be obtained.

The scattered field for plane wave incidence on periodic corrugated surfaces with soft and hard boundary conditions was calculated by John Desanto [22-23].

Hiroyoshi and Yasuura [24] presented a computer aided procedure based on the method of modal expansions and applied it to the scattering from a periodic structure composed of a perfectly conducting surface. Several physical characteristics of the reflection grating including the diffraction anomalies were explored.

Numerical integral equation was extended to penetrable media by Kalhor and Neureuther [25]. They used numerical solution of integral equation to explore the effects of material parameters and the groove geometry on diffraction grating performance. The material parameters were studied by first developing and verifying a surface impedance model.

Kalhor and Moaveni [26] analyzed a numerical technique for diffraction grating of arbitrary groove shape as electromagnetic boundary value problems. The method yields the scattered far field modal amplitude without the necessity of computing the induced surface currents. This makes the technique very simple and convenient for analyzing the performance of diffraction grating under normal and anomalous conditions.

William et al. [27] developed a technique for making rapid RCS measurement over wide frequency bands. The HP automatic network analyzer, which measures scattering parameters at discrete frequencies over a wide band, corrects for system errors before presenting measured data. It has been adopted to obtain the RCS. This new technique can be viewed as an automated form of the two antenna RCS measurement method.

A solution to the problem of scattering of a plane wave using an infinite periodic array of thin conductors on a dielectric slab was formulated by Montgomery [28].

Hessel et al. [29] showed that Bragg condition($\lambda = 2d\sin\theta$) is a necessary condition for perfect blazing of infinite perfectly conducting diffraction gratings that produce only a single diffracted order, n = -1. The rectangular profile grating was analyzed as an illustration.

Maystre and Petit [30] reported the theoretical and numerical study of grating anomalies linked with the absorption of energy. They showed that metallic gratings can exhibit anomalies like total absorption of planewave.

The reflection and transmission characteristics of an arbitrary, periodic interface characterized by either a surface admittance function or surface impedance function was presented by Mayhan and Tsai [31].They also gave the peculiar resonances associated with certain periodic structures.

Roumiguieres et al. [32] investigated the possibility of making perfectly conducting rectangular groove gratings which are perfectly blazed simultaneously in both polarizations.

Levine [33] presented a physical optics solution for the scattering of plane wave from a perfectly conducting corrugated surface in the case of waves incident from an arbitrary direction and in the case of an observer far from the surface. This solution was used to compute the radar cross section of the surface with irregular corrugations.

Knot [34] had shown that the deformation of metallic flat plates into cylindrical segments reduces the large specular echo but does not necessarily reduce the mean cross section by more than 1 dB or so.

An analysis of the diffraction of parallel polarized electromagnetic waves from corrugated periodic perfectly conducting surfaces by both a rigorous method and a method based on Rayleigh hypothesis was presented by Kalhor [35].

Ebbeson [36] has given the results of an analytical and numerical investigation of TM polarized plane wave scattering from an infinite fin-corrugated surface. The surface was composed of infinitely thin, perfectly conducting fins of spacing $\lambda/2 < a < \lambda$. Specular reflection from this ideal surface were completely converted to backscatter in a direction opposite to the incident wave when the fin period and height were properly chosen. A procedure for the design and performance prediction of a finite fin-corrugated surface composed of finitely thick fins were also described.

John et al. [37] described a bistatic RCS measurement technique. It used the variation of CW null balance approach, resulting in rapid measurement time. A network analyzer and process computer were incorporated into the existing image ground plane system to improve the bistatic capability and add flexibility.

Jull et al. [38] reported that perfect blazing of reflection gratings to the $n = -1$ spectral order for both TE and TM polarizations is possible with rectangular grooves with angle of incidence in the range 19.5° to 59.4°. Design dimensions were verified experimentally at 35 GHz.

Jull and Ebbeson [39] proposed the use of corrugated surfaces to reduce interfering reflections from buildings. Numerical examination was made for infinite comb grating under H - polarised plane wave illumination with grating space between λ and $\lambda/2$. Model measurements at 35 GHz on finned surfaces of finite size under non plane wave illumination are given to verify whether the surfaces behave essentially as predicted for the infinite comb.

A theory of scattering by periodic metallic surfaces was given by Whitman and Felix [40]. They utilized physical optics approximation to determine the first order current distribution in the metal surface.

Numerical results for plane wave scattering from a perfectly conducting diffraction grating with triangular groove profile was presented by Cheo et al. [41]. They could obtain simultaneous blazing with 100 % efficiency in both polarizations. The angles of incidences for which such simultaneous blazing occur are narrower than that obtained with rectangular groove profile.

Kalhor [42] analyzed diffraction of electromagnetic waves by a planar array of perfectly conducting strips by a simple numerical technique based on mode expansion and point matching. The results were compared against other numerical results available in the literature. Further numerical results which show the usefulness of these structures as shielding grids, reflection less metallic supports, polarizers and diffractors in obstructed communication links are also included.

Knop [43] treated diffraction of light by deep rectangular groove transmission phase grating by numerically solving Maxwell's equations.

Heath and Jull [44] calculated the coefficients of the matrices governing the scattered mode amplitudes for plane electromagnetic wave incidence on a perfectly conducting periodic surface with a rectangular groove profile. These matrices were decomposed when the bragg condition was satisfied facilitating computation. For the comb grating, the numerical results converged when the groove width approached the period. Perfect blazing with arbitrary polarisation for near grazing incidence was shown to be possible in principle, with deep grooves.

Montgomery [45] formulated the solution to the problem of scattering of a plane wave by an infinite periodic array of thin conductors on a dielectric slab. Numerical results as well as comparison of theory with experimental data were also given.

The numerical values of the depth and width of rectangular grooves, a profile suitable for multipath interference suppression for TM and TE polarisation, was given by Jull et al. [46]. They showed that angular and frequency range over which the surfaces were effective decreased with groove depth.

Heath and Jull [47] described that corrugations could completely convert specular reflection from a conducting surface to backscatter. They showed that this was possible with rectangular groove surface profile for either TE or TM polarisations or for both simultaneously. Numerical and experimental results were illustrated for a surface, designed for plane wave incidence at 50° from the normal.

The design of dichroic subreflector for dual frequency reflector antenna has been described by Agrawal and Imbriale [48]. The surface had crossed dipoles printed on a dielectric sheet. The influence of parameters on transmission and reflection coefficients were experimentally evaluated. They presented the analysis based upon floquet mode theory to predict the experimental results correctly.

Montgomery [49] worked out the solutions for electromagnetic scattering using the perturbational form of the modified residue calculus technique. This is for an infinite array of multiple parallel strips for TE and TM polarisations.

Based on physical optics method Kalhor [50] analyzed the scattering of electromagnetic waves by planar arrays of perfectly conducting strips. The induced current as determined by physical optics was used to find out the amplitudes of various propagating space harmonics. He also compared the results against a few exact results available in the literature.

Jull and Heath [51] developed triangular and rectangular groove surfaces which reflect only TE polarization while totally backscattering TM polarization. It was found that complete elimination of TM polarized reflection with simultaneous elimination of TE polarized backscatter required a unique combination of rectangular groove dimensions.

An unusual reflection grating which is capable of efficiently diffracting the antenna beam over a wide angular range due to frequency variation was presented by Jull and Beauliew [52].

Kalhor et al. [53] analyzed diffraction of plane electromagnetic waves by a planar array of perfectly conducting strips. This numerical technique is based on mode expansion and minimization of error in the field values at the boundary. They compared the results with other numerical results available in the literature.

Jerome et al. [54] presented a complete solution of plane wave scattering from a twist reflector of infinite extent for arbitrary incidence. The solution was accomplished through the use of an E and H type modal representation of the fields in the twister and free space region.

Tsao and Mittra [55] employed an iterative technique in the spectral domain to solve the problem of scattering from two dimensional periodic structures. The formulations were carried out in spectral domain where a set of algebraic equations was obtained directly for the spectral coefficients of aperture field distribution. These equations were then solved simultaneously using an iterative procedure.

It was reported by Paul and Nair [56] that corrugated metal surfaces showed the property of rotatory polarisation. Orientation of the corrugations with plane of polarisation of incident radiation determines the extent of the tilt. They established that rotatory polarisation was additive when two corrugated reflecting surfaces were successively employed.

Kalhor and Ilyas [57] presented a numerical integral equation technique for the problem of scattering of electromagnetic waves by periodic conducting cylinders embedded in a dielectric slab backed by a plane reflector. The solution of the integral equation yielded the induced surface currents on the cylinders from which the power in various reflected modes were calculated. A comparison of experimental and numerical results were also given.

A simple, closed form approximate solution for the transmission coefficient of a normally incident e.m. plane wave through a screen made of periodic metal grids or metal plates was given by Lee et al. [58]. Explicit formulas were also presented for cascading screens and dielectric slabs.

Mohram and Gaylord [59] analyzed corrugated gratings using rigorous coupled wave theory. The analysis applied to arbitrary grating profiles, groove depths, angle of incidence and wavelengths.

A method of analysis of strip gratings with more than one conducting strip per period was given by Archer [60]. The method was then applied to a periodic twin - strip grating with two unequal gaps. The scattering parameters were found from a set of linear equations which could be solved numerically.

Shmoys and Hessel [61] presented an approach to construct frequency scanned antenna using a periodic structure. The periodic structure considered was a transmission grating consisting of perfectly conducting rectangular bars. The periodicity of the grating was selected in such a way hat the first higher order diffracted mode was propagated. Since the direction of propagation of the higher order mode depended on the frequency, the frequency scanning was obtained by dimensioning the bars so that the power of the incident field was converted to the transmitted higher order mode.

Bhattacharya et al. [62] has described a monostatic CW radar cross section measurement facility in X-band. This set up is capable of automatically measuring the CW monostatic RCS over the range of aspect angle 0 to $\pm 180^{\circ}$ for both parallel and perpendicular polarisations.

Tsao and Mittra [63] has presented a full wave analysis for the problem of scattering from frequency selective surfaces using the spectral domain approach. A detailed investigation is given for the special cases of cross type and jerusalem cross. The role of junction type basis functions in representing the current distribution has also been studied.

A computationally efficient method for analyzing the scattering from FSS comprised of circular metal patches has been presented by Mittra et al. [64]. The formulation was carried out in the spectral domain where the convolution form of the integral equation for the induced current reduced to an algebraic one and the spectral Galerkin technique was used to solve the resulting equation.

Hurd and Jull [65] investigated theoretically the scattering of a plane H-polarized wave from a grating composed of narrow grooves in a perfectly conducting surface using conformal transformation techniques. The necessary condition was also derived for the elimination of specularly reflected wave. Only when the -1 and 0 order space waves are present, this condition becomes the bragg condition.

Bhattacharya and Tandon [66] designed, fabricated and tested a low backscatter corrugated metal surface for H-polarised incident waves. They formulated the problem using the scattering matrix approach and determined the reflection and transmission coefficients at the fin air interface using an integral equation approach. The RCS has been experimentally measured and an expression for monostatic RCS is also obtained.

An experimental investigation of the scattering from crossed gratings of square pyramids was conducted by Cai et al. [67]. They have provided examples of the use of equivalent singly periodic grating surfaces as a guide to the design of crossed grating surfaces.

The problem of diffraction of e.m.wave by a thick grating was analyzed with the aid of Wiener - Hopf technique by Kobayashi [68]

Jull et al [69] presented a numerical analysis of thin corrugated strips with rectangular groove profiles, dual blazed to n = -1 spectral order. It has shown that, high efficiency gratings remain efficient as the number of grating elements is reduced to as few as two, provided that incidence is not near grazing. Numerical results show that the main effect of reduced grating size is a broadening of the diffracted beam, which can be predicted from a simple formula.

Jose and Nair [70] compared perfect blazing of reflector backed thin strip gratings to n = -1 spectral order for both TE and TM polarisations with corrugated reflection gratings. They found that, the strip gratings simulate effects of rectangular corrugations in conducting surfaces.

Wu [71] described a fast convergent integral equation solution to the scattering problem of a TE or TM plane wave by a one - dimensional periodic array of thin metal strips on a dielectric substrate.

The possibility of designing a reflective frequency scanning surface by using periodic array of metallic elements etched on a dielectric substrate and placed over a ground plane was investigated by Johansson [72]. The frequency scanning was obtained by letting the reflected first higher order mode be propagating and serve as the frequency scanned main beam, while the reflected zero order mode is suppressed. They obtained an integral equation for the induced current on the metallic elements. The Galerkins method was applied on the integral equations to get a system of linear equations which were then solved with the aid of computer.

The fundamentals of radar cross section measurements was reviewed by Robert B. Dybdal [73]. Measurement facilities including the present research activities on compact range techniques are then described. Those factors that limit the accuracy of RCS measurements are discussed.

Matsushima and Itakura [74] analyzed the scattering of electromagnetic waves by arrays of conducting strips using a singular integral equation technique.

Jose et al [75] reported the development of reflector backed strip gratings exhibiting properties like the elimination of specular reflection from a conducting surface for normal and near normal incidences, which is not possible by conventional corrugated surfaces.

The scattering of electromagnetic waves from a dielectric slab loaded with a periodic array of perfectly conducting strips by a mode matching technique was analyzed by Kalhor [76]. The fields were expanded in terms of suitable propagating and evanescent modes in various regions. He presented the variation of energy of significant scattered modes with various structure parameters for both principal polarizations of the incident wave.

Kildal [77] defined artificially soft and hard surfaces for e.m. waves. Transversely corrugated surfaces and other alternative surfaces form soft surfaces and longitudinally corrugated surfaces form hard surfaces.

Kalhor [78] analyzed the diffraction of e.m. waves by plane gratings of finite extent. Results were compared against those of structures of infinite extent to determine the minimum structure sizes that should be used in experimental measurements to obtain meaningful results.

The scattering of obliquely incident plane waves by a cascade connection of periodic strip gratings was analyzed by Matsushima and Itakura [79]. A set of integral equations was derived and solved using the moment method.

Johansson et al. [80] presented theoretical and experimental results for a frequency scanned antenna composed of a line source and a frequency scanned reflection grating, shaped to a cylindrical reflector. The grating structure considered consisted of an array of dipoles placed over a ground plane. The design of the dipole grating for optimum blazing has been discussed. They used Floquet's theorem and method of moments for theoretical analysis.

The frequency scanned gratings consisting of periodic arrays of thin conducting elements of single dipoles and crossed dipoles were investigated by Johansson [81]. The principle used were to let the first higher order diffracted wave propagate and serve as the frequency scanned beam. Both reflection and transmission gratings were considered. Theoretical analysis was made on the basis of floquets theorem and method of moments. He also compared theoretical results with experimental results.

Zakharov et al. [82] proposed an effective method for the numerical analysis of the diffraction of an H-polarized wave by a grating consisting of ideally conducting surface.

A new robust approach for the analysis of strip gratings for TE and TM cases was described by Sohail et al. [83]. The field distributions in the plane of the grating were expanded in Fourier series, whose coefficients were derived as the solution of an infinite dimensional system of linear equations.

Jin and Volakis [84] discussed the scattering characterization of an infinite and truncated periodic array of perfectly conducting patches on a dielectric slab. The scattering pattern of the finite array was computed approximately by integrating the infinite periodic array currents over the extent of the given finite array.

Kildal [85] presented the concept of soft and hard surfaces in detail considering different geometries. Both geometrical optics and asymptotic diffraction theories were used to calculate scattering from hard and soft surfaces.

The scattering and guidance of e.m waves from two dimensionally periodic metal grating structure was investigated by Wu and Chen [86]. The dispersion characteristics for this structure were obtained by the spectral domain analysis. Numerical results provide valuable information for the design of new devices in two dimensional periodic structure.

Armen and Webb [87] investigated a planar technique for determining the forward scattered field from a generally shaped inductive FSS with nonplanar illumination.

An analysis of infinite FSS's with patches of various aspect ratios, using two types of basis functions was presented by Peston et al. [88]. The analysis was based on Green's function formulation in the spectral domain and the resulting equation was solved using the method of moments.

Jon [89] interpreted the concepts of artificially hard and soft surfaces in terms of plane wave reflection properties of surfaces. Numerical results for surfaces with longitudinally oriented dielectrically filled corrugations and longitudinally oriented strips on a grounded dielectric substrate were presented.

An accurate numerical solution for the electromagnetic scattering from a periodic array of a finite number of conducting strips using a singular integral equation approach was presented by Matsushima and Itakura [90].

Johansson [91] investigated the periodic array of thin conducting ring patches etched on a dielectric substrate and placed over a ground plane for the use as blazed grating. The theoretical analysis used was based on floquets theorem and the method of moments.

An investigation on the problem of diffraction of e.m. wave by a thick conducting grating situated in an inhomogeneous dielectric slab using generalised network formulation was made by Gedney and Mittra [92]. Solutions for both TE and TM polarisations were presented.

Borkar et al. [93] described the design procedure of a millimeter wave twist reflector. They accounted the loss factor of the dielectric material for the prediction of twist reflector performance.

Kruzis et al. [94] gave the characteristic spectral response of an inclined strip grating, either free standing or embedded in a dielectric slab to variations of the oblique angle. The inclined strip grating was analyzed through an indirect mode matching technique based on Greens second theorem. Calculations focused on the effect of oblique angle on the magnitude of all propagating floquet harmonics on both sides.

The possibilities of diffraction gratings like reflection echelons and echeletts to be used as antennas in the quasi optical millimetre wave bands was examined by Chakraborti et al. [95]

Kipp and Chan [96] presented a numerically efficient technique for the calculation of the method of moments impedance matrix for planar periodic structures rendered in arbitrary triangular discretizations and embedded in layer media.

The scattering properties of perfectly conducting and resistive strips was predicted by Shively [97]. The strips were located on a dielectric slab backed by a perfectly conducting ground plane. The spectral domain Greens functions were used to relate the currents and fields on the strip and the resulting integral equation was solved using the method of moments.

Gemino et al. [98] presented a numerical model to analyze a system formed by the cascade connection of slanted strip grating plates to rotate the polarisation plane of a linearly polarized wave.

Inorder to establish design data for rectangular groove gratings with TM blazing at non bragg incidence Chen et al. [99] reported a rigorous analysis by mode matching with computer search routines for zeroes in specular reflection.

The importance of the study of scattering properties of strip gratings is well understood from the above review of past work in the field. The behaviour of strip grating to reduce reflections from targets is an area of current interest for the reduction of RCS. It can be seen from the review that, investigations for improving frequency bandwidth and angular range using these structures are not been well established. The work presented in this thesis is mainly oriented towards these problems.

Chapter

METHODOLOGY

3

Measurement Techniques

The fundamental objective of RCS measurements is to demonstrate techniques for distinguishing different types of targets, modifying target scattering properties, separating targets from background clutter and determining the response of targets to radar waveforms and processing.This chapter highlights the methodology adopted for the measurement of RCS of targets. The facilities required and fabrication of structures brought into this study are described in detail.

Almost all schemes for measuring RCS involve three basic elements.

(i) A source or radiator of electromagnetic energy.

(ii) An obstacle or scatterer of energy.

(iii) A receiving antenna or probe which measures the properties of an electromagnetic field at points in space.

Methods of measurement can broadly be classified according to how the transmitted and received fields are separated. The incident field and scattered field may be separated by a difference in propagation directions [CW cancellation method using magic tee, two antenna systems etc], by a frequency difference [Doppler and FM systems], or by a time delay [Pulsed systems]. FM and Pulsed systems are useful for measurement of large models at long ranges. CW cancellation method is adopted in the present study, since it is the least costly method and most useful for RCS measurements of small models in indoor measurement systems.

The separation of the transmitted signal from the received signal and the elimination of the unwanted signals that are reflected from the foreground and the model mount cause the principal difficulty experienced in measuring RCS. Other difficulties are in determining the minimum distance between antenna and target, and in devising a support whose cross section does not significantly affect the measurements.

Reflection from the surrounding walls, objects and external electromagnetic interactions may create error in the measurements. Hence inorder to avoid such reflections anechoic chambers are used. This is an artificially simulated free space environment in which e.m.wave propagation can be performed without interactions from the external signal sources. The room is large enough to allow the target to be well away from the backwall, and the backwall has the best possible absorbing material. Absorbers are used to control the energy to and from the target. Polyurethane foam impregnated with carbon and fire retardant chemicals are used as absorbers. The critical parameters of absorbers are the shape and size of the absorber. The absorbers have good coefficient of absorption in the frequency of interest. The walls of the chamber provide protection from the environment. With proper shielding it can isolate the measurement from external effects and protect the environment outside the chamber from energy emitted during the measurement.

The field that illuminates the model also illuminates the model supports and surrounding objects as a result of which the scattered field at the receiver becomes a combination of the desired field from the model and fields scattered by the surrounding objects.

These undesired echoes are reduced by careful design and fabrication of the support fixture. The support fixture used in this study is a turn table on which is mounted a wooden cylindrical rod of minimum circumference fitted with absorbing materials. The height of the rod from the ground can be adjusted to minimise ground reflection effects. The transmit - receive antennas and the target are kept at about the same height. Ground illumination is kept to the minimum by mounting antennas and target well above the ground and by using antennas having narrow beams.

The minimum distance between the antenna and the target is one of the important parameters in RCS measurements. Short distance requires less power and this reduces background problems. The target is sufficiently separated from the radar so that the incident energy is plane over the complete target. The scattered wave is also kept plane over the radar receiving antenna. The distance $2\,D^2 / \lambda$ is usually taken as beginning of far field region. At a distance of $2\,D^2_{tar} / \lambda$ the wave scattered from the target appears as if it is infinite distance away. This wave is received by the antenna, and the plane wave must be $1.5\,D^2_{ant} / \lambda$ away for the antenna to operate in the expected manner upon an incident plane wave. Thus the range between the antenna and the scatterer can be considered consisting of two distances added together. So in the case of an unfocussed antenna, the total range is $R = 1.5\,D^2_{ant} / \lambda + 2\,D^2_{tar} / \lambda$.The range criteria can be expressed as $R \geq pD^2_{tar} / \lambda$ where p has been empirically chosen to be between 2.5 and 4.

Echoes from the walls of the chamber and that from within the system itself are always present in the receiving system and unless eliminated they will contaminate the target signal to be measured. The CW system relies on cancellation inorder to separate the desired target echo from the undesired echoes by the use of hybrid junction. A CW radar radiates and receives RF signals continuously. Because the radar operates continuously at a constant frequency of extremely narrow bandwidth, it is possible to extract a small portion of the transmitted signal and to use it to cancel the unwanted reflection which is constant over the time required for measurement. A CW system for measuring RCS is shown in the figure 3.1.

The source used is HP 8350 B sweep oscillator [0.01-20 GHz] fed through precision attenuator. The power is fed to one of the asymmetrical port of the hybrid tee.

Hybrid Tee is a four port waveguide device with a pair of symmetrical ports and a pair of asymmetrical ports. It possesses the useful property that no energy can be transferred between the asymmetrical ports when the symmetrical ports are suitably matched. Energy injected into one of the asymmetrical ports is delivered to each symmetrical port, but none is delivered to the other asymmetric port. The advantage of this isolation property of the hybrid tee is used by feeding the transmitted signal into one of the asymmetrical ports, and by connecting the receiver to the other asymmetrical port and by attaching the antenna to one of the symmetrical ports and matched load with tuners at the other, as shown in fig. 3.2.

The transmitted signal is split by the tee into two paths, one towards the antenna and the other towards the tuning network. Chamber reflections and the antenna mismatch reflect part of the signal back toward the junction of the four waveguides. Some of this returned-signals enter the receiver line, even when there is no target installed on the support column. Similarly energy is reflected from the imperfect termination due to the tuning network, and some of this energy also enters the receiver line. The controllable reflections from the tuning network are adjusted in amplitude and phase so that they have the same amplitude but the opposite phase of those returning from the antenna port. These unwanted

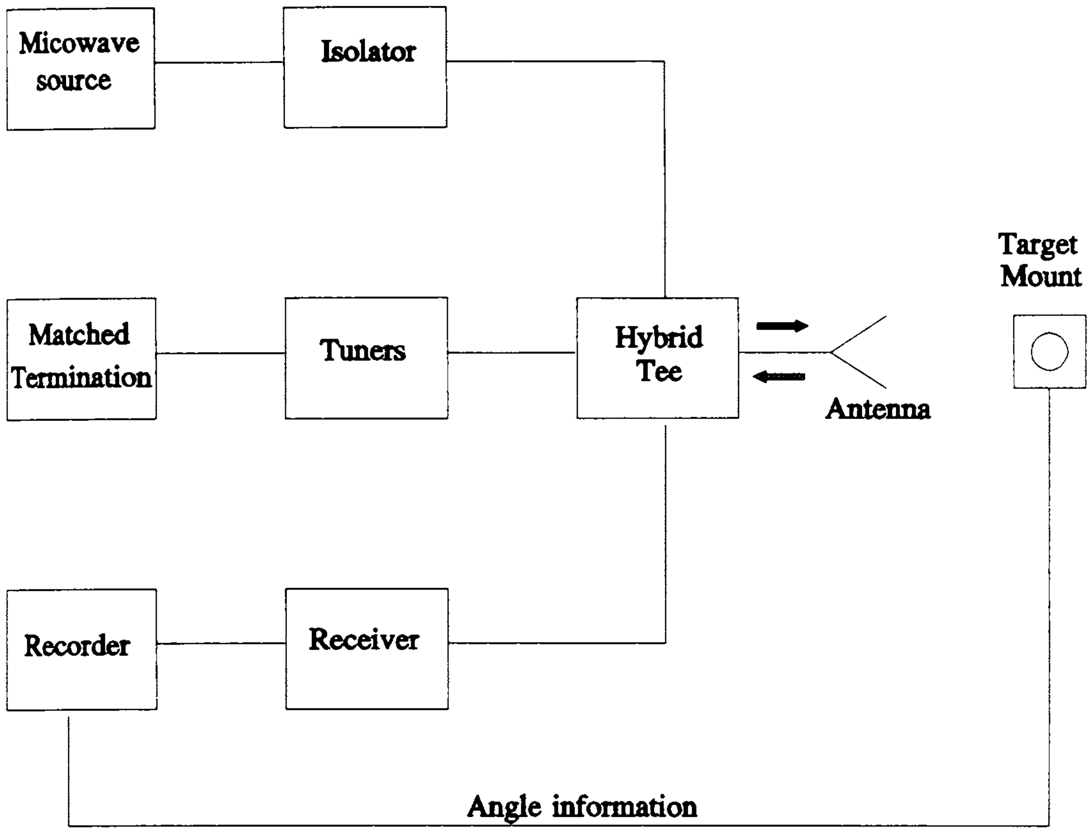

Fig.3.1 Typical CW system for measuring RCS

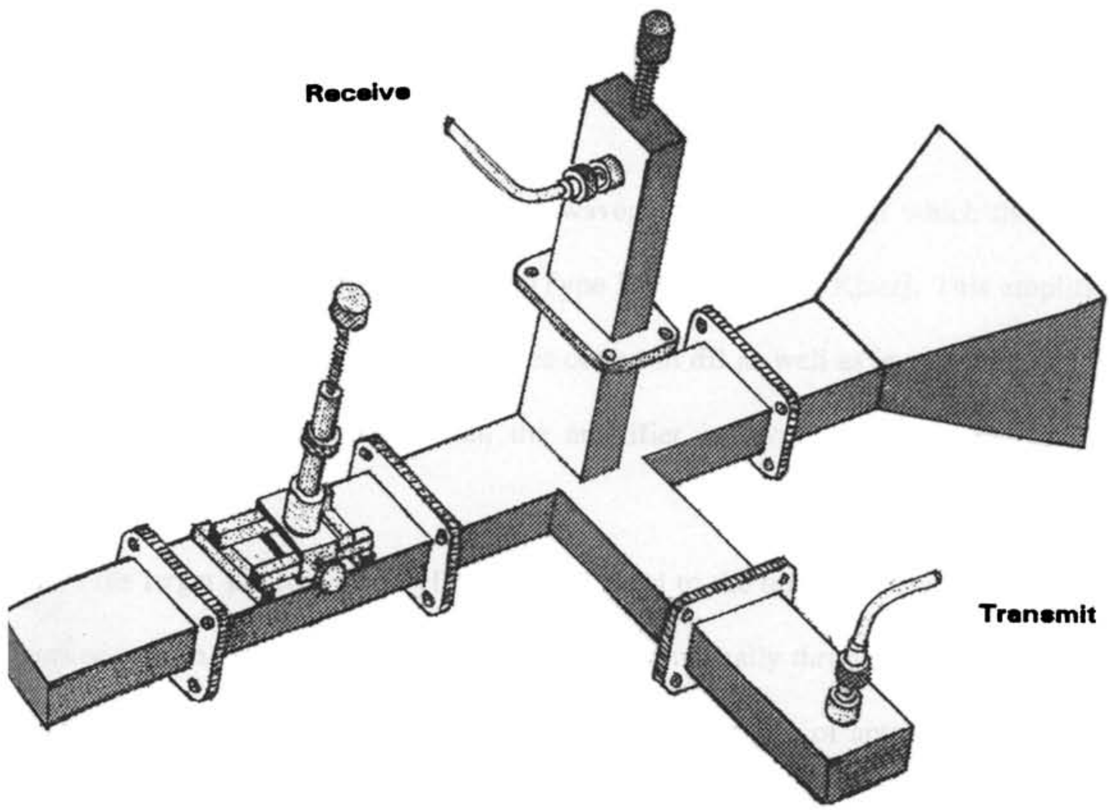

Fig.3.2 Magic Tee method

reflections from the chamber walls and from mismatches in the system itself are cancelled by a controllable reflection from the tuning network. The adjustment is performed in the absence of the target. When this adjustment is made, no signal indication is achieved in the receiver line.

The receiving system consists of a waveguide detector from which the rectified output is given to a measuring amplifier [Type 2636 Bruel and Kjaer]. This amplifier is provided with proper RF filters and it gives output in dB as well as in volts directly from the meter. The recorder output from the amplifier is given to XY/t recorder [Type HP7047A].

The target is fitted on a cylindrical rod fixed to the turn table and is placed at the centre of an arch. The turn table can be rotated automatically through 360° in the desired direction. The arch is a wooden frame work that allows a pair of antennas to be fixed at a constant radius from the centre of the test panel, for a variety of subtended angles. Each antenna is mounted on a carriage which can be rotated in the desired direction. The carriage is designed to keep the horn pointed to the centre of the test target, no matter where the carriage is positioned. The transmitting and receiving horns are fitted to ball bearings so that they can be rotated in any direction for polarisation measurements. To reduce direct coupling of energy from transmitter and receiver, absorbers are lined around the antennas and thus adequate isolation is obtained. Fig. 3.3 shows the experimental setup.

To avoid the mismatch signals due to the presence of operator, a remote control is designed to control both the antennas and the turntable.Using this system the direction of rotation of the target as well as the movement of the receiver is controlled.

The measurement procedure starts with the target support in place without the target. The tuning unit is adjusted until there is no detectable signal in the receiver arm of the tee. The SCS is then placed on target support producing an uncancelled signal in the

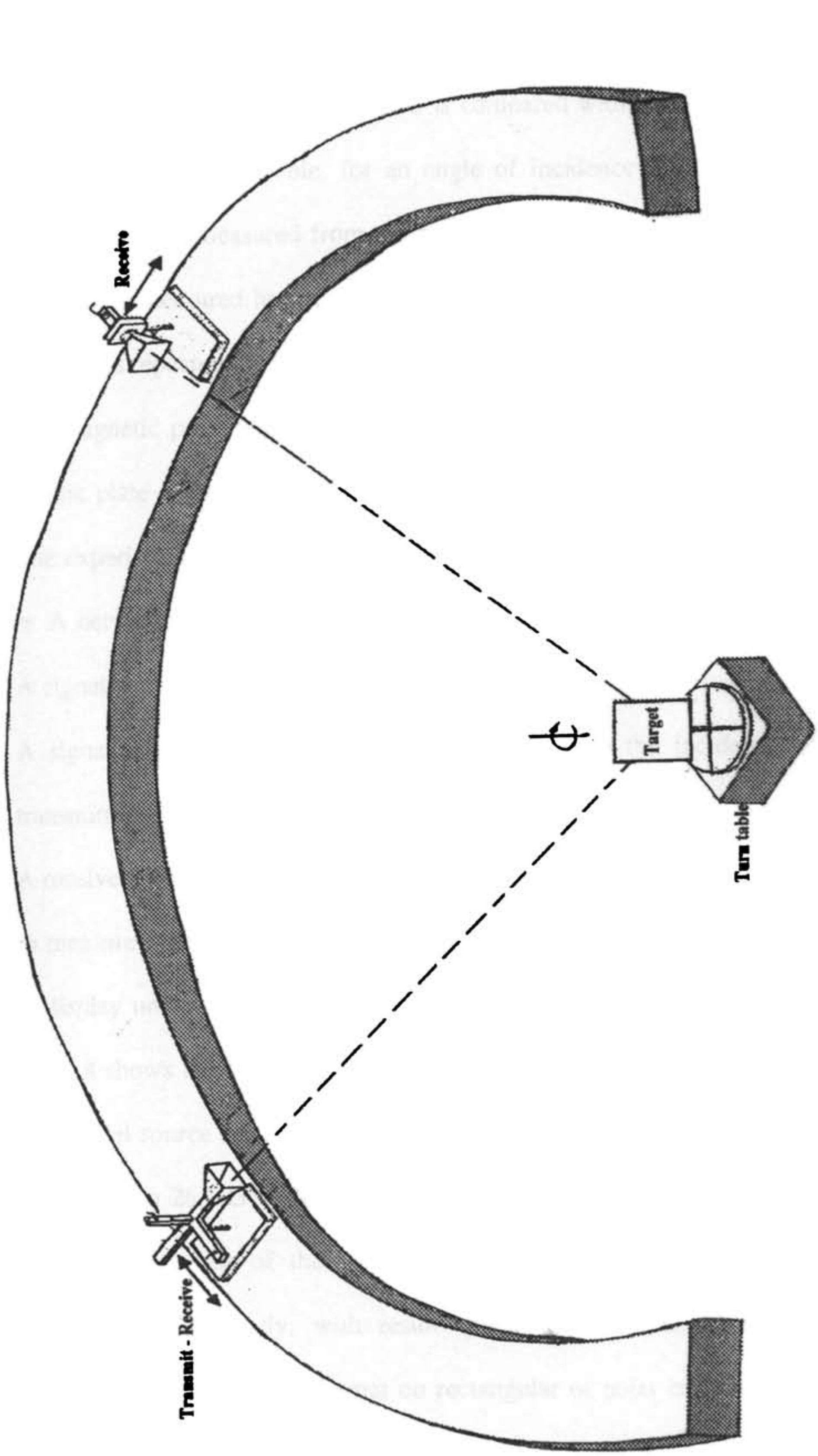

Fig. 3.3 Experimental setup

receiver arm. The signal is recorded. The SCS is then replaced by a standard object, a plane metallic plate of the same dimension of the SCS. The uncancelled signal from the standard is recorded. The signal due to SCS is compared with that of the standard. Then the SCS is set using the turntable, for an angle of incidence θ_i from the transmitter. Backscattered power is measured from the receiver arm of the hybrid tee and specularly reflected power is measured by the receiver antenna set at an angle of reflection $\theta_r = \theta_i$. The experiment is repeated for various angles of incidences for both Transverse electric and Transverse magnetic polarisations in X-band. The results are compared with that of the plane metallic plate of the same dimensions of the SCS.

The experiments described in the appendix were done using HP 8510 B Network Analyzer. A network analyzer is generally comprised of

(i) A signal source to provide the stimulus.

(ii) A signal separation network or test set, to sample the incident, reflected and transmitted signals.

(iii) A receiver to convert the microwave signals to a lower intermediate frequency, and to measure the signal levels and phase differences

(iv) A display unit to present the measured results in the desired format.

Fig 3.4 shows the block diagram of Network Analyzer.

The signal source used in the present study is capable of working in the frequency range of 45 MHz to 26.5 GHz. The measurement results can be displayed on one of the two independent channels of the Network analyzer. The channels can be displayed individually or simultaneously, with results presented in either logarithmic / linear magnitude, phase or group delay format on rectangular or polar co-ordinates. The entire measurement result can be recorded using a plotter.

RCS measurement using automated Network analyzer increases measurement speed,

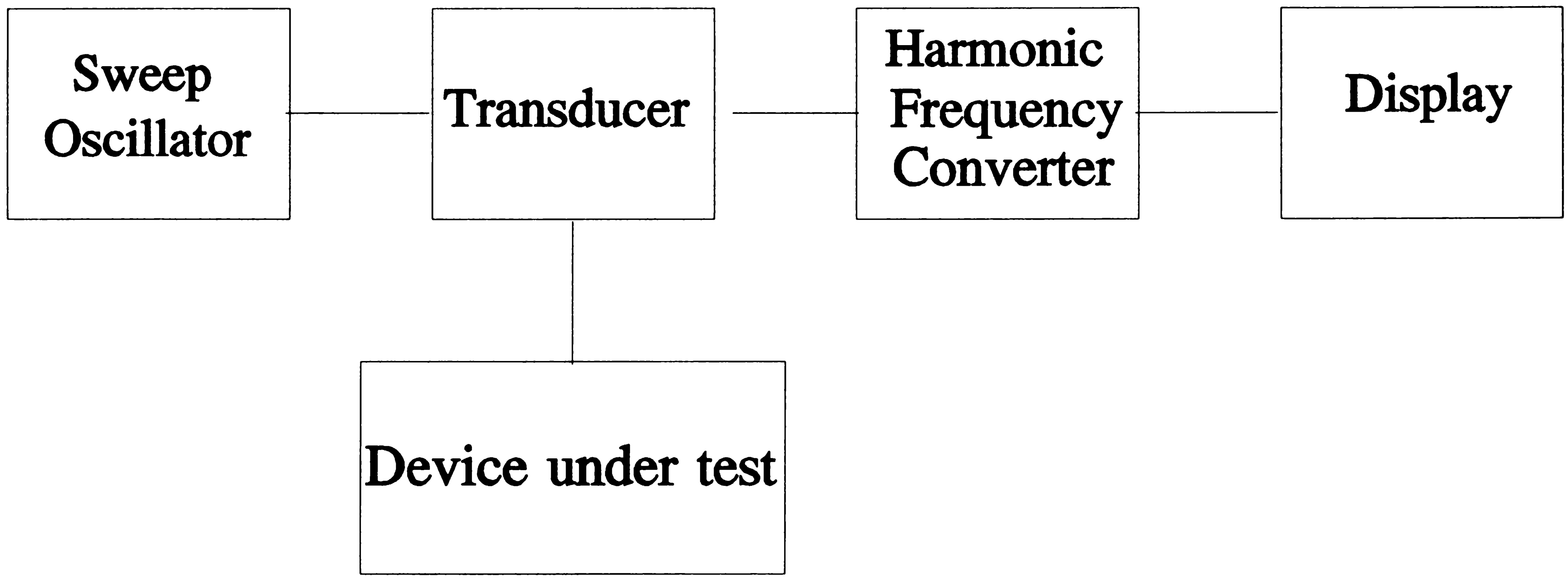

Fig.3.4 Block diagram of a Network Analyzer

convenience and accuracy. A digital computer is used in the measurement system to control the equipment as well as to perform the data processing. The network analyzer can be configured to make swept frequency RCS measurements in the frequency domain and perform the required corrections automatically. The internal correction capability of the analyzer can be used to remove measurement errors at a speed that allows real - time measurements of the test target. In addition the HP 8510 B also has the optional capability to compute the inverse Fourier transform of the measured data to give the time domain response, which displays reflections from the target as a function of time or distance. The time domain gating feature can also be used to analyze the measured responses and further reduce the effects of unwanted signals.

In RCS measurements, the response of a target is analyzed by bouncing radar signals off the target and picking up the return signals with a receiving antenna. At each discrete frequency for which RCS measurements are to be obtained, the system measures the characteristics of the measurement equipment, such as errors due to finite isolation between the reference and receiver channels, losses and phase deviations of the cable. In addition to that cross coupling between the transmitter and receiver antennas and the clutter from fixed obstacles such as supports for the targets without the target are measured and stored in the memory. These measurements are vectorially subtracted from the received target-plus-clutter signal to obtain the backscattered signal from the target alone. Fig 3.5 shows RCS measurements with HP 8510B network analyzer and 8511A frequency converter.

Fabrication of strip gratings

Thin metallic strips etched on a dielectric substrate and placed over a metallic conducting surface simulates the characteristics of a corrugated surface. These surfaces are

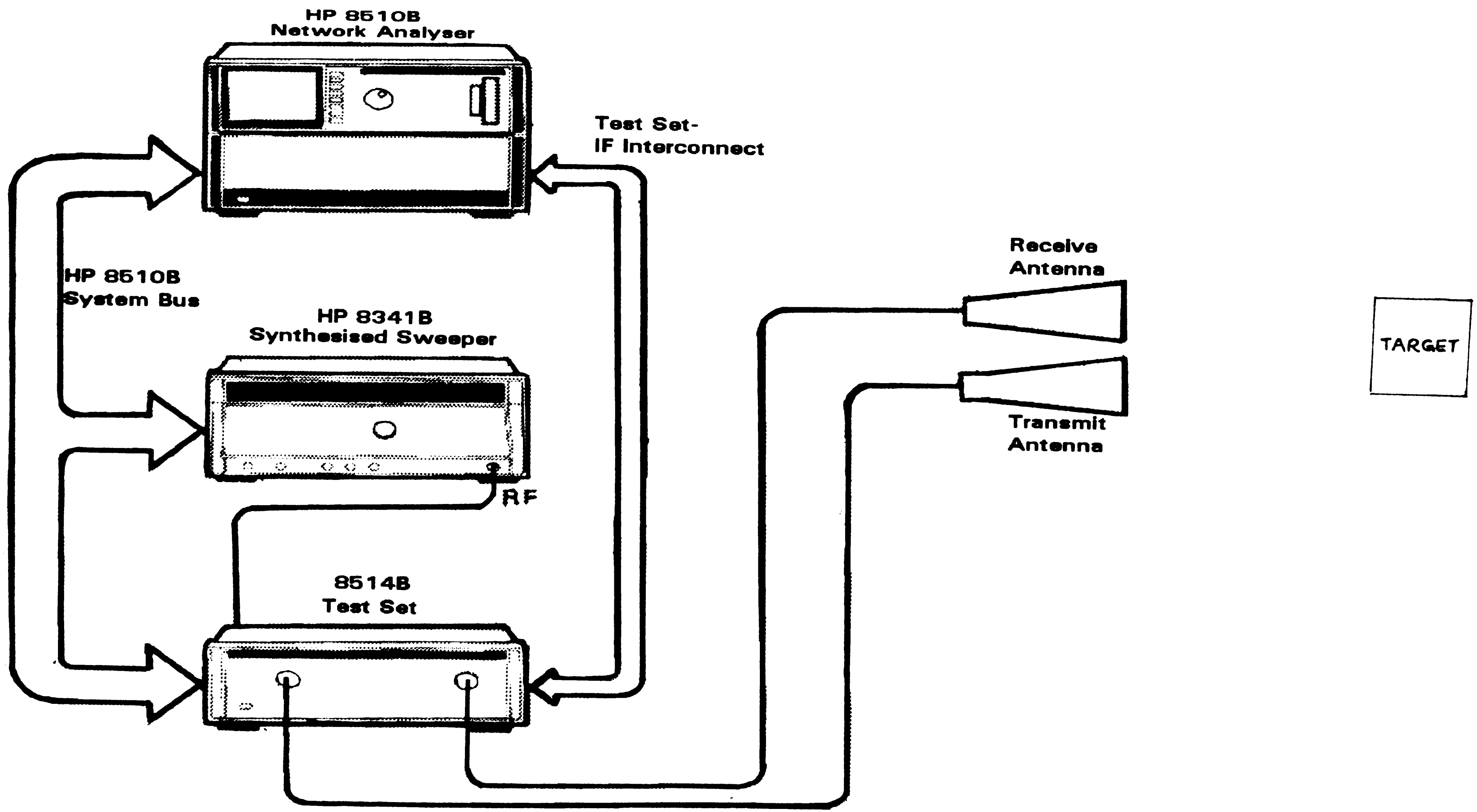

Fig.3.5 RCS Measurements with HP 8510 B Network Analyser

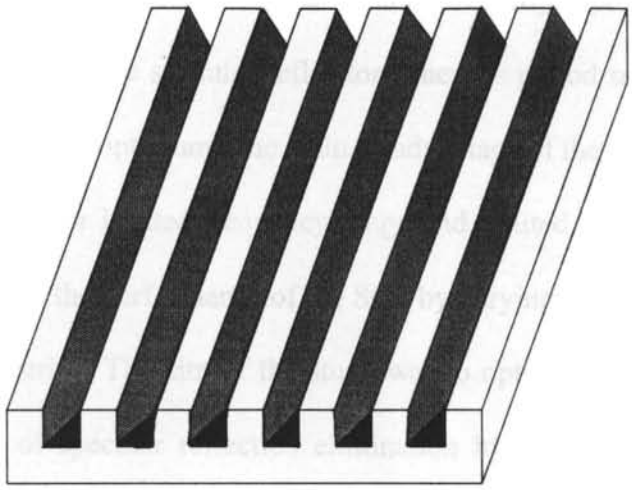

(a)

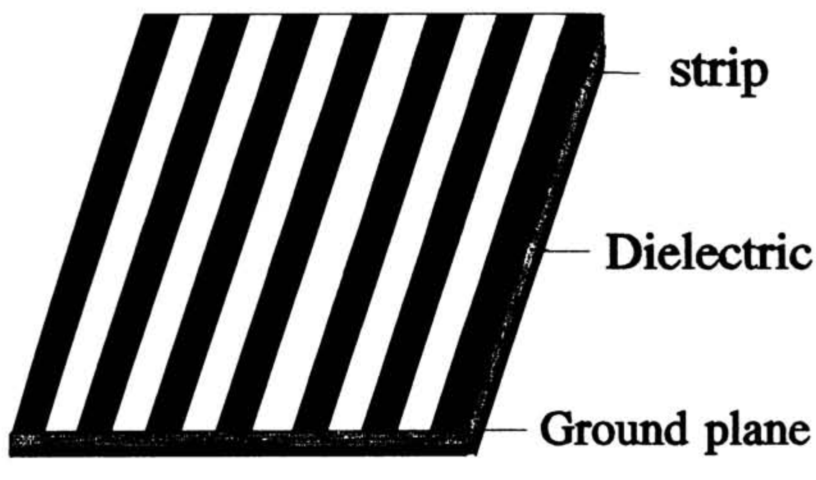

(b)

Fig.3.6 (a) Corrugated surface

(b) Equivalent SCS

called Simulated Corrugated Surfaces (SCS). The corrugated surface and its equivalent SCS are shown in fig 3.6. The dielectric substrate used in the study is poly methyl methacrylate. These SCS can eliminate the specular reflection when its period satisfies bragg condition and dielectric thickness is optimum. The main disadvantage of the system is the elimination of specular reflection for limited frequency range and limited angular range. However it is possible to improve the performance of the SCS by varying other parameters like, shape and aspect ratio of strips. The aim of the study was to optimise the frequency bandwidth and angular range of specular reflection elimination by modifying the size, shape and period of the strips. Different types of structures brought into study are as follows.

1. Progressively varied SCS

This structure is made by etching thin metallic strips on a reflector backed dielectric substrate of size 30cm × 30cm. Fig. 3.7 shows the diagram of progressively varied SCS. The width 'a' of the strip is progressively varied by keeping the period $d = a+b$ constant. The common ratio 'r' [ratio of widths of adjacent strips] with which stripwidth varies is selected in such a way that the values of 'a' lies in the range $0 < a < d$. Three types of variations used are given in terms of central frequency in table 3.1. First the structures were fabricated for common period and strip widths varying in geometric progression for various common ratios. Then strip widths were varied for a common period and common ratio. Finally the period was varied keeping all other parameters constant.

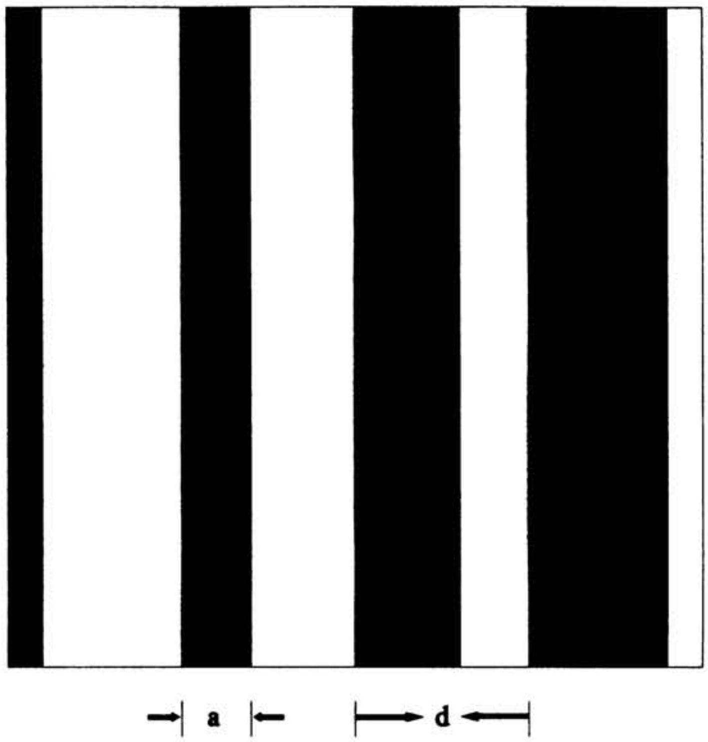

Fig.3.7 Progressively varied strips

No	a/λ	r	d/λ
P1	0.500 .... 0.500	1.000	1.000
P2	0.466 .... 0.533	1.015	1.000
P3	0.433 .... 0.566	1.032	1.000
P4	0.400 .... 0.600	1.046	1.000
P5	0.366 .... 0.633	1.063	1.000
P6	0.333 .... 0.666	1.080	1.000
P7	0.300 .... 0.700	1.098	1.000
P8	0.266 .... 0.733	1.119	1.000
P9	0.250 .... 0.750	1.130	1.000
P10	0.233 .... 0.766	1.141	1.000
P11	0.200 .... 0.800	1.167	1.000
P12	0.166 .... 0.833	1.196	1.000
P13	0.133 .... 0.866	1.231	1.000
P14	0.100 .... 0.900	1.276	1.000
P15	0.066 .... 0.933	1.341	1.000
P16	0.033 .... 0.966	1.454	1.000
P17	0.166 .... 0.333	1.080	1.000
P18	0.200 .... 0.400	1.080	1.000
P19	0.233 .... 0.466	1.080	1.000
P20	0.250 .... 0.500	1.080	1.000
P21	0.266 .... 0.533	1.080	1.000
P22	0.300 .... 0.600	1.080	1.000
P23	0.366 .... 0.733	1.080	1.000
P24	0.400 .... 0.800	1.080	1.000
P25	0.416 .... 0.833	1.080	1.000
P26	0.333 .... 0.666	1.080	0.833
P27	0.333 .... 0.666	1.080	0.900
P28	0.333 .... 0.666	1.080	1.100
P29	0.333 .... 0.666	1.080	1.166
P30	0.333 .... 0.666	1.080	1.233
P31	0.333 .... 0.666	1.080	1.333

Table 3.1 Design details of progressively varied SCS.

2. Tapered SCS

Tapered SCS was fabricated by etching thin metallic strips on a reflector backed dielectric substrate of size 30cm x 30 cm. Here variation was given along the y-axis of the conventional SCS as shown in fig. 3.8. Various tapering structures fabricated are shown in terms of cental frequency in table 3.2. Initially structures were fabricated with 'a_2' kept constant and period 'd' was varied for different 'a_1' values. Then keeping period and 'a_2' values constant, structures with different 'a_1' were constructed. Finally 'a_1' and 'a_2' were varied keeping period 'd' constant to optimise the structure.

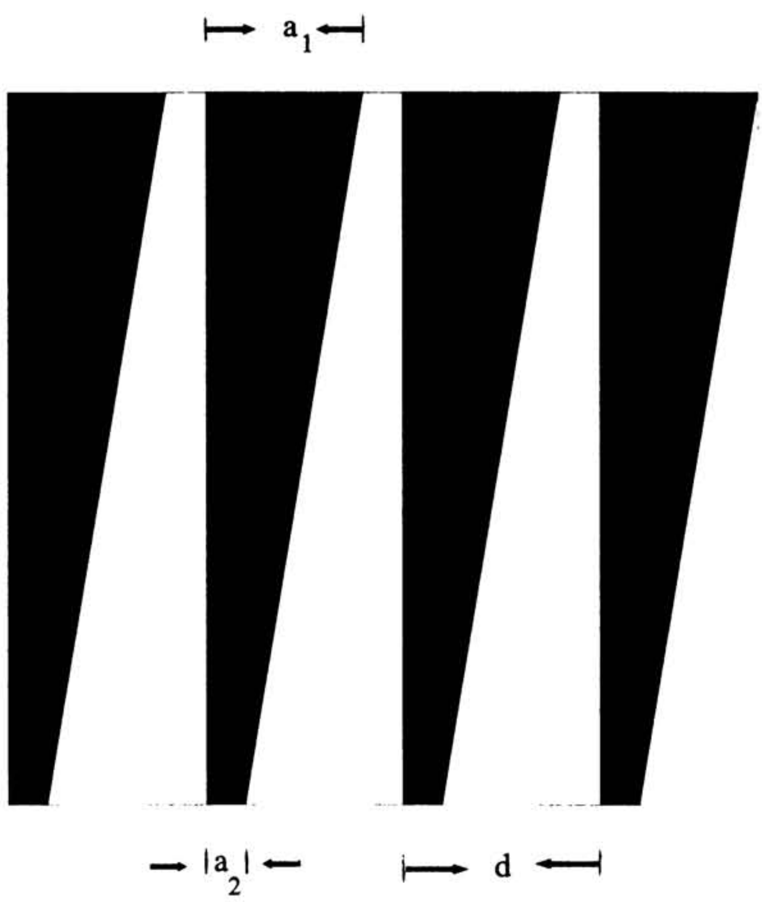

Fig 3.8 Tapered strips

No	a_1/λ	a_2/λ	d/λ
T1	1.066	0.000	1.060
T2	1.000	0.000	1.000
T3	0.933	0.000	0.933
T4	0.833	0.000	0.833
T5	0.733	0.000	0.733
T6	0.733	0.100	0.833
T7	0.666	0.166	0.833
T8	0.600	0.233	0.833
T9	0.566	0.266	0.833
T10	0.500	0.333	0.833
T11	0.417	0.417	0.833
T12	0.333	0.166	0.833
T13	0.566	0.166	0.833
T14	0.733	0.166	0.833
T15	0.833	0.166	0.833
T16	0.666	0.000	0.833
T17	0.666	0.100	0.833
T18	0.666	0.233	0.833
T19	0.666	0.333	0.833

Table 3.2 Design details of tapered SCS.

3. Dual aspect ratio strips

This structure was fabricated by etching thin metallic strips of single periodicity and double aspect ratio on a reflector backed dielectric substrate of size 30cm x 30cm. Variations were made as shown in the figure 3.9. Keeping periodicity 'd', 'l_1', 'l_2', and 'a_1' constant, structures were fabricated with different 'a_2' values. Then keeping 'a_1', 'a_2' and period constant, 'l_1' and 'l_2' were varied to obtain another set of structures. The parameters are chosen approximately to avail experimental data of corresponding self complementary gratings (a=0.5d) from earlier works. Table 3.3. shows the various structures fabricated for the study.

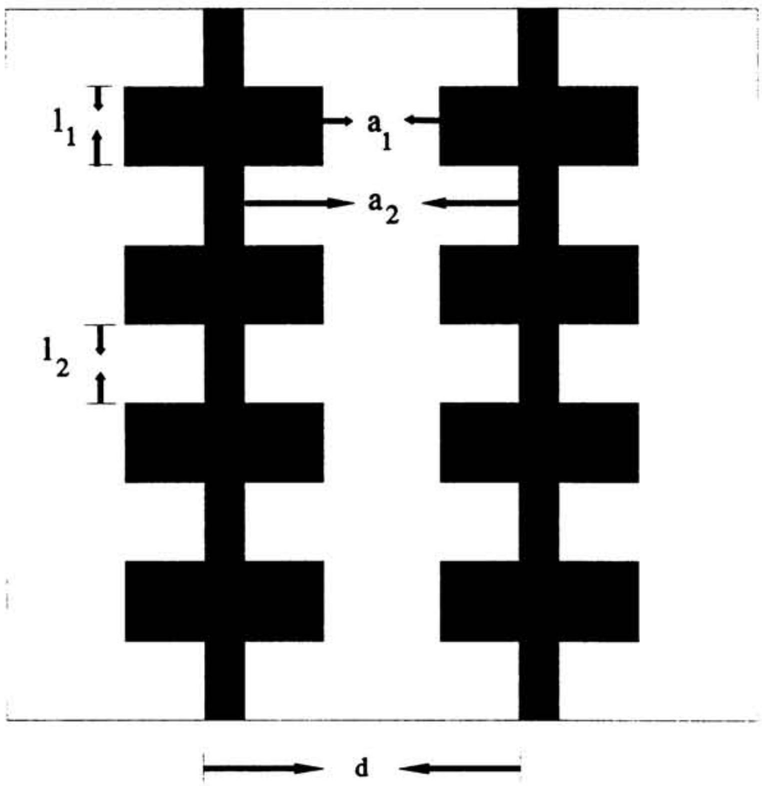

Fig. 3.9 Dual aspect ratio strips.

No	l_1/λ	l_2/λ	a_1/λ	a_2/λ	d/λ
D1	0.500	0.500	0.500	0.633	1.00
D2	0.500	0.500	0.500	0.700	1.00
D3	0.500	0.500	0.500	0.766	1.00
D4	0.500	0.500	0.500	0.833	1.00
D5	0.500	0.500	0.500	0.900	1.00
D6	0.500	0.600	0.500	0.700	1.00
D7	0.500	0.666	0.500	0.700	1.00
D8	0.500	0.833	0.500	0.700	1.00
D9	0.666	0.666	0.500	0.700	1.00
D10	0.833	0.833	0.500	0.700	1.00

Table 3.3 Design details of dual aspect ratio strips.

4. Dual periodic rhombic shaped structure

This is also a modification of the SCS. The grating structure has a periodicity 'd' for the strips, and each strip is given a regular periodic variation in dimension along its length as shown in fig. 3.10. Thus the structure provides a two dimensional or dual periodicity. This is fabricated by etching thin metallic strips on one side of a double cladded dielectric substrate of size 30cm x 30cm. The period of the strip is a constant. Each strip is made up of a number of rhombic shaped elements of side length 'l' and angles 'α' & 'β'. Each structure used in the study has ten regular symmetric strips. Various structures fabricated are shown in terms of central frequency in table 3.4. Initially, structures are constructed by varying 'l' and keeping 'd', 'α' & 'β' constant. then angles 'α' & 'β' are varied keeping 'l' & 'd' constant for another set of structures. Finally structures are fabricated with 'α', 'β' and 'l' constant and period varied.

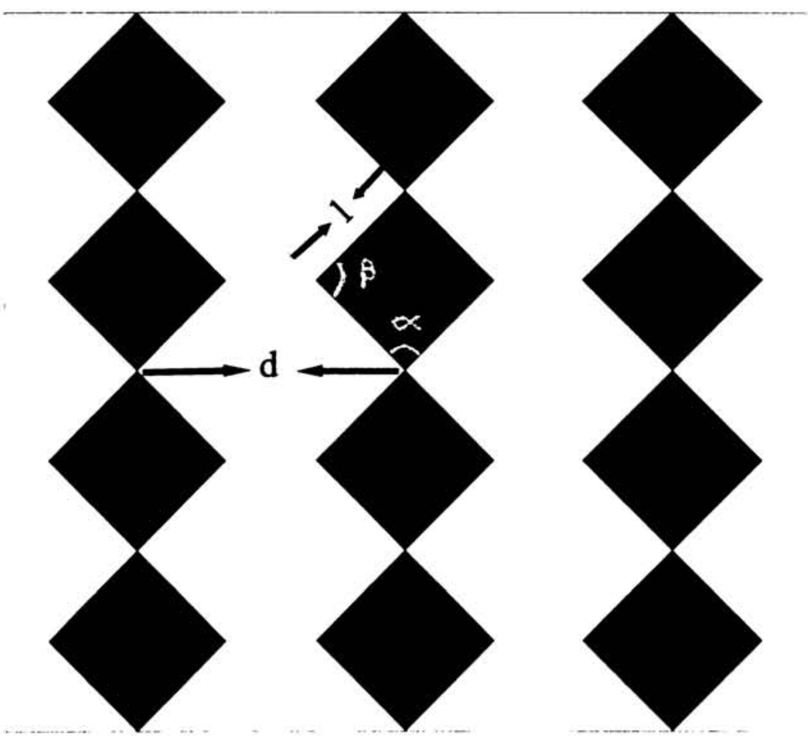

Fig. 3.10 Dual periodic rhombic shaped strips.

No	l/λ	α deg.	β deg.	d/λ
R1	0.166	90°	90°	1.000
R2	0.200	90°	90°	1.000
R3	0.233	90°	90°	1.000
R4	0.266	90°	90°	1.000
R5	0.300	90°	90°	1.000
R6	0.333	90°	90°	1.000
R7	0.363	90°	90°	1.000
R8	0.404	90°	90°	1.000
R9	0.437	90°	90°	1.000
R10	0.471	90°	90°	1.000
R11	0.500	90°	90°	1.000
R12	0.533	90°	90°	1.000
R13	0.566	90°	90°	1.000
R14	0.600	90°	90°	1.000
R15	0.633	90°	90°	1.000
R16	0.666	90°	90°	1.000
R17	0.471	30°	150°	1.000
R18	0.471	45°	135°	1.000
R19	0.471	60°	120°	1.000
R20	0.471	75°	105°	1.000
R21	0.471	105°	70°	1.000
R22	0.471	120°	60°	1.000
R23	0.471	135°	45°	1.000
R24	0.471	150°	30°	1.000
R25	0.471	90°	90°	0.666
R26	0.471	90°	90°	0.833
R27	0.471	90°	90°	0.900
R28	0.471	90°	90°	1.066
R29	0.471	90°	90°	1.166
R30	0.471	90°	90°	1.333

Table 3.4 Design details of dual periodic rhombic shaped structure.

5. Periodic structures with 'V' shaped elements

This is also a structure designed for RCS reduction. 'V' shaped conducting elements are etched on the reflector backed dielectric substrate of dimension 30cm x 30cm as shown in fig. 3.11. Each element is arranged with a regular period. The values of 'w' and 'l' are chosen in such a way that elements do not overlap, while period 'd' and interelement spacing 'b' are varied. Table 3.5 shows the various structures used in the study. Two sets of structures are fabricated. One by varying 'b', keeping all other parameters constant and the other by varying 'd' keeping all other parameter constant.

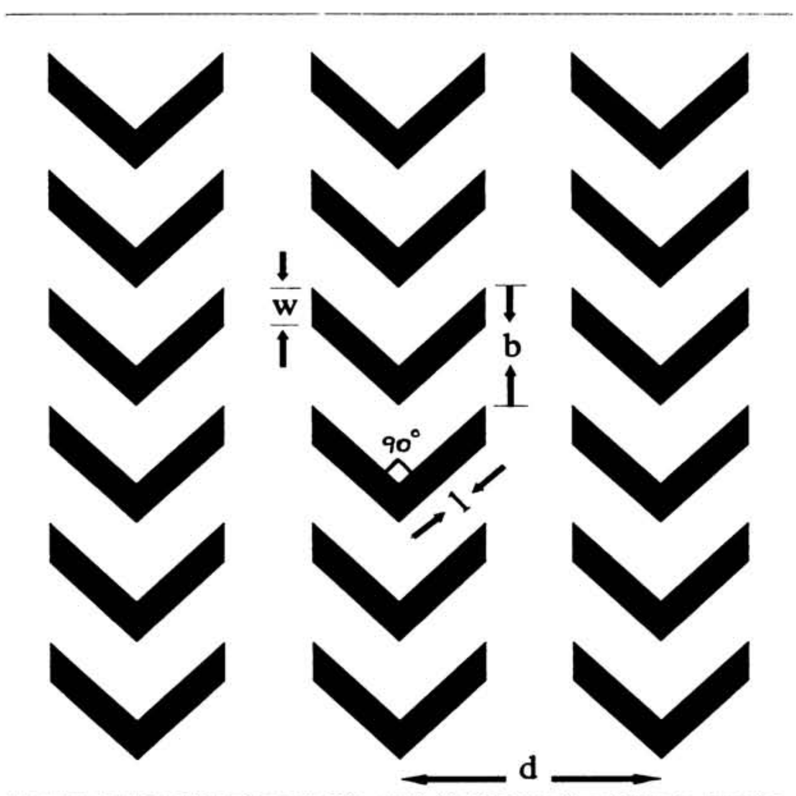

Fig. 3.11 Periodic structure with V-shaped elements.

The parameters are chosen approximately to avail experimental data of corresponding self complementary gratings (a=0.5d) from earlier works.

No	w/λ	l/λ	d/λ	b/λ
V_1	0.166	0.500	1.000	0.333
V_2	0.166	0.500	1.000	0.400
V_3	0.166	0.500	1.000	0.500
V_4	0.166	0.500	1.000	0.600
V_5	0.166	0.500	1.000	0.666
V_6	0.166	0.500	1.000	0.833
V_7	0.166	0.500	0.800	0.400
V_8	0.166	0.500	0.866	0.400
V_9	0.166	0.500	0.900	0.400
V_{10}	0.166	0.500	1.067	0.400

Table 3.5 Design details of periodic structure with V-shaped elements.

Chapter

EXPERIMENTAL RESULTS

4

This chapter gives an account of the experimental results obtained for various SCS's and other periodic structures. The studies were conducted in the frequency range 8-12 GHz. The chapter is divided into five sections :-

1. Progressively varied SCS;
2. Tapered SCS;
3. Dual aspect ratio strips;
4. Dual periodic rhombic shaped structures;
5. Periodic structures with V-shaped elements;

As theoretical modelling of strip grating is not available in open literature, it is found difficult to design various shapes of strip grating. Hence the structures described here were optimised for desired characters through experimental iterations.

This chapter concentrates on the design and performance evaluation of different types of strip gratings which possess properties which reduce RCS to a considerable extend. The main concentration in the performance evaluation is the reflected RF power. Little attention is given to the actual calculation of RCS. However, the magnitude of the reflected power from a target, as such, gives an indication of the magnitude of its RCS.

Specular reflections from a conducting surface can be eliminated by corrugations of proper period and depth. The corrugations of period between one half and one wavelength in a conducting surface will scatter only two spectral orders, specular reflection and backscatter. When the period satisfies the Bragg condition required for perfect blazing, the specular reflection (n = 0, mode) is completely cancelled and the corrugated surface becomes a 100% backscatter (n = -1, mode). If the period satisfies the condition for constructive interference in the direction of incidence, specular reflection is minimised and it can be eliminated by proper choice of corrugation depth. Fabrication of metallic corrugations is a time consuming and difficult task. Thin conducting strips etched on a dielectric substrate backed with a metallic reflector can produce equivalent effects of perfectly blazed rectangular grooves. This is a very simple, easy and less time consuming procedure. Schematic diagram of a self complementary strip grating is shown in fig.4.1 (a). Variation of reflected power against the angle of incidence and frequency for such an SCS, compared to the variation of a plane metallic plate of same dimensions is shown in fig. 4.1 (b) and (c).

It is clear from the fig. 4.1 (b & c) that limitations of these structures are mainly, the elimination of specular reflection is restricted for limited angular range and for limited frequency range. Several other parameters of this structure are to be modified to eliminate these restrictions in angular range and frequency.

The investigations carried out for the development of new types of SCS's, which can eliminate specular reflection for wide angular range and wide frequency range are

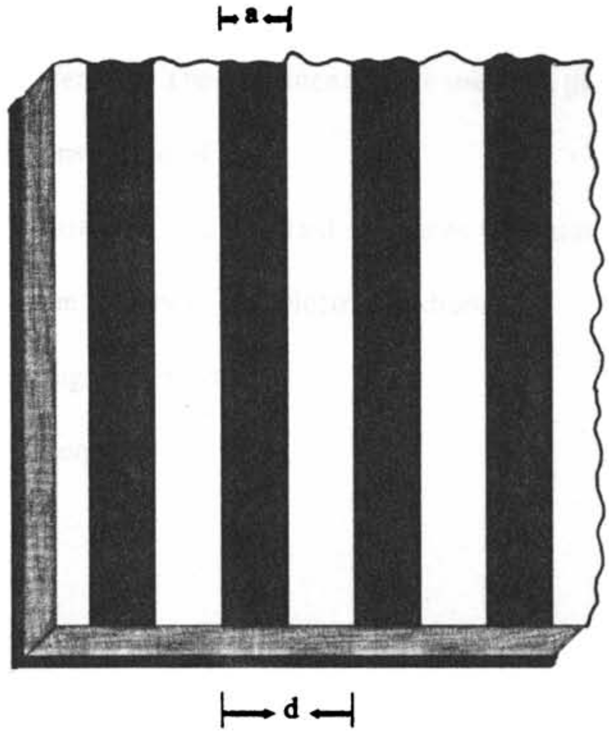

(a)

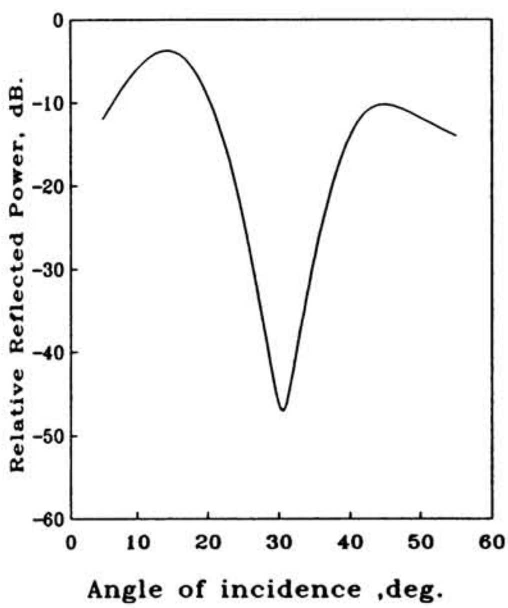

(b)

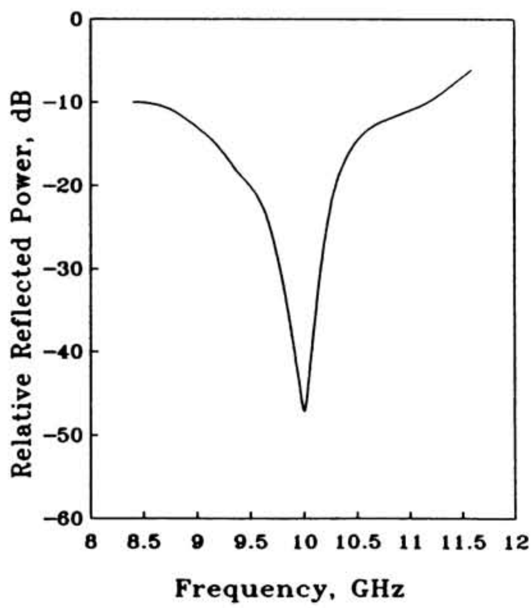

(c)

Fig.4.1 (a) Schematic representation of SCS
(b) Variation of relative reflected power with angle of incidence.
(c) Variation of relative reflected power with frequency.

highlighted in this chapter. Each and every characteristic of the developed structure is compared to that of a reference. The reference surface used is a plane metallic plate, which is of the same dimensions as the SCS.

The following characteristics of the modified structures are studied in detail:-

1. Variation with the thickness of dielectric medium.
2. Variation with angle of incidence.
3. Variation with frequency.

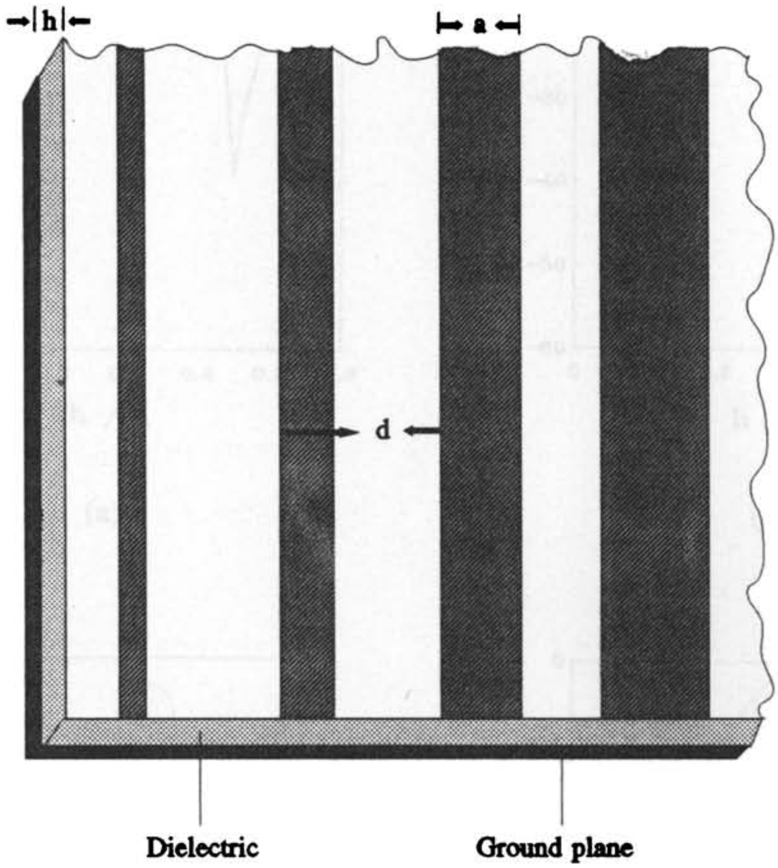

.Fig.4.2 Schematic diagram of progressively varied SCS.

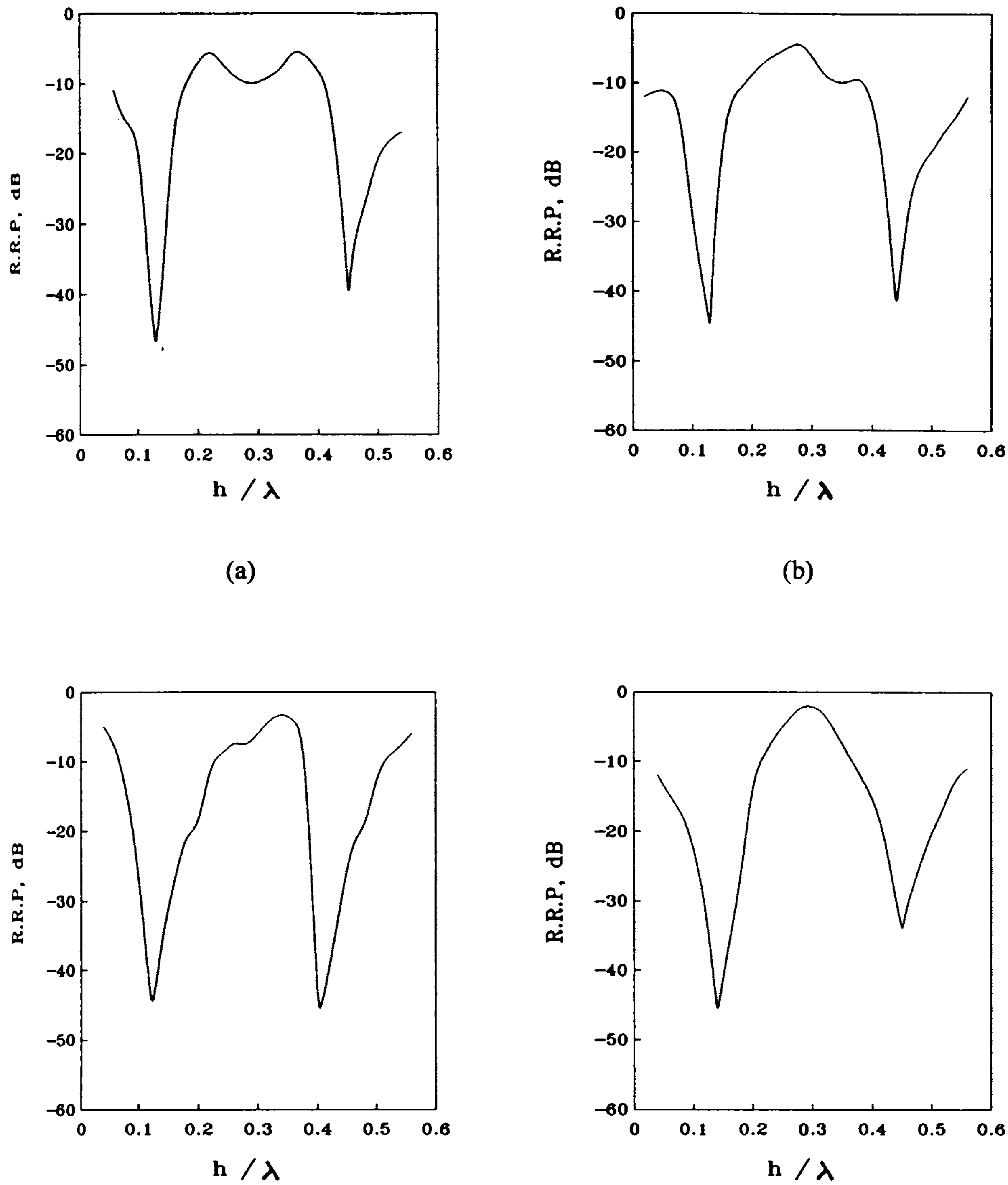

Fig.4.3. Variation of Relative reflected power with dielectric thickness.

(a) [P4]. d = λ, a' = 0.50 λ, r = 1.046, θ_i = 37.5°, f = 10GHz
(b) [P8]. d = λ, a' = 0.50 λ, r = 1.119, θ_i = 40°, f = 10GHz
(c) [P11]. d = λ, a' = 0.50 λ, r = 1.167, θ_i = 37.5°, f = 10GHz
(d) [P19]. d = λ, a' = 0.35 λ, r = 1.080, θ_i = 32.5°, f = 10GHz

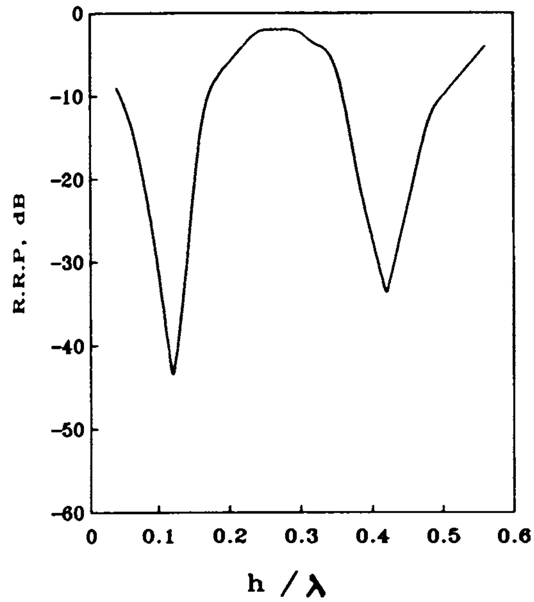

(e)

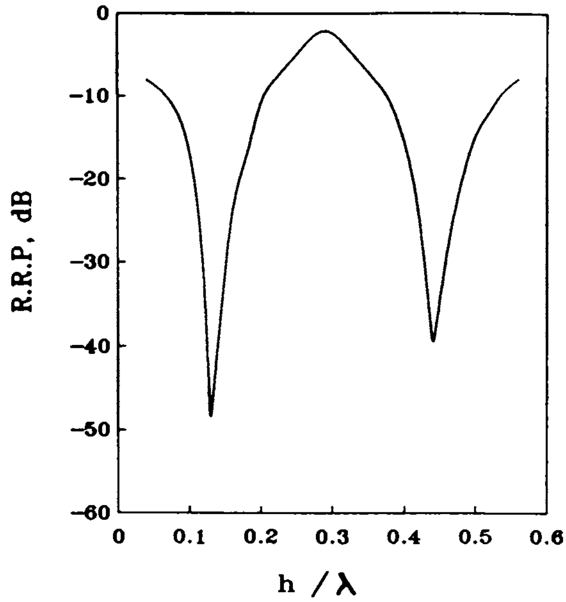

(f)

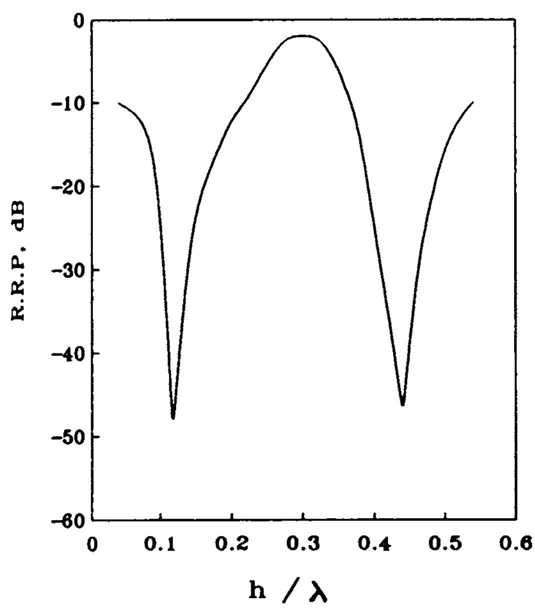

(g)

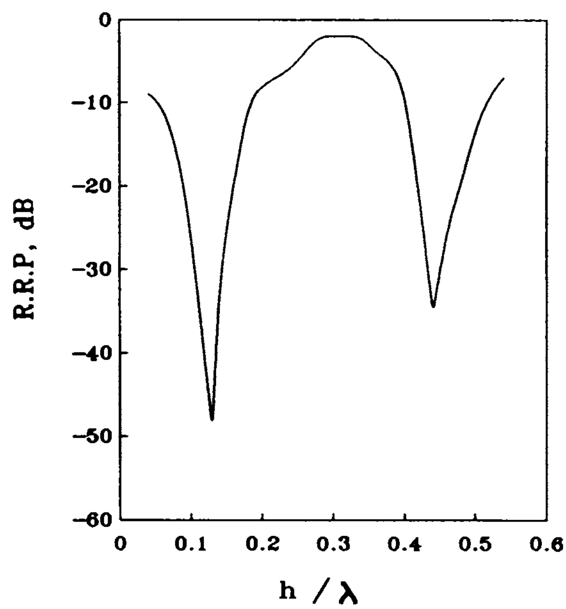

(h)

Fig.4.3. Variation of Relative reflected power with dielectric thickness.

(e) [P24]. $d = \lambda$, $a' = 0.60\ \lambda$, $r = 1.08$, $\theta_i = 57.5°$, $f = 10GHz$
(f) [P6]. $d = \lambda$, $a' = 0.50\ \lambda$, $r = 1.08$, $\theta_i = 40°$, $f = 10GHz$
(g) [P26]. $d = 0.833\lambda$, $a' = 0.50\ \lambda$, $r = 1.08$, $\theta_i = 50°$, $f = 10GHz$
(h) [P29]. $d = 1.166\lambda$, $a' = 0.50\ \lambda$, $r = 1.08$, $\theta_i = 40°$, $f = 10GHz$

[P19] of dimensions d = λ, r = 1.08, a′ = 0.35λ

[P24] of dimensions d = λ, r = 1.08, a′ = 0.60λ and

[P6] of dimensions d = λ, r = 1.08, a′ = 0.50λ

is shown in fig. 4.3 (d, e & f).

(c) Period

The plots of R.R.P Vs h / λ for SCS's

[P26] of dimensions d = 0.833λ, r = 1.08, a′ = 0.5λ and

[P29] of dimensions d = 1.166λ, r = 1.08, a′ = 0.5λ

are shown in fig. 4.3 (g & h). These structures have different period, while other parameters are the same.

From fig. 4.3, it is observed that reflected power is minimum only for certain values of dielectric thickness. The minimum dielectric thickness obtained is used for further experimental investigations.

4.1.2 Angle of incidence

With proper choice of dielectric thickness, the reflected power from the SCS, at various angles of incidence, is measured and compared with that of the reference target. Variation of relative reflected power with angle of incidence for typical structures at constant frequency for TM polarisation is shown in fig. 4.4. The power diverted to n = -1 mode at blazing angle is also shown. The variations for the three sets of structure parameters (r, a′ & d) described earlier are investigated.

Variation of relative reflected power with angle of incidence for SCS's [P4], [P8], [P11], [P19],[P6], [P26] and [P29] are shown in fig. 4.4 (a.i), (b.i), (c.i), (d.i), (e.i), (f.i), (g.i) and (h.i) respectively. The scattered power with receiving angle from normal, at blazing angle of incidence is plotted in fig. 4.4 (a.ii), (b.ii), (c.ii), (d.ii), (e.ii), (f.ii), (g.ii) & (h.ii)

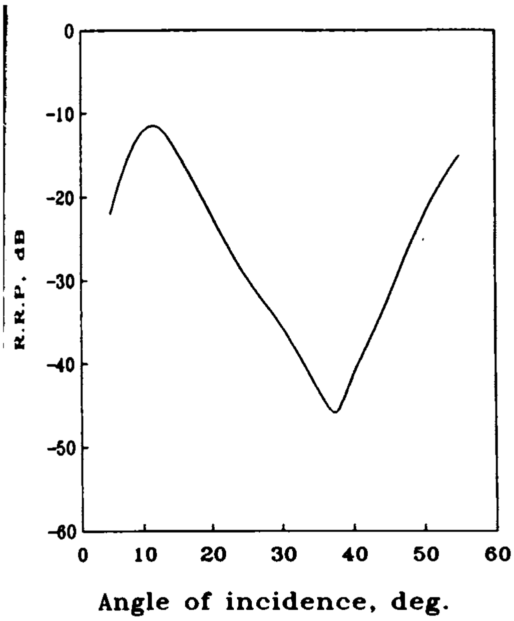

(a.i)

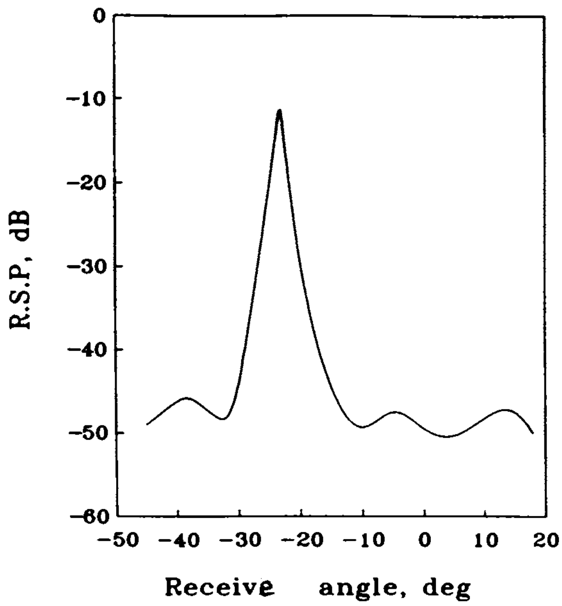

(a.ii)

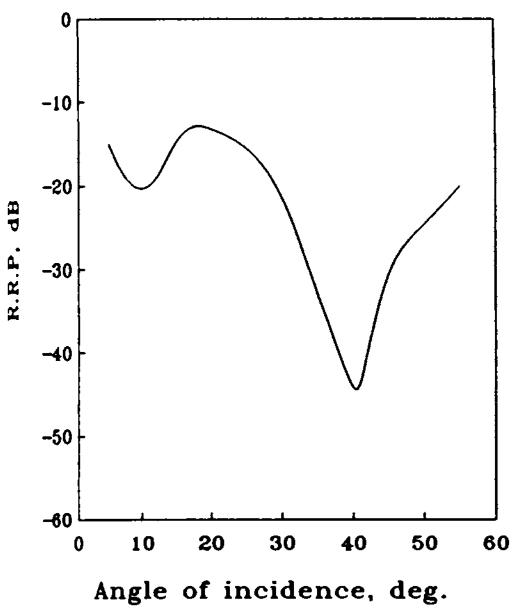

(b.i)

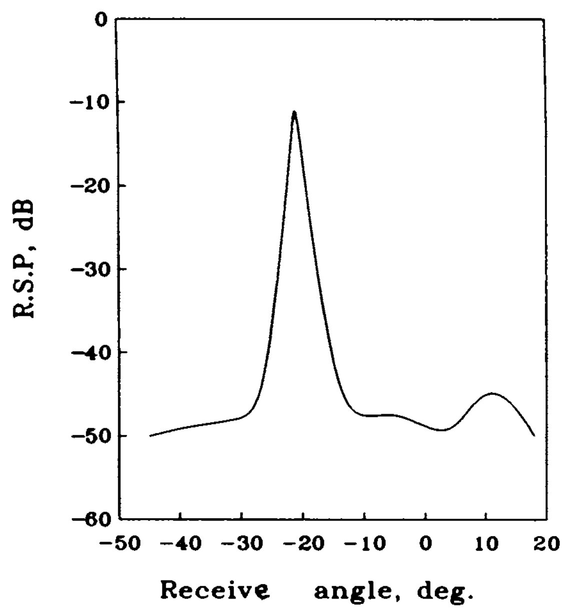

(b.ii)

Fig.4.4. (i) Variation of Relative reflected power with incident angle.
(ii) Measured relative scattered power with receive angle.

(a) [P4]. d = λ, a′ = 0.50 λ, r = 1.046, h/λ = 0.130, f = 10GHz
(b) [P8]. d = λ, a′ = 0.50 λ, r = 1.119, h/λ = 0.130, f = 10GHz

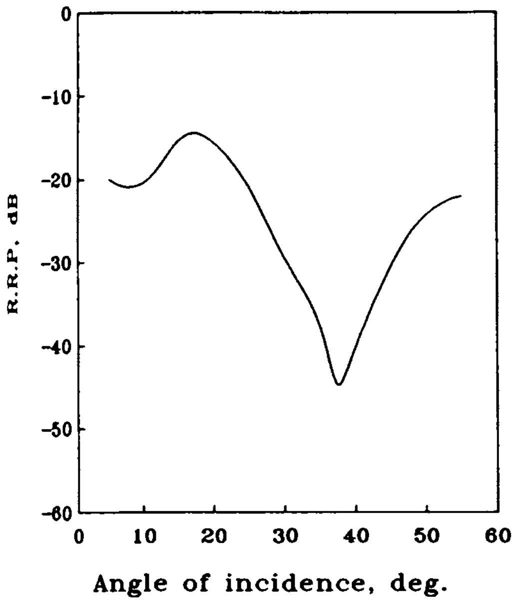

(c.i)

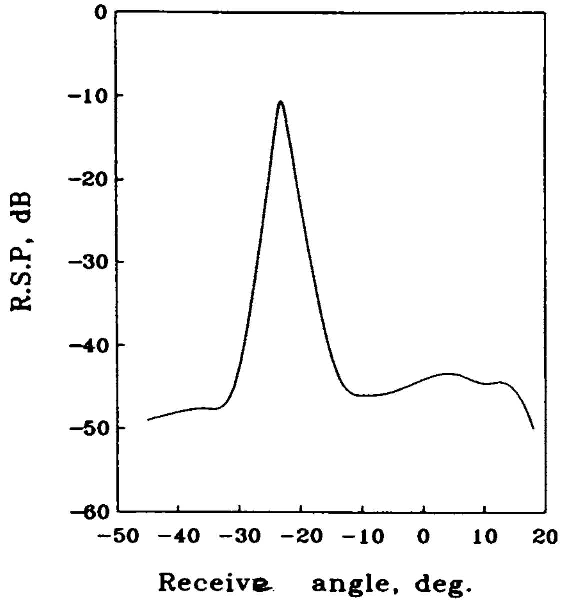

(c.ii)

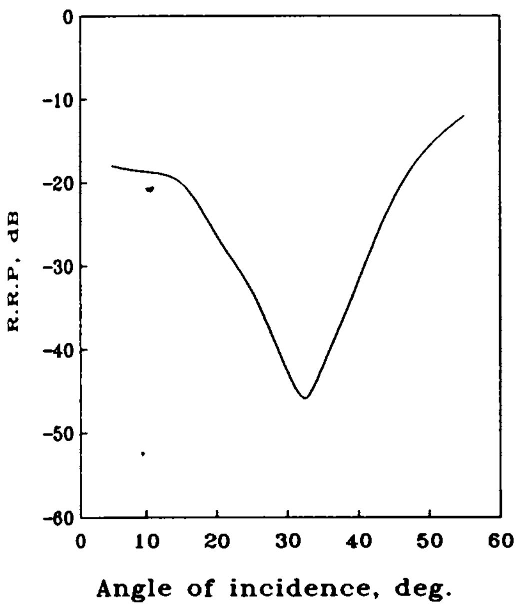

(d.i)

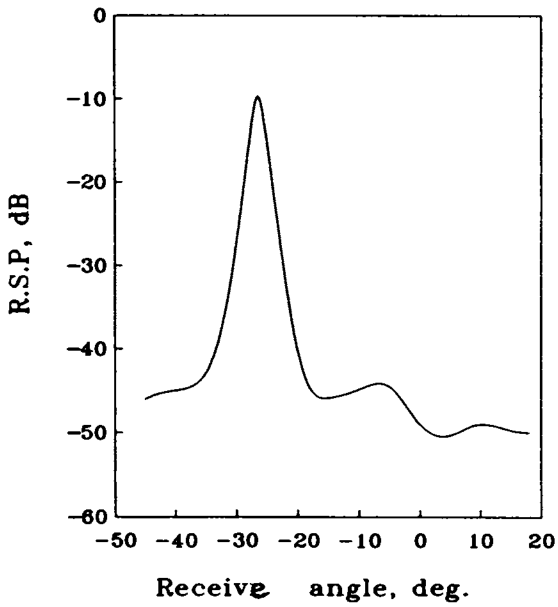

(d.ii)

Fig.4.4. (i) Variation of Relative reflected power with incident angle.
(ii) Measured relative scattered power with receive angle.

(c) [P11]. d = λ, a' = 0.50 λ, r = 1.167, h/λ = 0.130, f = 10GHz
(d) [P19]. d = λ, a' = 0.35 λ, r = 1.08, h/λ = 0.117, f = 10GHz

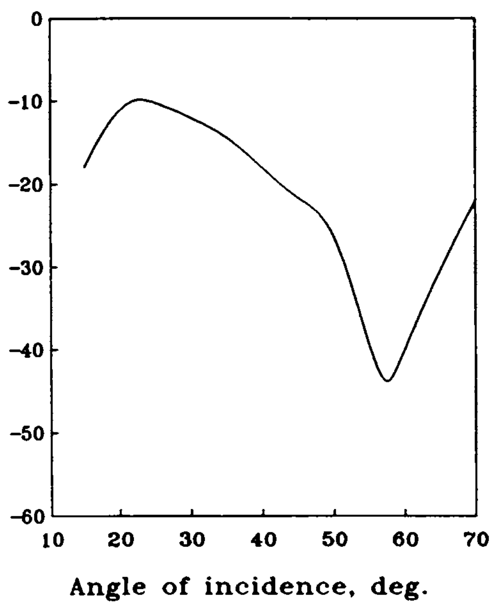

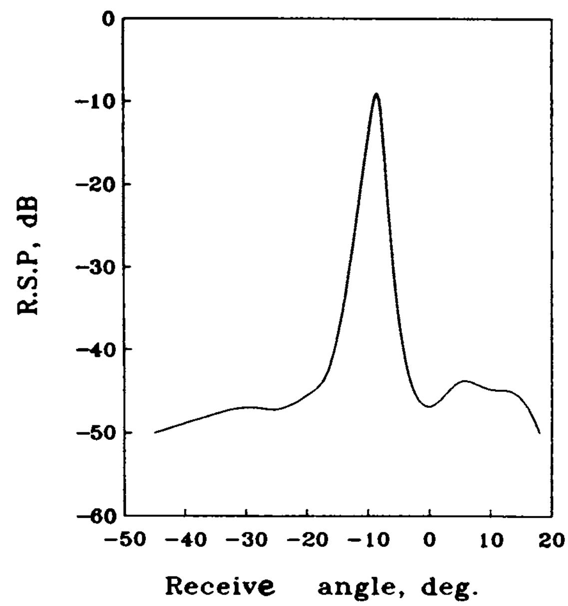

(e.i) (e.ii)

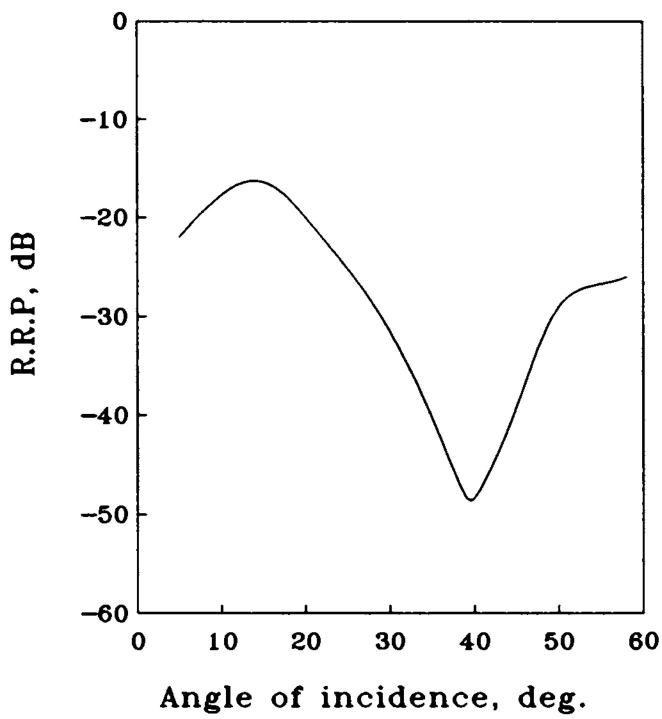

(f.i)

Fig.4.4 (i) Variation of Relative reflected power with incident angle.
(ii) Measured scattered power with receive angle.

(e) [P24]. $d = \lambda$, $a' = 0.60\ \lambda$, $r = 1.08$, $h/\lambda = 0.117$, $f = 10$ GHz
(f) [P6]. $d = \lambda$, $a' = 0.50\ \lambda$, $r = 1.08$, $h/\lambda = 0.130$, $f = 10$ GHz

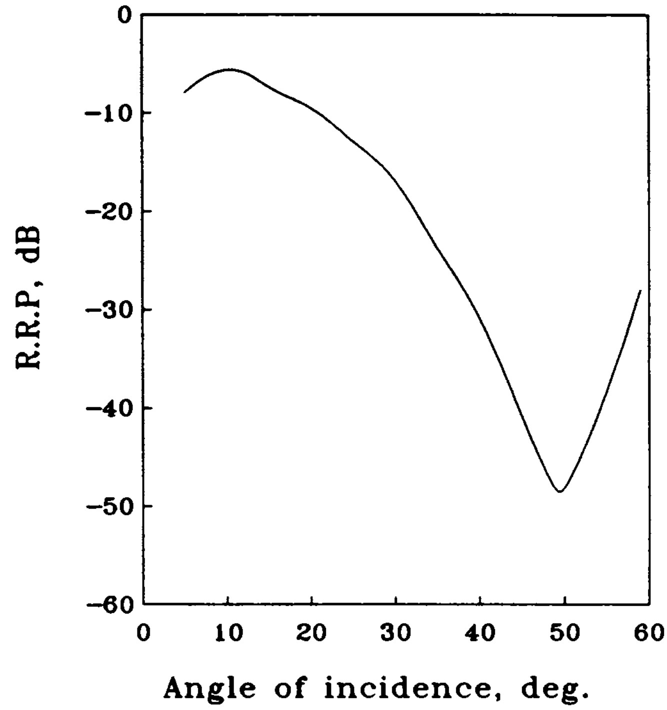

(g.i)

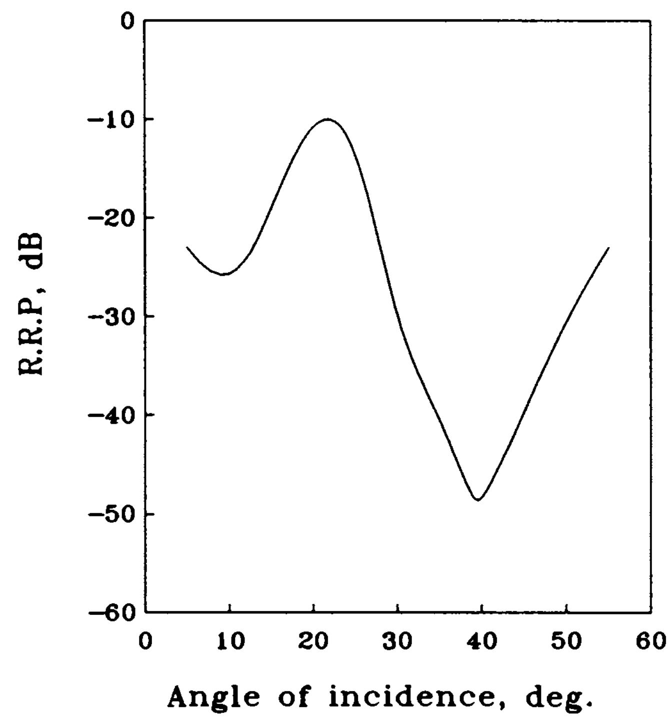

(h.i)

Fig.4.4 (i) Variation of relative reflected power with incident angle

(g) [P26]. d = 0.833λ, a′ = 0.50 λ, r = 1.08, h/λ = 0.117, f = 10 GHz

(h) [P29]. d = 1.166λ, a′ = 0.50 λ, r = 1.08, h/λ = 0.130, f = 10 GHz

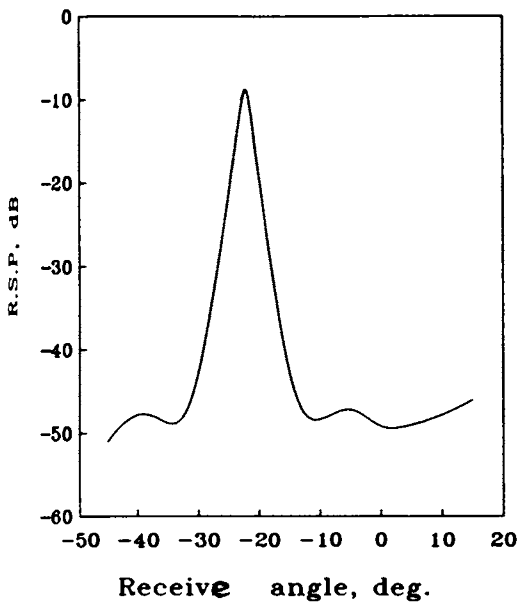

(f.ii)

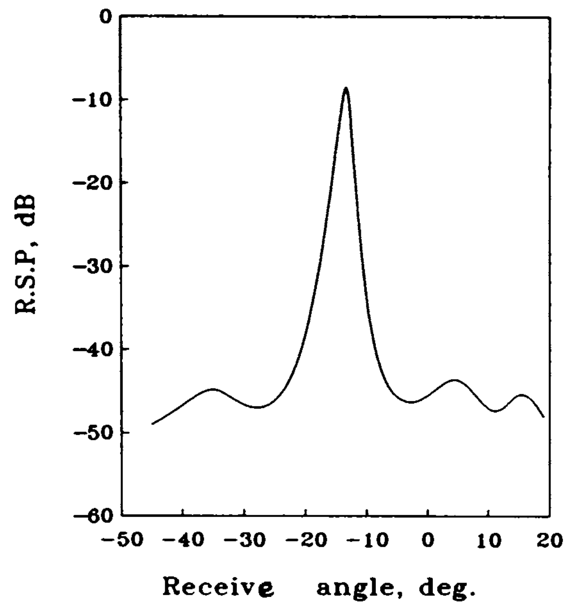

(g.ii)

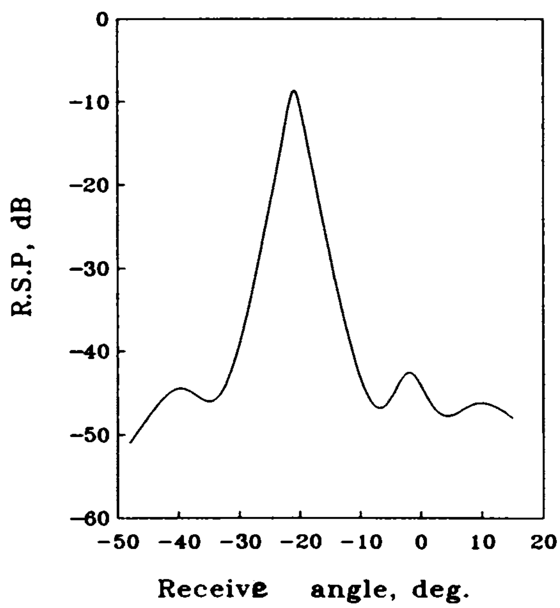

(h.ii)

Fig.4.4 (ii) Measured scattered power with receive angle

(f) [P6]. $d = \lambda$, $a' = 0.50\ \lambda$, $r = 1.08$, $\theta_i = 40°$, $f = 10$ GHz
(g) [P26]. $d = 0.833\lambda$, $a' = 0.50\ \lambda$, $r = 1.08$, $\theta_i = 50°$, $f = 10$ GHz
(h) [P29]. $d = 1.166\lambda$, $a' = 0.50\ \lambda$, $r = 1.08$, $\theta_i = 40°$, $f = 10$ GHz

for the same configuration of SCS's. It is clear from the above plots that blazing is possible only for a particular incident angle.

4.1.3 Frequency

After selecting the dielectric thickness and angle of incidence where blazing is obtained, frequency is changed. Keeping the structure at blazing angle, the corresponding reflected power is measured. Variation of relative reflected power with frequency for typical structures from all sets of structures for TM polarisation is shown in fig. 4.5. Fig. 4.5 (a), (b), (c), (d), (e), (f), (g) and (h) represents the variation of relative reflected power with frequency for structures SCS [P4], [P8], [P11], [P19],[P6], [P26] and [P29] respectively.

In fig. 4.5 (h) solid line shows the variation of R.R.P with frequency for progressively varied SCS and dotted line represents that for self complementary strip grating. 'Self complementary strip gratings' are corresponding plane gratings of identical dimensions (a=0.5d) of grating elements [75]. From this it is observed that the bandwidth for specular reflection elimination (less than - 40 dB) is about 2.14 GHz for progressively varies SCS, while that for self complementary strip grating it is only 0.142 GHz. Using progressively varied SCS, it is possible to increase the bandwidth of elimination of specular reflection.

Table 4.1 presents the various strip geometries which were brought into study for elimination of reflected power in TM polarisation. The varying strip width of the structure, the period, the common factor, the minimum dielectric thickness, the angle at which blazing is obtained and the bandwidth obtained are also presented.

In the first set, period is kept constant and strip widths are varied in different progression values. In the second set period is kept constant and strip widths are varied with the same progression and in the third set common ratio and strip widths are kept the same but the period is changed. The results are tabulated.

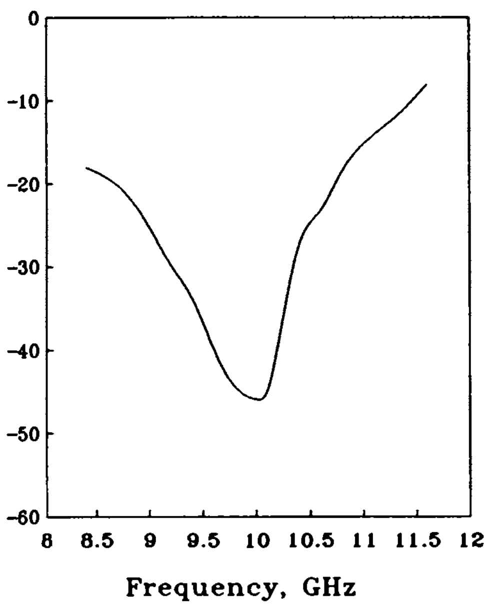

(a)

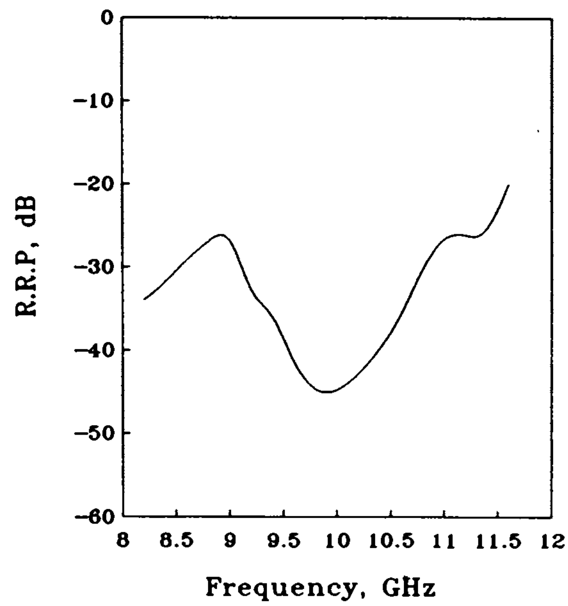

(b)

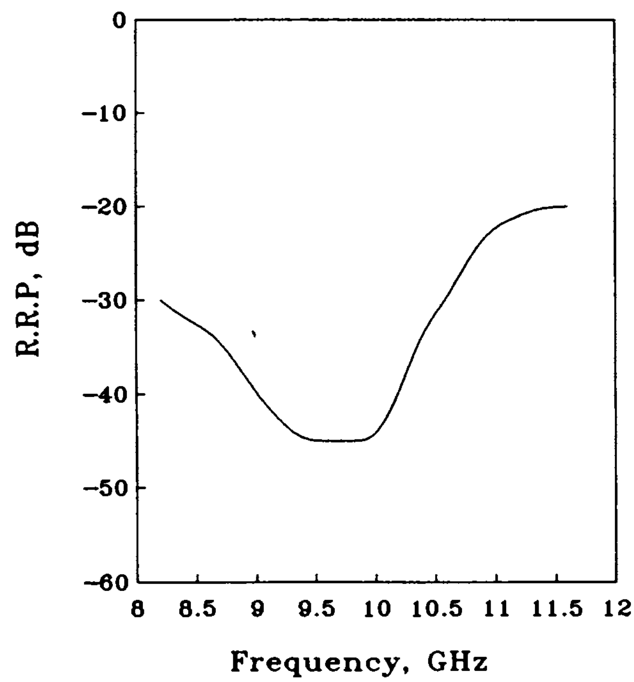

(c)

Fig.4.5 Variation of relative reflected power with frequency

(a) [P4]. $d = \lambda$, $a' = 0.50\ \lambda$, $r = 1.046$, $\theta_i = 37.5°$, $h/\lambda = 0.130$
(b) [P8]. $d = \lambda$, $a' = 0.50\ \lambda$, $r = 1.119$, $\theta_i = 40°$, $h/\lambda = 0.130$
(c) [P11]. $d = \lambda$, $a' = 0.50\ \lambda$, $r = 1.167$, $\theta_i = 37.5°$, $h/\lambda = 0.130$

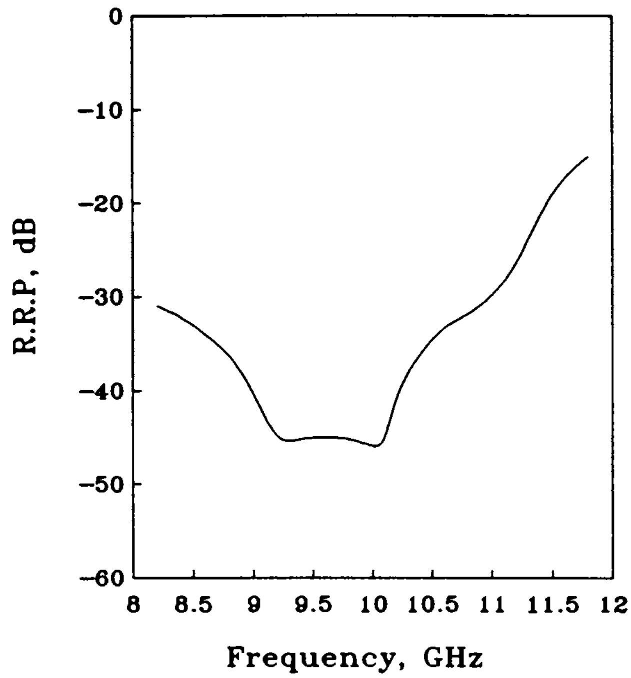

(d)

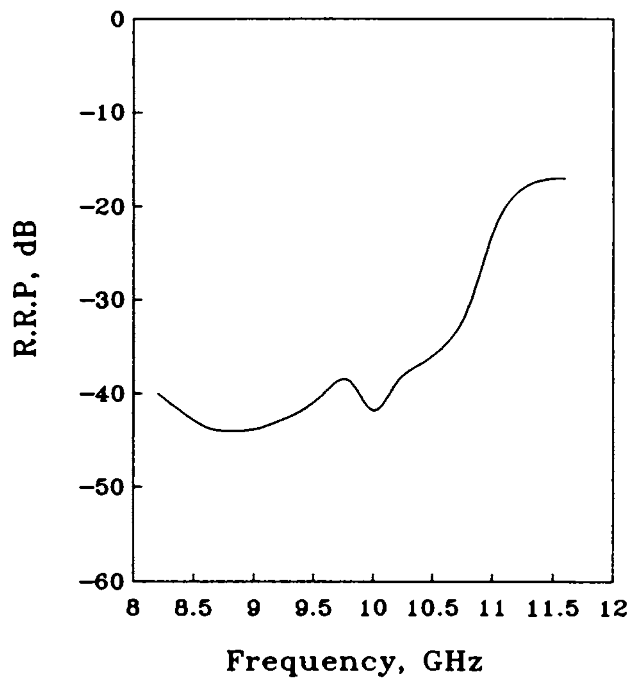

(e)

Fig.4.5. Variation of relative reflected power with frequency

(d) [P19]. d = λ, a′ = 0.35 λ, r = 1.080, θ_i = 32.5°, h/λ = 0.117
(e) [P24]. d = λ, a′ = 0.60 λ, r = 1.080, θ_i = 57.5°, h/λ = 0.117

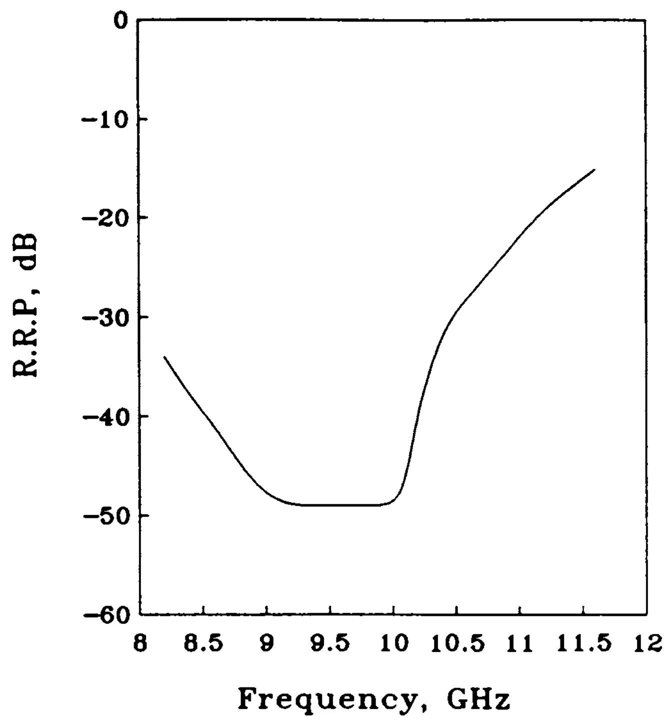

(f)

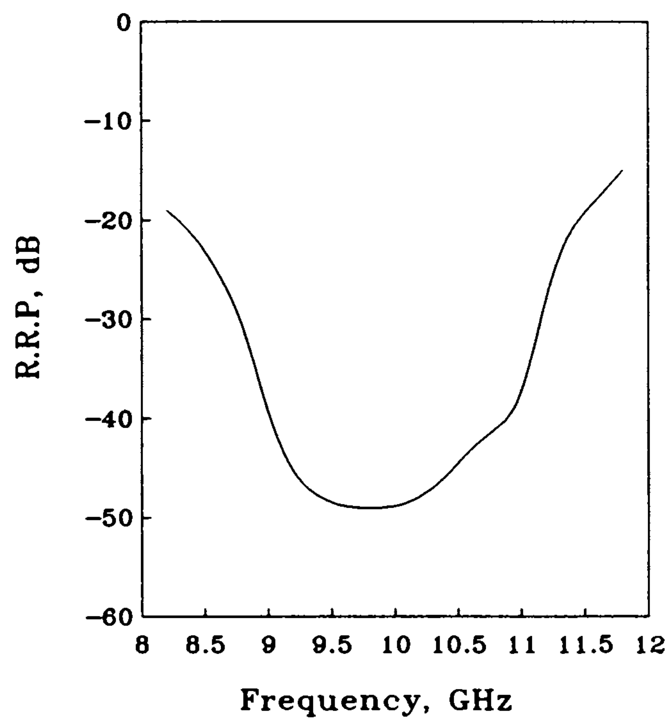

(g)

Fig.4.5 Variation of relative reflected power with frequency.

(f) [P6]. $d = \lambda$, $a' = 0.50\ \lambda$, $r = 1.08$, $\theta_i = 40°$, $h/\lambda = 0.130$

(g) [P26]. $d = 0.833\lambda$, $a' = 0.50\ \lambda$, $r = 1.08$, $\theta_i = 50°$, $h/\lambda = 0.117$

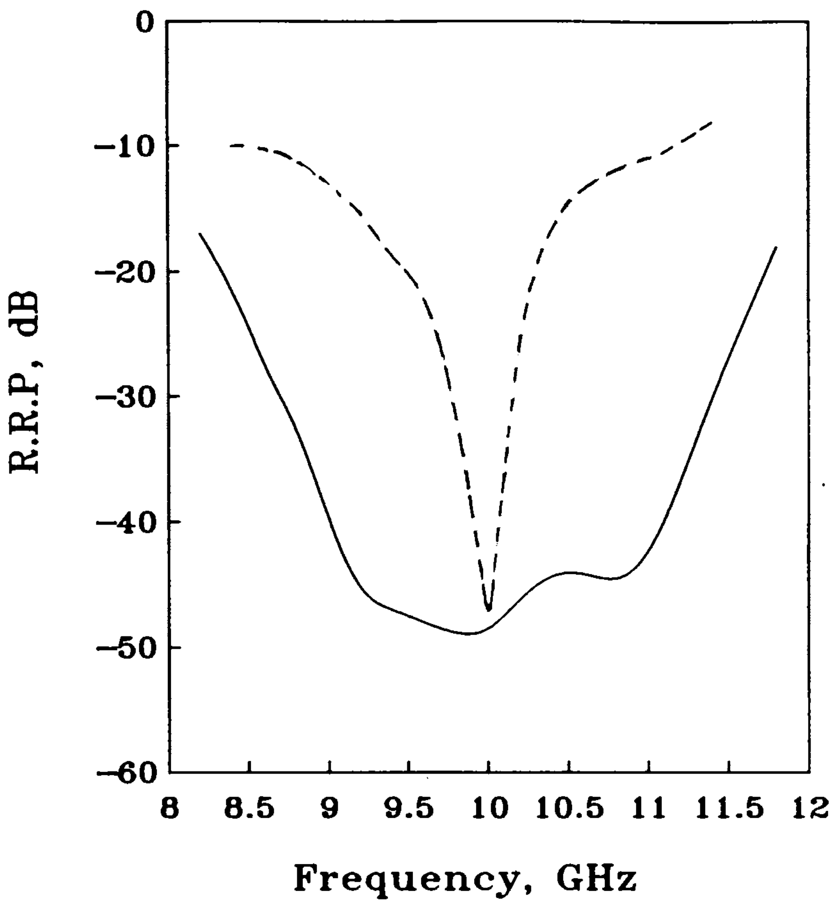

(h)

Fig.4.5 (h) Variation of relative reflected power with frequency.

———— [P29]. d = 1.166 λ, a′ = 0.50 λ, r = 1.08, h/λ = 0.130, f = 10 GHz

- - - - - - - Self complimentary strip grating. (a = b = 0.5 λ)

TABLE 4.1
Various structure parameters studied and results obtained
TM - POLARISATION

a/λ	d/λ	r	Optimum h/λ	Blazing angle θ	Band width GHz
0.500..........0.500	1.000	1.000	0.103	30°	0.142
0.466..........0.533	1.000	1.015	0.106	30°	0.550
0.433..........0.566	1.000	1.032	0.107	37.5°	0.199
0.400..........0.600	1.000	1.046	0.130	37.5°	0.580
0.366..........0.633	1.000	1.063	0.130	40°	0.600
0.333..........0.666	1.000	1.080	0.130	40°	1.540
0.300..........0.700	1.000	1.098	0.130	40°	0.826
0.266..........0.733	1.000	1.119	0.130	40°	0.952
0.250..........0.750	1.000	1.130	0.130	40°	1.375
0.233..........0.766	1.000	1.141	0.130	40°	1.212
0.200..........0.800	1.000	1.167	0.130	37.5°	1.200
0.166..........0.833	1.000	1.196	0.130	35°	1.083
0.133..........0.866	1.000	1.231	0.167	25°	0.147
0.100..........0.900	1.000	1.276	0.130	22.5°	0.145
0.066..........0.933	1.000	1.341	0.150	20°	0.145
0.033..........0.966	1.000	1.454	-	-	-
0.166...........0.333	1.000	1.080	0.117	20°	0.050
0.200...........0.400	1.000	1.080	0.117	30°	1.002
0.233...........0.466	1.000	1.080	0.117	32.5°	1.200
0.250...........0.500	1.000	1.080	0.123	30°	1.406
0.266...........0.533	1.000	1.080	0.137	37.5°	1.305
0.300...........0.600	1.000	1.080	0.133	37.5°	1.042
0.333...........0.666	1.000	1.080	0.117	40°	1.540
0.366...........0.733	1.000	1.080	0.117	55°	1.153
0.400...........0.800	1.000	1.080	0.117	57.5°	1.400
0.416...........0.833	1.000	1.080	0.167	20°	0.241
0.333...........0.666	0.833	1.080	0.117	50°	1.740
0.333...........0.666	0.900	1.080	0.117	50°	1.721
0.333...........0.666	1.000	1.080	0.130	40°	1.540
0.333...........0.666	1.100	1.080	0.130	42.5°	1.802
0.333...........0.666	1.166	1.080	0.130	40°	2.140
0.333...........0.666	1.233	1.080	0.143	37.5°	1.300
0.333...........0.666	1.333	1.080	0.150	40°	1.103

Fig 4.6 represents the characteristics of structure SCS [P6] for TE polarised incident waves. Variation of relative reflected power with dielectric thickness, angle of incidence and frequency are shown in fig. 4.6 (a), (b) and (d). Scattered power Vs receiving angle at blazing angle is shown in fig. 4.6 (c). The figure illustrates that these structures behave similar to that of conventional SCS for TE polarization.

Table 4.2 presents the results obtained in TE polarisation for various structure configuration explained earlier.

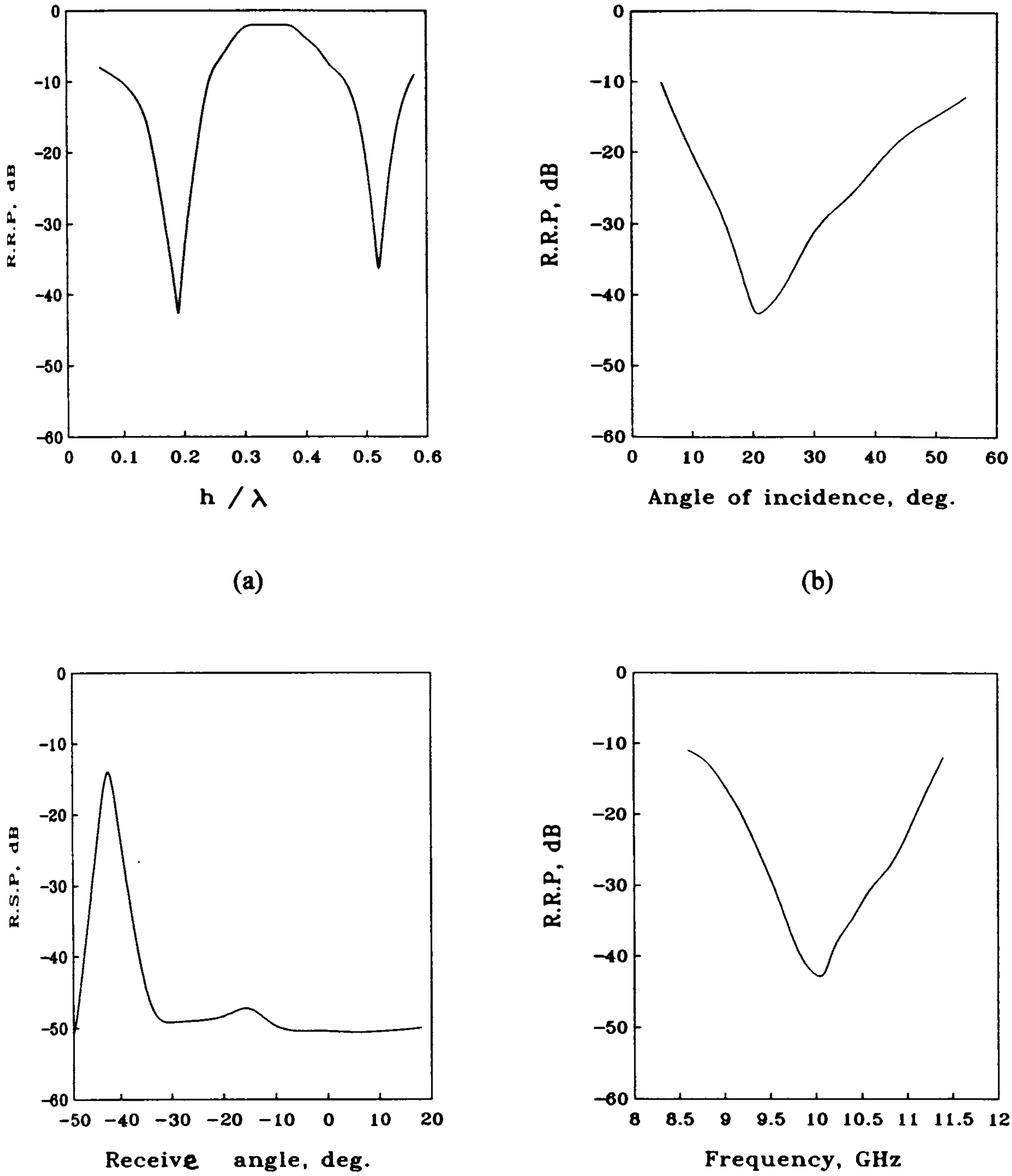

Fig.4.6 Characteristics of [P6]. $d = \lambda$, $r = 1.08$, $a' = 0.5\ \lambda$. (TE Polarisation)

(a) Variation of relative reflected power with dielectric thickness.
(b) Variation of relative reflected power with angle of incidence.
(c) Variation of relative scattered power with receive angle.
(d) Variation of relative reflected power with frequency.

TABLE 4.2

Various structure parameters studied and results obtained
TE - POLARISATION

a/λ	d/λ	r	Optimum h/λ	Blazing angle θ	Band width GHz
0.500..........0.500	1.000	1.000	0.200	30°	0.35
0.466..........0.533	1.000	1.015	0.200	25°	0.30
0.433..........0.566	1.000	1.032	0.197	22.5°	0.40
0.400..........0.600	1.000	1.046	0.200	30°	0.40
0.366..........0.633	1.000	1.063	0.201	25°	0.36
0.333..........0.666	1.000	1.080	0.190	20°	0.30
0.300..........0.700	1.000	1.098	0.173	30°	0.58
0.266..........0.733	1.000	1.119	0.201	20°	0.42
0.250..........0.750	1.000	1.130	0.190	25°	0.40
0.233..........0.766	1.000	1.141	0.187	17.5°	0.60
0.200..........0.800	1.000	1.167	0.187	20°	0.64
0.166..........0.833	1.000	1.196	0.173	25°	0.70
0.133..........0.866	1.000	1.231	0.202	25°	0.56
0.100..........0.900	1.000	1.276	0.190	25°	0.88
0.066..........0.933	1.000	1.341	0.200	25°	0.60
0.033..........0.966	1.000	1.454	0.200	40°	0.60
0.166...........0.333	1.000	1.080	0.183	27.5°	0.68
0.200...........0.400	1.000	1.080	0.183	25°	0.80
0.233...........0.466	1.000	1.080	0.183	30°	0.50
0.250...........0.500	1.000	1.080	0.183	25°	0.45
0.266...........0.533	1.000	1.080	0.190	20°	0.35
0.300...........0.600	1.000	1.080	0.190	20°	0.30
0.333...........0.666	1.000	1.080	0.190	20°	0.30
0.366...........0.733	1.000	1.080	0.203	10°	0.10
0.400...........0.800	1.000	1.080	0.233	7.5°	0.02
0.416...........0.833	1.000	1.080	0.233	5°	-
0.333...........0.666	0.833	1.080	-	-	-
0.333...........0.666	0.900	1.080	0.220	10°	0.02
0.333...........0.666	1.000	1.080	0.190	20°	0.30
0.333...........0.666	1.100	1.080	0.183	20°	0.45
0.333...........0.666	1.166	1.080	0.183	22.5°	0.60
0.333...........0.666	1.233	1.080	0.183	22.5°	0.60
0.333...........0.666	1.333	1.080	0.217	25°	0.35

2 TAPERED SCS

The schematic diagram of tapered SCS is shown in fig 4.7. The bandwidth for ecular reflection elimination could be increased to a considerable extent, i.e from 0.142 Hz to 2.14 GHz, by giving variation along x - direction [progressively varied SCS]. order to increase the bandwidth further, variations were given along y - axis to form the pered SCS. The structure parameters varied for the study were period 'd', stripwidths 'a_1' 'a_2', dielectric thickness 'h', incident angle 'θ', and frequency 'f'

.2.1 Dielectric thickness

The variation of relative reflected power with dielectric thickness for various ructure parameters at optimum blazing angle (angle of incidence corresponding to which flection is minimum) in TM polarisation are shown in fig. 4.8.

1) *Strip width 'a_2=0'*

The plots of R.R.P with h / λ for SCS [T2] of period d = λ, strip widths a_2 = 0, a_1 λ and SCS [T4] of period d = 0.833λ, stripwidths a_2 = 0, a_1 = 0.833λ are shown in fig. .8 (a) & (b).

b) *Constant period*

Variation of relative reflected power with h / λ for SCS's [T6] of dimensions d = 0.833λ, a_1 = 0.733λ, a_2 = 0.1λ and [T9] of dimensions d = 0.833λ, a_1 = 0.566λ, a_2 = .266λ which form typical structures with constant period are shown in fig. 4.8 (c) & (d).

c) *Constant period & constant stripwidth 'a_2'*

Plot of R.R.P with h / λ of a typical structure SCS [T14] of dimensions d = 0.833λ, a_1 = 0.733λ, a_2 = 0.166λ which is one among the set of structures with constant period and constant stripwidth a_2 is shown in fig. 4.8 (e).

d) *Constant period & constant stripwidth 'a_1'*

Relative reflected power with changes in thickness of dielectric for typical structures

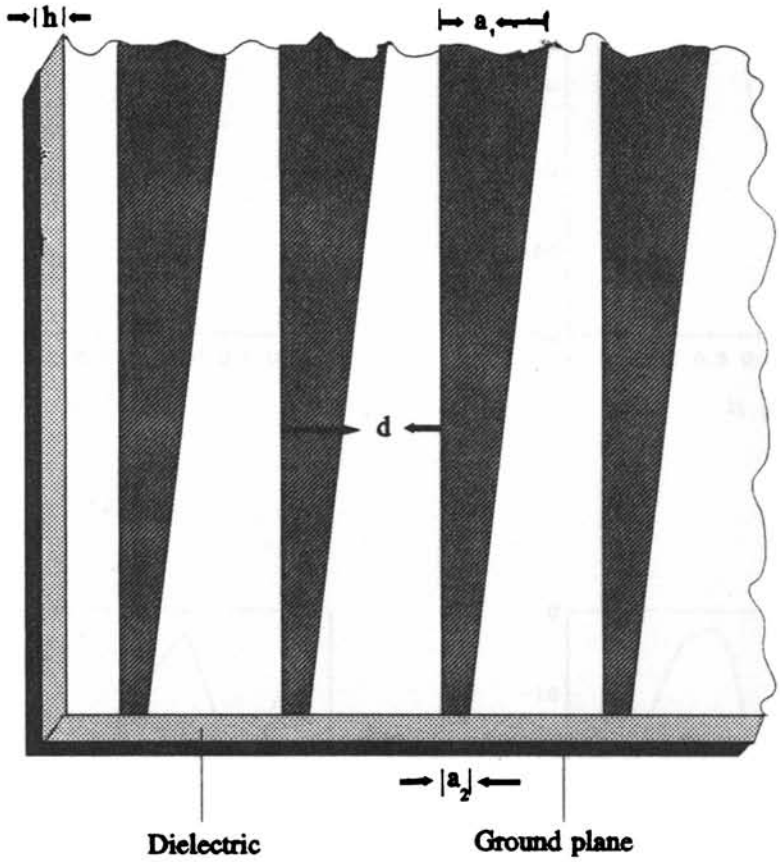

Fig.4.7 Schematic representation of tapered SCS.

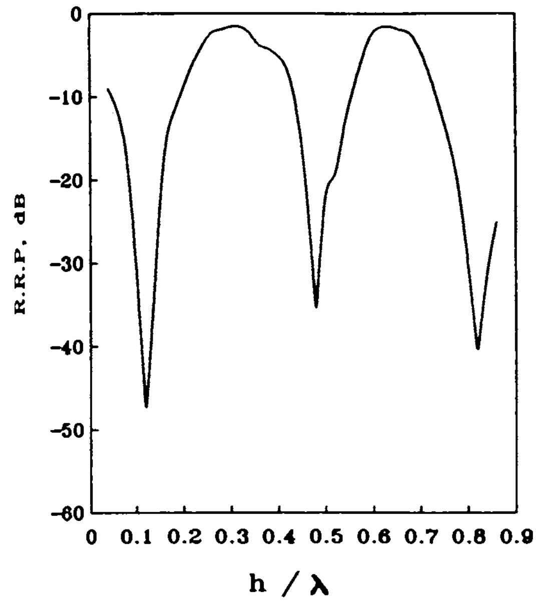

(a)

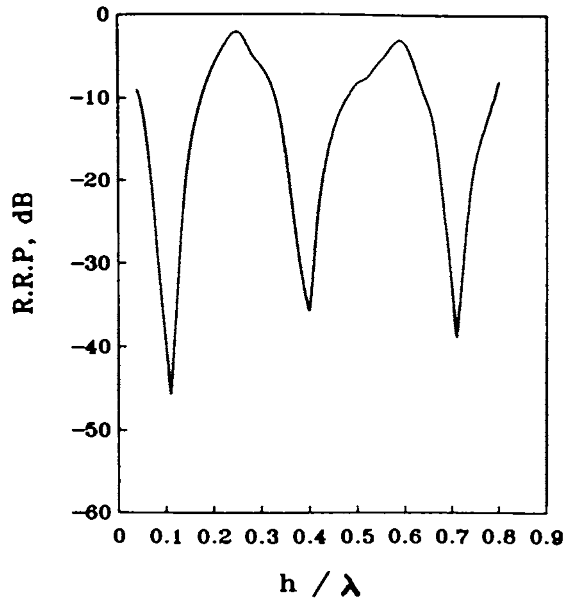

(b)

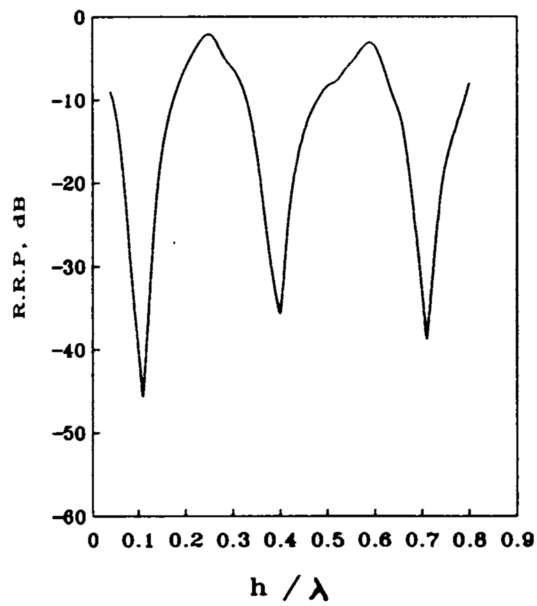

(c)

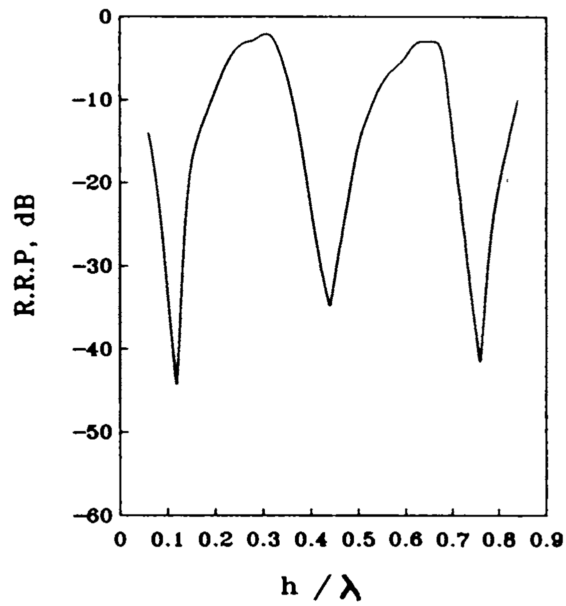

(d)

Fig.4.8 Variation of relative reflected power with dielectric thickness.

(a) [T2]. $d = \lambda$, $a_1 = \lambda$, $a_2 = 0$, $\theta_i = 45°$, f = 10 GHz
(b) [T4]. $d = 0.833\lambda$, $a_1 = 0.833\lambda$, $a_2 = 0$, $\theta_i = 36°$, f = 10 GHz
(c) [T6]. $d = 0.833\lambda$, $a_1 = 0.733\lambda$, $a_2 = 0.1\lambda$, $\theta_i = 44°$, f = 10 GHz
(d) [T9]. $d = 0.833\lambda$, $a_1 = 0.566\lambda$, $a_2 = 0.266\lambda$, $\theta_i = 45°$, f = 10 GHz

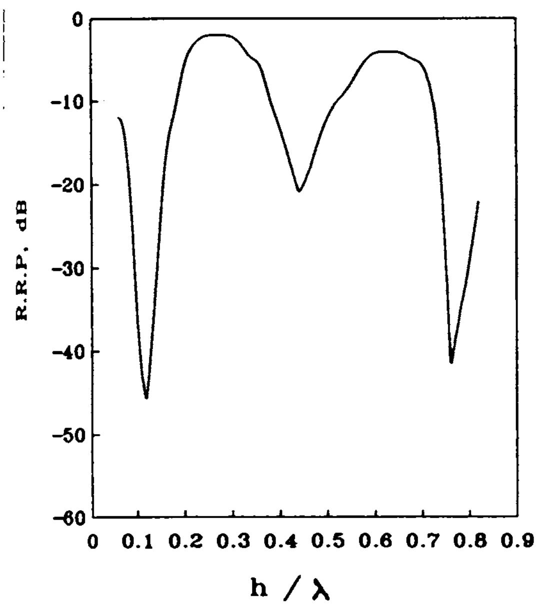

(e)

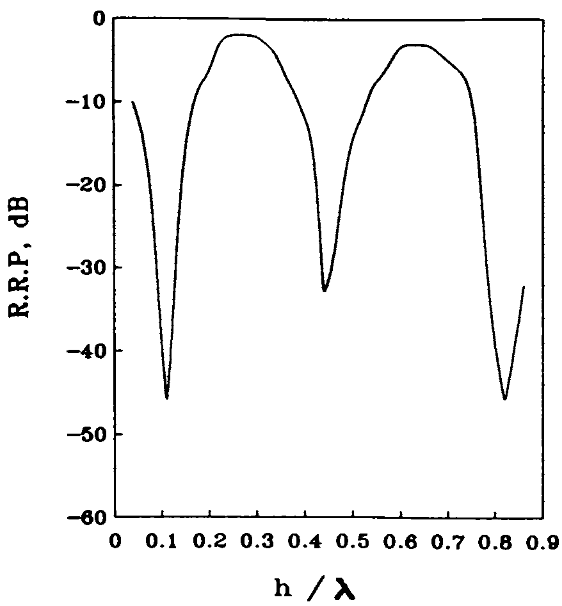

(f)

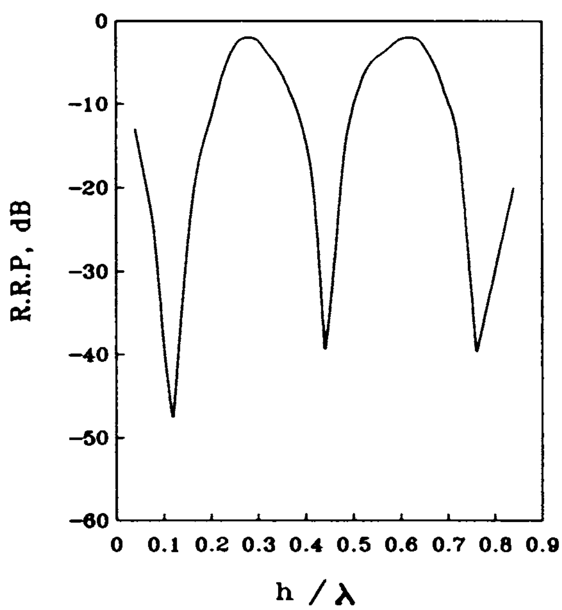

(g)

Fig.4.8 Variation of relative reflected power with dielectric thickness.

(e) [T14]. $d = 0.833\lambda$, $a_1 = 0.733\lambda$, $a_2 = 0.166\lambda$, $\theta_i = 50°$, $f = 10$ GHz
(f) [T18]. $d = 0.833\lambda$, $a_1 = 0.666\lambda$, $a_2 = 0.233\lambda$, $\theta_i = 50°$, $f = 10$ GHz
(g) [T7]. $d = 0.833\lambda$, $a_1 = 0.666\lambda$, $a_2 = 0.166\lambda$, $\theta_i = 50°$, $f = 10$ GHz

in the set of constant period and constant strip width a_1 are illustrated. Fig. 4.8 (f & g) shows the plots for SCS's [T7] of d = 0.833λ, a_1 = 0.666λ, a_2 = 0.166λ and [T18] of dimensions d = 0.833λ, a_1 = 0.666λ, a_2 = 0.233λ.

From the figures it can be noted that reflected power varies with dielectric thickness. For further experimental investigations the thickness where reflected power is minimum is chosen.

4.2.2 Angle of incidence

Variation of relative reflected power with angle of incidence, for various structure parameters with optimum dielectric thickness, in TM polarisation is given in fig. 4.9. The power scattered to n = -1 mode at blazing angle incidence is also shown. The characteristics for all the four sets of structures described earlier were investigated. The variation of relative reflected power with angle of incidence for SCS's [T2], [T4], [T6], [T9], [T14], [T18] & [T7] are illustrated in fig. 4.9 (a.i),(b.i), (c.i), (d.i), (e.i) (f.i) and (g.i) respectively. The plots of scattered power with receiving angle from normal for the above structures are shown in fig. 4.9 (a.ii), (b.ii), (c.ii), (d.ii).(e.ii), (f.ii) and (g.ii) respectively. From all these plots it is clear that blazing is possible only for a particular angle of incidence and n = -1 mode obeys the basic grating equation.

4.2.3 Frequency

Effect of the variation of frequency on reflected power for typical SCS structures from all sets described earlier are shown in fig. 4.10.

Fig. 4.10 (a), (b), (c), (d), (e) & (f) shows the variation of relative reflected power with frequency for SCS's [T2], [T4], [T6], [T9], [T14], & [T18] respectively. The solid lines of fig. 4.10 (g) represents the variation of R.R.P with frequency for tapered SCS [T7], and

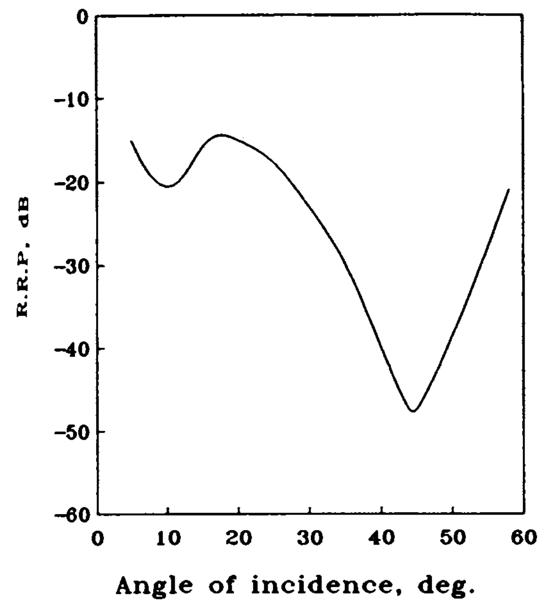

(a.i)

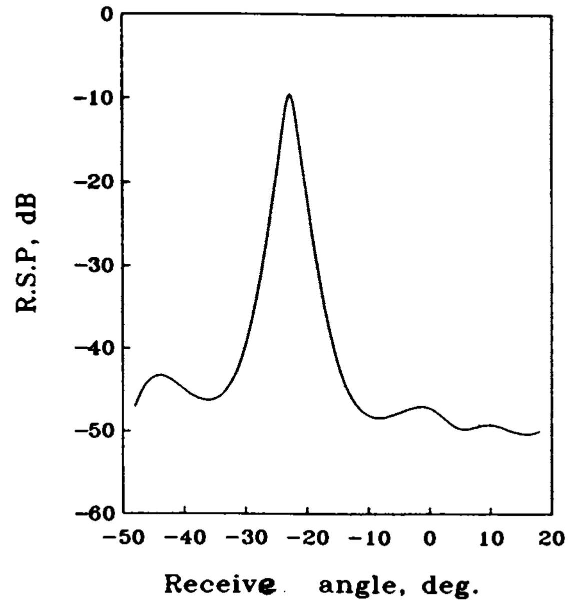

(a.ii)

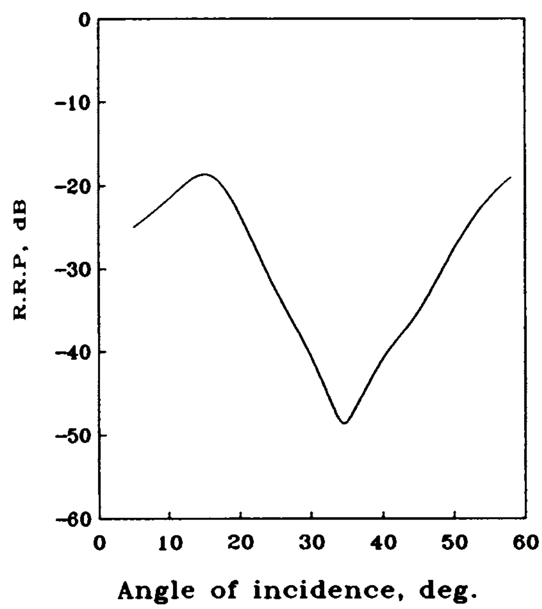

(b.i)

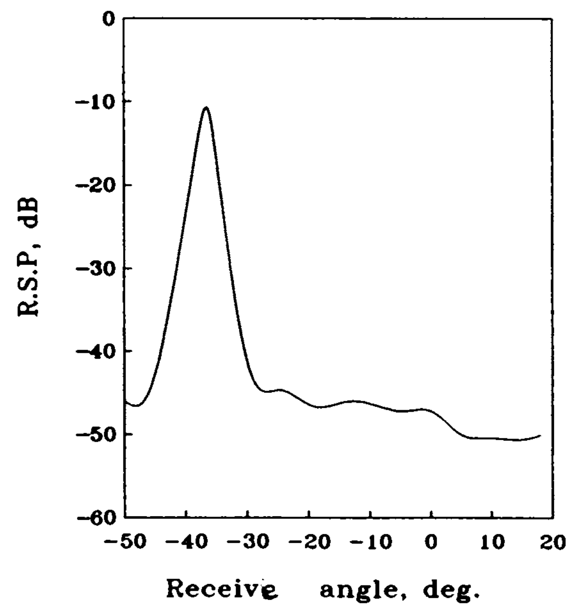

(b.ii)

Fig.4.9 (i) Variation of relative reflected power with angle of incidence.
(ii) Measured relative scattered power with receive angle.

(a) [T2]. $d = \lambda$, $a_1 = \lambda$, $a_2 = 0$, $h = 0.127\lambda$, $f = 10$ GHz
(b) [T4]. $d = 0.833\lambda$, $a_1 = 0.833\lambda$, $a_2 = 0$, $h = 0.116\lambda$, $f = 10$ GHz

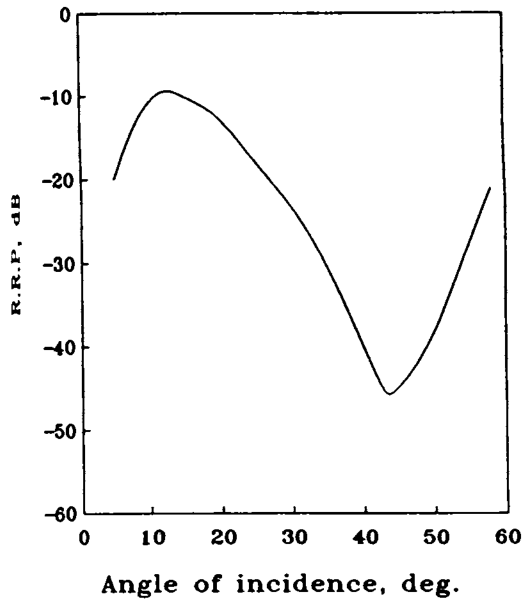

(c.i)

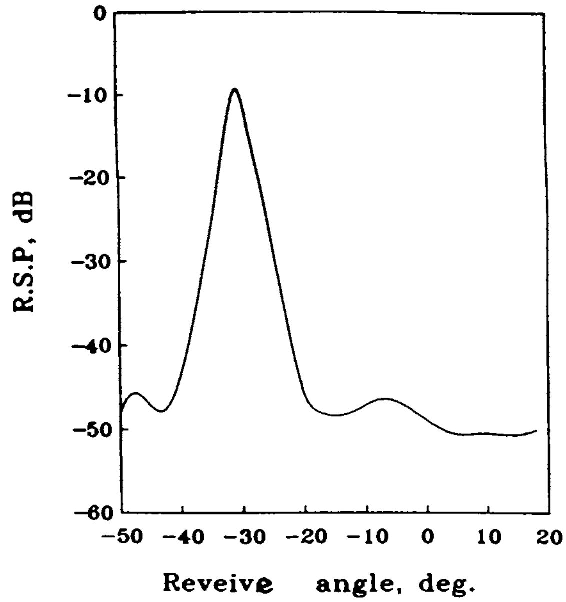

(c.ii)

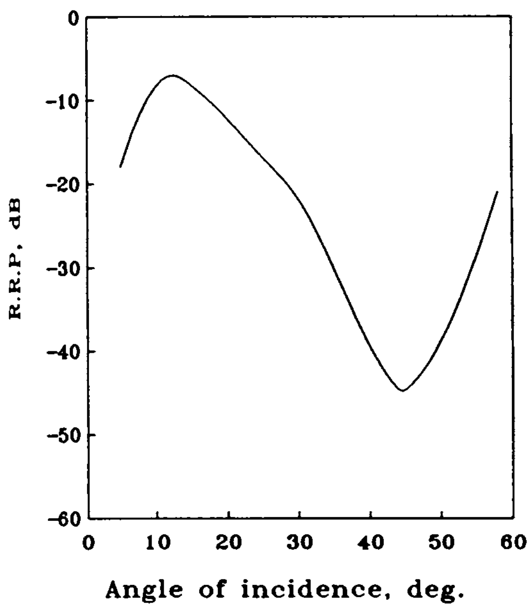

(d.i)

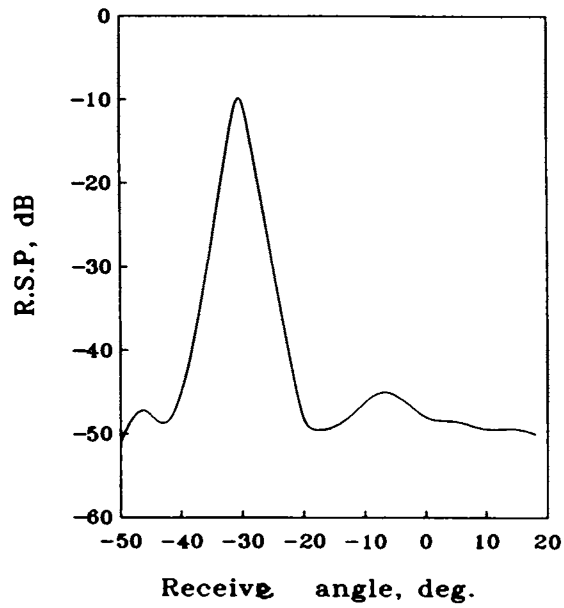

(d.ii)

Fig.4.9 (i) Variation of relative reflected power with angle of incidence.
(ii) Measured relative scattered power with receive angle.

(c) [T6]. $d = 0.833\lambda$, $a_1 = 0.733\lambda$, $a_2 = 0.1\lambda$, $h = 0.166\lambda$, $f = 10$ GHz
(d) [T9]. $d = 0.833\lambda$, $a_1 = 0.566\lambda$, $a_2 = 0.266\lambda$, $h = 0.120\lambda$, $f = 10$ GHz

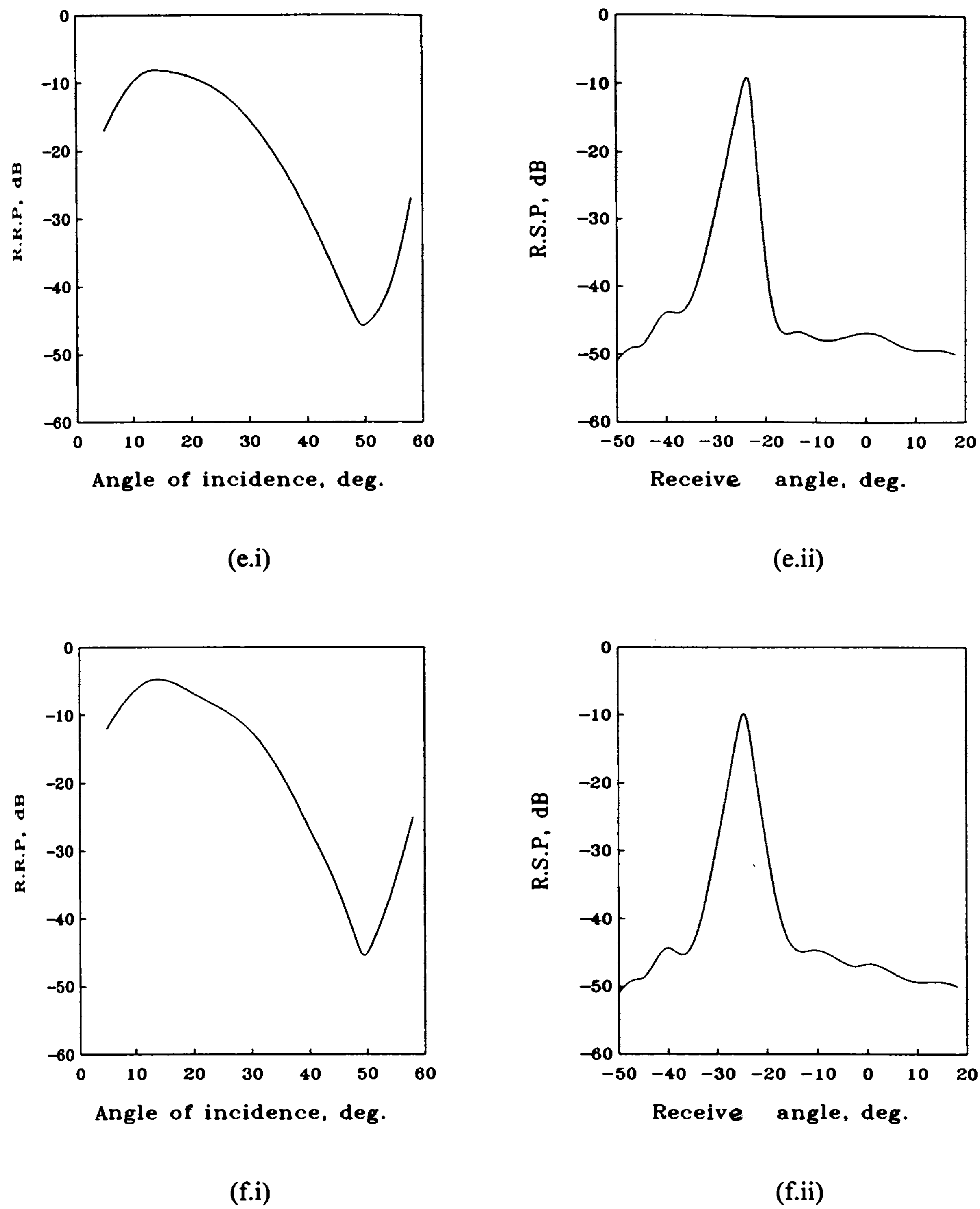

Fig.4.9 (i) Variation of relative reflected power with angle of incidence.
(ii) Measured relative scattered power with receive angle.

(e) [T14]. $d = 0.833\lambda$, $a_1 = 0.733\lambda$, $a_2 = 0.166\lambda$, $h = 0.117\lambda$, $f = 10$ GHz
(f) [T18]. $d = 0.833\lambda$, $a_1 = 0.666\lambda$, $a_2 = 0.233\lambda$, $h = 0.120\lambda$, $f = 10$ GHz

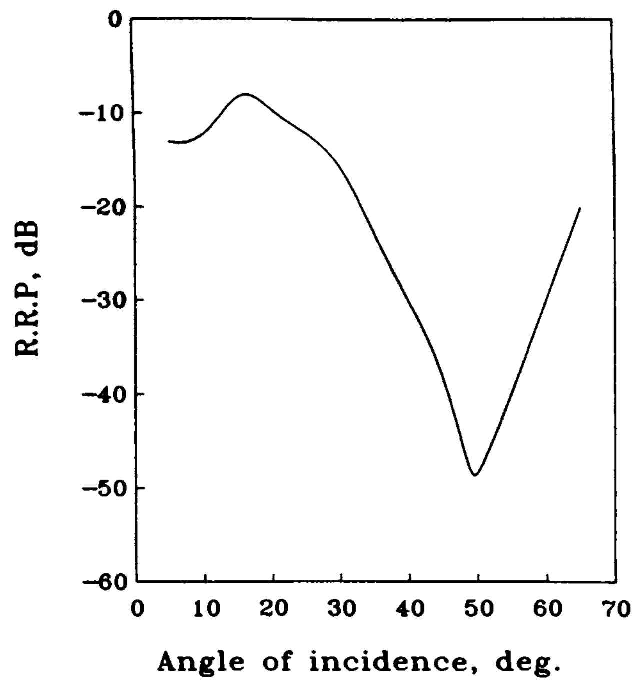

(g.i)

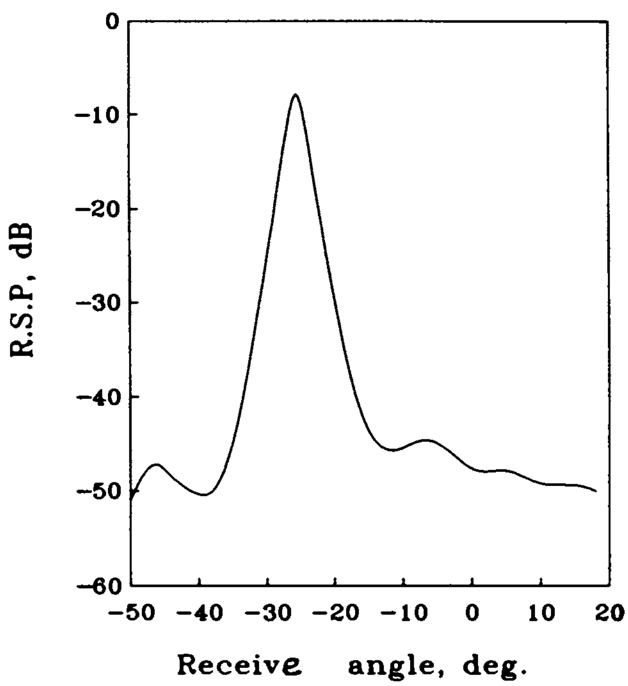

(g.ii)

Fig.4.9 (i) Variation of relative reflected power with angle of incidence.
(ii) Measured relative scattered power with receive angle.
(g) [T7]. $d = 0.833\lambda$, $a_1 = 0.666\lambda$, $a_2 = 0.166\lambda$, $h = 0.123\lambda$, $f = 10$ GHz

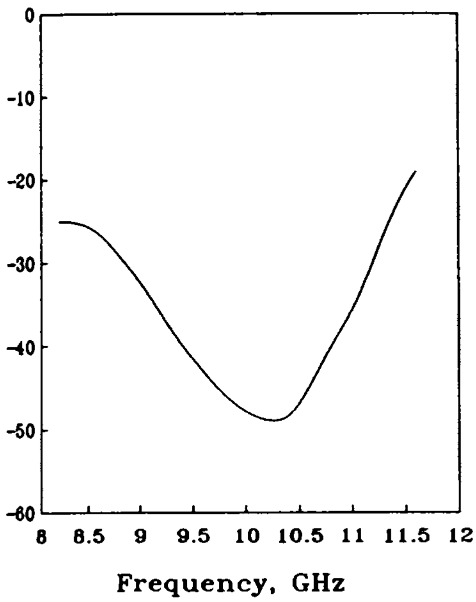

(a)

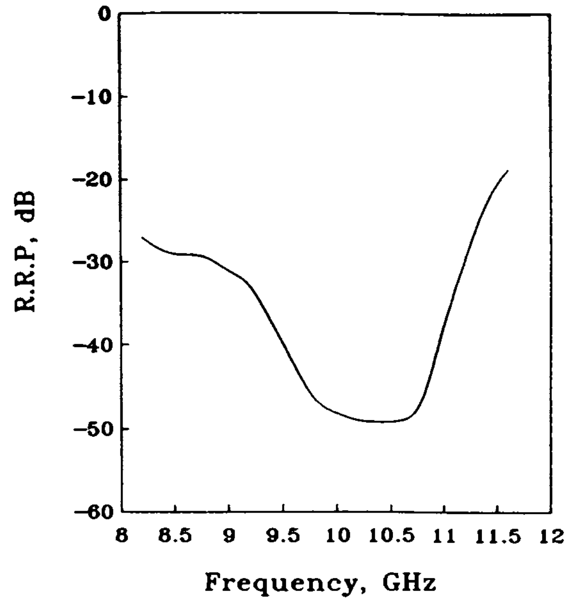

(b)

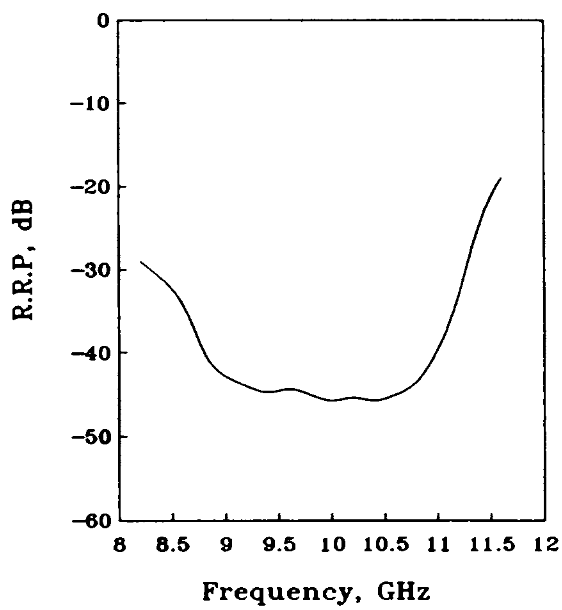

(c)

Fig.4.10 Variation of relative reflected power with frequency.

(a) [T2]. $d = \lambda$, $a_1 = \lambda$, $a_2 = 0$, $\theta_i = 45°$, $h = 0.127$
(b) [T4]. $d = 0.833\lambda$, $a_1 = 0.833\lambda$, $a_2 = 0$, $\theta_i = 36°$, $h = 0.116$
(c) [T6]. $d = 0.833\lambda$, $a_1 = 0.733\lambda$, $a_2 = 0.1\lambda$, $\theta_i = 44°$, $h = 0.116$

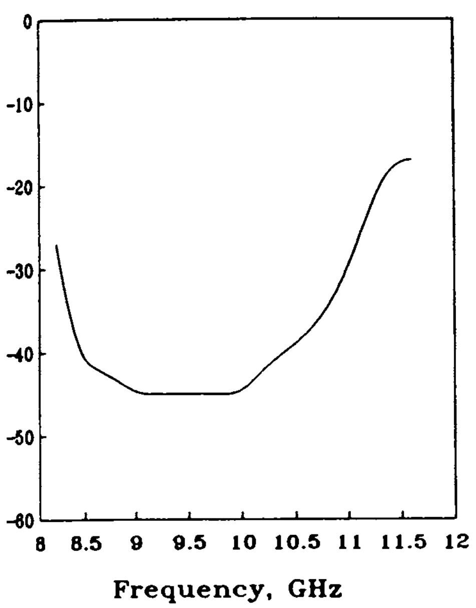

(d)

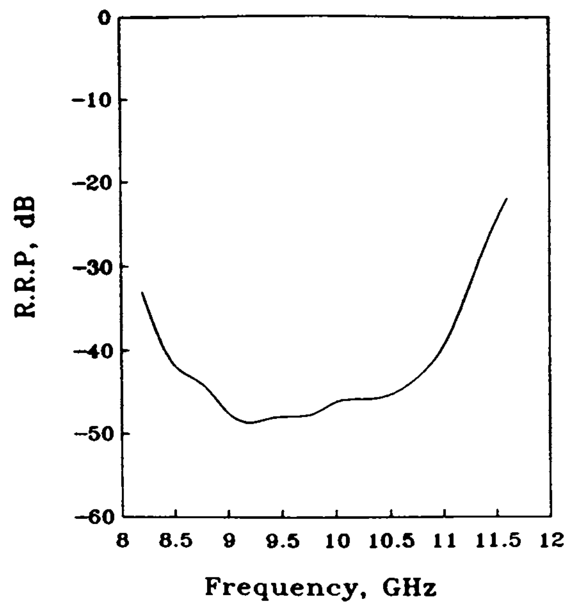

(e)

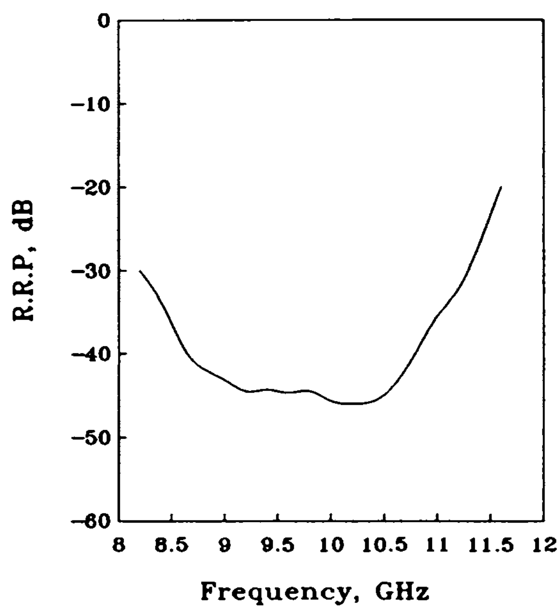

(f)

Fig.4.10 Variation of relative reflected power with frequency.

(d) [T9]. $d = 0.833\lambda$, $a_1 = 0.566\lambda$, $a_2 = 0.266\lambda$, $\theta_i = 45°$, $h = 0.120\lambda$
(e) [T14]. $d = 0.833\lambda$, $a_1 = 0.733\lambda$, $a_2 = 0.166\lambda$, $\theta_i = 50°$, $h = 0.117\lambda$
(f) [T18]. $d = 0.833\lambda$, $a_1 = 0.666\lambda$, $a_2 = 0.233\lambda$, $\theta_i = 50°$, $h = 0.120\lambda$

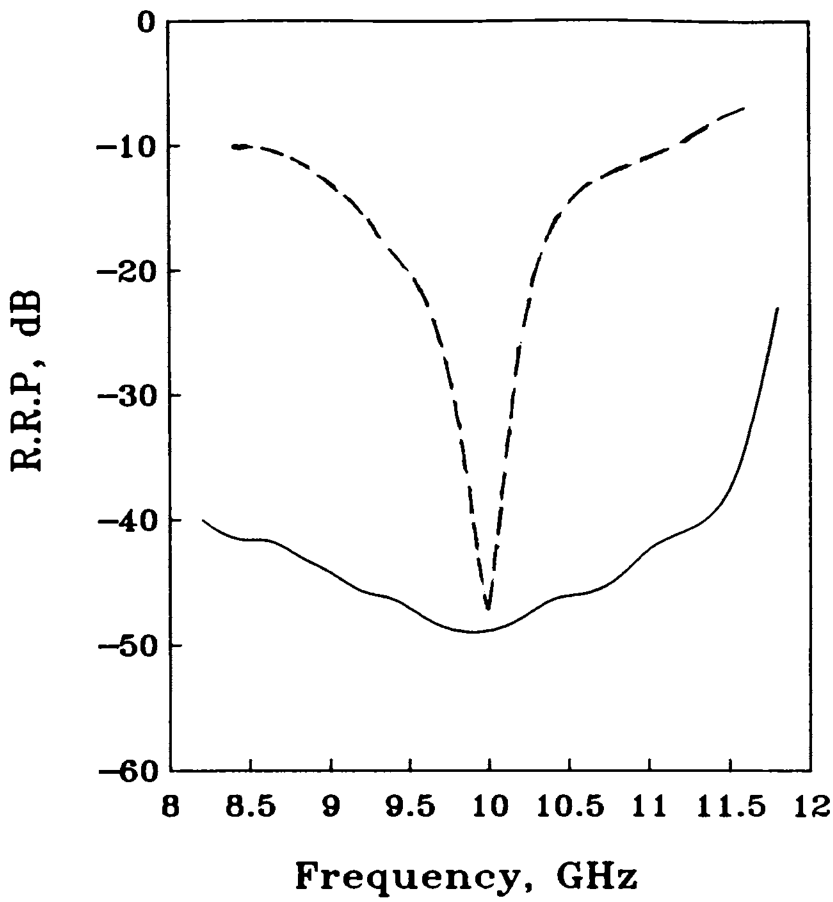

(g)

Fig.4.10 Variation of relative reflected power with frequency.

——— (g) [T7]. $d = 0.833\lambda$, $a_1 = 0.666\lambda$, $a_2 = 0.166\lambda$, $h = 0.123\lambda$, $\theta_i = 50°$

- - - - - Self complementary strip grating.

dotted line that for conventional SCS.

It is clear from the plot 4.10 (g) that bandwidth (below – 40 dB) for specular reflection elimination is about 3.6 GHz with tapered SCS. This is much greater than conventional SCS [0.142 GHz] and progressively varied SCS [2.14 GHz]. Since the strip widths are changing in y - direction, it results in a large number of elementary gratings of various 'a' & 'b' values. These elementary gratings may resonate for different frequencies This may be the reason for the increase in bandwidth.

4.2.4 Bandwidth with period and strip widths

The variation of frequency bandwidth for specular reflection elimination with strip widths 'a_1' & 'a_2' and period 'd' are shown in fig. 4.11 (a), (b),& (c). It is observed that bandwidth is more when a_1 values lies between $\lambda / 2$ and $3\lambda / 4$, and a_2 values lies between $\lambda / 8$ and $\lambda / 4$.

Characteristics of the structure [T7] for TE polarised incident wave are illustrated in fig. 4.12. Variation of relative reflected power with dielectric thickness, angle of incidence and frequency are shown in fig. 4.12. (a), (b) & (d). The scattered power with receiving angle from normal at blazing angle incidence is shown fig. 4.12 (c). The results confirm that there is not much deviation from the characteristics of conventional SCS.

Different structure geometries designed in the study and results obtained for most effective reduction in RCS are tabulated. Table 4.3 presents the period 'd', stripwidths 'a_1', & 'a_2', optimum dielectric thickness h / λ, Blazing angle θ, and frequency bandwidth at blazing angle incidence obtained for TM polarisation. Four sets of structures are shown. The first set of SCS is structures with same stripwidth 'a_2'. The second set is structures with same period 'd', the third set is structures with same period 'd' and strip width 'a_2', and the fourth set is structures with same period 'd' and same strip width 'a_1'.

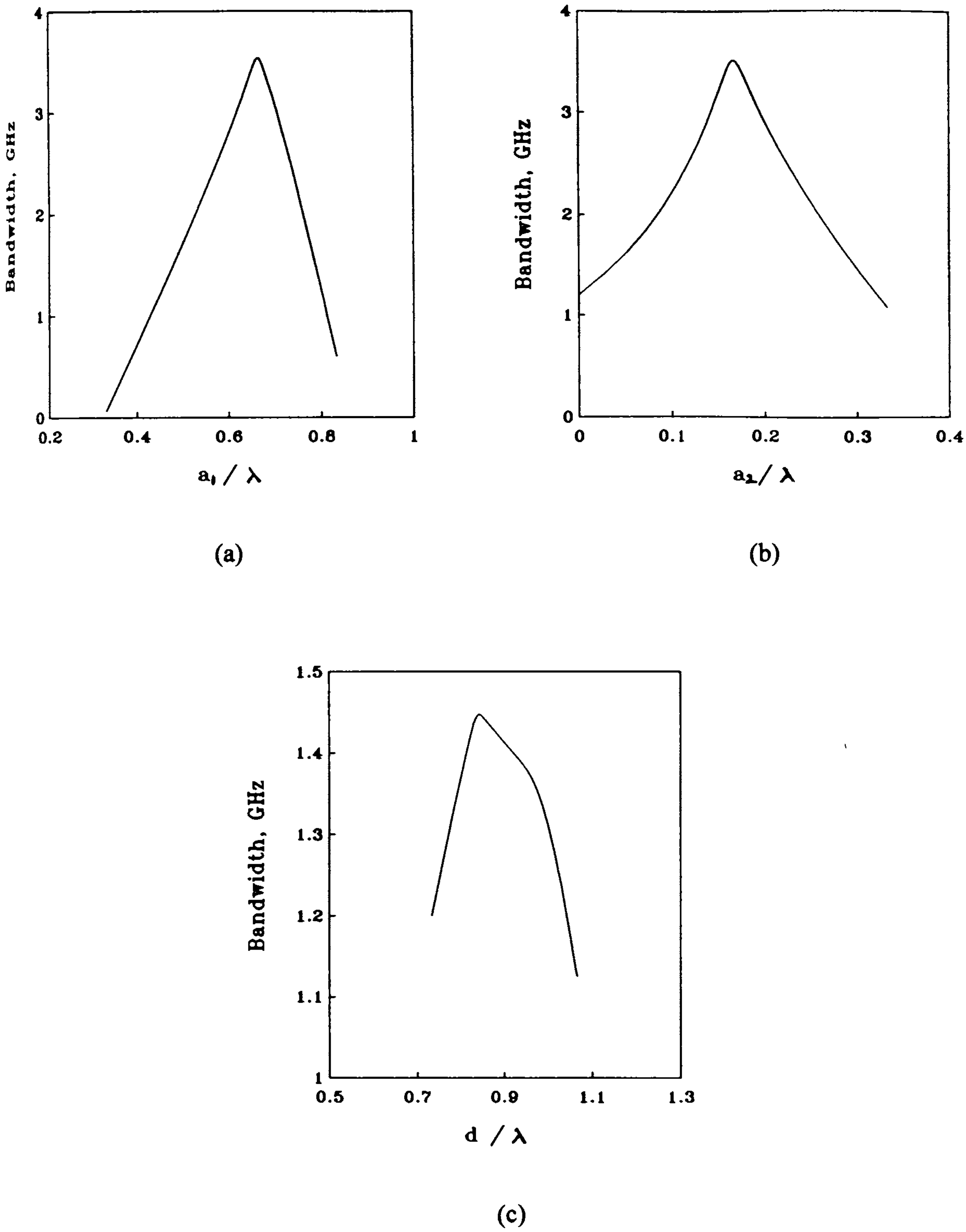

Fig.4.11 Variation of Bandwidth with structure paramters.

(a) Bandwidth Vs a_1 / λ
(b) Bandwidth Vs a_2 / λ
(c) Bandwidth Vs d / λ

TABLE 4.3

Different structure parametres varied and results obtained

TM - POLARISATION

period d/λ	Strip width a_1/λ	Strip width a_2/λ	Optimum dielectric thickness h/λ	Blazing angle θ	Frequency Band-width GHz
1.066	1.066	0.000	0.130	40°	1.125
1.000	1.000	0.000	0.127	45°	1.350
0.933	0.933	0.000	0.117	35°	1.392
0.833	0.833	0.000	0.116	36°	1.455
0.733	0.733	0.000	0.103	30°	1.200
0.833	0.833	0.000	0.116	36°	1.455
0.833	0.733	0.100	0.116	44°	2.305
0.833	0.666	0.166	0.123	50°	3.600
0.833	0.600	0.233	0.127	45°	2.108
0.833	0.566	0.266	0.120	45°	2.000
0.833	0.500	0.333	0.120	40°	0.950
0.833	0.417	0.417	0.123	37.5°	0.150
0.833	0.333	0.166	0.103	30°	0.060
0.833	0.566	0.166	0.107	40°	2.300
0.833	0.666	0.166	0.123	50°	3.600
0.833	0.733	0.166	0.117	50°	2.640
0.833	0.833	0.166	0.110	50°	0.600
0.833	0.666	0.000	0.110	30°	1.200
0.833	0.666	0.100	0.110	40°	1.900
0.833	0.666	0.166	0.123	50°	3.600
0.833	0.666	0.233	0.120	50°	2.200
0.833	0.666	0.333	0.110	55°	1.078

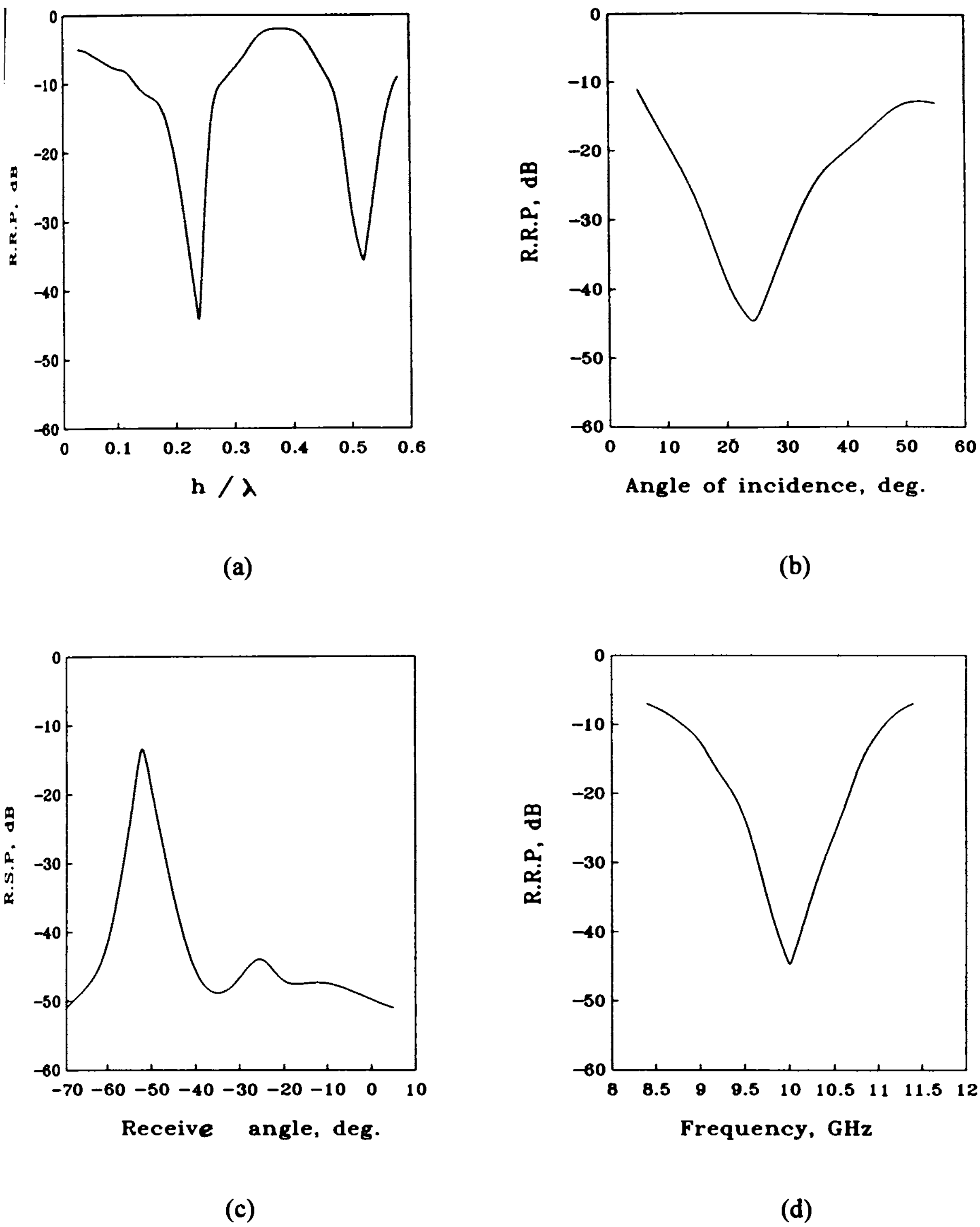

Fig.4.12. Characteristics of [T7]. $d = 0.833\lambda$, $a_1 = 0.666\lambda$, $a_2 = 0.166\lambda$ in TE polarisation.

(a) Variation of relative reflected power with dielectric thickness.
(b) Variation of relative reflected power with angle of incidence.
(c) Measured relative scattered with receive angle.
(d) Variation of relative reflected power with frequency.

4.3 DUAL ASPECT RATIO STRIPS

After trying variations of the width of the strips along the x and y directions for the SCS, periodic variation were given along the strip direction. This led to the formation of dual aspect ratio (a / d) strips. The schematic representation of dual aspect ratio strips is shown in fig. 4.13. The parameters which were varied to optimise the structure are gap widths 'a_1 & a_2', lengths 'l_1 & l_2', dielectric thickness 'h', angle of incidence 'θ_i' and frequency 'f'.

4.3.1 Dielectric thickness

Changes in relative reflected power with dielectric thickness for various structure parameters in TE and TM polarisations at blazing angle are plotted in fig. 4.14. Structure parameters varied are given below.

(a) Gap width

Variation of R.R.P with h / λ for structures with same period 'd', same lengths 'l_1 & l_2' and different gap widths 'a' were investigated. The characteristics for typical structures [D2] of dimensions $d = \lambda$, $l_1 = l_2 = 0.5\lambda$, $a_1 = 0.5\lambda$, $a_2 = 0.7\lambda$ and [D4] of dimensions $d = \lambda$, $l_1 = l_2 = 0.5\lambda$, $a_1 = 0.5\lambda$, $a_2 = 0.833\lambda$ are shown in fig. 4.14 (a.i) and (b.i) for TM polarisation. Variations for the same structures in TE polarisation is plotted in fig. 4.14 (a.ii) and (b.ii).

(b) Length

Relative reflected power variations with dielectric thickness for structures with same period 'd' same gap widths 'a_1 & a_2' and different lengths 'l_1 & l_2' were also investigated. Typical variations for structures

[D7] of dimensions $d = \lambda$, $l_1 = 0.5\lambda$, $l_2 = 0.666\lambda$, $a_1 = 0.5\lambda$, $a_2 = 0.7\lambda$ and

[D10] of dimensions $d = \lambda$, $l_1 = 0.833\lambda$, $l_2 = 0.833\lambda$, $a_1 = 0.5\lambda$, $a_2 = 0.7\lambda$ are presented in

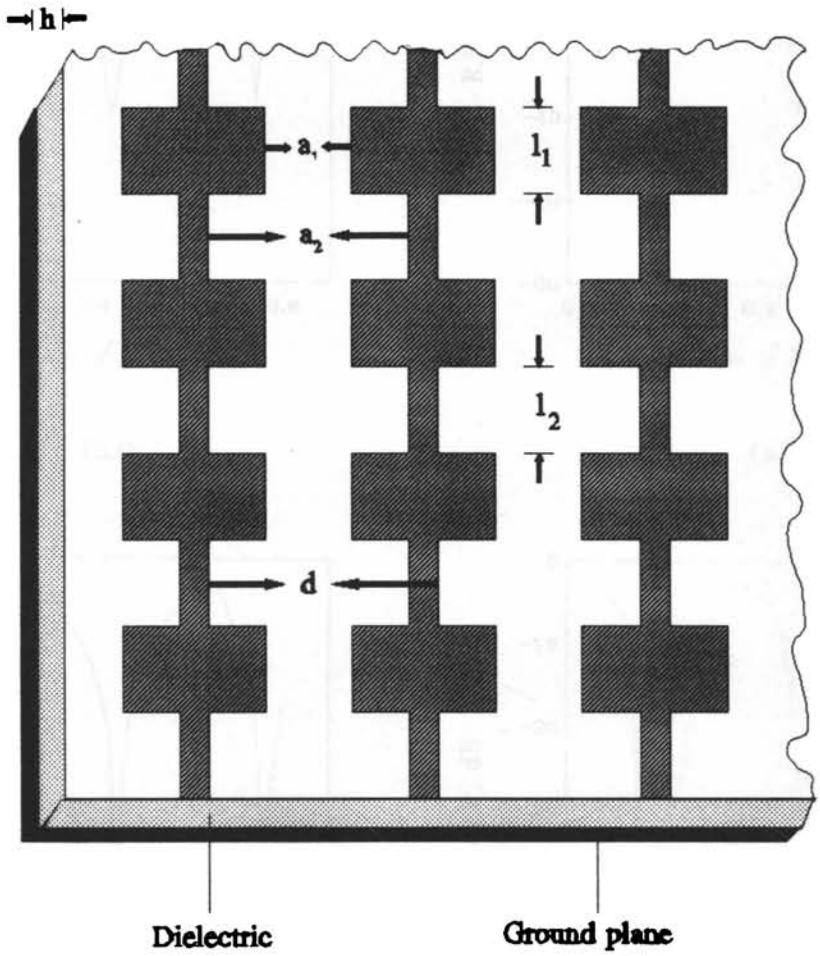

Fig.4.13 Schematic diagram of dual aspect ratio strips.

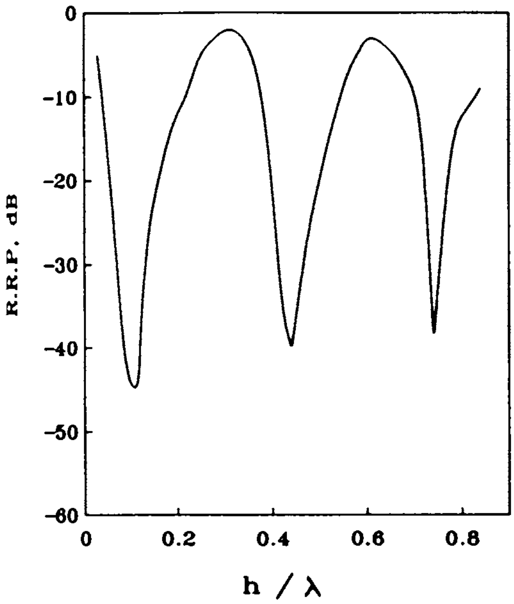

(a.i)

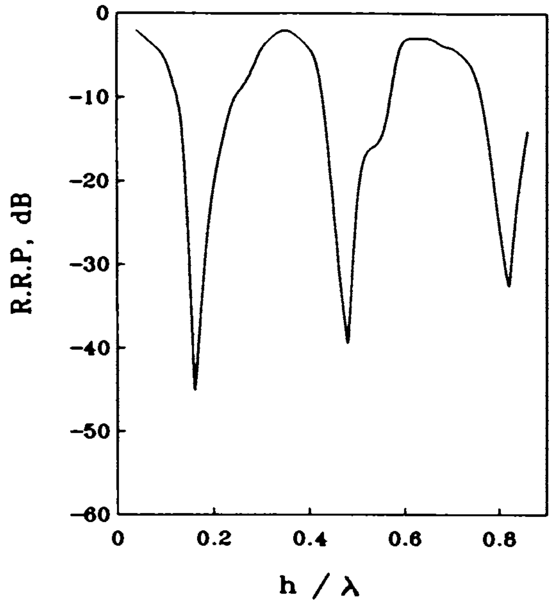

(a.ii)

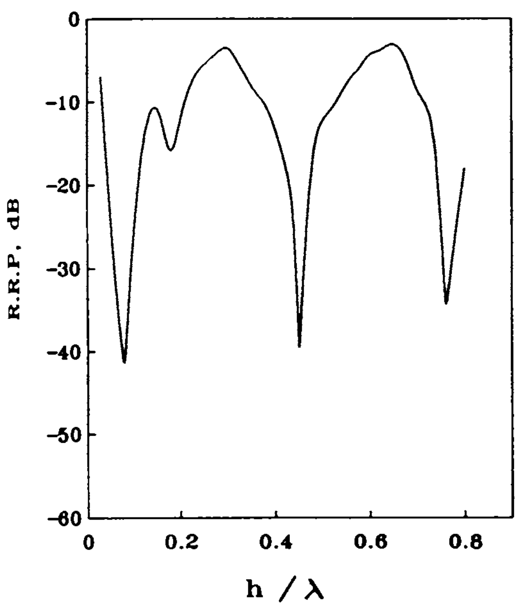

(b.i)

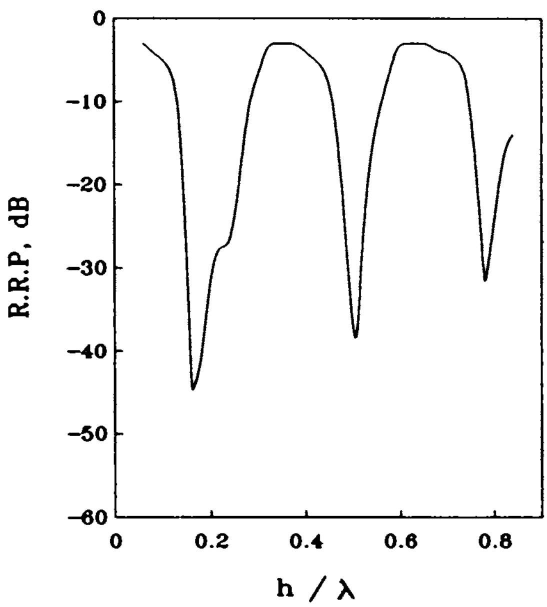

(b.ii)

Fig.4.14 Variation of Relative reflected power with dielectric thickness.

(a) [D2]. $d = \lambda$, $l_1 = 0.5\lambda$, $l_2 = 0.5\lambda$, $a_1 = 0.5\lambda$, $a_2 = 0.7\lambda$, $f = 10$ GHz
(b) [D4]. $d = \lambda$, $l_1 = 0.5\lambda$, $l_2 = 0.5\lambda$, $a_1 = 0.5\lambda$, $a_2 = 0.833\lambda$, $f = 10$ GHz

(i) TM polarisation (ii) TE polarisation

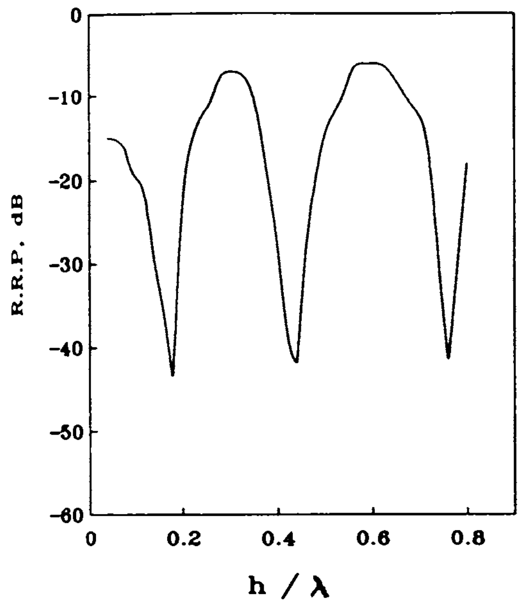

(c.i)

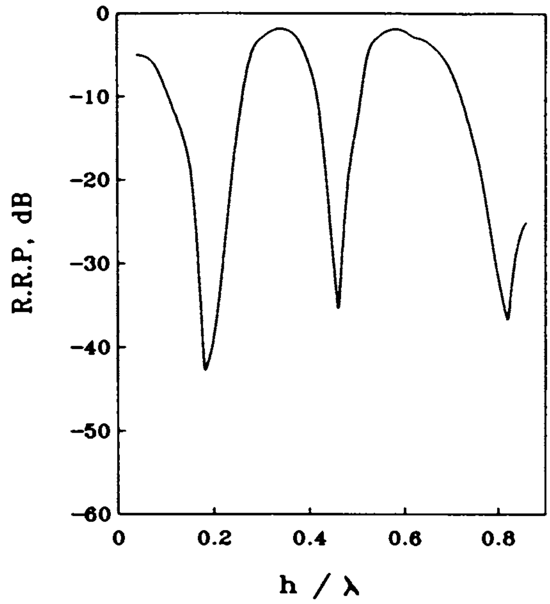

(c.ii)

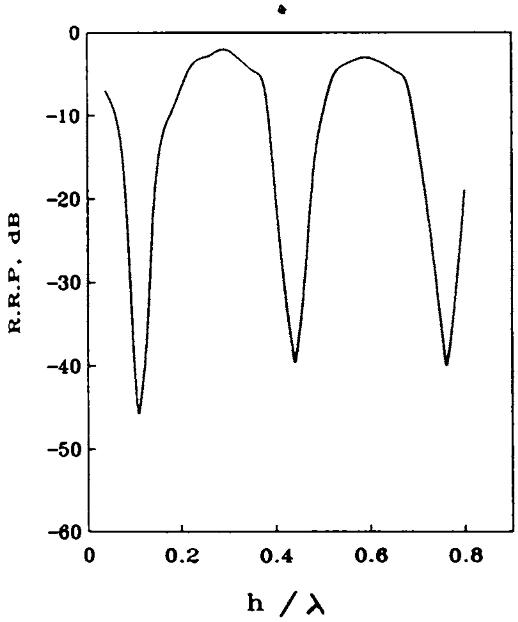

(d.i)

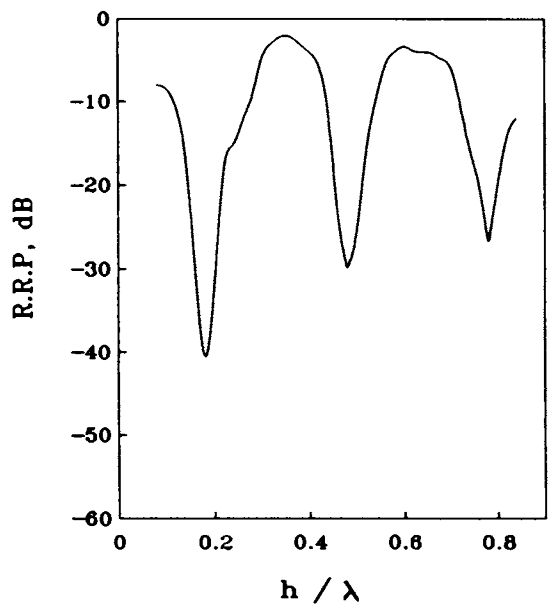

(d.ii)

Fig.4.14 Variation of Relative reflected power with dielectric thickness.

(c) [D7]. $d = \lambda$, $l_1 = 0.5\lambda$, $l_2 = 0.666\lambda$, $a_1 = 0.5\lambda$, $a_2 = 0.7\lambda$, $f = 10$ GHz
(d) [D10]. $d = \lambda$, $l_1 = 0.833\lambda$, $l_2 = 0.833\lambda$, $a_1 = 0.5\lambda$, $a_2 = 0.7\lambda$, $f = 10$ GHz

(i) TM polarisation (ii) TE polarisation

fig. 4.14 (c.i) and (d.i) for TM polarisation . The variations for the same structures in TE polarisations are plotted in fig. 4.14 (c.ii) & (d.ii).

4.3.2 Angle of incidence

Plots of relative reflected power (R.R.P) and relative backscattered power (R.B.S.P) against incident angles for structures [D2]. [D4], [D7] & [D10] in TM polarisation are shown in fig. 4.15 (a.i), (b.i), (c.i) & (d.i). Variations in TE polarisation for the same structures are plotted in fig. 4.15. (a.ii), (b.ii), (c.ii) & (d.ii).

It is noted that, in all these structures, specular reflection is eliminated only for a particular incident angle. The advantage obtained by this type of structures is that, simultaneous elimination of specular reflection is possible for TE and TM polarisation as is illustrated for structure D[7] in fig. 4.15 (c). Here, the specular reflection is eliminated for the structure with same dielectric thickness, same frequency and same incident angle for TE and TM polarisations.

4.3.3 Frequency

Keeping the SCS at blazing angle, the frequency is varied and the changes in relative reflected power with frequency for structures [D2], [D4], [D7] & [D10] in TM polarisation is noted and given in fig. 4.16 (a.i), (b.i), (c.i) & (d.i). Variations in TE polarisation for the same structures are shown in fig. 4.16. (a.ii), (b.ii), (c.ii) & (d.ii).

The bandwidth provided by these structures is not much greater than that of the self complementary strip gratings. For TE polarisation the bandwidth is found to be slightly increased. It can be noted that the angular range for specular reflection elimination is also not increased. The advantage of such structures is that simultaneous blazing can be achieved for TE and TM polarisations.

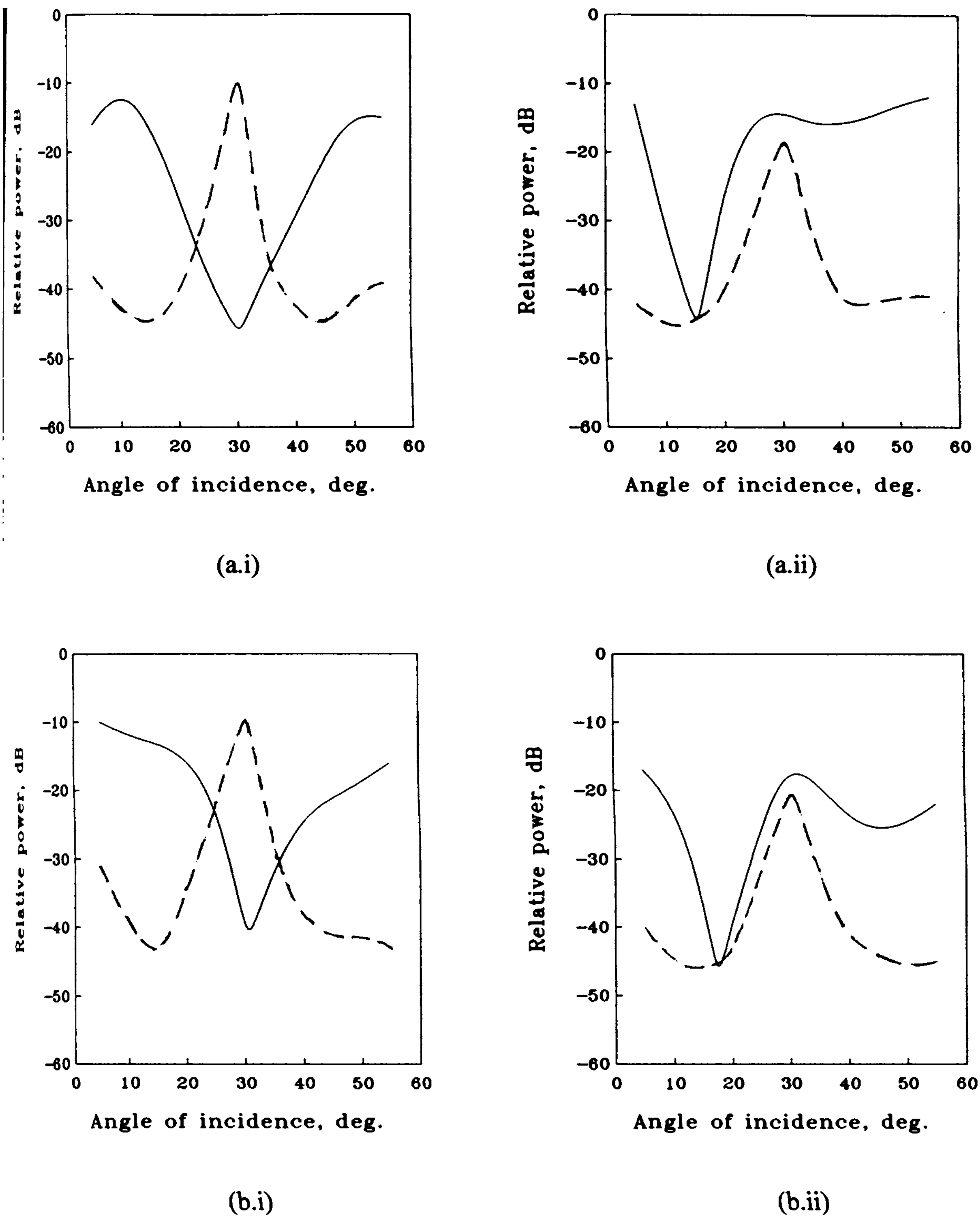

Fig.4.15 Variation of R.R.P and R.B.S.P with angle of incidence

(i) TM polarisation (ii) TE polarisation

——— Relative reflected power - - - - - Relative backscattered power

(a) [D2]. $d = \lambda$, $l_1 = 0.5\lambda$, $l_2 = 0.5\lambda$, $a_1 = 0.5\lambda$, $a_2 = 0.7\lambda$, f = 10 GHz

(b) [D4]. $d = \lambda$, $l_1 = 0.5\lambda$, $l_2 = 0.5\lambda$, $a_1 = 0.5\lambda$, $a_2 = 0.833\lambda$, f = 10 GHz

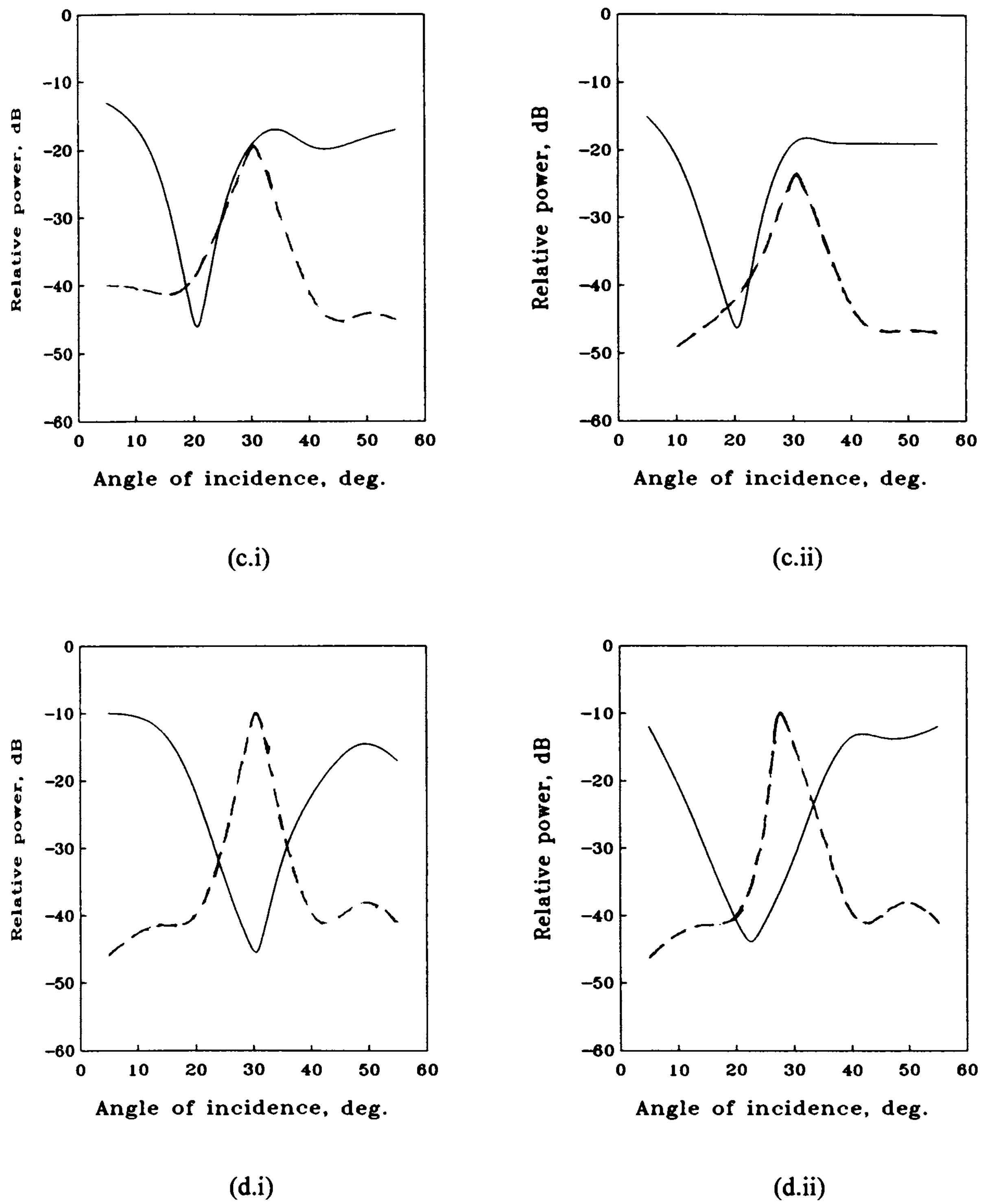

Fig.4.15 Variation of R.R.P and R.B.S.P with angle of incidence

(i) TM polarisation (ii) TE polarisation

——— Relative reflected power - - - - - Relative backscattered power

(c) [D7]. $d = \lambda$, $l_1 = 0.5\lambda$, $l_2 = 0.666\lambda$, $a_1 = 0.5\lambda$, $a_2 = 0.7\lambda$, f = 10 GHz

(d) [D10]. $d = \lambda$, $l_1 = 0.833\lambda$, $l_2 = 0.833\lambda$, $a_1 = 0.5\lambda$, $a_2 = 0.7\lambda$, f = 10 GHz

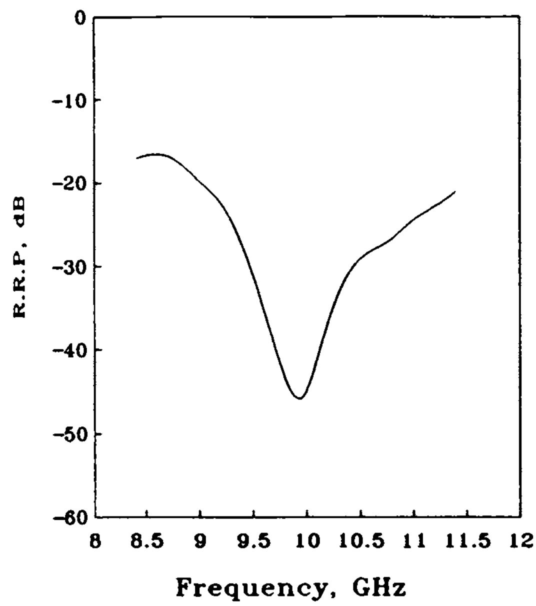

(a.i)

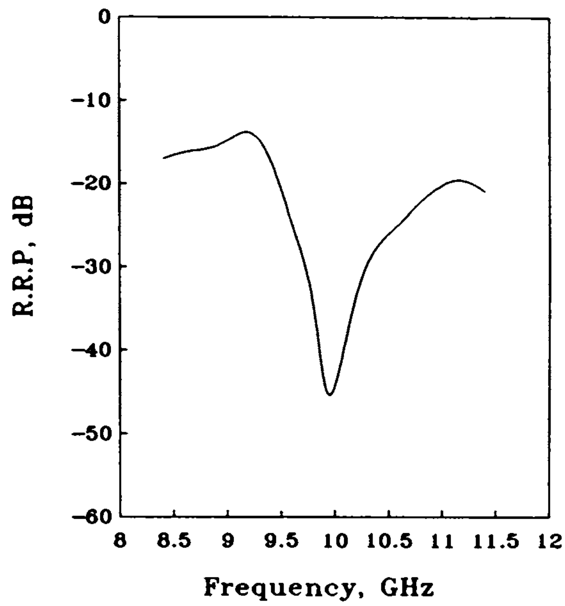

(a.ii)

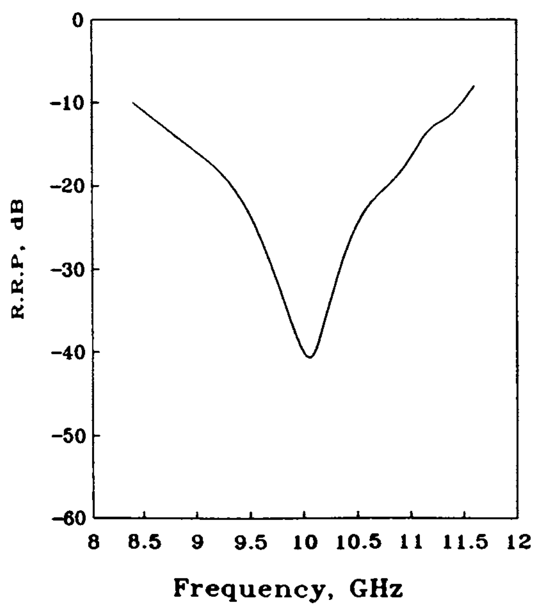

(b.i)

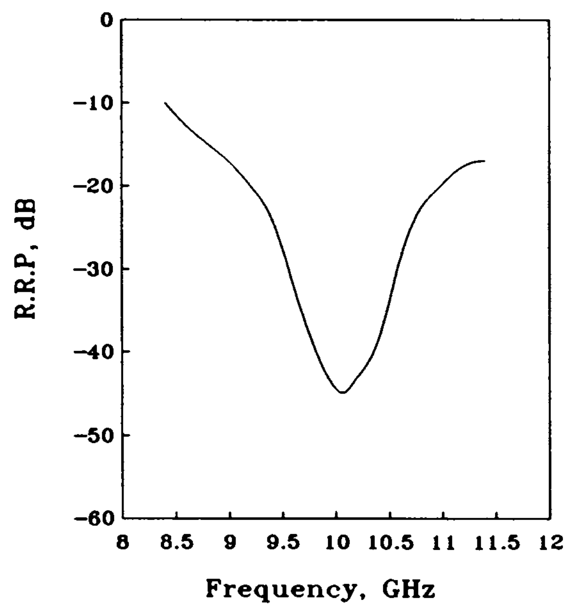

(b.ii)

Fig.4.16 Variation of Relative reflected power with frequency.

(i) TM polarisation (ii) TE polarisation

(a) [D2]. $d = \lambda$, $l_1 = 0.5\lambda$, $l_2 = 0.5\lambda$, $a_1 = 0.5\lambda$, $a_2 = 0.7\lambda$

(b) [D4]. $d = \lambda$, $l_1 = 0.5\lambda$, $l_2 = 0.5\lambda$, $a_1 = 0.5\lambda$, $a_2 = 0.833\lambda$

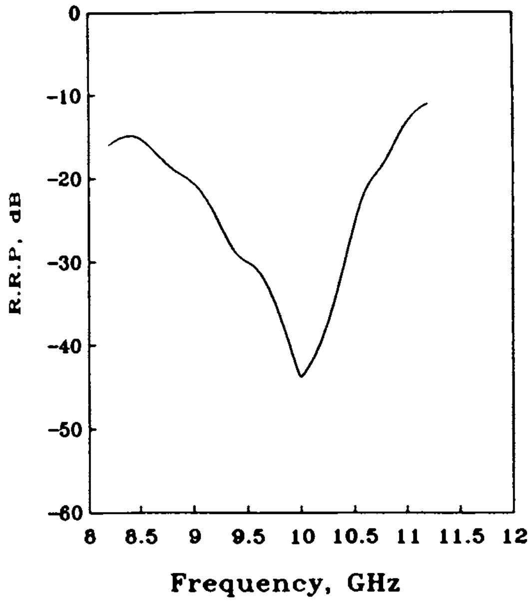

(c.i)

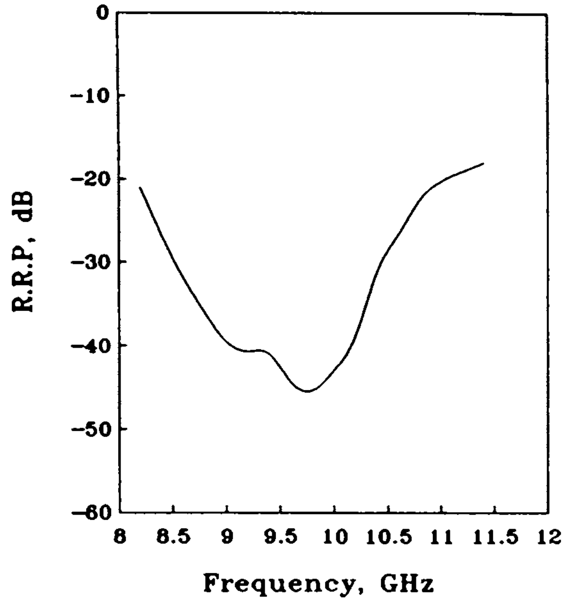

(c.ii)

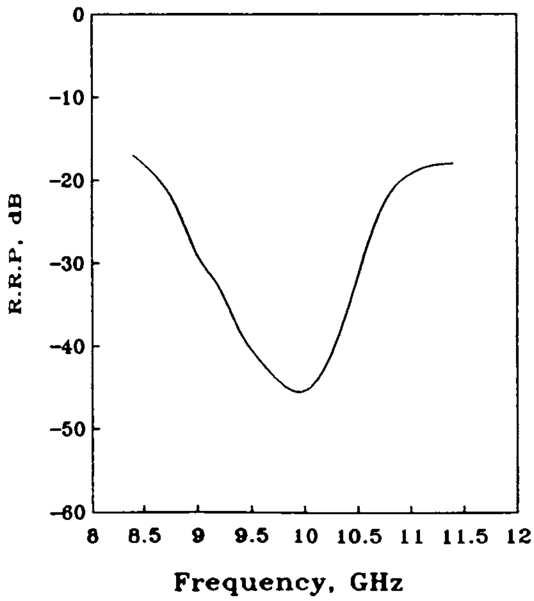

(d.i)

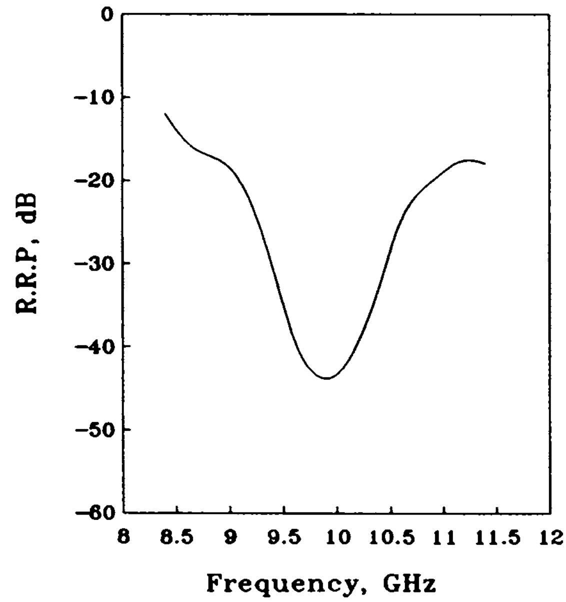

(d.ii)

Fig.4.16 Variation of Relative reflected power with frequency.

(i) TM polarisation (ii) TE polarisation

(c) [D7]. $d = \lambda$, $l_1 = 0.5\lambda$, $l_2 = 0.666\lambda$, $a_1 = 0.5\lambda$, $a_2 = 0.7\lambda$

(d) [D10]. $d = \lambda$, $l_1 = 0.833\lambda$, $l_2 = 0.833\lambda$, $a_1 = 0.5\lambda$, $a_2 = 0.7\lambda$

The structure parameters varied and the results obtained are tabulated. Table 4.4 shows the period 'd', lengths 'l_1 & l_2', gapwidths 'a_1 & a_2', optimum dielectric thickness 'h', blazing angle θ and bandwidth for TM polarisation. Table 4.5 shows the results obtained in TE polarisation for the same structure variations.

TABLE 4.4
Structure parameters and results for dual aspect ratio strips
TM POLARISATION

d=λ

Length		Gap width		Dielctric thickness	Blazing angle	Frequency Bandwidth
l_1/λ	l_2/λ	a_1/λ	a_2/λ	h/λ	θ	GHz
0.500	0.500	0.500	0.633	0.110	30°	0.231
0.500	0.500	0.500	0.700	0.100	30°	0.480
0.500	0.500	0.500	0.766	0.097	35°	0.200
0.500	0.500	0.500	0.833	0.083	30°	0.120
0.500	0.500	0.500	0.900	0.103	30°	0.025
0.500	0.500	0.500	0.700	0.100	30°	0.480
0.500	0.600	0.500	0.700	0.180	25°	0.280
0.500	0.666	0.500	0.700	0.187	20°	0.280
0.500	0.833	0.500	0.700	0.127	25°	0.630
0.500	0.500	0.500	0.700	0.100	30°	0.480
0.666	0.666	0.500	0.700	0.120	20°	0.500
0.833	0.833	0.500	0.700	0.117	30°	0.800

TABLE 4.5
Structure parameters and results for dual aspect ratio strips
TE POLARISATION

d=λ

Length		Gap width		Dielctric thickness	Blazing angle	Frequency Bandwidth
l_1/λ	l_2/λ	a_1/λ	a_2/λ	h/λ	θ	GHz
0.500	0.500	0.500	0.633	0.190	20°	0.150
0.500	0.500	0.500	0.700	0.167	15°	0.160
0.500	0.500	0.500	0.766	0.153	12.5°	0.172
0.500	0.500	0.500	0.833	0.173	18°	0.600
0.500	0.500	0.500	0.900	0.143	37.5°	0.020
0.500	0.500	0.500	0.700	0.167	15°	0.160
0.500	0.600	0.500	0.700	0.180	20°	0.862
0.500	0.666	0.500	0.700	0.187	20°	1.200
0.500	0.833	0.500	0.700	0.183	22.5°	0.600
0.500	0.500	0.500	0.700	0.167	15°	0.160
0.666	0.666	0.500	0.700	0.183	25°	0.702
0.833	0.833	0.500	0.700	0.190	22.5°	0.600

4.4 DUAL PERIODIC RHOMBIC SHAPED STRUCTURE

The search for wide angular range and wide bandwidth of specular reflection elimination led to another type of structure which is dual periodic. It is also a modification of SCS. In dual periodic, the grating structure has a periodicity 'd' for the strips, and each strip is given a regular periodic variation in dimension along its length. Each strip is made up of a number of rhombic shaped elements of sidelength 'l' and internal angles 'α & β'. The schematic diagram of dual periodic rhombic shaped structure is shown in fig. 4.17. The parameters varied to optimise the structure are side length 'l', internal angles 'α & β', period 'd', dielectric thickness 'h', incident angle 'θ' and frequency 'f'.

4.4.1 Dielectric thickness

The reflected power from the SCS is found to be changing with the thickness of the dielectric and it is illustrated in fig. 4.18. Structure parameters varied for the study are given below.

(a) Sidelength

The sidelength of rhombic shaped elements was varied keeping the angles and the period same for the structures. The variation of relative reflected power with dielectric thickness for typical structures

[R3] of dimensions period $d = \lambda$, angles $\alpha = \beta = 90°$, $l = 0.233\lambda$ and

[R10] of dimensions period $d = \lambda$, angles $\alpha = \beta = 90°$, $l = 0.471\lambda$ for TE polarisation are shown in fig. 4.18 (a) & (b).

(b) Internal angle

Structures with same sidelength and period but having different internal angles were studied. Plots of R.R.P with h / λ for the following structures for TE polarisation are illustrated in fig. 4.18 (c) & (d)

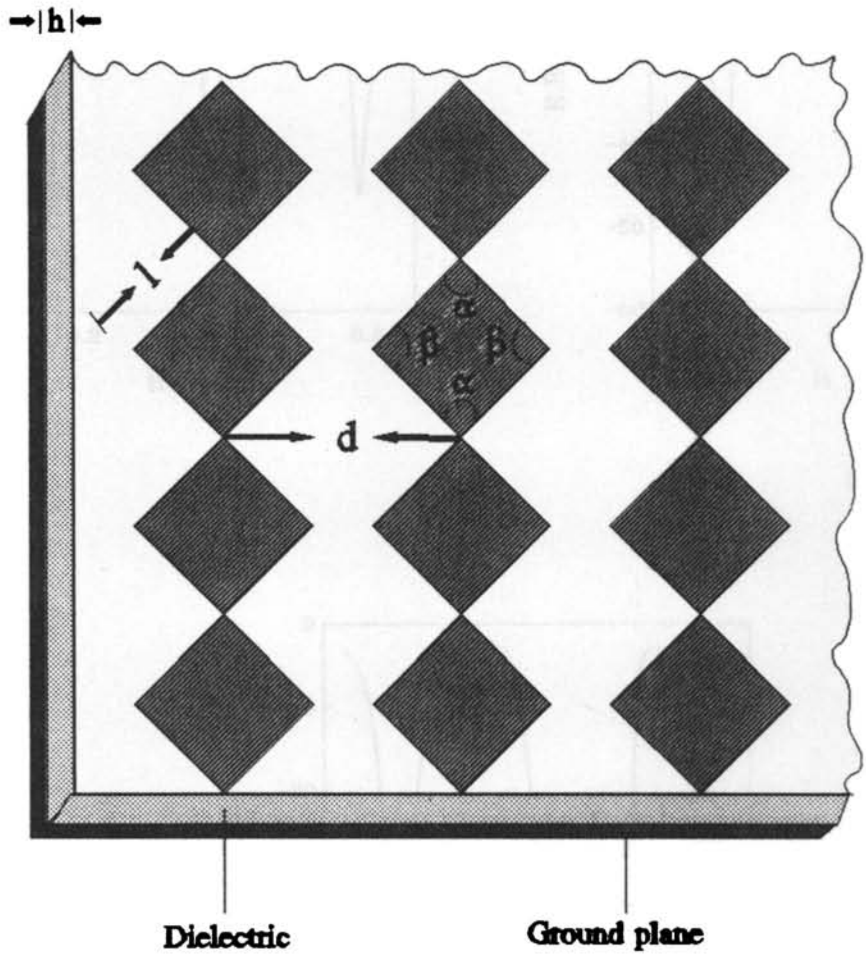

Fig.4.17 Schematic diagram of dual periodic rhombic shaped structure.

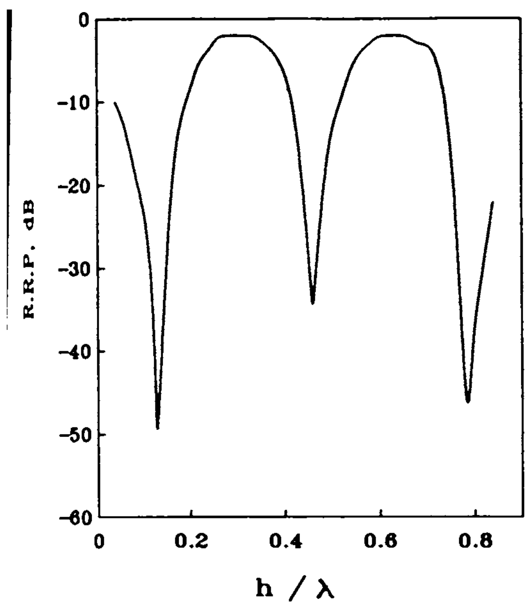

(a)

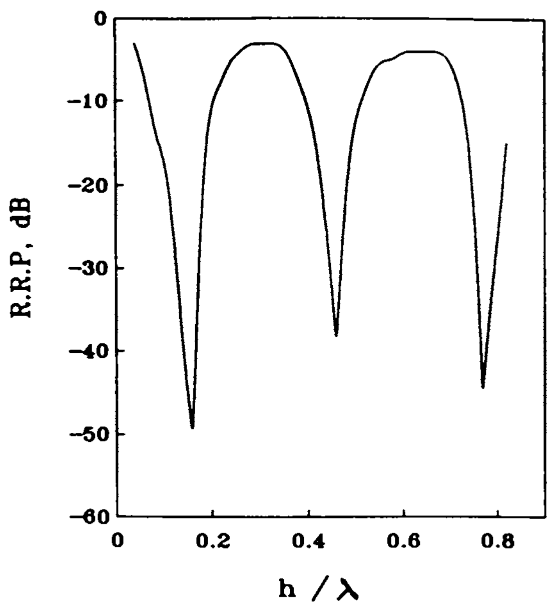

(b)

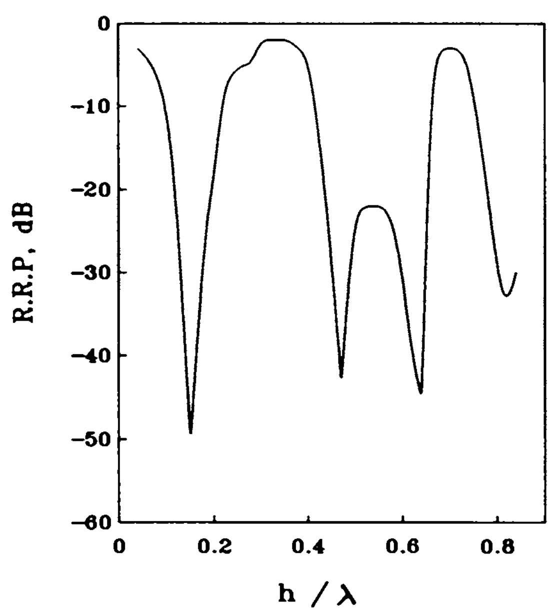

(c)

Fig.4.18 Variation of relative reflected power with dielectric thickness.

(a) [R3]. $d = \lambda$, $l = 0.233\lambda$, $\alpha = 90°$, $\beta = 90°$, $\theta_i = 30°$, $f = 10$ GHz
(b) [R10]. $d = \lambda$, $l = 0.471\lambda$, $\alpha = 90°$, $\beta = 90°$, $\theta_i = 30°$, $f = 10$ GHz
(c) [R19]. $d = \lambda$, $l = 0.471\lambda$, $\alpha = 60°$, $\beta = 120°$, $\theta_i = 42.5°$, $f = 10$ GHz

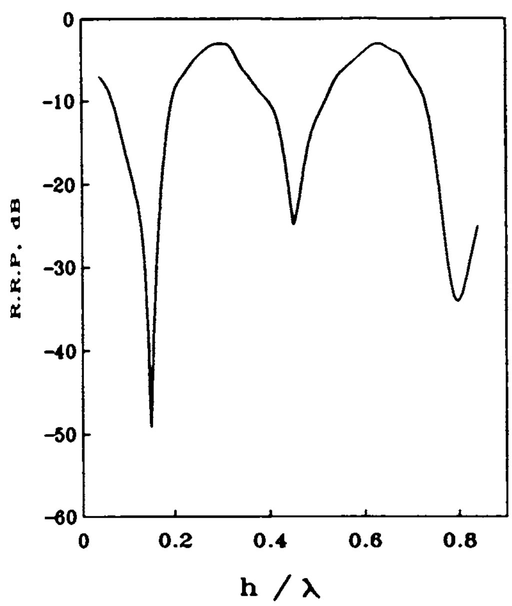

(d)

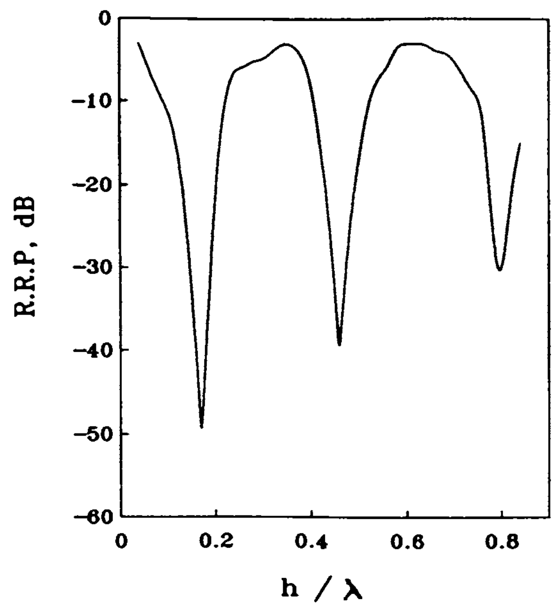

(e)

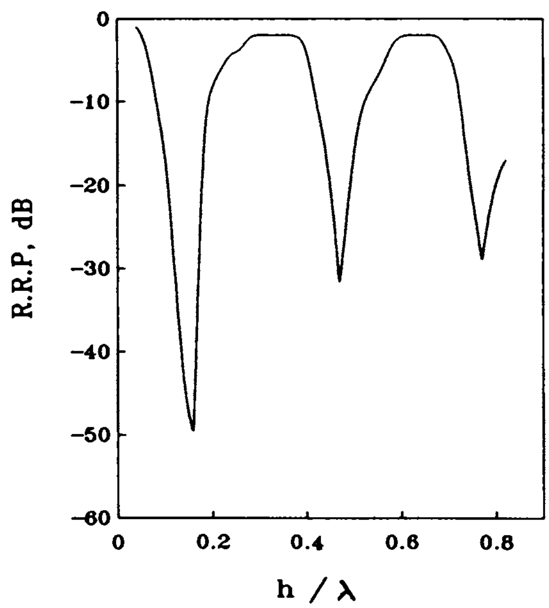

(f)

Fig.4.18 Variation of relative reflected power with dielectric thickness.

(d) [R22]. $d = \lambda$, $l = 0.471\lambda$, $\alpha = 120°$, $\beta = 60°$, $\theta_i = 32.5°$, $f = 10$ GHz
(e) [R26]. $d = 0.833\lambda$, $l = 0.471\lambda$, $\alpha = \beta = 90°$, $\theta_i = 37.5°$, $f = 10$ GHz
(f) [R29]. $d = 1.166\lambda$, $l = 0.471\lambda$, $\alpha = \beta = 90°$, $\theta_i = 30°$, $f = 10$ GHz

[R19] of dimensions $d = \lambda$, $\alpha = 60°$, $\beta = 120°$, $l = 0.471\lambda$

[R22] of dimensions $d = \lambda$, $\alpha = 120°$, $\beta = 60°$, $l = 0.471\lambda$

(c) Period

Investigations were carried out for structures with same sidelength, same internal angles but different periods. Variation of R.R.P with h / λ for typical structures

[R26] of dimensions $\alpha = \beta = 90°$, $l = 0.471\lambda$, $d = 0.833\lambda$ and

[R29] of dimensions $\alpha = \beta = 90°$, $l = 0.471\lambda$, $d = 1.166\lambda$ in TE polarisation are shown in fig. 4.18 (e) & (f).

It is clear from the plots that the reflected power is dependent on the dielectric thickness.

4.4.2 Incident angle

Fig. 4.19 illustrates the changes in reflected power due to the change in incident angle for constant dielectric thickness and frequency. Variations of R.R.P with angle of incidence for structures [R3], [R6], [R8], [R12], [R19], [R22], [R26] & [R29] in TE polarisation are shown in fig. 4.19. (a.i), (b.i), (c.i), (d.i), (e.i), (f.i), (g.i) and (h.i). The power levels scattered corresponding to $n = -1$ mode with receiving angle at blazing angle of incidence for the same structures are shown in fig 4.19 (a.ii), (b.ii), (c.ii), (d.ii), (e.ii), (f.ii), (g.ii) and (h.ii).

In fig. 4.19 (i) the solid line represents the variation of relative reflected power with incident angle for structure [R10], while dotted line represents that for conventional SCS. By modifying the structure, the angular range has been increased by 30° (i.e from 15° incidence to 45° incidence). It is noted that for conventional structure, blazing is possible only for a particular angle of incidence. When blazing occurs, all the power is diverted to $n = -1$ mode in accordance with the basic grating equation.

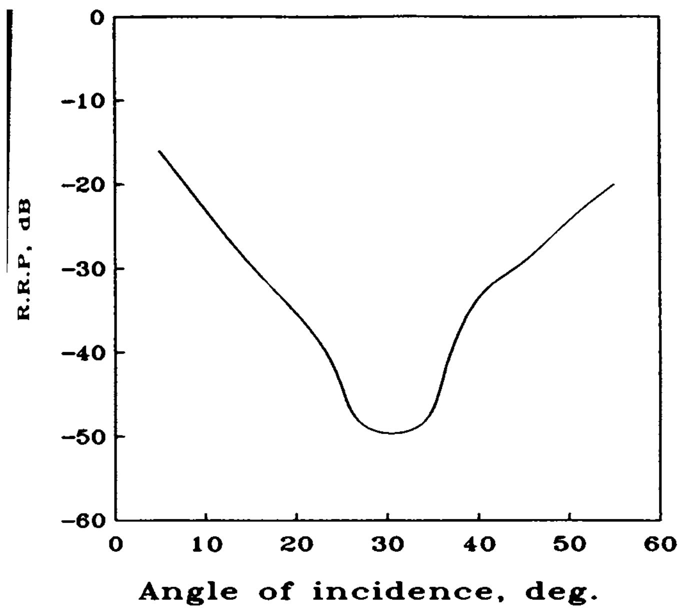

(a.i)

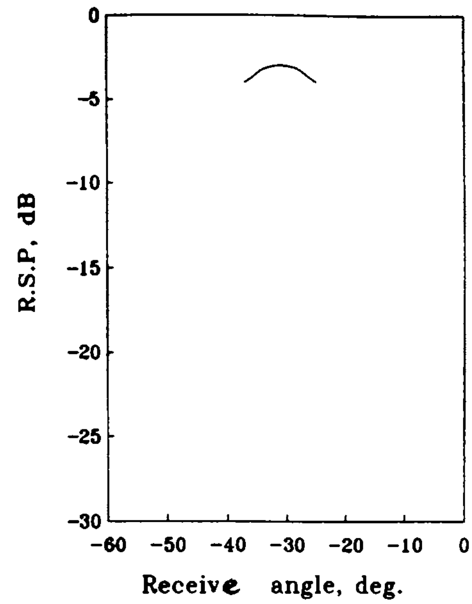

(a.ii)

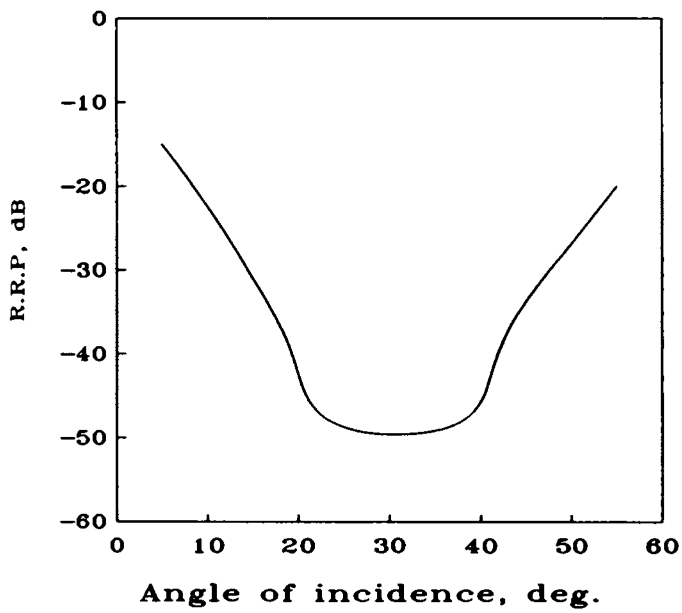

(b.i)

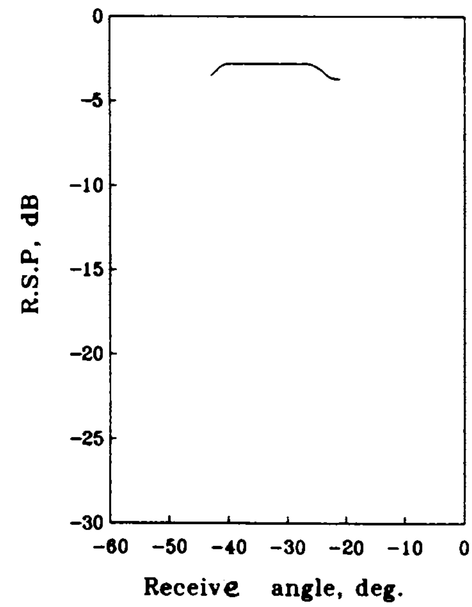

(b.ii)

Fig.4.19 (i) Variation of relative reflected power with angle of incidence.
(ii) Scattered power level at blazing angles.

(a) [R3]. $d = \lambda$, $l = 0.233\lambda$, $\alpha = 90°$, $\beta = 90°$, $h = 0.130\lambda$, $f = 10$ GHz
(b) [R6]. $d = \lambda$, $l = 0.333\lambda$, $\alpha = 90°$, $\beta = 90°$, $h = 0.154\lambda$, $f = 10$ GHz

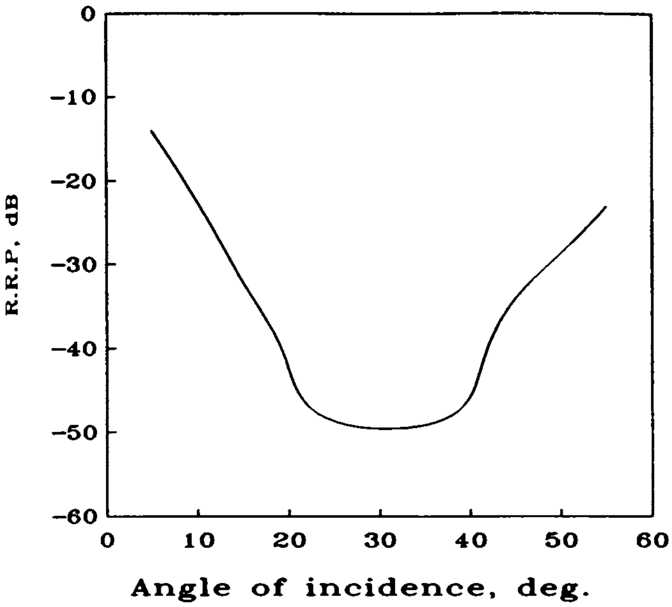

(c.i)

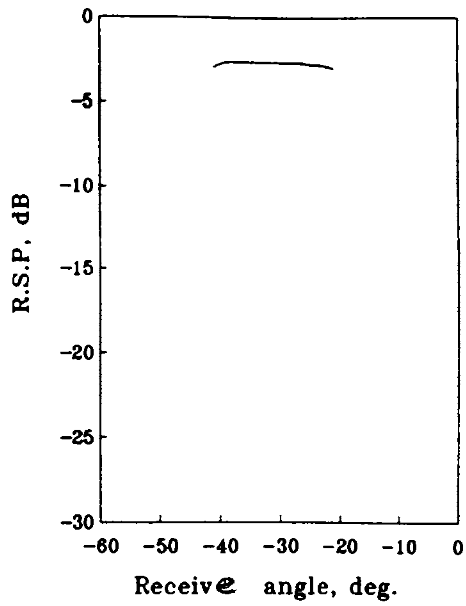

(c.ii)

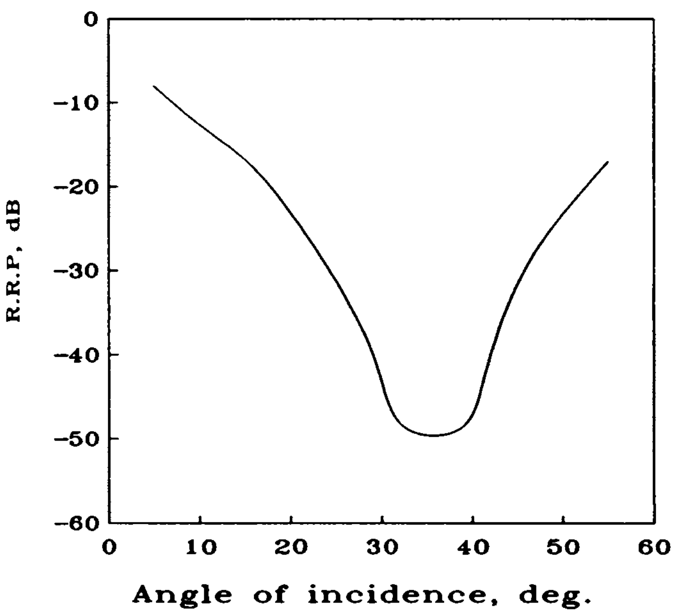

(d.i)

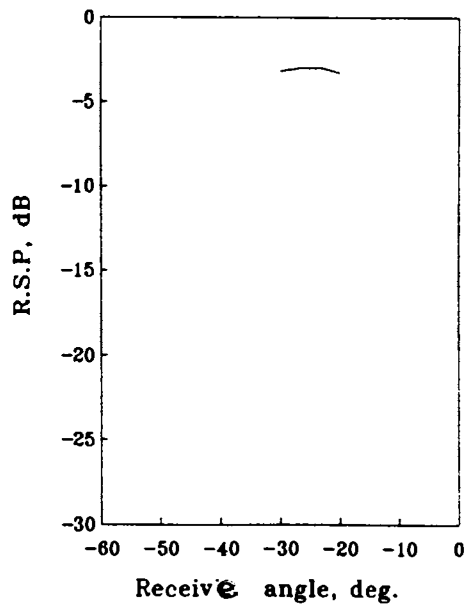

(d.ii)

Fig.4.19 (i) Variation of relative reflected power with angle of incidence.
(ii) Scattered power level at blazing angles.

(c) [R8]. $d = \lambda$, $l = 0.404\lambda$, $\alpha = 90°$, $\beta = 90°$, $h = 0.155\lambda$, $f = 10$ GHz
(d) [R12]. $d = \lambda$, $l = 0.533\lambda$, $\alpha = 90°$, $\beta = 90°$, $h = 0.140\lambda$, $f = 10$ GHz

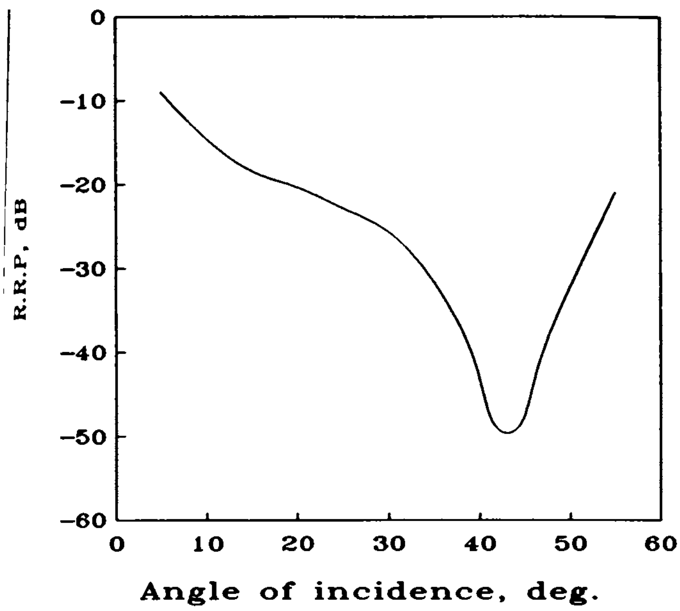

(e.i)

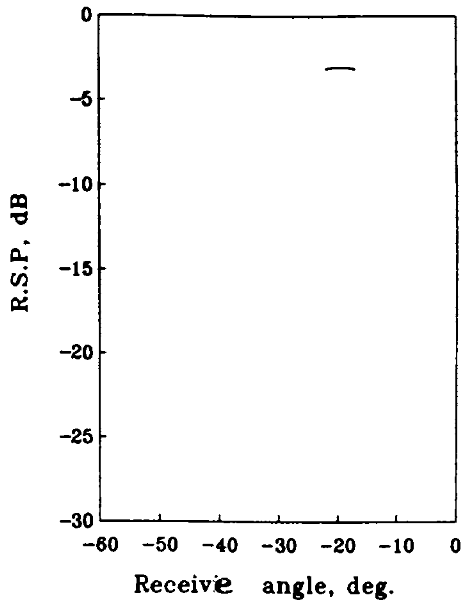

(e.ii)

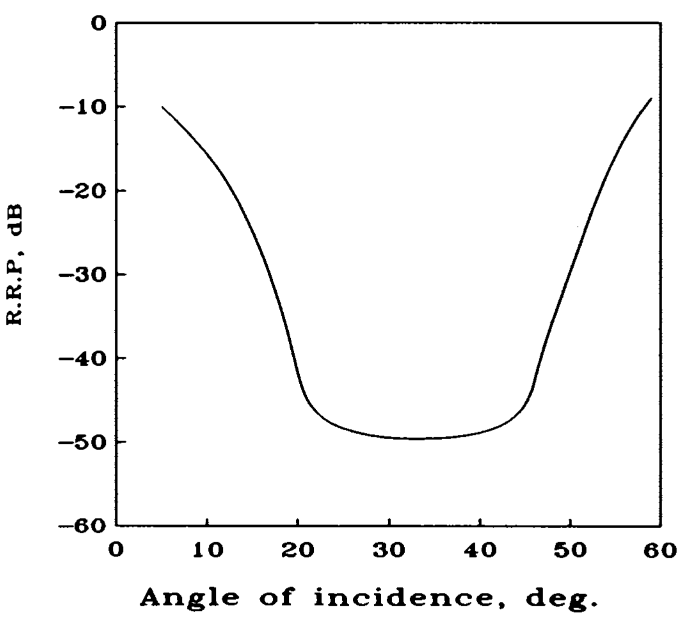

(f.i)

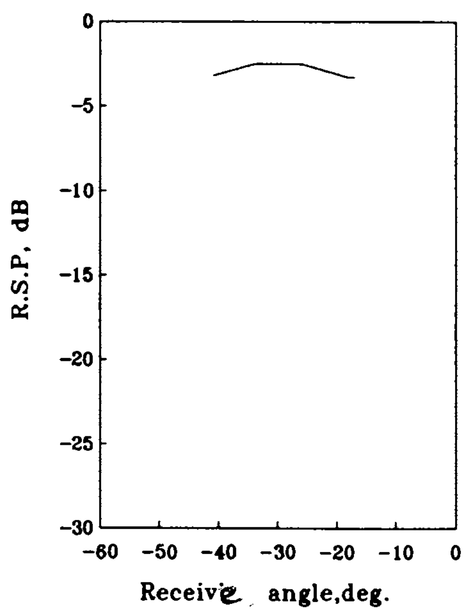

(f.ii)

Fig.4.19 (i) Variation of relative reflected power with angle of incidence.
(ii) Scattered power level at blazing angles.

(e) [R19]. $d = \lambda$, $l = 0.471\lambda$, $\alpha = 60°$, $\beta = 120°$, $h = 0.15\lambda$, $f = 10$ GHz
(f) [R22]. $d = \lambda$, $l = 0.471\lambda$, $\alpha = 120°$, $\beta = 60°$, $h = 0.153\lambda$, $f = 10$ GHz

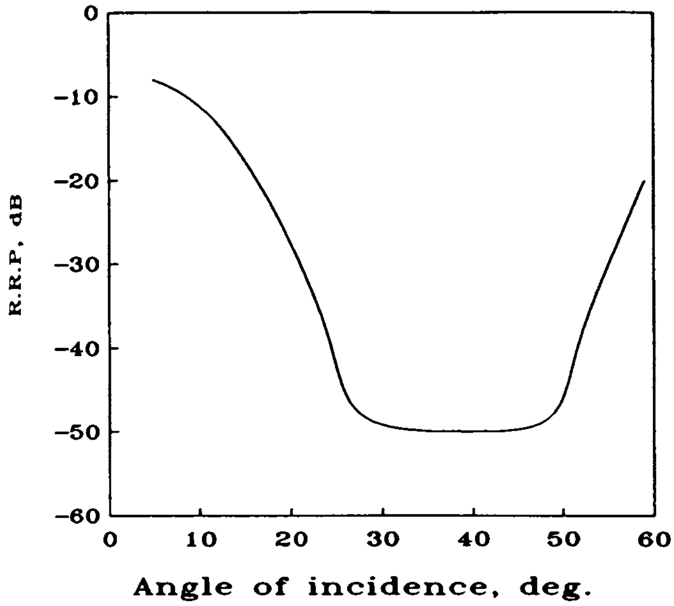

(g.i)

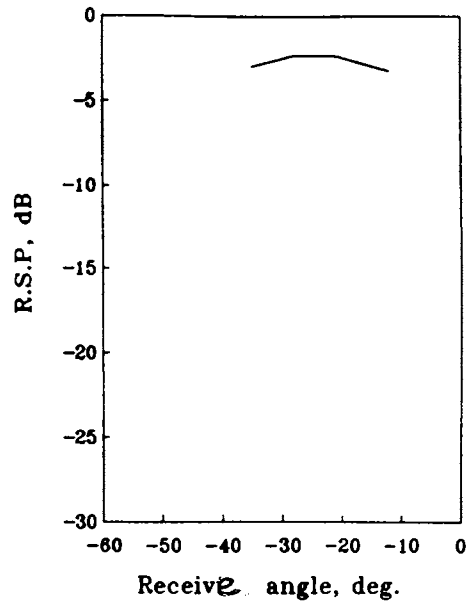

(g.ii)

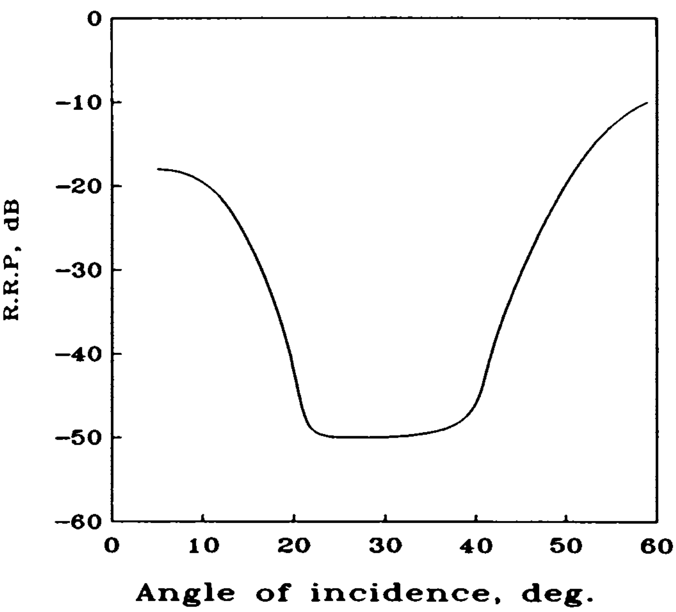

(h.i)

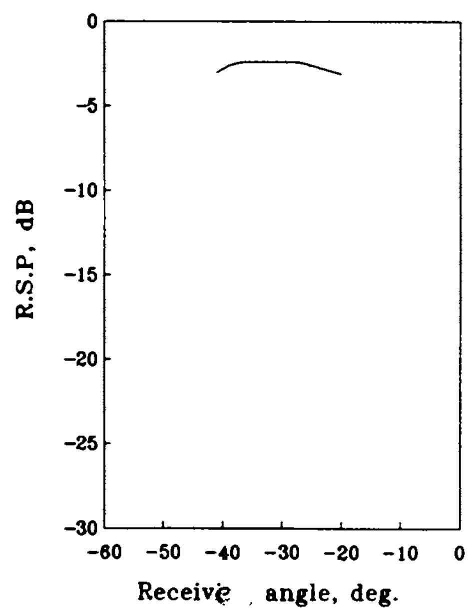

(h.ii)

Fig.4.19 (i) Variation of relative reflected power with angle of incidence.
(ii) Scattered power level at blazing angles.

(g) [R26]. $d = 0.833\lambda$, $l = 0.471\lambda$, $\alpha = \beta = 90°$, $h = 0.170\lambda$, $f = 10$ GHz
(h) [R29]. $d = 1.166\lambda$, $l = 0.471\lambda$, $\alpha = \beta = 90°$, $h = 0.156\lambda$, $f = 10$ GHz

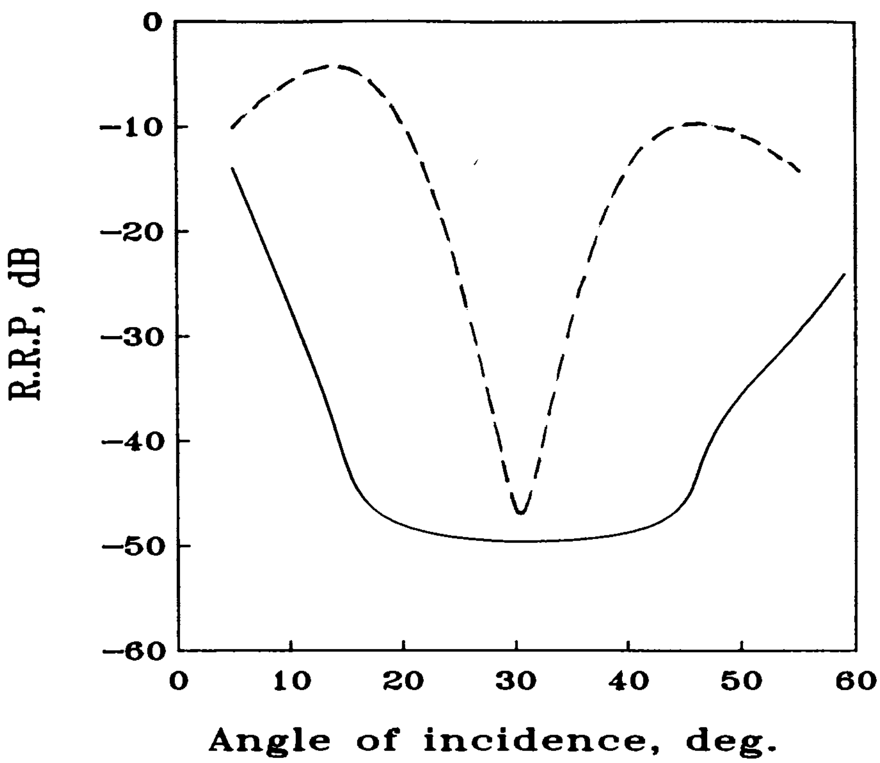

(i.i)

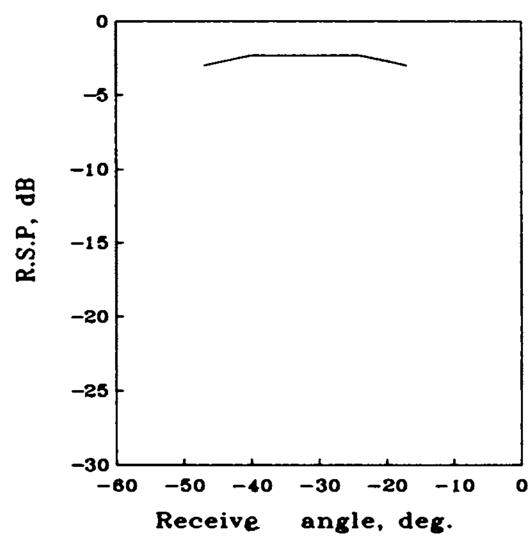

(i.ii)

Fig.4.19 (i) Variation of relative reflected power with angle of incidence.
(ii) Scattered power level at blazing angles.

(i) ——— [R10]. $d = \lambda$, $l = 0.471\lambda$, $\alpha = \beta = 90°$, $h = 0.158\lambda$, $f = 10$ GHz
- - - - - Self complementary strip grating.

4.4.3 Frequency

Variation of R.R.P with frequency for structures [R6], [R8], [R10], [R12], [R19], [R22], [R26] & [R29] is shown in fig. 4.20 (a), (b), (c), (d), (e), (f), (g) & (h) respectively for TE polarisation. The solid line in fig. 4.20 (h) represent the variation of R.R.P with frequency for structure [R3] and dotted line show that for conventional SCS. As is clear from the figure, wide bandwidth for TE polarisation is achieved using this structure.

4.4.4 Angular range & Frequency bandwidth

Variation of angular range and frequency bandwidth with length l / λ is shown in fig. 4.21 (a) & (b). The change of angular range and bandwidth with internal angle is plotted in fig. 4.21 (c) & (d). It is observed that when 'l' is around $\lambda / 4$ frequency bandwidth is high and when l is around $\lambda / 2$, angular range is high. Also angular range is high when $\alpha = \beta = 90°$

The results obtained for various structure parameters of the dual periodic structures in TE polarisation is shown in table 4.6. The first set represents structures with different 'l' values. The second set represents structures with different angles and the third set with structures of different periods. The table shows the parameters; side length 'l', internal angle α & β, period 'd', dielectric thickness h / λ, blazing angle θ and frequency bandwidth below -40 dB.

The reflection characteristics with incident angles in TM polarisation for structures

[R5] of dimensions $d = \lambda$, $\alpha = \beta = 90°$, $l = 0.300\lambda$, $h = 0.12\lambda$,

[R6] of dimensions $d = \lambda$, $\alpha = \beta = 90°$, $l = 0.333\lambda$, $h = 0.13\lambda$,

[R7] of dimensions $d = \lambda$, $\alpha = \beta = 90°$, $l = 0.363\lambda$, $h = 0.133\lambda$ and

[R19] of dimensions $d = \lambda$, $\alpha = 60°$, $\beta = 120°$, $l = 0.471\lambda$, $h = 0.15\lambda$, are plotted in fig. 4.22 (a.i), (b.i), (c.i) & (d.i) respectively. The variation of R.R.P with frequency in TM

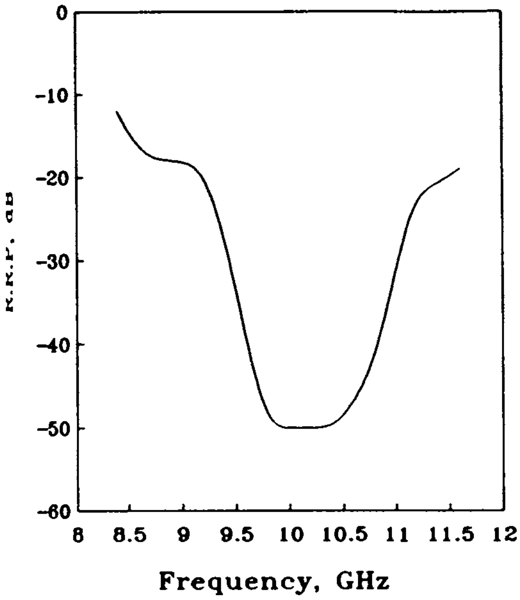

(a)

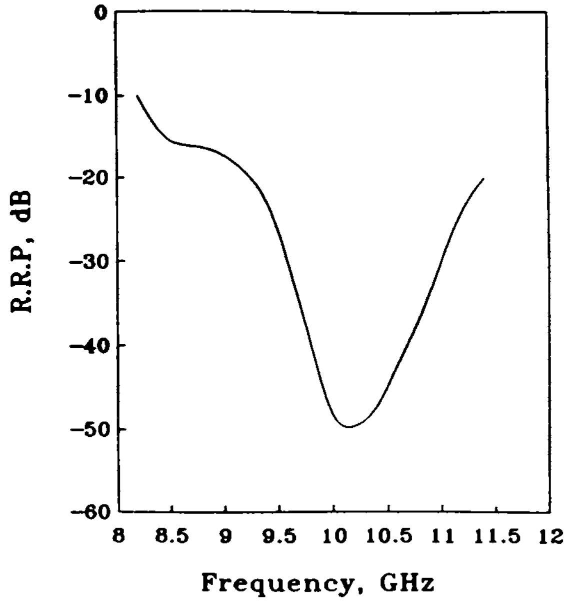

(b)

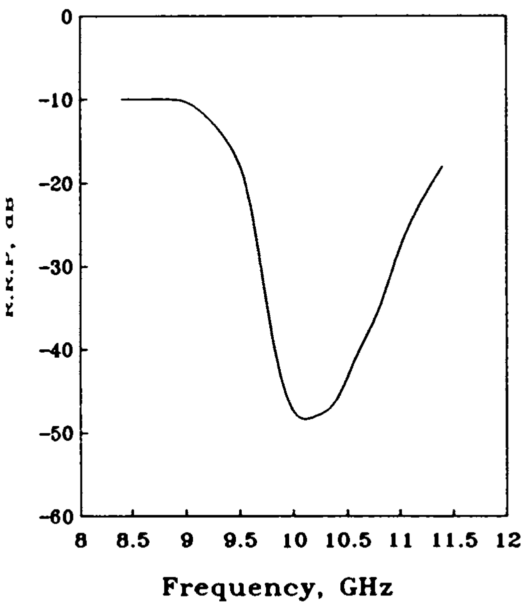

(c)

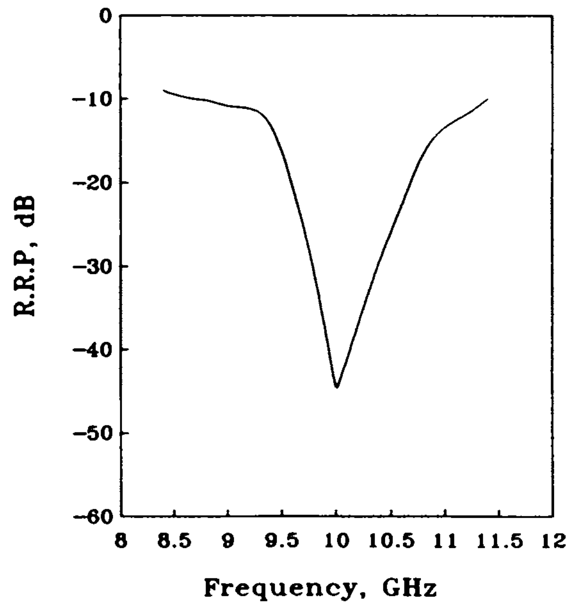

(d)

Fig.4.20 Variation of relative reflected power with frequency.

(a) [R6]. $d = \lambda$, $l = 0.333\lambda$, $\alpha = 90°$, $\beta = 90°$, $\theta_i = 30°$, $h = 0.154\lambda$
(b) [R8]. $d = \lambda$, $l = 0.404\lambda$, $\alpha = 90°$, $\beta = 90°$, $\theta_i = 30°$, $h = 0.155\lambda$
(c) [R10]. $d = \lambda$, $l = 0.471\lambda$, $\alpha = 90°$, $\beta = 90°$, $\theta_i = 30°$, $h = 0.158\lambda$
(d) [R12]. $d = \lambda$, $l = 0.533\lambda$, $\alpha = 90°$, $\beta = 90°$, $\theta_i = 35°$, $h = 0.140\lambda$

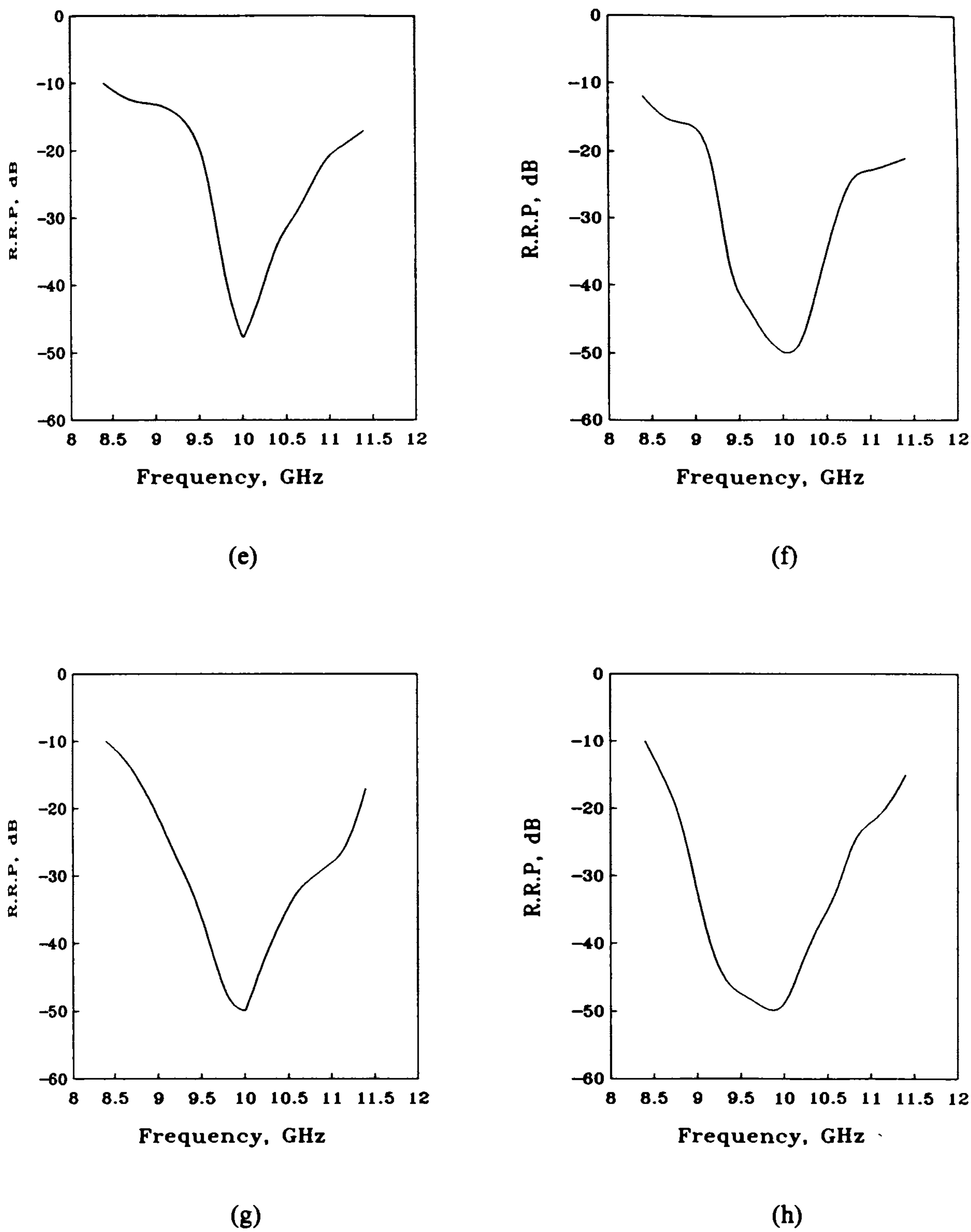

Fig.4.20 Variation of relative reflected power with frequency.

(e) [R19]. $d = \lambda$, $l = 0.471\lambda$, $\alpha = 60°$, $\beta = 120°$, $\theta_i = 42.5°$, $h = 0.150\lambda$
(f) [R22]. $d = \lambda$, $l = 0.471\lambda$, $\alpha = 120°$, $\beta = 60°$, $\theta_i = 32.5°$, $h = 0.153\lambda$
(g) [R26]. $d = 0.833\lambda$, $l = 0.471\lambda$, $\alpha = \beta = 90°$, $\theta_i = 37.5°$, $h = 0.170\lambda$
(h) [R29]. $d = 1.166\lambda$, $l = 0.471\lambda$, $\alpha = \beta = 90°$, $\theta_i = 27.5°$, $h = 0.156\lambda$

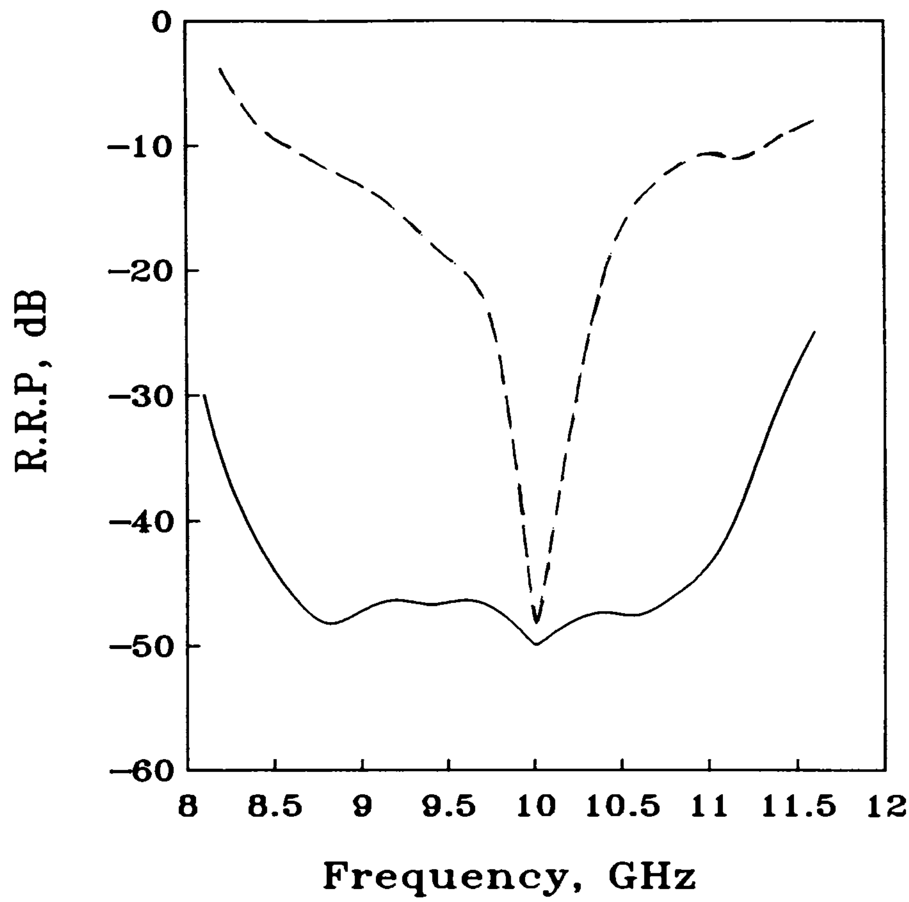

(i)

Fig.4.20 Variation of relative reflected power with frequency.

——— (i) [R3]. $d = \lambda$, $l = 0.233\lambda$, $\alpha = \beta = 90°$, $\theta_i = 30°$, $h = 0.13\lambda$

- - - - - Self complementary strip grating.

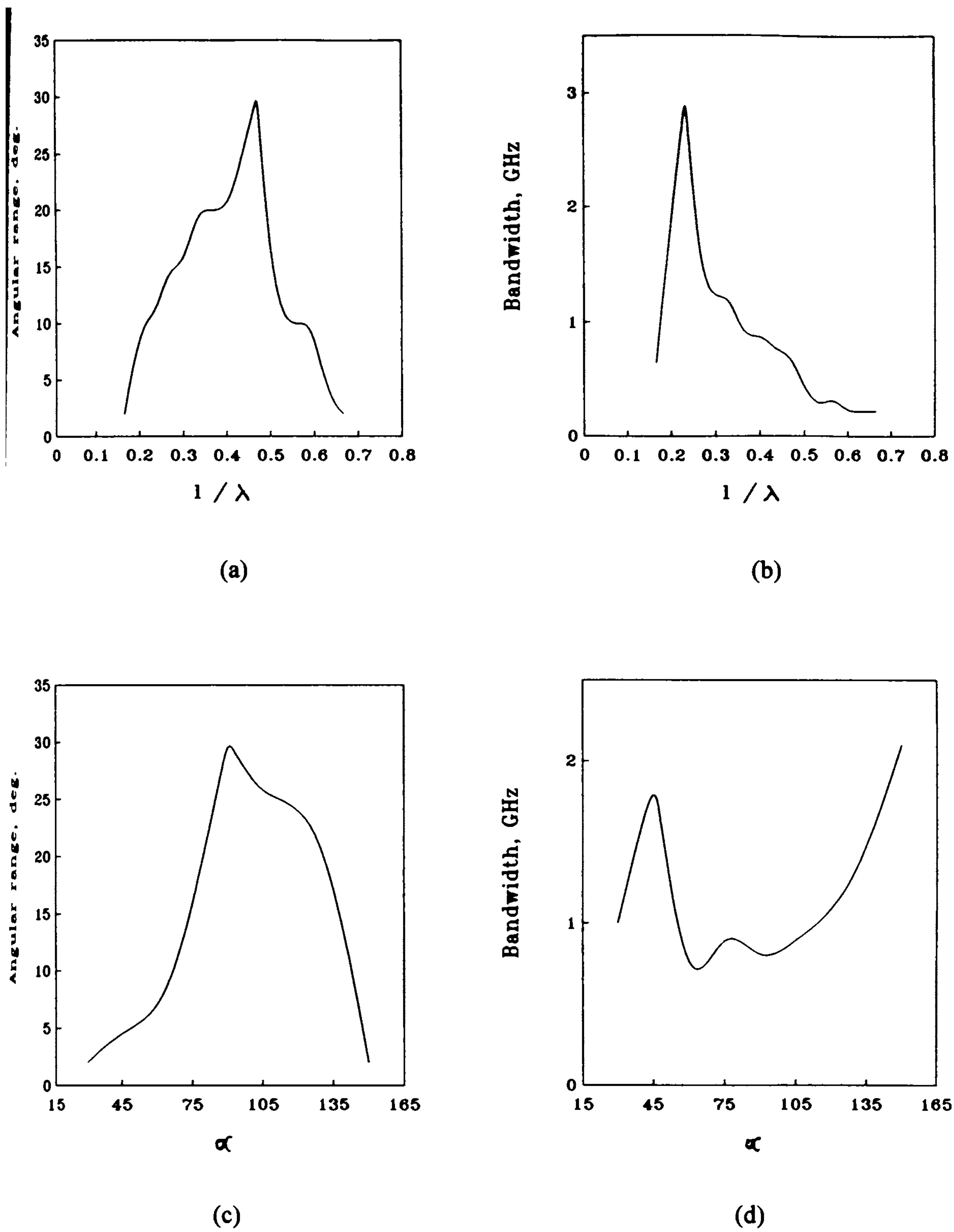

Fig.4.21 (a) Variation of angular range with length 'l'
(b) Variation of frequency bandwidth with length 'l'
(c) Variation of angular range with angle 'α'
(d) Variation of frequency bandwidth with angle 'α'

TABLE 4.6

Structure parameters and results for rhombic shaped periodic structures

TE POLARISATION

Side length l/λ	Angle α	Angle β	Period d/λ	Dielectric thickness h/λ	Blazing angle θ	Frequency Bandwidth GHz
0.166	90	90	1.000	0.117	5°	0.64
0.200	90	90	1.000	0.110	20°-30°	1.90
0.233	90	90	1.000	0.130	25°-35°	2.95
0.266	90	90	1.000	0.153	25°-40°	1.40
0.300	90	90	1.000	0.154	25°-40°	1.20
0.333	90	90	1.000	0.154	20°-40°	1.24
0.363	90	90	1.000	0.155	20°-40°	0.85
0.404	90	90	1.000	0.155	20°-40°	0.90
0.437	90	90	1.000	0.155	20°-45°	0.75
0.471	90	90	1.000	0.158	15°-45°	0.72
0.500	90	90	1.000	0.140	30°-45°	0.42
0.533	90	90	1.000	0.140	30°-40°	0.25
0.566	90	90	1.000	0.103	30°-40°	0.35
0.600	90	90	1.000	0.087	45°-55°	0.20
0.633	90	90	1.000	0.170	20°	0.22
0.666	90	90	1.000	0.173	15°	0.22
0.471	30°	150°	1.000	0.173	35°	1.00
0.471	45°	135°	1.000	0.167	30°-35°	1.90
0.471	60°	120°	1.000	0.150	40°-45°	0.40
0.471	75°	105°	1.000	0.157	30°-45°	1.05
0.471	90°	90°	1.000	0.158	15°-45°	0.72
0.471	105°	75°	1.000	0.155	15°-40°	0.90
0.471	120°	60°	1.000	0.153	20°-45°	1.05
0.471	135°	45°	1.000	0.147	20°-40°	1.40
0.471	150°	30°	1.000	0.133	20°	2.10
0.471	90°	90°	0.666	0.170	40°-55°	0.30
0.471	90°	90°	0.833	0.170	25°-50°	0.70
0.471	90°	90°	0.900	0.163	30°-50°	0.50
0.471	90°	90°	1.000	0.158	15°-45°	0.72
0.471	90°	90°	1.066	0.150	20°-35°	0.70
0.471	90°	90°	1.166	0.156	20°-40°	1.20
0.471	90°	90°	1.333	0.170	20°	0.02

polarisation for the same structures is shown in fig. 4.22 (a.ii), (b.ii), (c.ii) & (d.ii). From the figures it is observed that eventhough the bandwidth is increased, it has not increased so much as that obtained in tapered SCS.

The results obtained for TM polarisation for the same structures described above in TE polarisation are shown in table 4.7.

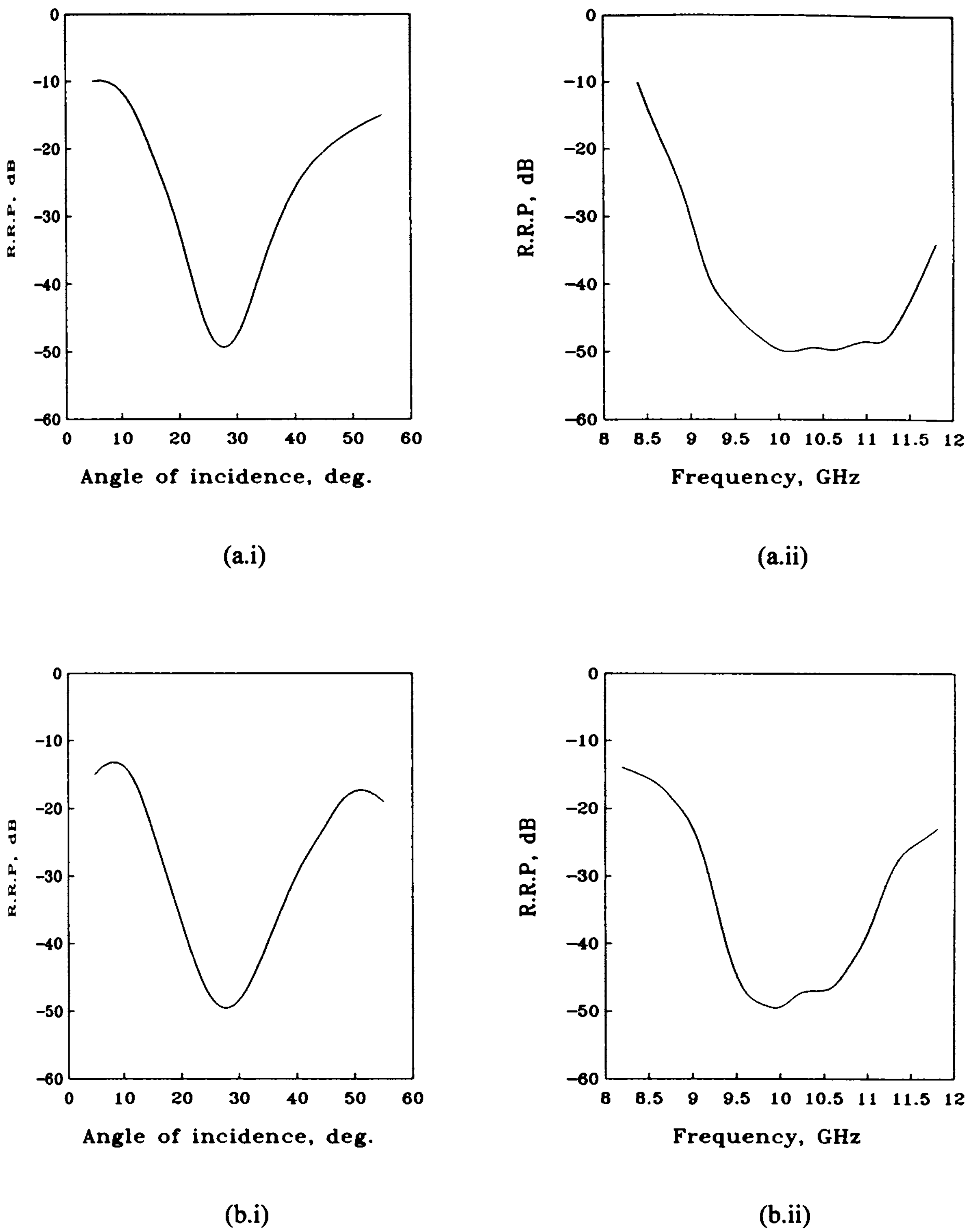

Fig.4.22 (i) Variation of relative reflected power with angle of incidence.
(ii) Variation of relative reflected power with frequency.

(a) [R5]. $l = 0.300\lambda$, $\alpha = \beta = 90°$, $d = \lambda$, $h = 0.12\lambda$
(b) [R6]. $l = 0.333\lambda$, $\alpha = \beta = 90°$, $d = \lambda$, $h = 0.13\lambda$

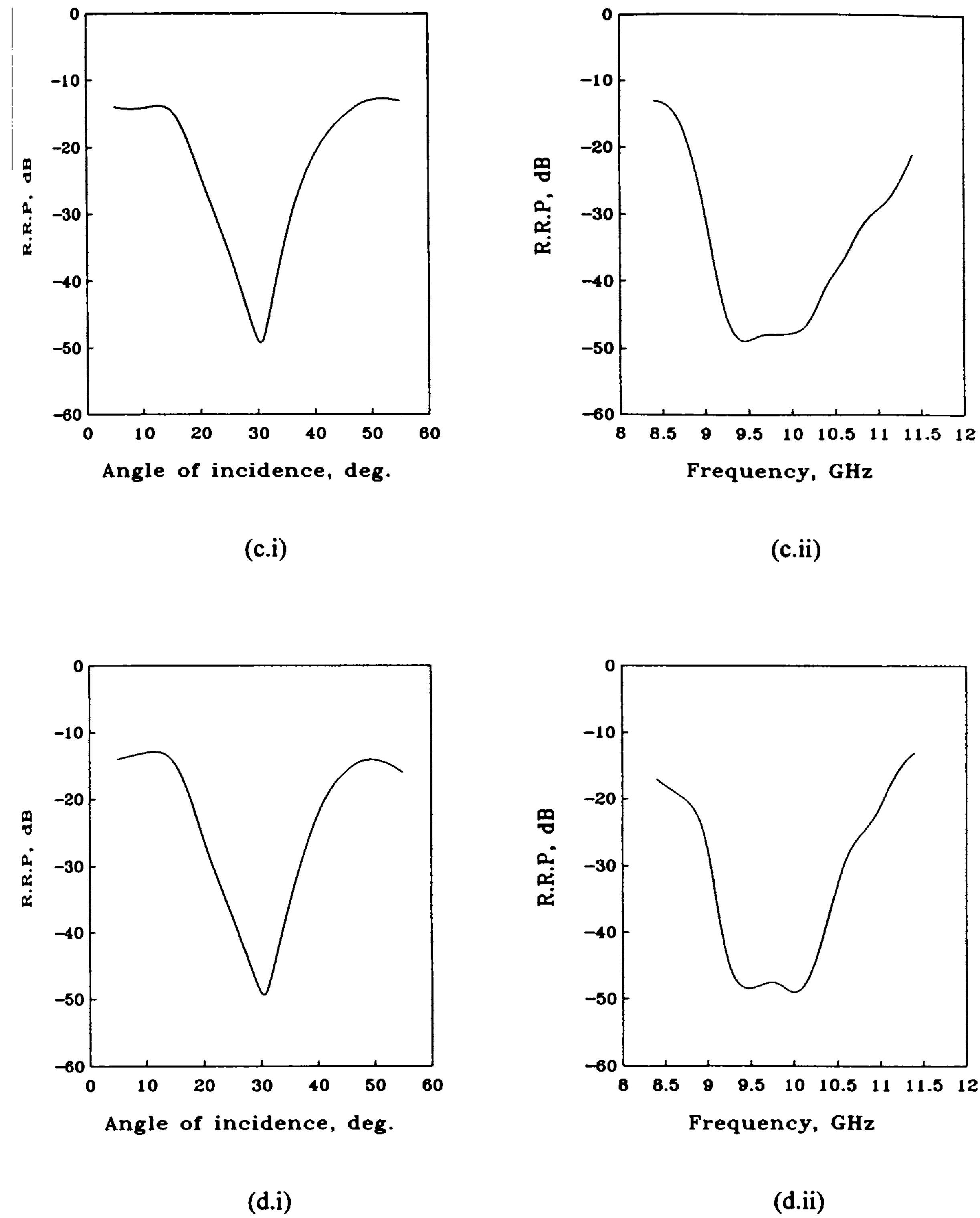

Fig.4.22 (i) Variation of relative reflected power with angle of incidence.
(ii) Variation of relative reflected power with frequency.

(c) [R7]. $l = 0.363\lambda$, $\alpha = 90°$, $\beta = 90°$, $d = \lambda$, $h = 0.133\lambda$
(d) [R19]. $l = 0.471\lambda$, $\alpha = 60°$, $\beta = 120°$, $d = \lambda$, $h = 0.15\lambda$

TABLE 4.7

Structure parameters and results for rhombic shaped periodic structures

TM POLARISATION

Side length l/λ	Angle α	Angle β	Period d/λ	Dielectric thickness (h/λ)	Blazing angle θ	Frequency Bandwidth GHz
0.166	90	90	1.000	-	-	-
0.200	90	90	1.000	0.123	10°	0.10
0.233	90	90	1.000	0.110	25°-30°	0.62
0.266	90	90	1.000	0.072	25°	0.56
0.300	90	90	1.000	0.120	25°-30°	2.40
0.333	90	90	1.000	0.130	25°-30°	1.60
0.363	90	90	1.000	0.133	30°	1.30
0.404	90	90	1.000	0.117	30°	0.40
0.437	90	90	1.000	0.100	30°	0.12
0.471	90	90	1.000	0.150	10°	0.12
0.500	90	90	1.000	0.173	15°,40°	0.40
0.533	90	90	1.000	0.127	35°	0.10
0.566	90	90	1.000	0.107	35°,50°	0.30
0.600	90	90	1.000	0.110	50°	0.36
0.633	90	90	1.000	0.050	55°	0.24
0.666	90	90	1.000	0.157	15°	0.10
0.471	30°	150°	1.000	-	-	-
0.471	45°	135°	1.000	0.127	30°	0.55
0.471	60°	120°	1.000	0.150	30°	1.10
0.471	75°	105°	1.000	0.153	35°-40°	0.30
0.471	90°	90°	1.000	0.150	10°	0.12
0.471	105°	75°	1.000	0.137	10°	0.10
0.471	120°	60°	1.000	0.117	10°,55°	0.34
0.471	135°	45°	1.000	0.103	55°	0.35
0.471	150°	30°	1.000	0.103	55°	0.22
0.471	90°	90°	0.666	-	-	-
0.471	90°	90°	0.833	0.077	50°	0.40
0.471	90°	90°	0.900	0.083	60°	0.46
0.471	90°	90°	1.000	0.150	10°	0.12
0.471	90°	90°	1.066	0.183	25°	0.10
0.471	90°	90°	1.166	0.187	25°	0.38
0.471	90°	90°	1.333	0.117	60°	0.44

4.5 PERIODIC STRUCTURES WITH 'V' SHAPED ELEMENTS

As described earlier, modification of strip grating along x & y directions and periodic variations along the strip length has led to interesting and encouraging results. The single strip is divided into a large number of V-shaped elements. Investigations with these V-shaped periodic elements are presented here. The schematic representation of V-shaped structures is shown in fig. 4.23. Actually this is also a modification of strip gratings. i.e. giving gaps in a strip grating. It has been noticed that with small rectangular gaps, the structure behaves like conventional strip gratings. Inclined gaps were given along the strips and these gratings are found to behave as reflection polarisers. The gaps were given in an angular way to form V-shaped elements. The parameters studied include strip period 'd', inter element period 'b', dielectric thickness 'h', incident angle 'θ' & frequency 'f'.

4.5.1 Thickness of dielectric

Variation of R.R.P with dielectric thickness for structures [V2] with dimensions period $d = \lambda$, sidelength $l = 0.5\lambda$, stripwidth $a = 0.666\lambda$, element width $w = 0.166\lambda$, interelement period $b = 0.4\lambda$ and [V9] of dimensions $d = 0.9\lambda$, $l = 0.5\lambda$, $a = 0.666\lambda$, $w = 0.166\lambda$ and $b = 0.4\lambda$ are shown in fig. 4.24. (a.i) and (b.i) for TM polarisation. Variation for the same structures in TE polarisation is given in fig. 4.24. (a.ii) and (b.ii)

4.5.2 Incident angle

Plots of relative reflected power with angle of incidence for the following structures in TM polarisation are shown in fig. 4.25. (a), (b), (c) & (d).

[V2] of dimensions $d = \lambda$, $a = 0.666\lambda$, $w = 0.166\lambda$, $l = 0.5\lambda$, $b = 0.4\lambda$

[V4] of dimensions $d = \lambda$, $a = 0.666\lambda$, $w = 0.166\lambda$, $l = 0.5\lambda$, $b = 0.6\lambda$

[V6] of dimensions $d = \lambda$, $a = 0.666\lambda$, $w = 0.166\lambda$, $l = 0.5\lambda$, $b = 0.833\lambda$ and

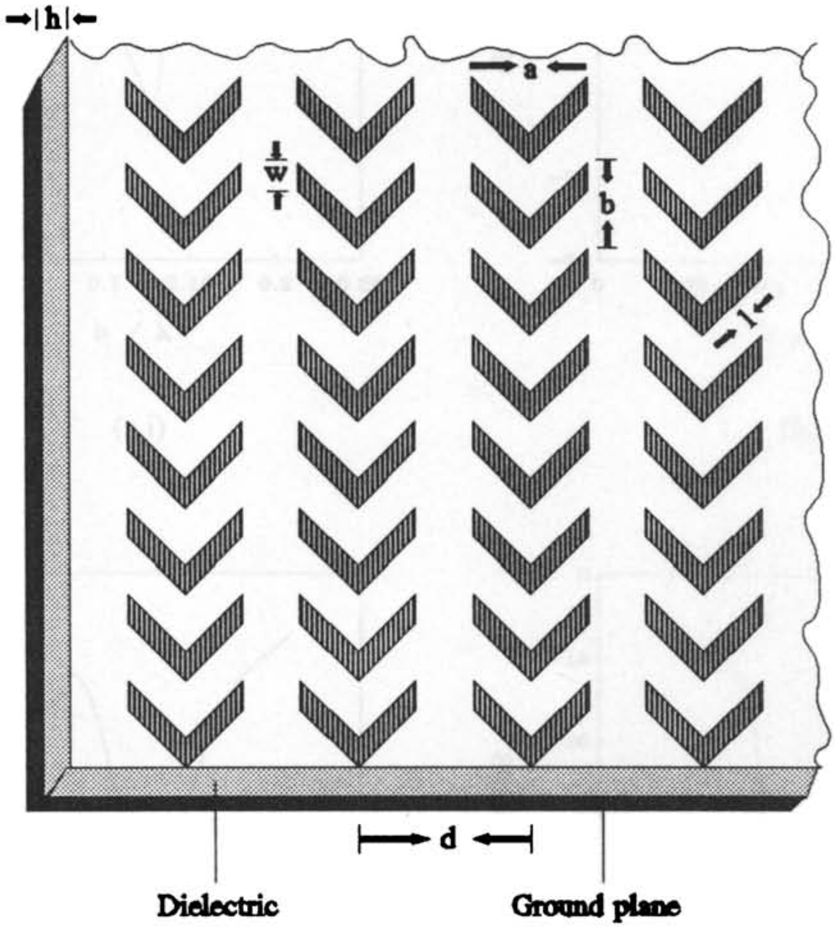

Fig.4.23 Schematic diagram of periodic structure with 'V' shaped elements.

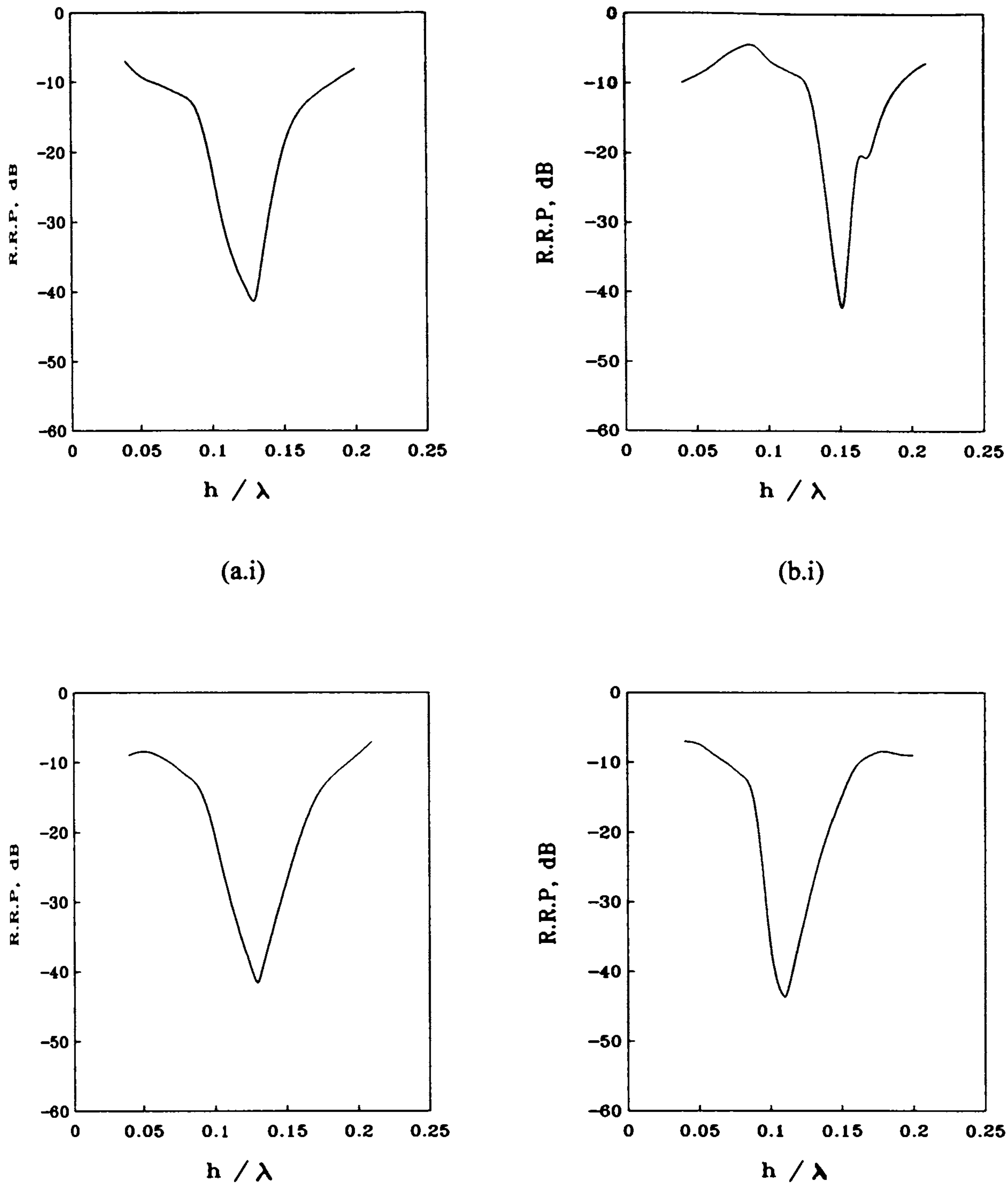

(a.i) (b.i)

(a.ii) (b.ii)

Fig.4.24 Variation of relative reflected power with dielectric thickness.

(a) [V2]. w = 0.166λ, l = 0.5λ, d = λ, b = 0.4λ, f = 10 GHz
(b) [V9]. w = 0.166λ, l = 0.5λ, d = 0.9λ, b = 0.4λ, f = 10 GHz

(i) TM polarisation (ii) TE polarisation

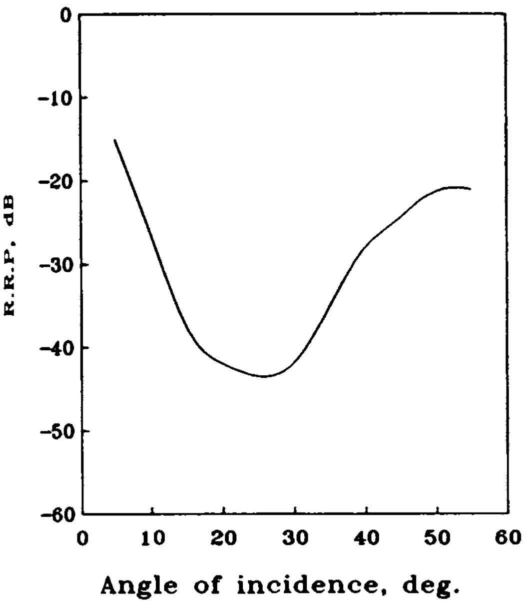

(a)

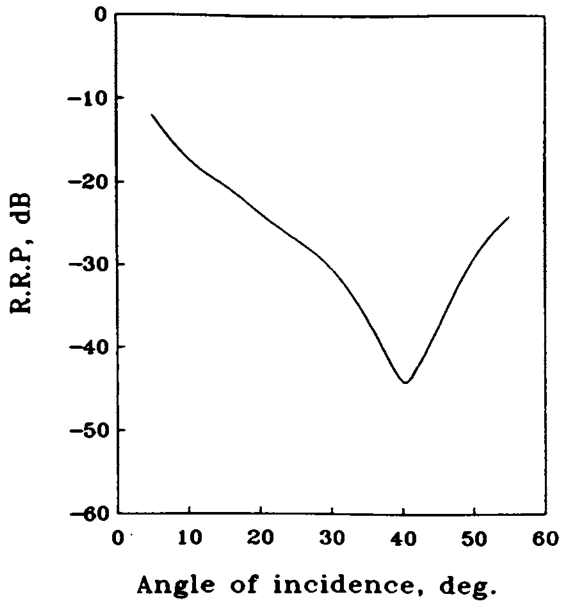

(b)

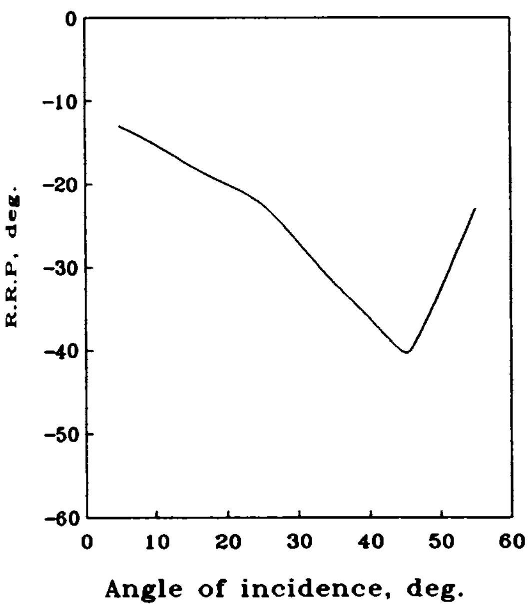

(c)

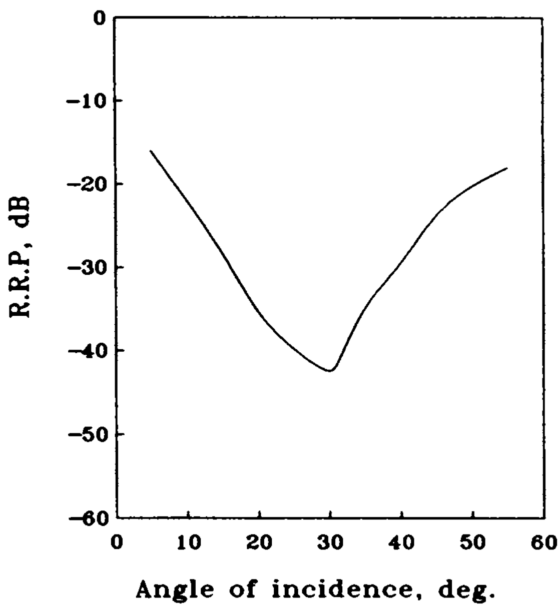

(d)

Fig.4.25 Variation of relative reflected power with angle of incidence.
TM polarisation

(a) [V2]. w = 0.166λ, l = 0.5λ, d = λ, b = 0.4λ, h = 0.130λ, f = 10 GHz
(b) [V4]. w = 0.166λ, l = 0.5λ, d = λ, b = 0.6λ, h = 0.163λ, f = 10 GHz
(c) [V6]. w = 0.166λ, l = 0.5λ, d = λ, b = 0.833λ, h = 0.173λ, f = 10 GHz
(d) [V9]. w = 0.166λ, l = 0.5λ, d = 0.9λ, b = 0.4λ, h = 0.153λ, f = 10 GHz

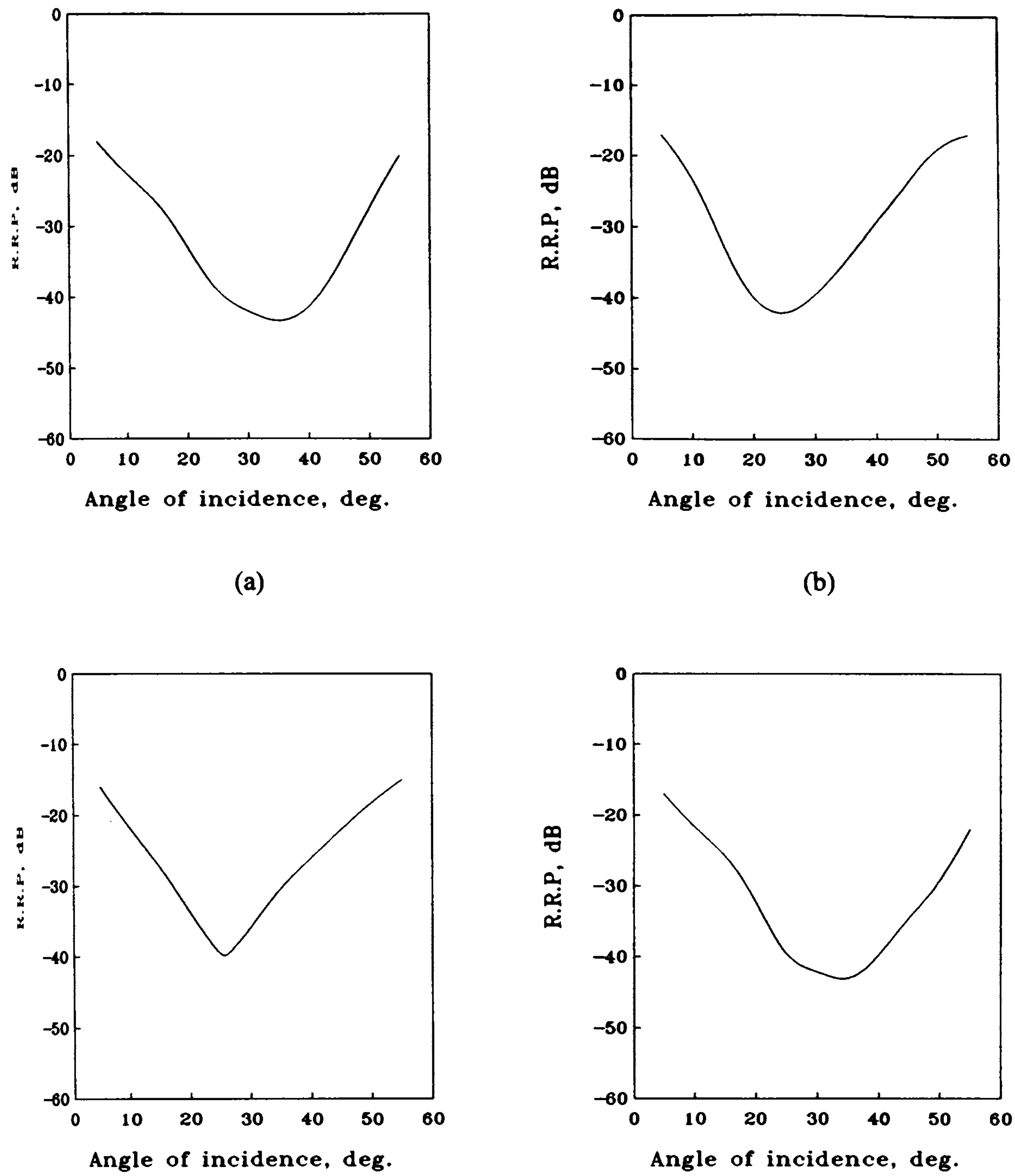

(a) (b) (c) (d)

Fig.4.26 Variation of relative reflected power with angle of incidence.
TE polarisation

(a) [V2]. w = 0.166λ, l = 0.5λ, d = λ, b = 0.4λ, h = 0.130λ, f = 10 GHz
(b) [V4]. w = 0.166λ, l = 0.5λ, d = λ, b = 0.6λ, h = 0.133λ, f = 10 GHz
(c) [V6]. w = 0.166λ, l = 0.5λ, d = λ, b = 0.833λ, h = 0.167λ, f = 10 GHz
(d) [V9]. w = 0.166λ, l = 0.5λ, d = 0.9λ, b = 0.4λ, h = 0.110λ, f = 10 GHz

[V9] of dimensions d = 0.9λ, a = 0.666λ, w = 0.166λ, l = 0.5λ, b = 0.4λ.

Variation for the same structures in TE polarisation is illustrated in fig. 4.26 (a), (b), (c) & (d). From the figures it is noted that angular range for specular reflection elimination increases for both TE and TM polarisations. But it is very much less than that achieved by rhombic shaped structure, where an angular range of 30° is obtained in TE polarisation.

4.5.3 Frequency

Changes in R.R.P with frequency for structures [V2], [V4], [V6] & [V9] in TM polarisation is shown in fig. 4.27 (a), (b), (c) & (d) respectively. Variations for the same structures in TE polarisation are illustrated in fig. 4.28 (a), (b), (c) & (d). It is observed that, bandwidth is increased slightly compared to conventional strip gratings, but this increase is not as much as that obtained in progressively varied and tapered structures.

4.5.4 Axial ratio

When blazing occurs, power is diverted to n = −1 spectral order. The power backscattered by strip gratings is normally in the same polarisation as incident wave. However, from the observations it is found that, with V-shaped structures, the power backscattered is elliptically polarised. Variation of axial ratio of backscattered power with frequency for structures [V2] & [V9] for TM polarisation is shown in fig. 4.29. (a.i) & (b.i). The same for TE polarisation is shown in fig. 4.29 (a.ii) & (b.ii). The plots make it clear that almost circular polarisation can be obtained at a particular frequency.

The structure parameters and observations in TE polarisation & TM polarisation is shown in tables 8 & 9 respectively. Table includes strip period, inter element period, dielectric thickness, blazing angle and frequency bandwidth.

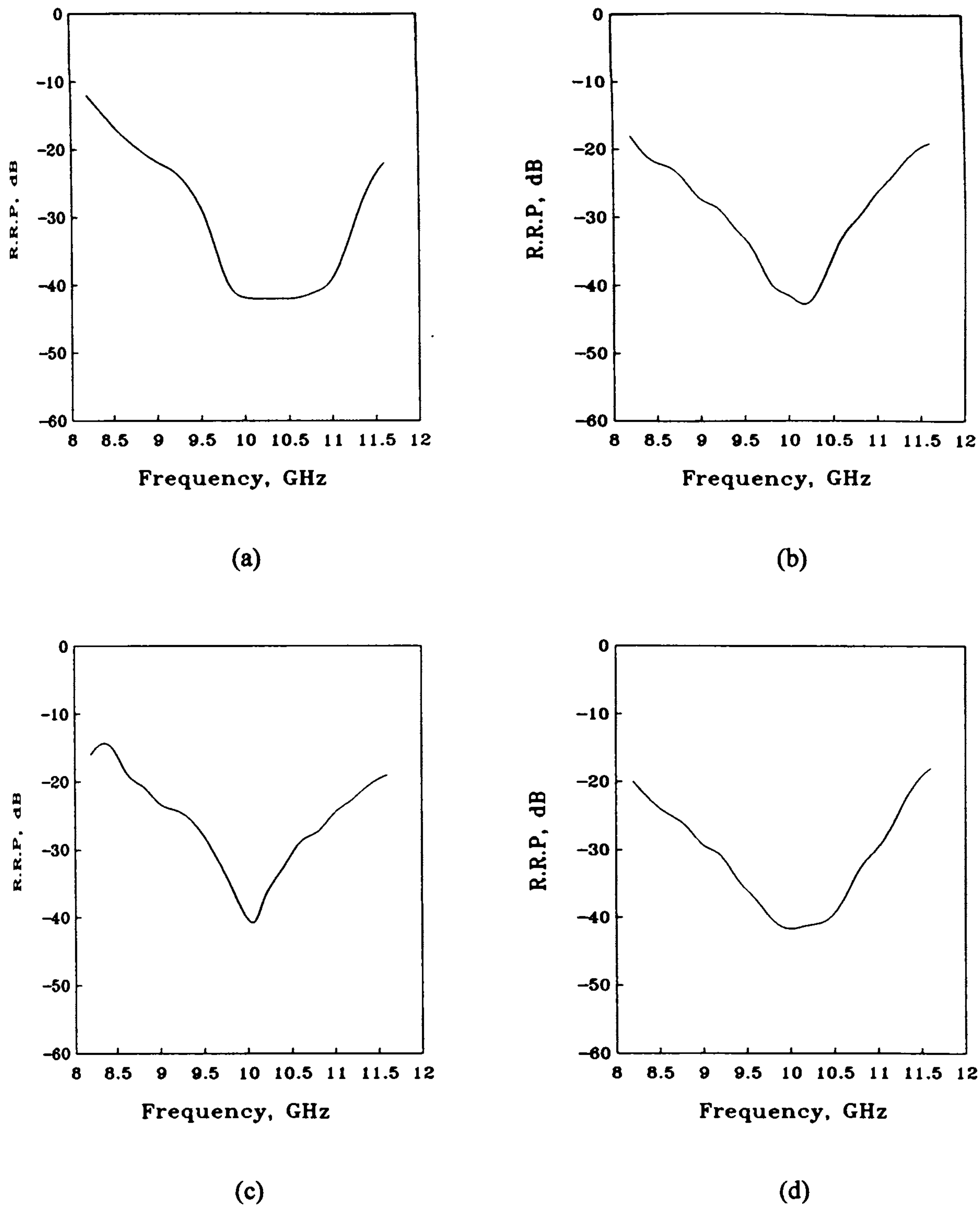

Fig.4.27 Variation of relative reflected power with frequency.
TM polarisation

(a) [V2]. $w = 0.166\lambda$, $l = 0.5\lambda$, $d = \lambda$, $b = 0.4\lambda$, $h = 0.130\lambda$, $\theta_i = 30°$
(b) [V4]. $w = 0.166\lambda$, $l = 0.5\lambda$, $d = \lambda$, $b = 0.6\lambda$, $h = 0.163\lambda$, $\theta_i = 40°$
(c) [V6]. $w = 0.166\lambda$, $l = 0.5\lambda$, $d = \lambda$, $b = 0.833\lambda$, $h = 0.173\lambda$, $\theta_i = 45°$
(d) [V9]. $w = 0.166\lambda$, $l = 0.5\lambda$, $d = 0.9\lambda$, $b = 0.4\lambda$, $h = 0.153\lambda$, $\theta_i = 30°$

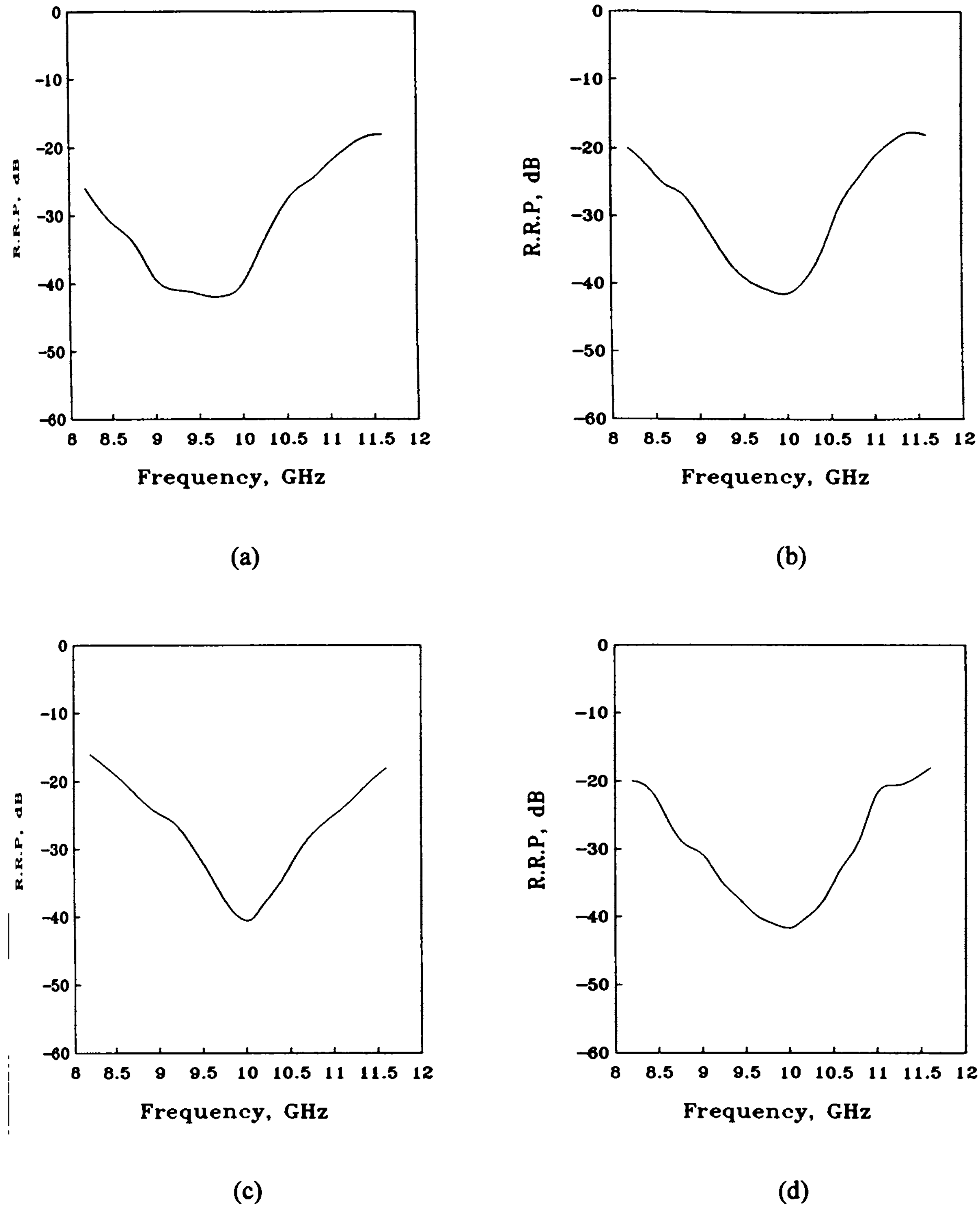

Fig.4.28 Variation of relative reflected power with frequency.
TE polarisation

(a) [V2]. w = 0.166λ, l = 0.5λ, d = λ, b = 0.4λ, h = 0.130λ, θ_i = 30°
(b) [V4]. w = 0.166λ, l = 0.5λ, d = λ, b = 0.6λ, h = 0.133λ, θ_i = 25°
(c) [V6]. w = 0.166λ, l = 0.5λ, d = λ, b = 0.833λ, h = 0.167λ, θ_i = 25°
(d) [V9]. w = 0.166λ, l = 0.5λ, d = 0.9λ, b = 0.4λ, h = 0.110λ, θ_i = 35°

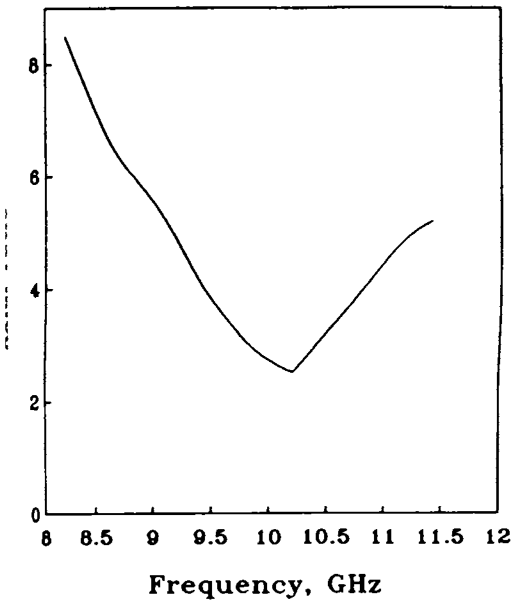

(a.i)

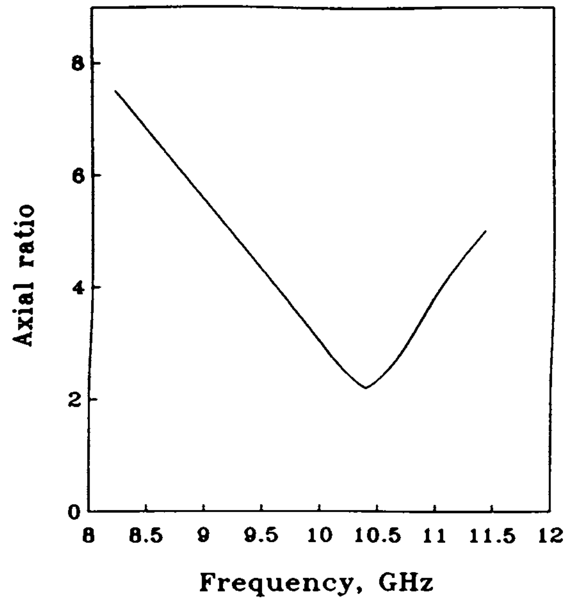

(b.i)

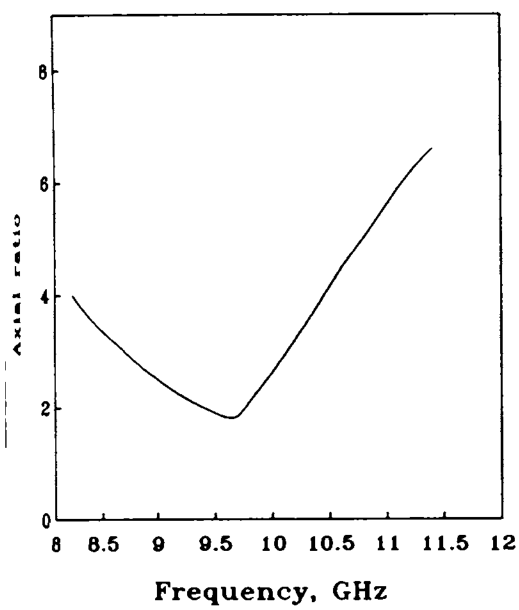

(a.ii)

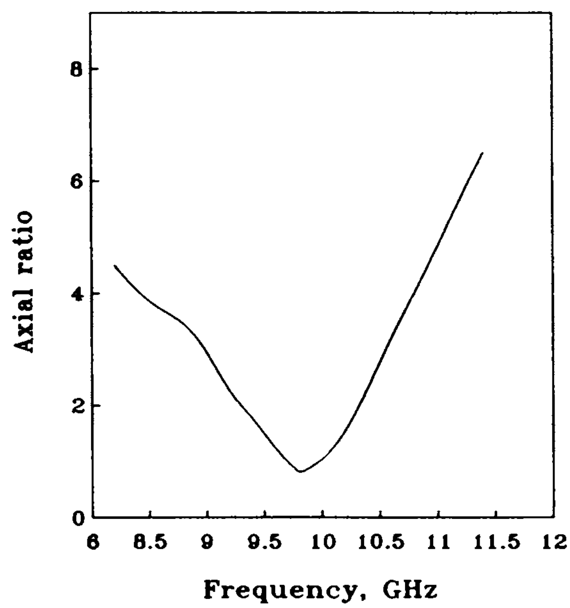

(b.ii)

Fig.4.29 Variation of axial ratio with frequency.

(a) [V2]. w = 0.166λ, l = 0.5λ, d = λ, b = 0.4λ
(b) [V9]. w = 0.166λ, l = 0.5λ, d = 0.9λ, b = 0.4λ

(i) TM polarisation (ii) TE polarisation

TABLE 4.8

Parameters varied in the study - TE POLARISATION

a = 0.666λ, l = 0.5λ, w = 0.166λ

Period d/λ	Separation b/λ	Dielectric thickness h/λ	Blazing angle θ	Bandwidth GHz
1.000	0.333	0.130	35°-45°	0.40
1.000	0.400	0.130	25°-40°	1.10
1.000	0.500	0.143	30°-40°	1.00
1.000	0.600	0.133	20°-30°	0.64
1.000	0.666	0.150	25°-30°	0.57
1.000	0.833	0.167	25°	0.16
0.800	0.400	0.100	30°-40°	0.58
0.866	0.400	0.123	30°-40°	0.70
0.900	0.400	0.110	25°-40°	0.88
1.000	0.400	0.130	25°-40°	1.10
1.067	0.400	0.127	25°-35°	0.76

TABLE 4.9

Parameters varied in the study - TM POLARISATION

a = 0.666λ, l = 0.5λ, w = 0.166λ

Period d/λ	Separation b/λ	Dielectric thickness h/λ	Blazing angle θ	Bandwidth GHz
1.000	0.333	0.130	20°	0.40
1.000	0.400	0.130	15°-30°	1.12
1.000	0.500	0.163	35°-45°	0.87
1.000	0.600	0.163	40°	0.64
1.000	0.666	0.170	40°	0.45
1.000	0.833	0.173	45°	0.20
0.800	0.400	0.133	20°	0.35
0.866	0.400	0.143	25°	0.63
0.900	0.400	0.153	25°-30°	0.88
1.000	0.400	0.130	15°-30°	1.12
1.067	0.400	0.170	30°	0.70

Chapter

THEORETICAL ANALYSIS 5

Theoretical explanation for the observed phenomena of scattering from various types of periodic strips over a dielectric sheet with a conducting ground plane is presented in this chapter. There are different methods to solve the problem of scattering from periodic structures. Most of these methods are highly tedious and require much computational time. The method adopted by Kalhor [76] is suitably extended in this thesis. Kalhor analyzed the scattering of electromagnetic waves, from a dielectric slab loaded with a periodic array of perfectly conducting strips, by a mode matching technique. This technique is relatively simple and straight forward.

PROGRESSIVELY VARIED SCS

A dielectric substrate of thickness 'h' loaded with perfectly conducting strips over a ground plane is shown in fig. 5.1. The dielectric is assumed to be lossless. The perfectly

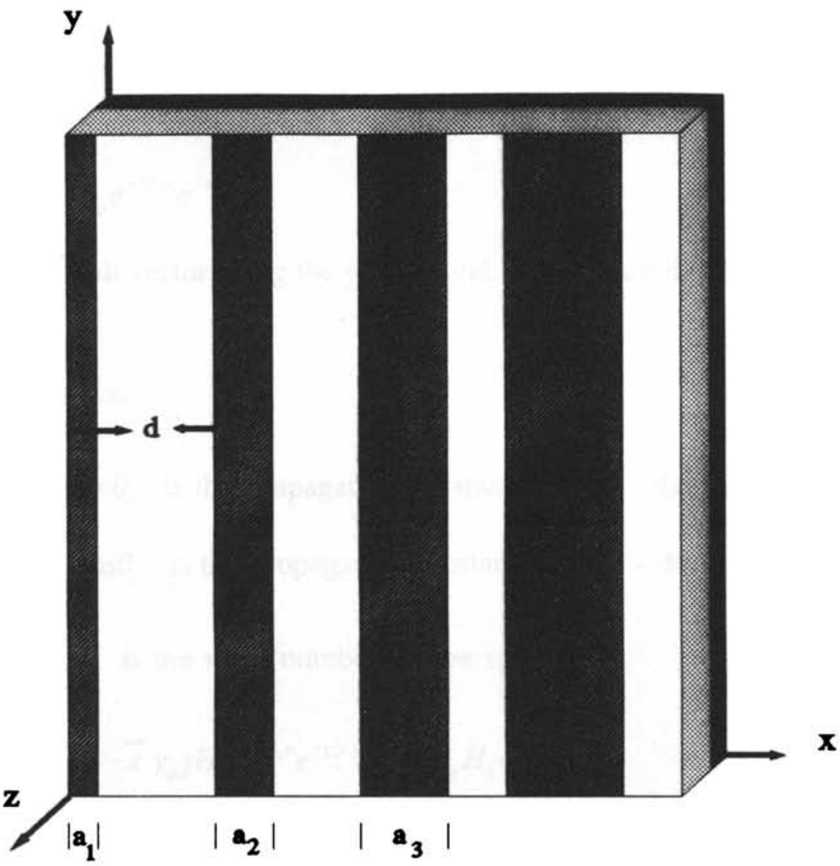

Fig. 5.1 Progressively varied SCS

conducting strips of width 'a' and negligible thickness are arranged with a constant period 'd'. The stripwidths increases in geometric progression.

A plane wave in TM polarisation is incident on the structure. The incident magnetic field at incident angle 'θ_i' after suppression of the exp(jωt) time dependence has the following form

$$\vec{H}_i = \vec{y} H_o e^{-j\beta_o x} e^{j\gamma_o z}$$

where $\vec{y}$ is the unit vector along the y - axis and H_o is the amplitude of the magnetic field

of the incident wave.

$\beta_o = k_o Sin\theta_i$ is the propagation constant along x - direction.

$\gamma_o = k_o Cos\theta_i$ is the propagation constant along z - direction.

$k_o = \dfrac{2\pi}{\lambda}$ is the wave number in free space.

$$\nabla \times \vec{H}_i = -\vec{x}\, \gamma_o j H_o e^{-j\beta_o x} e^{j\gamma_o z} - \vec{z} j\beta_o H_o e^{-j\beta_o x} e^{j\gamma_o z}$$

From Maxwell's equations

$$\nabla \times \vec{H} = j\omega\epsilon\vec{E}$$

$$E_i = -\vec{x}\left[\frac{H_o\gamma_o}{\omega\epsilon_o}\right] e^{-j\beta_o x} e^{j\gamma_o z} - \vec{z}\left[\frac{H_o\beta_o}{\omega\epsilon_o}\right] e^{-j\beta_o x} e^{j\gamma_o z} \qquad \ldots\ldots\ (1)$$

The reflected wave in the region z ≥ h is represented in terms of a summation of plane waves with fields

$$H_r = \vec{y}\sum_{n=-N}^{N} A_n e^{-j\beta_n x} e^{-j\gamma_n (z-h)}$$

where $\beta_n = \beta_o + \dfrac{2n\pi}{d}$

$$\gamma_n = \sqrt{k_o^2 - \beta_n^2} \qquad for \;\; k_o^2 > \beta_n^2$$

$$\gamma_n = -j\sqrt{\beta_n^2 - k_o^2} \qquad for \;\; k_o^2 < \beta_n^2$$

A_n are unknown mode amplitudes to be determined and N is a large integer. The two expressions for γ_n provide propagating and evanescent modes.

$$\nabla \times H_r = \vec{x}\sum_{n=-N}^{N} j\gamma_n A_n e^{-j\beta_n x} e^{-j\gamma_n (z-h)} - \vec{z}\sum_{n=-N}^{N} j\beta_n A_n e^{-j\beta_n x} e^{-j\gamma_n (z-h)}$$

$$E_r = \vec{x}\sum_{n=-N}^{N} \left(\frac{\gamma_n A_n}{\omega\epsilon_o}\right) e^{-j\beta_n x} e^{-j\gamma_n (z-h)} - \vec{z}\sum_{n=-N}^{N} \left(\frac{\beta_n A_n}{\omega\epsilon_o}\right) e^{-j\beta_n x} e^{-j\gamma_n (z-h)} \qquad \ldots\ldots\ldots \quad (2)$$

In the region $0 \le z \le h$ the fields are in terms of upward and downward travelling planewaves.

$$H_d = \vec{y}\sum_{n=-N}^{N} \left[C_n e^{-j\beta_n x} e^{-j\eta_n z} + D_n e^{-j\beta_n x} e^{j\eta_n z}\right]$$

where $\eta_n = \sqrt{k^2 - \beta_n^2} \qquad for \;\; k^2 > \beta_n^2$

$$\eta_n = -j\sqrt{\beta_n^2 - k^2} \qquad for \;\; k^2 < \beta_n^2$$

$$k = k_o\sqrt{\epsilon_r}$$

C_n and D_n are unknown field amplitudes

$$E_d = \vec{x}\sum_{n=-N}^{N} \left[\left(\frac{\eta_n C_n}{\omega\epsilon}\right) e^{-j\beta_n x} e^{-j\eta_n z} - \left(\frac{\eta_n D_n}{\omega\epsilon}\right) e^{-j\beta_n x} e^{j\eta_n z}\right]$$

$$+ \vec{z}\sum_{n=-N}^{N} \left[\left(\frac{-\beta_n C_n}{\omega\epsilon}\right) e^{-j\beta_n x} e^{-j\eta_n z} - \left(\frac{\beta_n D_n}{\omega\epsilon}\right) e^{-j\beta_n x} e^{j\eta_n z}\right] \qquad \ldots\ldots\ldots \quad (3)$$

The required boundary conditions are applied to obtain equations which are to be solved to find out unknown amplitudes.

At z = 0, the tangential electric field should vanish. Enforcing this condition on equation (3) forms

$$\sum_{n=-N}^{N}\left[\left(\frac{\eta_n C_n}{\omega\epsilon}\right)e^{-j\beta_n x}-\left(\frac{\eta_n D_n}{\omega\epsilon}\right)e^{-j\beta_n x}\right]=0$$

Because of the linear independence of the functions $e^{-j\beta_n x}$, the above equation must hold termwise.

$$C_n = D_n$$

At z = h, tangential electric field must be continuous.

Hence

$$-\left(\frac{H_o\gamma_o}{\omega\epsilon_o}\right)e^{-j\beta_o x}e^{j\gamma_o h}+\sum_{n=-N}^{N}\left(\frac{\gamma_n A_n}{\omega\epsilon_o}\right)e^{-j\beta_n x}$$
$$=\sum_{n=-N}^{N}\left[\left(\frac{\eta_n C_n}{\omega\epsilon}\right)e^{-j\beta_n x}e^{-j\eta_n h}-\left(\frac{\eta_n D_n}{\omega\epsilon}\right)e^{-j\beta_n x}e^{j\eta_n h}\right]$$

Since this equality must hold for all x and the exponential functions are linearly independent, the equation must hold for all mode values. So

$$-\left(\frac{H_o\gamma_o}{\omega\epsilon_o}\right)e^{j\gamma_o h}\delta(n)+\left(\frac{\gamma_n A_n}{\omega\epsilon_o}\right)=\left(\frac{\eta_n C_n}{\omega\epsilon}\right)e^{-j\eta_n h}-\left(\frac{\eta_n D_n}{\omega\epsilon}\right)e^{j\eta_n h}$$

$$C_n=\frac{\epsilon_r}{\eta_n(e^{-j\eta_n h}-e^{j\eta_n h})}\left[\gamma_n A_n-H_o\gamma_o e^{j\gamma_o h}\delta(n)\right]$$

At z = h, the tangential electric field must vanish on the conductor $[o \leq x \leq a]$

$$-H_o \gamma_o e^{-j\beta_o x} e^{j\gamma_o h} + \sum_{n=-N}^{N} \gamma_n A_n e^{-j\beta_n x} = 0 \qquad \ldots\ldots\ (4)$$

At z = h, the tangential magnetic field must be continuous in the opening $[a \leq x \leq d]$

$$H_o e^{-j\beta_o x} e^{j\gamma_o h} + \sum_{n=-N}^{N} A_n e^{-j\beta_n x} = \sum_{n=-N}^{N} \left[C_n e^{-j\beta_n x} e^{-j\eta_n h} + D_n e^{-j\beta_n x} e^{j\eta_n h} \right]$$

$$H_o e^{-j\beta_o x} e^{j\gamma_o h} \left[1 + \frac{j\epsilon_r \gamma_o Cot\eta_o h}{\eta_o} \right]$$

$$= \sum_{n=-N}^{N} A_n e^{-j\beta_n x} \left[\frac{\epsilon_r \gamma_n}{\eta_n} \left(\frac{1 + e^{-2j\eta_n h}}{-1 + e^{-2j\eta_n h}} \right) - 1 \right] \qquad \ldots\ldots\ (5)$$

The structure studied consists of ten strips arranged in regular period. The stripwidths in each period increases in geometric progression ($a_1, a_2, \ldots\ldots\ldots a_{10}$). Equations (4) and (5) are enforced at (2N + 1) points over $0 \leq x \leq 10d$ (entire region) to obtain (2N + 1) equations which are to be solved to find out the unknown A_n. N is chosen to be 35 to get good convergence. Equation (5) is applied when x lies between [a_1 & d], [($d+a_2$) & 2d], [($2d + a_3$) & 3d], [($3d + a_4$) & 4d], [($4d + a_5$) & 5d], [($5d + a_6$) & 6d], [($6d + a_7$) & 7d], [($7d + a_8$) & 8d], [($8d + a_9$) & 9d] and [($9d + a_{10}$) & 10d]. Equation (4) is applied when x has values other than the above region and within the range $0 \leq x \leq 10d$. The matching points are chosen so that they are equally distributed over the whole structure.

Figure 5.2 shows the variation of zeroth mode with frequency for a structure with $\varepsilon_r = 2.5$, period d = 3cm, common ratio r = 1.08, angle of incidence $\theta_i = 40°$ and dielectric thickness h = 0.39cm in comparison with that of a plane reflecting surface of the same dimensions. For the sake of comparison, the experimentally obtained results are superimposed on the theoretically calculated power. Fig. 5.3 shows the variation of relative reflected power with angle of incidence for the same structure and fig. 5.4 shows the

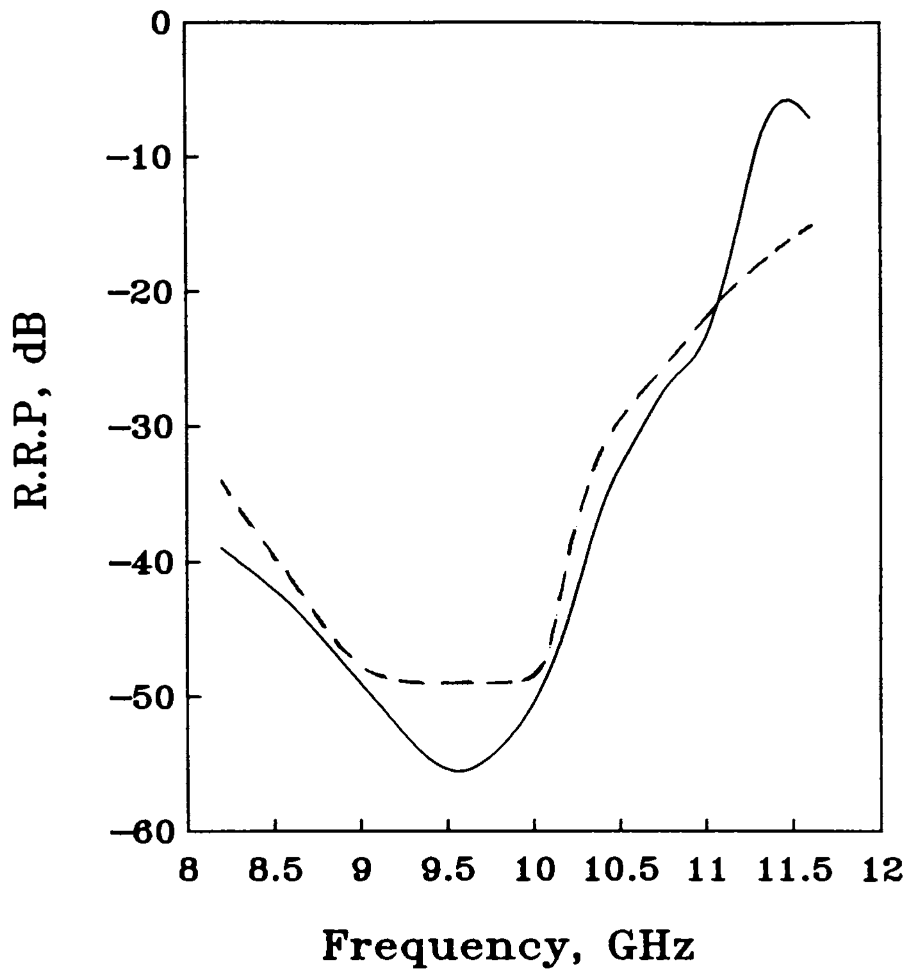

Fig. 5.2 Variation of relative reflected power with frequency

[Progressively varied SCS] d = 3cm, r = 1.08, θ_i = 40°, h = 0.39cm

——— Theoretical - - - - - - - Experimental

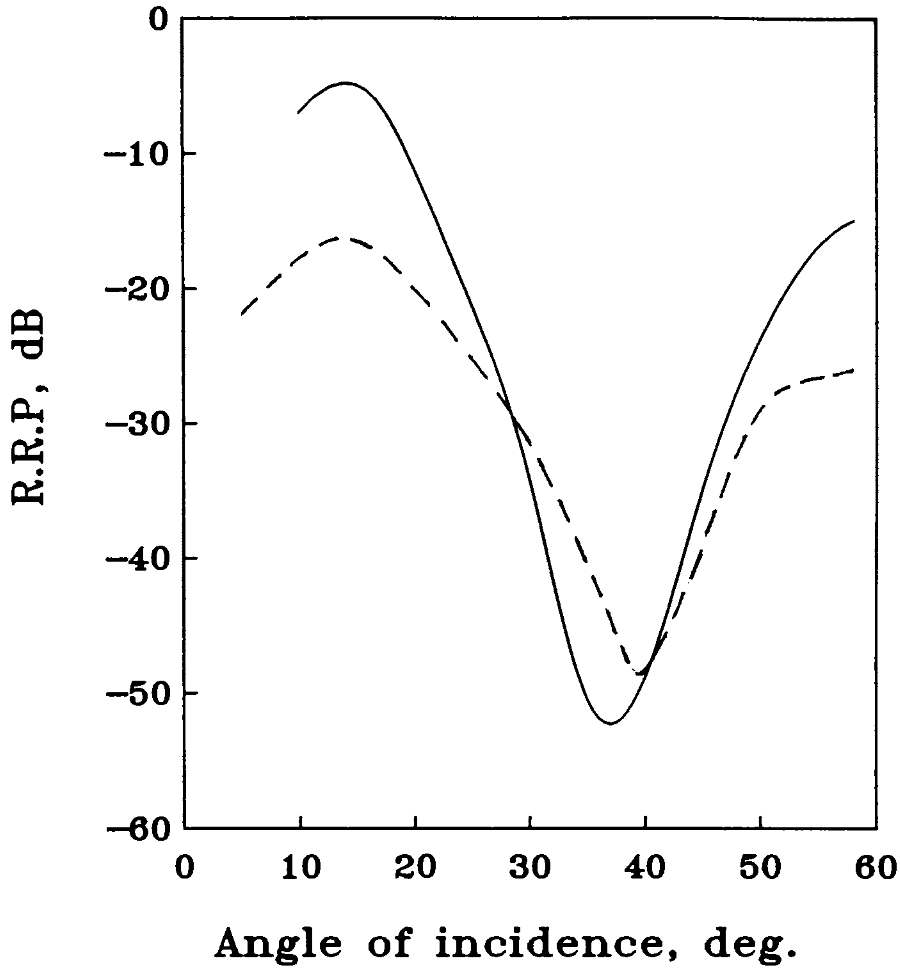

Fig. 5.3 Variation of relative reflected power with angle of incidence.

[Progressively varied SCS] d = 3cm, r = 1.08, f = 10 GHz, h = 0.39cm

———— Theoretical - - - - - - - Experimental

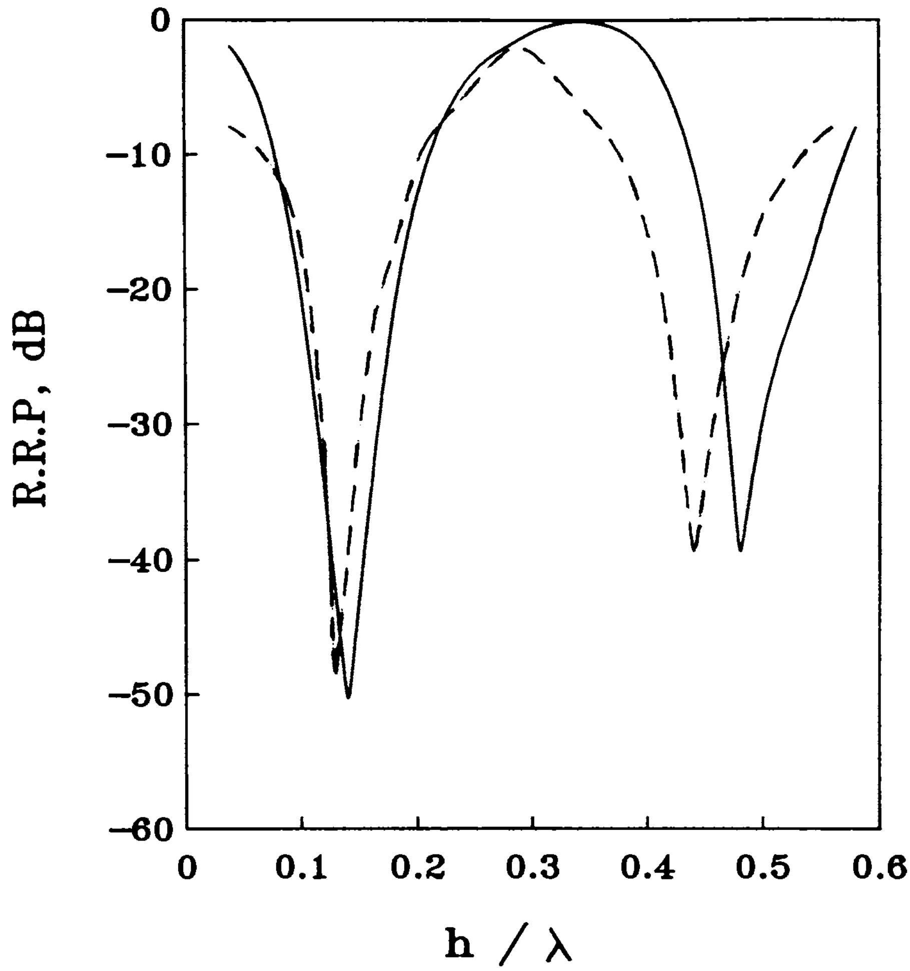

Fig. 5.4 Variation of relative reflected power with dielectric thickness.

[Progressively varied SCS] d = 3cm, r = 1.08, f = 10 GHz, θ_i = 40°

———— Theoretical - - - - - - - Experimental

variation of R.R.P with that of dielectric thickness. The reduction in RCS obtained experimentally is found to be theoretically true. The small discrepancy in fig.5.4 for very large h / λ may be due to experimental error in measurements on dielectric material thickness and small approximations used in the theoretical analysis.

TAPERED SCS

The above equations can be applied for tapered SCS also. Bandwidth enhancement is obtained experimentally in TM polarisation. The structure is segmented into 'n' sections as shown in fig. 5.5. Each section is considered independent. Equations (4) & (5) are enforced at (2N + 1) points over $0 \le x \le d$ to obtain (2N + 1) equations which are to be solved to find out unknown A_n from each segment. The matching points are chosen so as to be equally distributed over the whole structure. The reflected mode from each segment is vectorially added to obtain the overall reflected power from the whole SCS. The number of segments 'n' and number of modes 'N' are selected as 50 and 35 respectively. Fig. 5.6 shows the variation of relative reflected power with frequency for the structure of dimensions d = 2.5 cm, a_1 = 2cm, a_2 = 0.5 cm and h = 3.7mm. The experimentally obtained result is superimposed on the curve obtained theoretically. Fig. 5.7 gives the variation of R.R.P with angle of incidence and fig. 5.8 that of with dielectric thickness. Fairly good agreement between theoretical and experimental results is observed from the figures.

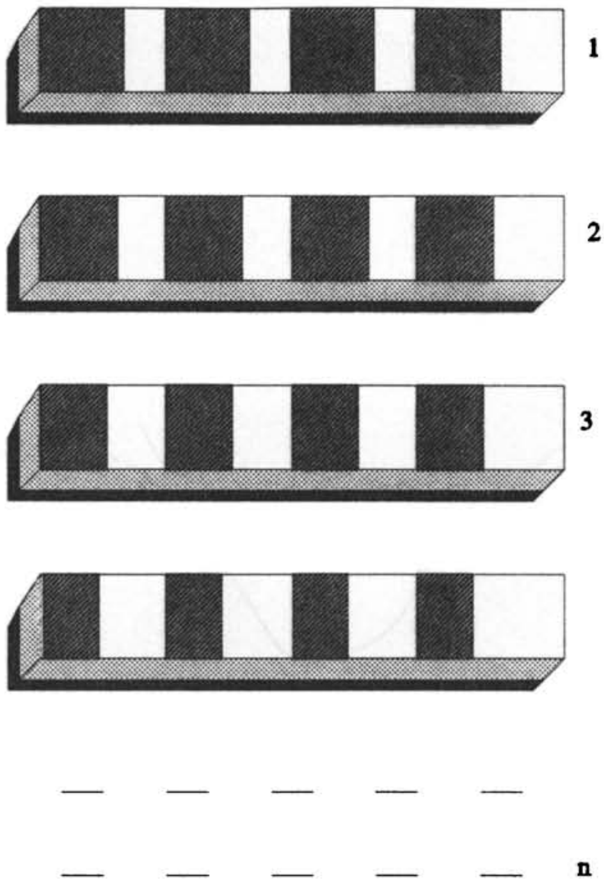

Fig. 5.5 Segmented Tapered SCS

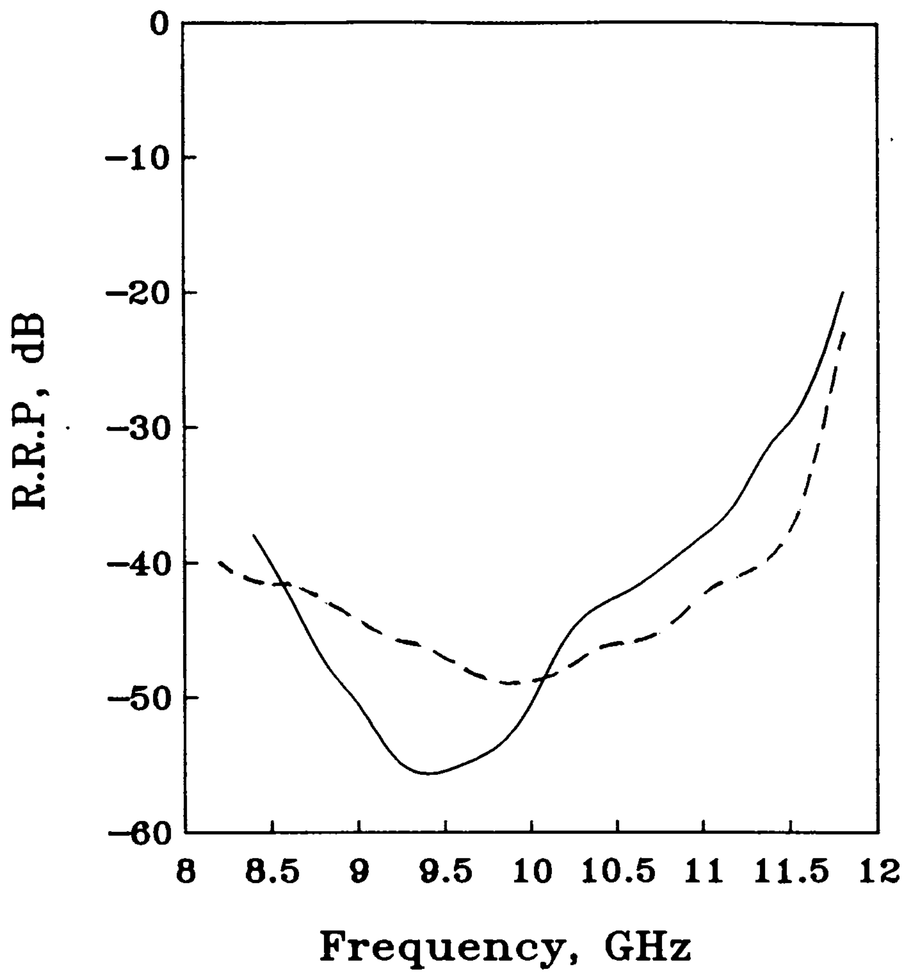

Fig. 5.6 Variation of relative reflected power with frequency

[Tapered SCS] d = 2.5cm, a_1 = 2cm, a_2 = 0.5cm, θ_i = 50°, h = 0.37cm

———— Theoretical - - - - - - - Experimental

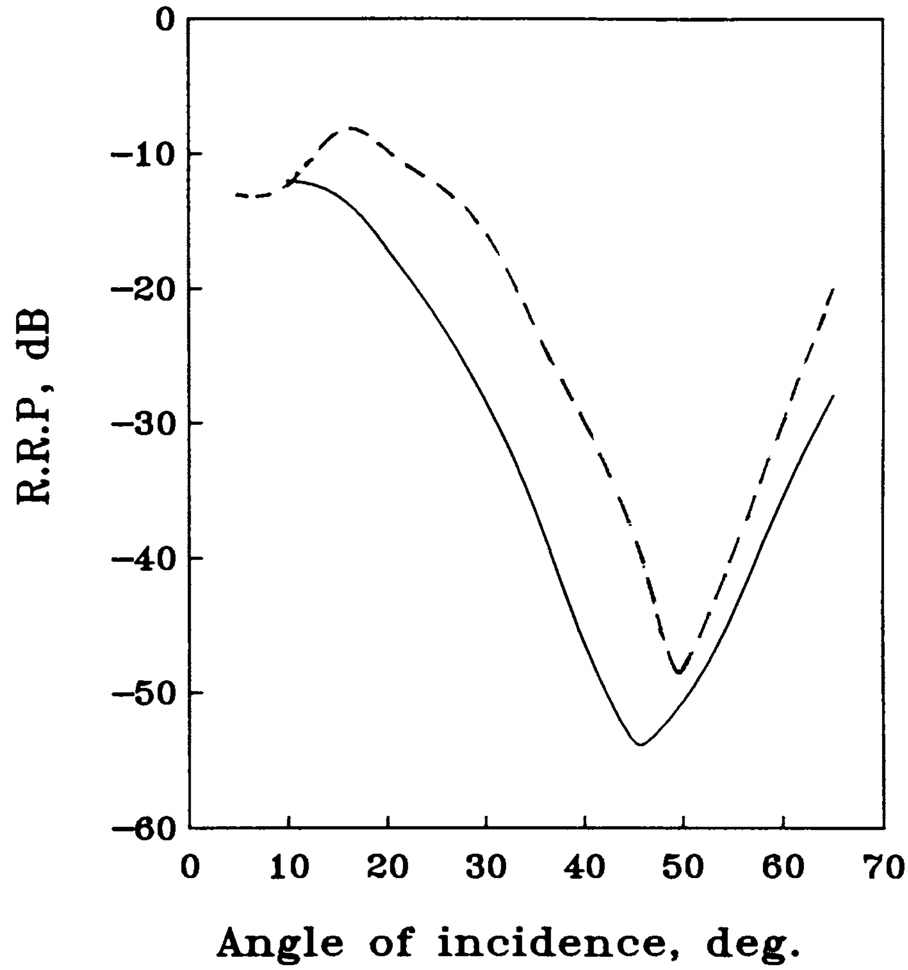

Fig. 5.7 Variation of relative reflected power with angle of incidence

[Tapered SCS] $d = 2.5cm$, $a_1 = 2cm$, $a_2 = 0.5cm$, $f = 10GHz$, $h = 0.37cm$

———— Theoretical - - - - - - - Experimental

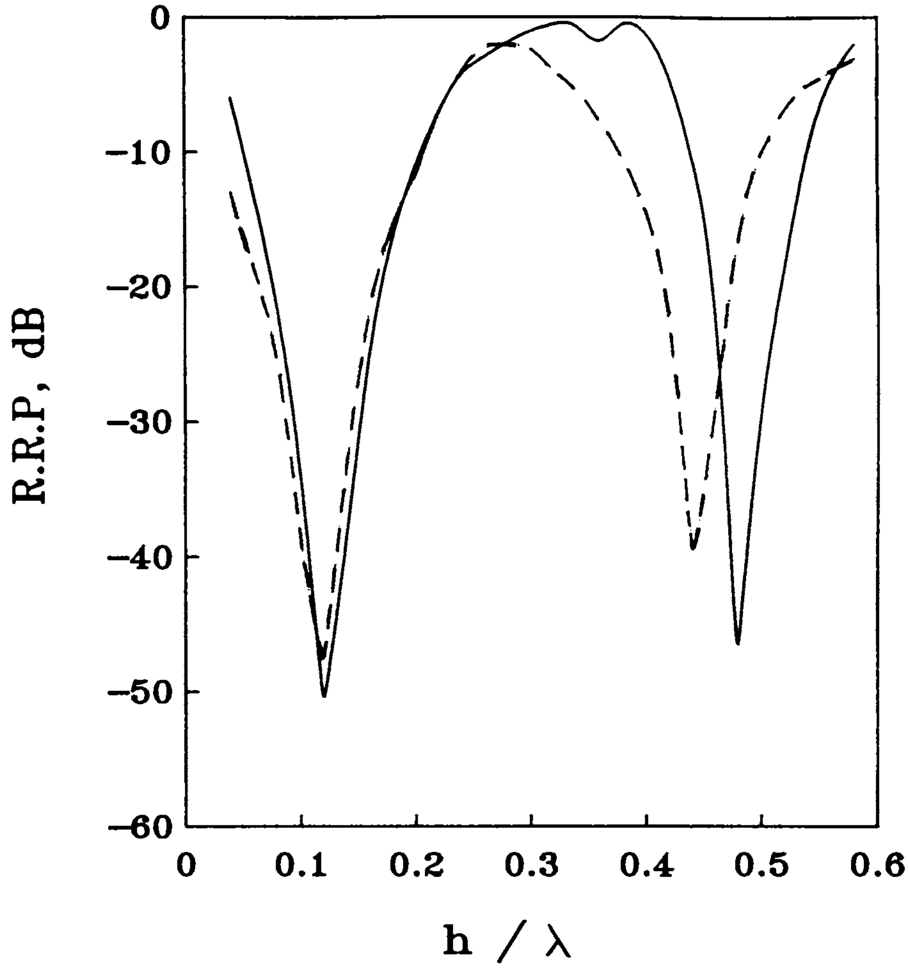

Fig. 5.8 Variation of relative reflected power with dielectric thickness

[Tapered SCS] d = 2.5cm, a_1 = 2cm, a_2 = 0.5cm, θ_i = 50°, f = 10 GHz

——————— Theoretical - - - - - - - Experimental

DUAL PERIODIC RHOMBIC SHAPED STRUCTURE

Strip grating structure modified to rhombic shaped structure, as explained earlier, is represented in fig. 5.9. The basic unit which gets repeated over the whole structure is shown in fig. 5.10.

When a plane wave is incident on an array of such a structure in TE polarisation, the incident electric field at incident angle θ_i, after suppression of exp $(j\omega t)$ time dependence, has the following form

$$E_i = \vec{y} E_o e^{-j\beta_o x} e^{j\gamma_o z} \qquad \ldots\ldots\ (6)$$

where $\vec{y}$ is the unit vector along the y-axis and E_o is the amplitude of the electric field of the incident wave.

$\beta_o = k_o Sin\theta_i$ is the propagation constant along the x-direction

$\gamma_o = k_o Cos\theta_i$ is the propagation constant along the z-direction

$k_o = \frac{2\pi}{\lambda}$ is the wave number in free space.

$$\nabla \times E_i = -\vec{x} j\gamma_o E_o e^{-j\beta_o x} e^{j\gamma_o z} - \vec{z} j\beta_o E_o e^{-j\beta_o x} e^{j\gamma_o z}$$

$$H_i = \vec{x}\left[\frac{E_o\gamma_o}{\omega\mu_o}\right] e^{-j\beta_o x} e^{j\gamma_o z} + \vec{z}\left[\frac{E_o\beta_o}{\omega\mu_o}\right] e^{-j\beta_o x} e^{j\gamma_o z}$$

The reflected wave in the region $z \geq h$ is represented in terms of a summation of plane waves with fields

$$E_r = \vec{y}\sum_{n=-N}^{N} A_n e^{-j\beta_n x} e^{-j\gamma_n (z-h)} \qquad \ldots\ldots\ (7)$$

where $\beta_n = \beta_o + \frac{2n\pi}{d}$

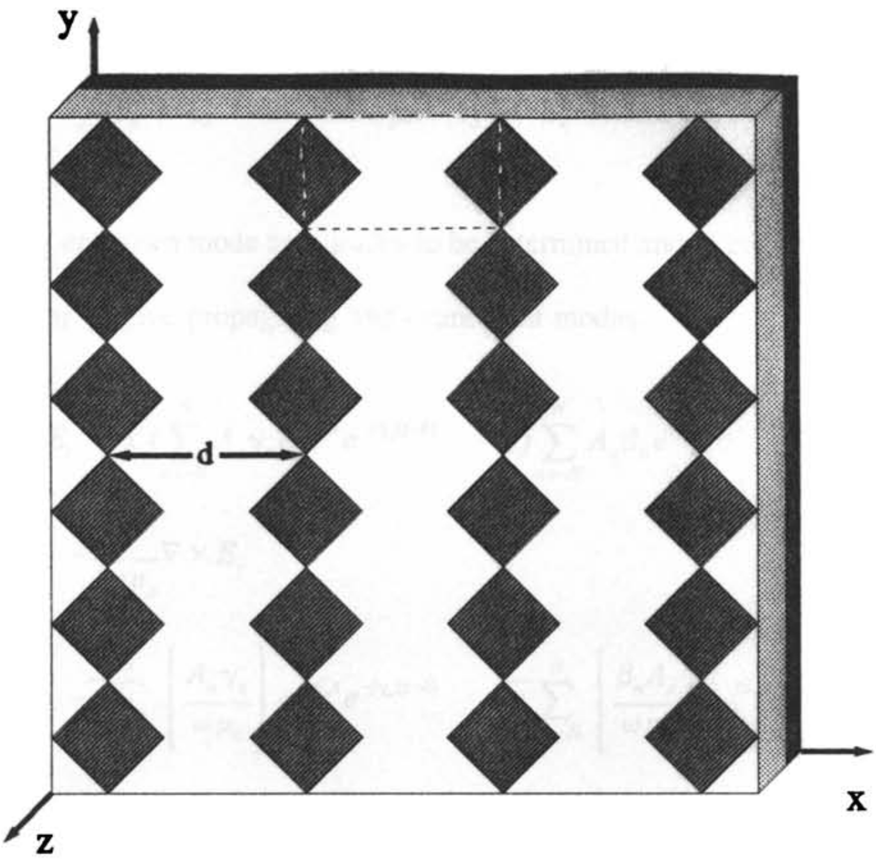

Fig. 5.9 Dual periodic rhombic shaped structure

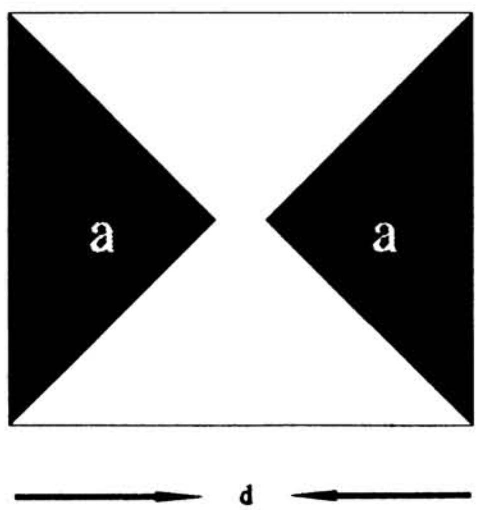

Fig. 5.10 Unit cell

$$\gamma_n = \sqrt{k_o^2 - \beta_n^2} \qquad for \;\; k_o^2 > \beta_n^2$$

$$\gamma_n = -j\sqrt{\beta_n^2 - k_o^2} \qquad for \;\; k_o^2 < \beta_n^2$$

A_n are unknown mode amplitudes to be determined and N is a large integer. The two expressions for γ_n give propagating and evanescent modes.

$$\nabla \times E_r = \vec{x} j \sum_{n=-N}^{N} A_n \gamma_n e^{-j\beta_n x} e^{-j\gamma_n (z-h)} \quad - \vec{z} j \sum_{n=-N}^{N} A_n \beta_n e^{-j\beta_n x} e^{-j\gamma_n (z-h)}$$

$$H_r = -\frac{1}{j\omega\mu_o} \nabla \times E_r$$

$$H_r = -\vec{x} \sum_{n=-N}^{N} \left[\frac{A_n \gamma_n}{\omega \mu_o} \right] e^{-j\beta_n x} e^{-j\gamma_n (z-h)} \quad + \vec{z} \sum_{n=-N}^{N} \left[\frac{\beta_n A_n}{\omega \mu_o} \right] e^{-j\beta_n x} e^{-j\gamma_n (z-h)}$$

In the region $0 \le z \le h$ the solution is formed in terms of upward and downward travelling plane waves.

$$E_d = \vec{y} \sum_{n=-N}^{N} \left[C_n e^{-j\beta_n x} e^{-j\eta_n z} + D_n e^{-j\beta_n x} e^{j\eta_n z} \right] \qquad \ldots\ldots\ldots \quad (8)$$

where $\eta_n = \sqrt{k^2 - \beta_n^2} \qquad for \;\; k^2 > \beta_n^2$

$$\eta_n = -j\sqrt{\beta_n^2 - k^2} \qquad for \;\; k^2 < \beta_n^2$$

$$k = k_o \sqrt{\epsilon_r}$$

C_n and D_n are unknown field amplitudes.

$$H_d = \vec{x} \sum_{n=-N}^{N} \left[\left[\frac{-C_n \eta_n}{\omega \mu_o} \right] e^{-j\beta_n x} e^{-j\eta_n z} + \left[\frac{D_n \eta_n}{\omega \mu_o} \right] e^{-j\beta_n x} e^{j\eta_n z} \right]$$
$$+ \vec{z} \sum_{n=-N}^{N} \left[\left[\frac{C_n \beta_n}{\omega \mu_o} \right] e^{-j\beta_n x} e^{-j\eta_n z} + \left[\frac{D_n \beta_n}{\omega \mu_o} \right] e^{-j\beta_n x} e^{j\eta_n z} \right]$$

The required boundary conditions are applied to obtain equations that are to be solved to findout unknown amplitudes.

At z = 0, the tangential electric field should vanish. Enforcing this condition on (8)

$$\sum_{n=-N}^{N} (C_n + D_n) e^{-j\beta_n x} = 0$$

Because of linear independence of functions $e^{-j\beta_n x}$ the above equations must hold termwise.

$$- C_n = D_n$$

At z = h, tangential electric field must be continuous.

$$E_o e^{-j\beta_o x} e^{j\gamma_o h} + \sum_{n=-N}^{N} A_n e^{-j\beta_n x} = \sum_{n=-N}^{N} \left(C_n e^{-j\beta_n x} e^{-j\eta_n h} + D_n e^{-j\beta_n x} e^{j\eta_n h} \right)$$

Since this equality must hold good for all x and the exponential functions are linearly independent, the equation must hold termwise.

$$E_o e^{j\gamma_o h} \delta(n) + A_n = C_n e^{-j\eta_n h} + D_n e^{j\eta_n h}$$

$$C_n = -D_n = \frac{E_o e^{j\gamma_o h} \delta(n)}{(e^{-j\eta_n h} - e^{j\eta_n h})} + \frac{A_n}{(e^{-j\eta_n h} - e^{j\eta_n h})}$$

At z = h, the tangential electric field must vanish on the conductor $[o \le x \le a]$

$$E_o e^{-j\beta_o x} e^{j\gamma_o h} + \sum_{n=-N}^{N} A_n e^{-j\beta_n x} = 0 \qquad \ldots\ldots\ldots (9)$$

At z = h, the tangential magnetic field must be continuous in the opening $[a \le x \le (d-a)]$

$$E_o \gamma_o e^{-j\beta_o x} e^{j\gamma_o h} - \sum_{n=-N}^{N} A_n \gamma_n e^{-j\beta_n x} = \sum_{n=-N}^{N} -C_n \eta_n e^{-j\beta_n x} e^{-j\eta_n h} + \sum_{n=-N}^{N} D_n \eta_n e^{-j\beta_n x} e^{j\eta_n h}$$

$$E_o e^{-j\beta_o x} e^{j\gamma_o h}\left[\gamma_o + j\eta_o Cot\eta_o h\right] = \sum_{n=-N}^{N} A_n e^{-j\beta_n x}\left[\gamma_n - \eta_n\left\{\frac{1 + e^{-2j\eta_n h}}{-1 + e^{-2j\eta_n h}}\right\}\right] \quad \ldots (10)$$

Equations (9) and (10) are enforced at (2N + 1) points over $0 \leq x \leq d$ to obtain (2N + 1) equations that are to be solved to find out unknown A_n. The matching points are chosen to be equally distributed over the whole structure.

Fig. 5.11 shows the zero mode variation with angle of incidence θ_i for the rhombic shaped structure with dimensions d = 3cm, l = 1.4cm, $\alpha = \beta = 90°$, h = 0.475cm. Results obtained experimentally are drawn along with theoretical results. Angular range for RCS reduction observed experimentally is found to be almost true theoretically also. Variation of relative reflected power with frequency and that of dielectric thickness are shown in figures 5.12 and 5.13 respectively.

For all the structures described above, the theoretical curves are in fairly good agreement with experimental results. The little discrepancies found are due to the assumptions adopted for theoretical analysis.

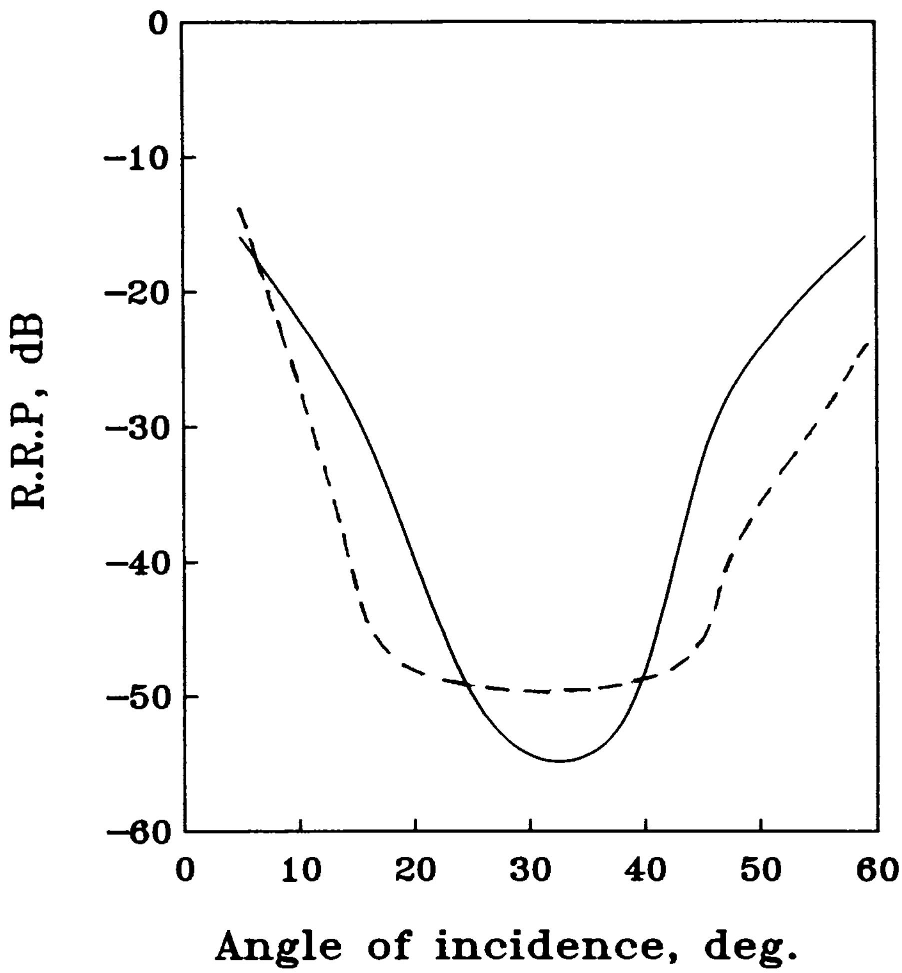

Fig. 5.11 Variation of relative reflected power with angle of incidence

[Dual periodic rhombic shaped structure]
d = 3cm, l = 1.4cm, $\alpha = \beta = 90°$, h = 0.475cm and f = 10 GHz

——— Theoretical - - - - - - - Experimental

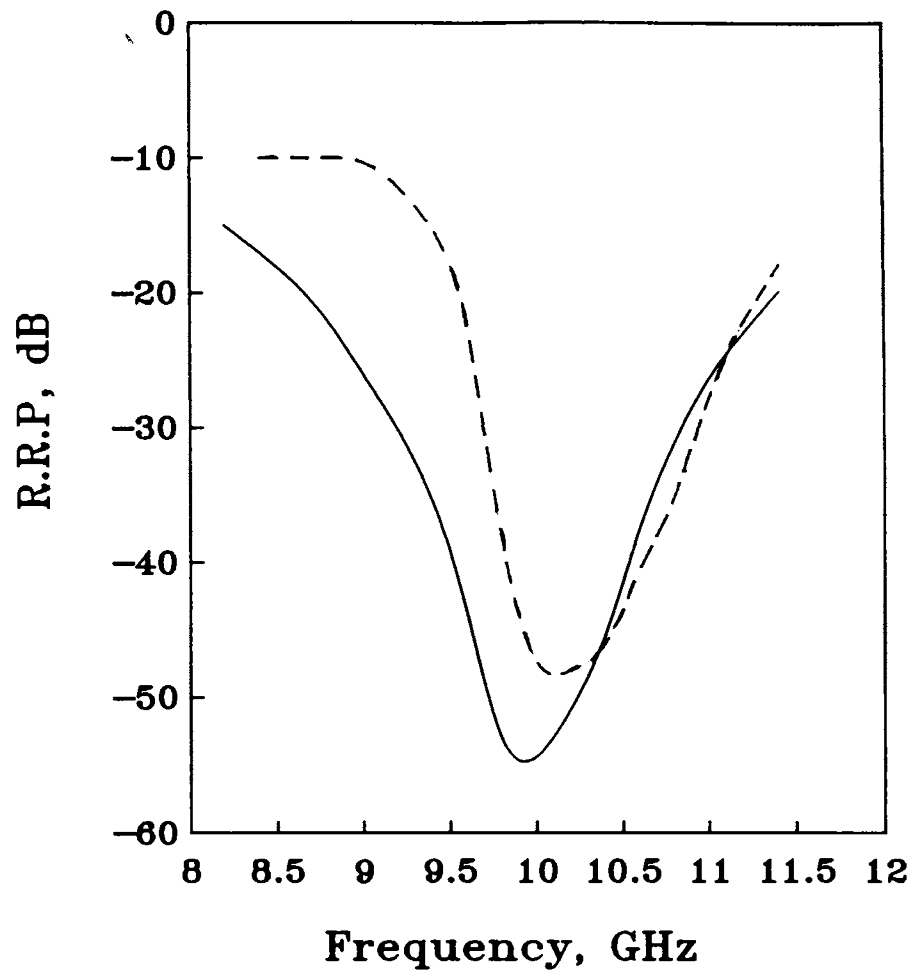

Fig. 5.12 Variation of relative reflected power with frequency

[Dual periodic rhombic shaped structure]
d = 3cm, l = 1.4cm, $\alpha = \beta = 90°$, h = 0.475cm and $\theta_i = 30°$

———— Theoretical - - - - - - - Experimental

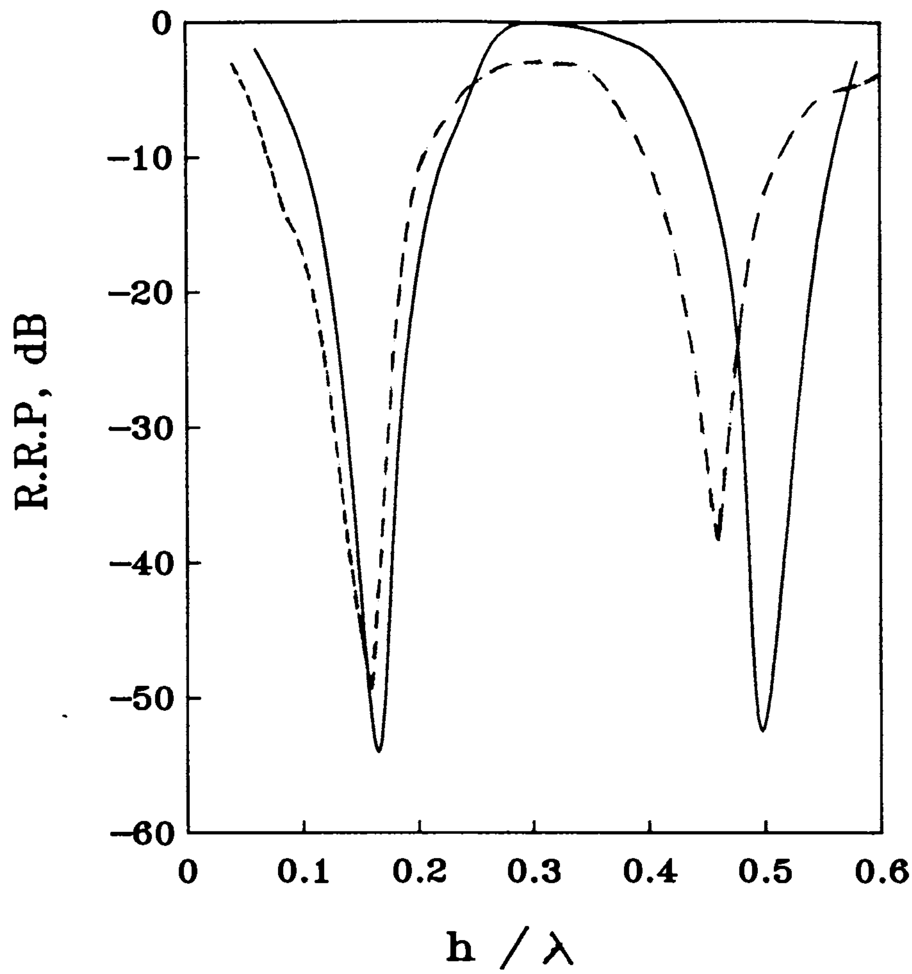

Fig. 5.13 Variation of relative reflected power with dielectric thickness.

[Dual periodic rhombic shaped structure]
d = 3cm, l = 1.4cm, $\alpha = \beta = 90°$, $\theta_i = 30°$, f = 10 GHz

———— Theoretical - - - - - - - Experimental

Chapter

CONCLUSIONS

6

Conclusions drawn and the comments on the results of the investigations carried out for the development of wideband SCS's and other periodic structures are presented in this chapter. Eventhough the attempt was development of techniques to reduce RCS of planar surfaces, the main interest was focused on determining the reflected RF power from metallic targets and thus to estimate their reflectivity. The electromagnetic power reflected from the strip-grating system is compared to that from plane metallic targets of same physical dimensions. From these facts, it is possible to evaluate the level of RCS of the target. This is useful in many ways, as the absolute value of RCS is not always necessary when the reflectivity of the target is known, provided that the other parameters like range, transmitting power and isolation between transmitter and receiver are kept unchanged. It has already been established [38] that reflections from a conducting surface can be eliminated using corrugations of proper period and depth. Fabrication of metallic corrugations is a time consuming and difficult task. Thin conducting strips loaded on a dielectric substrate backed with a metallic reflector can produce equivalent effects of perfectly blazed corrugations [70]. This is a very simple, easy and quicker procedure. The advantages of the newly developed structures over the existing structure are examined in this chapter. This chapter concludes with a description of the scope for further work in this field.

INFERENCES FROM THE EXPERIMENTAL & THEORETICAL STUDIES

Earlier studies on SCS's have already established that SCS can eliminate reflection and thereby reduce the RCS of plane metallic surfaces. But this property is restricted to limited angular range and limited frequency range. The available parameters of the structure are modified to overcome these limitations.

Progressively varied SCS formed by modifying the conventional SCS along the x-direction is found to increase the bandwidth of reflection elimination in TM polarisation. Figure 4.5 shows the recorded relative reflected power with frequency for certain structures. From table 4.1 it is clear that bandwidth of progressively varied SCS is greater when compared to that of conventional SCS. A bandwidth of more than ten times is obtained with most of the structures. Eventhough the variation of bandwidth with structure parameters is not regular, it is observed that bandwidth is more for structures whose stripwidths lie in the range between d / 4 and 3d / 4.

When SCS was modified along the y-direction, it forms a tapered SCS. The optimised structure was found to eliminate reflection almost over the entire X-band in TM polarisation. The bandwidth enhancement is also clear from the observation in figures 4.10

which show the variation of relative reflected power with frequency. The reason for the increase in bandwidth may be due to the changing stripwidth, which results in a large number of elementary gratings of different parameters, which resonate for different frequencies. The relation of bandwidth with structure parameters is clear from plots 4.11. It is observed that bandwidth is more when 'a_1' lies between $\lambda / 2$ and $3\lambda / 4$ and 'a_2' lies between $\lambda / 8$ and $\lambda / 4$.

Dual aspect ratio strips were fabricated by providing variations along the strip direction. The bandwidth provided by these structures is not much greater than that of self complementary strip grating. One advantage observed by this structure is that simultaneous elimination of specular reflection is possible for TE and TM polarisation as shown in fig.4.15 (c). That is a structure with same dielectric thickness, at same angle of incidence and same frequency eliminates specular reflection in TE and TM polarisation.

Dual periodic rhombic shaped structure has a periodicity 'd' for strips and each strip is given a regular periodic variation in dimension along its length. Each strip consists of a number of rhombic shaped elements of sidelength 'l' and internal angles 'α' & 'β'. These structures can eliminate reflection over a wide angular range in TE polarisation, which was not at all possible with conventional strip grating. Fig. 4.19 shows the variation of relative reflected power with angle of incidence for these types of structures. An angular range of 30° where reflection is low is made possible with the optimised structure. The variation of bandwidth and angular range with structure parameter is clear from table 4.6. It is observed that when the sidelength 'l' is around $\lambda / 4$ bandwidth is high and when 'l' is around $\lambda / 2$, angular range is high. It is also observed that when $\alpha = \beta = 90°$ angular range is higher than conventional SCS.

Another type of structure was formed by giving small gaps along the strip grating. When small rectangular gaps were given along the x-axis, the structure behaved like conventional strip gratings. When the gaps were given in an inclined way the structure behaved as reflection polariser. Gaps given in an angular way formed V-shaped elements arranged periodically. From plots 4.25 and 4.26, it is clear that angular range for reflection elimination increases for TE and TM polarisation compared to conventional strip grating. But the advantage gained in this case is less than that gained with rhombic shaped structures. Plots 4.27 and 4.28 makes clear that bandwidth also increases more than that obtained with conventional strip gratings. But it does not increase as it increases with progressively varied and tapered SCS's. One additional advantage of this structure is that circular polarisation can be achieved using this structure as illustrated in fig. 4.29.

Analysis of the scattering of electromagnetic waves from a dielectric slab loaded with a periodic array of perfectly conducting strips, using a mode matching technique is extended to explain the scattering from modified SCS's. In this approach the fields are expanded in terms of suitable propagating and evanescent modes in various regions. Boundary conditions are then enforced to obtain equations that are solved simultaneously to obtain the unknown wave amplitudes. Figures 5.2 to 5.8 and 5.11 to 5.13 show the experimental and theoretical results obtained for different grating structures. It is clear from the plots that theoretical results are almost in agreement with experimental results. The small discrepancies found are due to the approximations adopted for theoretical analysis. However this theory is found to be inadequate to explain the scattering from periodic elements with gaps and hence it needs further modifications. This leaves enough scope for further investigation in this field.

SCOPE FOR FURTHER WORK IN THE FIELD

Application of the SCS technique on real - time targets like models of aircrafts, ships, missiles etc. and reduction of their RCS is an important work to be taken up in this area. These complex shapes need much attention and careful analysis for implementing SCS technique. This is because same configuration may not be successful for different parts of the target. Each part of such target must have different type of configuration. More detailed investigation could be carried out in these directions. RCS reduction for wide angular range and wide frequency range for planar metallic targets can be achieved by this work. Investigations can be made whether this is possible with targets of other regular shapes. Giving gaps in the strip grating system has been suggested in this thesis. The advantages of this system is not fully studied. It is possible to take up different parameters, for detailed study, with strips of different dimensions. The effect of different dielectric materials for RCS reduction could be taken as a problem for further investigations.

The structure has potential applications as polarizers, frequency multiplexers and scanners in addition to multipath interference suppression and reduction of RCS of targets. The main disadvantage encountered in the present study is the enhancement of RCS in certain angles. This requires a further detailed investigation. The elimination of reflection for wider angle of incidences and wider frequency ranges than those obtained in this study for both polarisations may be possible by the critical selection of the available parameters. The final goal in the study should be to achieve complete reduction of RCS of targets.

Appendix

A

REDUCTION OF RCS OF CORNER REFLECTORS

INTRODUCTION

The enhanced backscattering cross section of corner reflectors make them an attractive target in RCS studies. The large echoes from these targets arise from multiple reflections between two or three mutually orthogonal flat surfaces forming the reflectors. Both dihedral and trihedral corners are usually formed in the mechanical structures of ships, aircrafts and vehicles, and they create the major scattering centres of such targets. The RCS reduction of such inevitable corner structures will be of great importance in the design and construction of these complex targets with reduced detectability in a radar system. It has been reported that RCS reduction of corners can be achieved by altering the mutual orthogonality of the flat surfaces [100]. The disadvantage of this technique is that it has to be incorporated at the engineering design phase itself. Simulated Corrugated Surfaces (SCS) have been reported for the RCS reduction of planar targets [70]. RCS reduction of corner reflectors using SCS technique is discussed in this appendix.

EXPERIMENTAL SETUP

SCS are fabricated by etching thin conducting strips with period 'd' over a dielectric substrate of thickness 'h'. They are loaded on dihedral corner reflector and trihedral corner reflector as shown in figures A.1 and A.2.

The corner reflector is mounted on a target support which is attached to a scientific Atlanta 4131 turn-table. This can be adjusted at different angular positions with respect to incident radiation. The RCS measurements at X-band were carried out inside a microwave anechoic chamber. The instrumentation radar consists of HP 8510B Network Analyser along with a synthesized sweep source and an S-parameter test set, controlled by HP 9000/300 series instrumentation computer. A bistatic method is used for the measurement of backscattered power in dBsm. dBsm means 'decibels above a square metre'. It is a unit referred for RCS in standard references [2]. Proper time gating and averaging is used for the measurement.

EXPERIMENTAL RESULTS

The RCS measurements of corner reflectors and SCS loaded corner reflectors were made for E-polarised electromagnetic wave. RCS reduction obtained for SCS loaded corner reflector with period d = 3cm, stripwidth a = 1.5cm and dielectric thickness h = 0.54 cm is discussed.

Figure A.3 (a) presents the variation of RCS with frequency for dihedral corner reflector (DCR). Dotted line shows the variation for DCR without SCS and solid line shows the variation for DCR with SCS at normal incidence. From the figure it is clear that RCS of

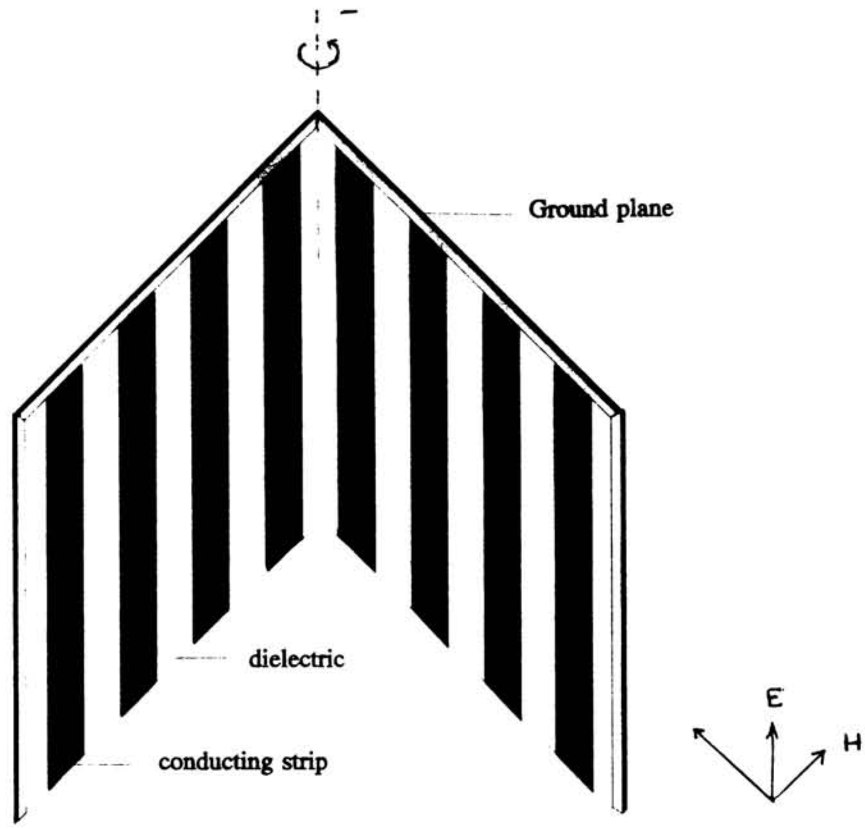

Fig. A.1 Strip loaded dihedral corner reflector

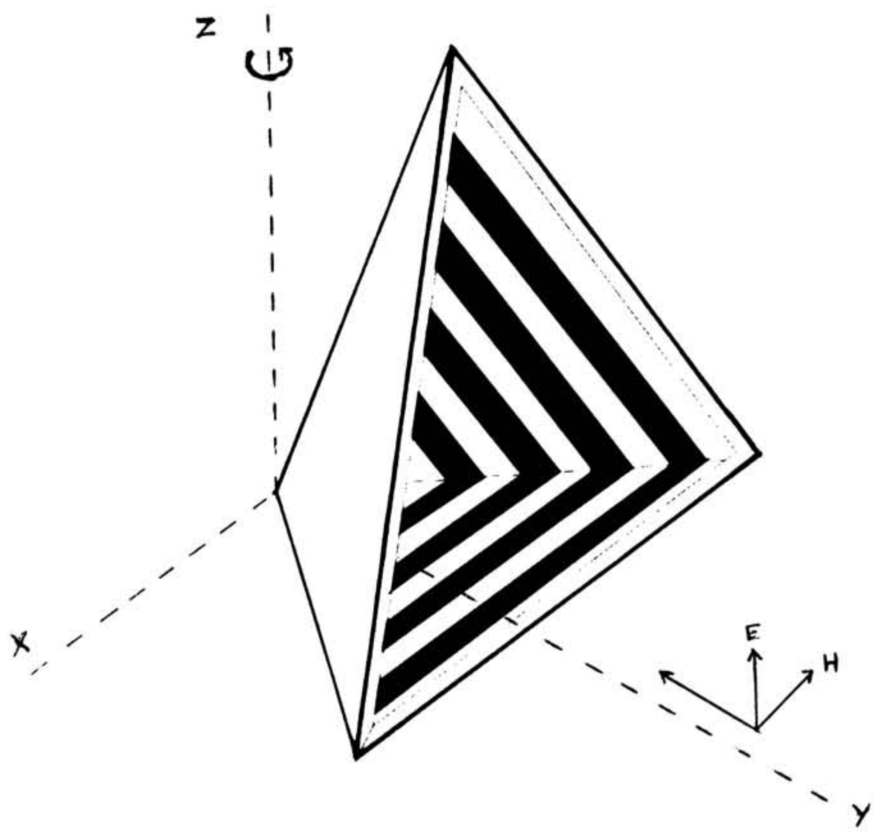

Fig. A.2 Strip loaded trihedral corner reflector

DCR is reduced by about 30 dBsm at 10.2 GHz with the loading of SCS. The variation of RCS with azimuth angle for strip loaded DCR compared to a DCR without SCS is shown in figure A.3 (b). RCS of dihedral corner reflector is found to be reduced appreciably with the loading of SCS.

The effect of SCS loading on the RCS of trihedral corner reflector (TCR) with frequency is shown in figure A.4 (a). Dotted line represents that for TCR and solid line represents that for strip loaded TCR. Variation of RCS with azimuth angle for strip loaded trihedral corner reflector with period d = 3 cm, stripwidth a = 1.5 cm and dielectric thickness h = 0.56 cm in comparison with TCR without SCS is given in figure A.4 (b). From the figures it is observed that RCS of Trihedral corner reflector can be reduced considerably with the application of SCS.

CONCLUSIONS

The backscattering cross section of corner reflectors, which is large due to the mutual perpendicularity of flat surface is greatly reduced by loading SCS. This need not be applied at the design step of the target, but can be used in the location found to be more hazardous for radar detection after the completion of the target. This technique shall find potential use in the RCS reduction of targets in defence and space applications.

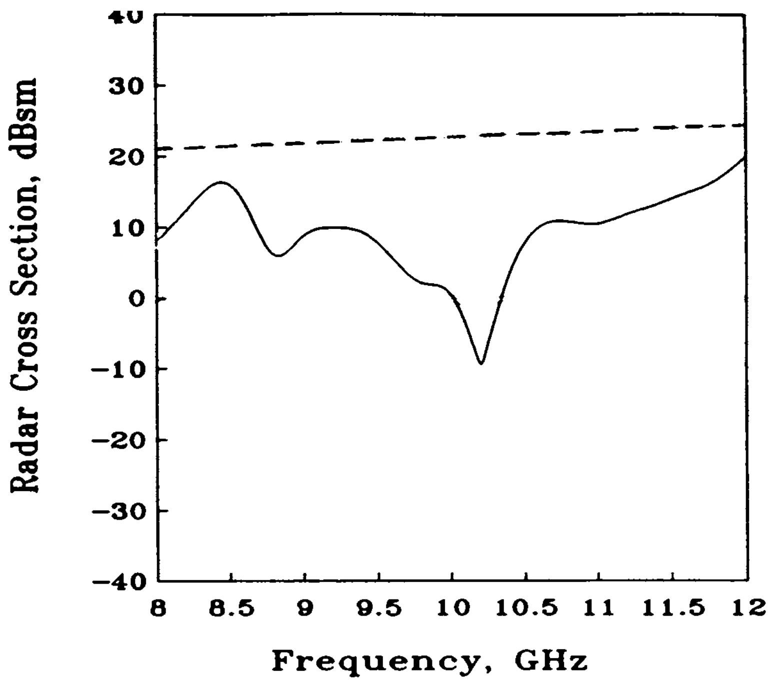

Fig. A.3(a). Variation of RCS with frequency.
- - - - - - DCR, ——— Strip loaded DCR

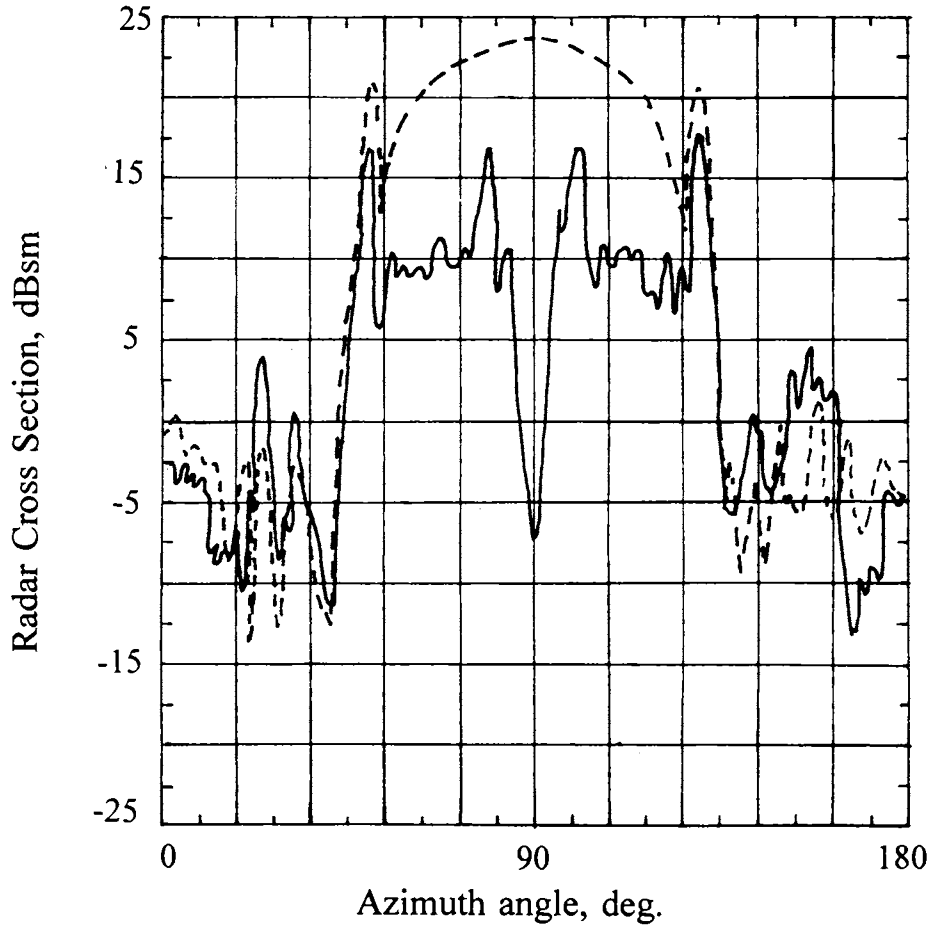

Fig. A.3(b) Variation of RCS with azimuth angle.
- - - - - - DCR ——— Strip loaded DCR

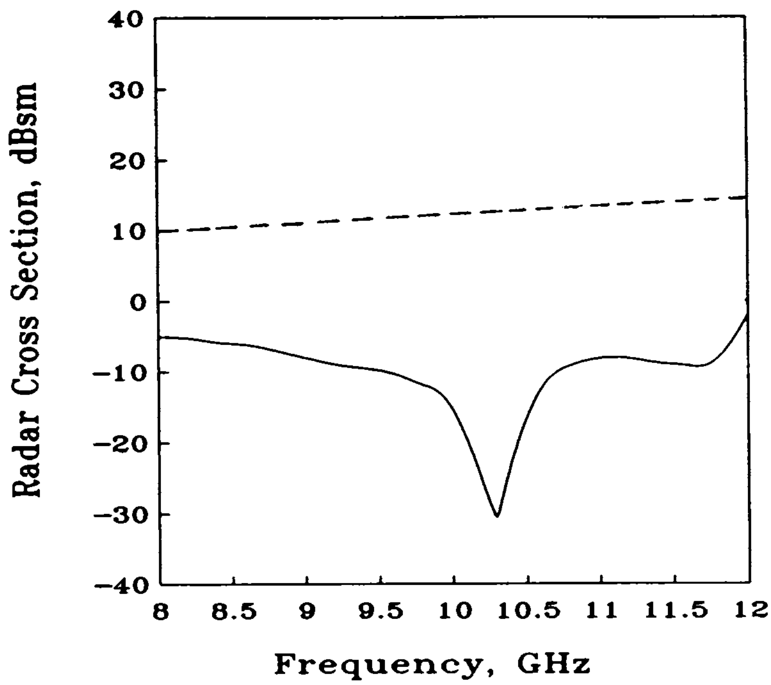

Fig. A.4(a). Variation of RCS with frequency.
- - - - - - TCR, ——— Strip loaded TCR

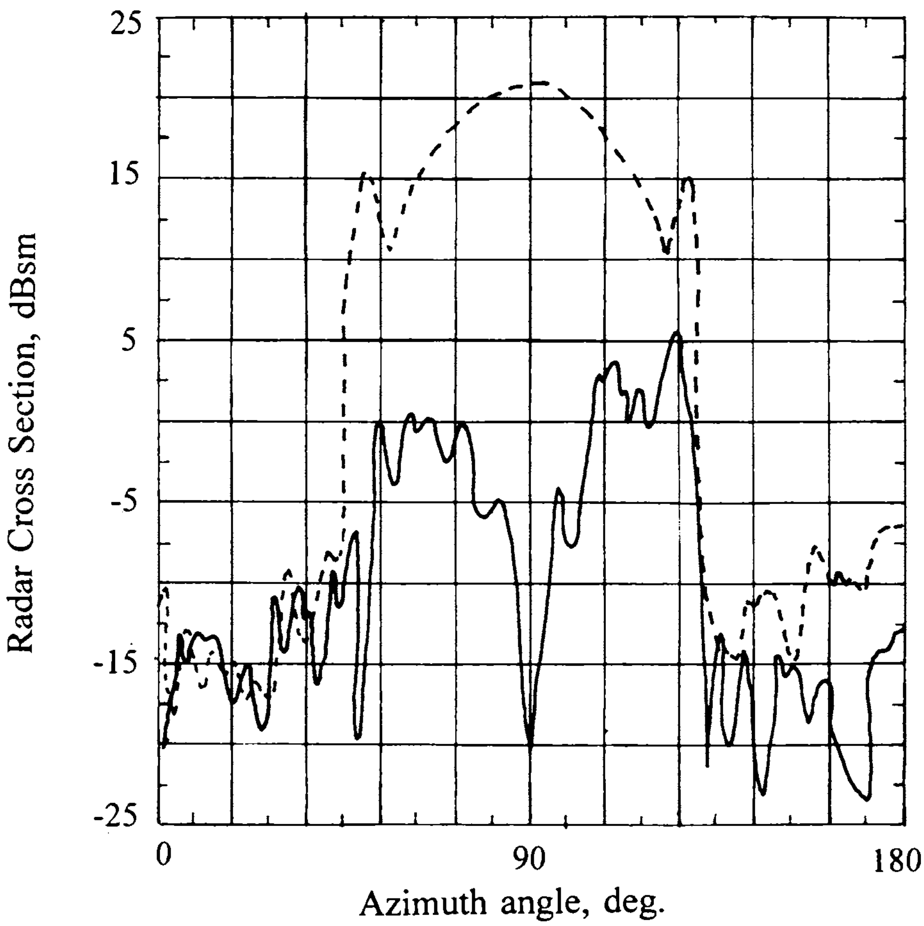

Fig. A.4(b) Variation of RCS with azimuth angle.
- - - - - - TCR ——— Strip loaded TCR

DEVELOPMENT OF A BROADBAND MICROSTRIP REFLECTARRAY ANTENNA

Appendix
B

INTRODUCTION

A class of antennas that utilizes arrays of elementary antennas as reflecting surfaces are called reflect array [101]. Reflector antennas are simple while arrays yield more precise control and versatility at the expense of simplicity. The reflect array combines much of the simplicity of the reflector-type antenna with the performance versatility of the array type. A variety of radiation patterns can be produced from the same aperture without the disadvantage of a complex corporate feed system.

The reflect array consists of a surface or aperture that is characterised by a surface impedance, and a primary radiator that illuminates this surface. The amplitude and phase of the fields reflected from the surface at any point is determined by the impedance presented by the surface at that point. In microstrip reflect array a short transmission line with variable lengths is connected to each patch at one end, with the other end of the line short or open circuited. When illuminated by the feed antenna, the dominant mode of each patch element is excited. Energy is coupled to the transmission line, reflected at the short (or open) end, and then re-radiated into free space. Thus, all the patches behave as re-radiators, and the short transmission lines serve as phase delay lines.

Variable reflection phase shifts from each element can be obtained simply by changing the patch size. This eliminates the requirement for variable length stubs. A reflectarray without tuning stubs simplifies the placement of elements in the array. The bandwidth of the microstrip reflectarray is narrow. A microstrip reflectarray with log periodic patches giving more bandwidth is explained in this appendix.

METHODOLOGY

The schematic diagram of a log periodic reflectarray is shown in figure B.1.
A 7 x 7 reflectarray is constructed in such a way that

$$\frac{L_n}{L_{n+1}} = \frac{W_n}{W_{n+1}} = \frac{d_n}{d_{n+1}} = \tau$$

where L_n and W_n are the length and width of the n^{th} patch, 'd' is the element spacing and τ is the constant scale factor.

The element spacing is adjusted to be less than $\dfrac{\lambda_o}{1 + Sin\theta}$ to avoid grating lobes. 'λ_o' is the free space wavelength and 'θ' is the design angle. The dimension 'L' of the central patch is taken to be slightly less than a half wavelength in the dielectric material. W is designed to be less than a wavelength in the dielectric inorder to prevent excitation of unwanted modes.

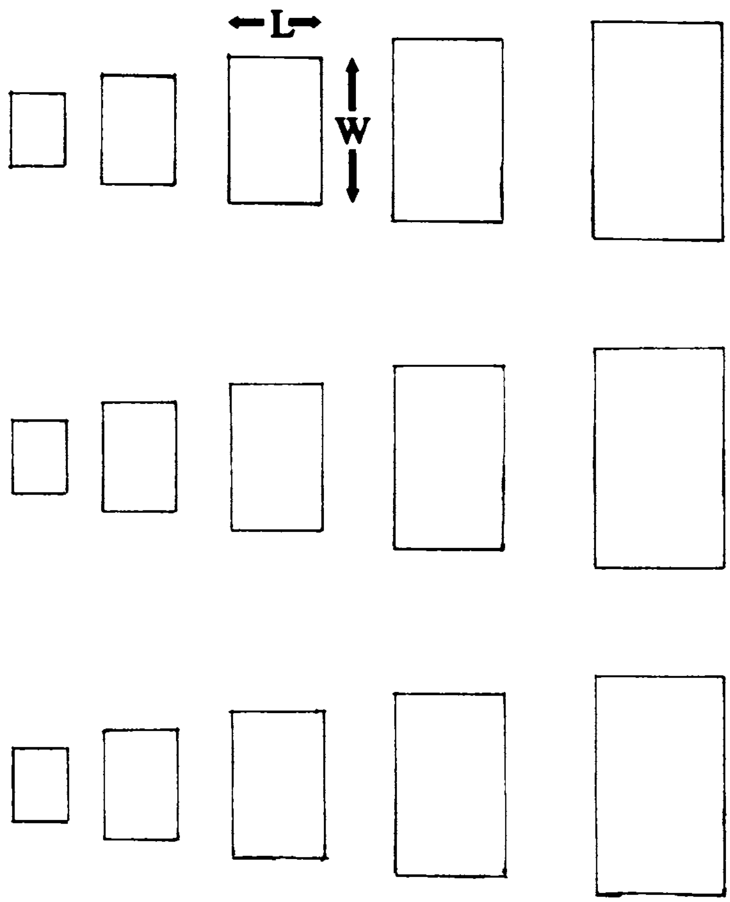

Fig. B.1 Log periodic reflectarray

The spacing between adjacent edges is more than 0.25 wavelengths in dielectric to minimise the mutual coupling of the patches in an array.

The microstrip reflectarray is kept at the centre of an arch. It is illuminated with a horn antenna located at an optimally designed distance from the array in the frequency range 5 to 7 GHz. The receiving antenna can be rotated along the arch in the desired direction. The tests were conducted using a HP 8510B Network Analyzer along with a synthesized sweep source and an S-parameter test set.

EXPERIMENTAL RESULTS

Plane waves were illuminated on the microstrip reflect array and redirected beam was measured using the receiver antenna. Figure B.2 shows the radiation redirected pattern with the incident wave at zero degrees, for a log periodic reflect array with the following dimensions.

$\varepsilon_r = 2.56$, $\tau = 0.9$, 'L' of the central element = 1.5 cm, 'W' of the central element = 2 cm.

The incident beam is found to be redirected to the design angle i.e 20° off broad side. Frequency variation of the redirected beam at normal incidence for the logperiodic microstrip reflect array in comparison with conventional microstrip reflectarray is shown in figure B.3. From the figure it is clear that bandwidth has been increased with log periodic reflect array.

CONCLUSIONS

Being flat, microstrip reflect array is cost effective than parabolic reflector. It can be easily mounted on to the surface of a structure, such as a space crafts main body or a building with less supporting structure volume and mass. The complex nature of stub tuned reflect array

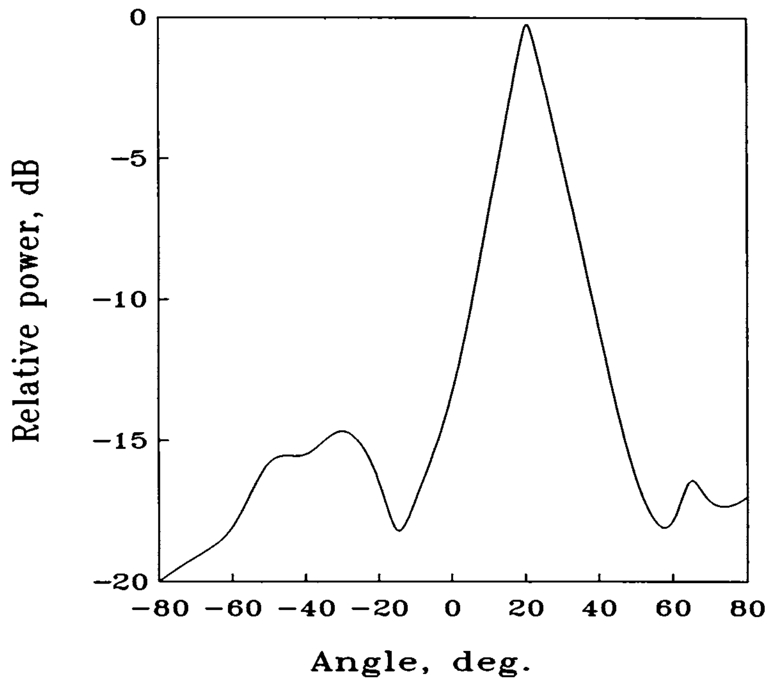

Fig. B.2. Redirected pattern with incident wave at 0 degrees

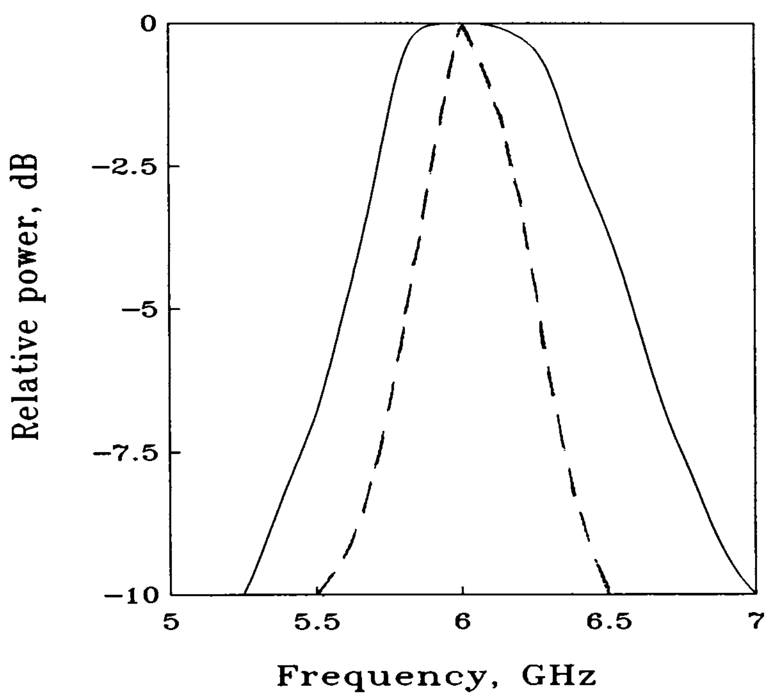

Fig. B.3. Variation of relative power with frequency

- - - - - Conventional reflect array
——— Log periodic reflect array

can be overcome by using log periodic microstrip reflect array. The placement of elements in the array is simplified and bandwidth of redirected beam is increased with such a structure.

REFERENCES

1. M.I.Skolnick, "Introduction to radar systems", Mc Graw Hill, 1988.

2. Eugene F.Knott, John F.Shaeffer and Michael T.Tuley, "Radar cross section", Artech House, Inc. 1985.

3. Nicholas C.Currie, "Techniques of radar reflectivity measurements", Artech house, Inc. 1984.

4. George T.Ruck, "Radar cross section handbook", Vol I & II, Plenum press, New York, 1970.

5. E.F.Knott, "Radar cross section measurements" Van nostrand Reinhold, 1993.

6. Edward A.Lewis and Joseph P.Casey, "Electromagnetic reflection and transmission by gratings of resistive wires", J.Appl.Phys., Vol.23, No.6, June 1952, pp. 605-608.

7. R.A.Hurd, "The propagation of an electromagnetic wave along an infinite corrugated surface", Canad.J.Phys., Vol.32, No.12, Dec.1954, pp.727-734.

8. Robin I.Primich, "Some electromagnetic transmission and reflection properties of a strip grating", IRE Trans. Antennas & Propagat., Vol.5, April 1957, pp 176-182.

9. T.B.A.Senior, "The scattering of electromagnetic waves by a corrugated sheet", Canad.J.Phys., Vol.37, No.7, July 1959, pp.787-797.

10. C.G.Bachman, H.E.King and R.C.Hansen, "Techniques for measurement of reduced radar cross sections - Part I", Microwave Journal, Vol.6, Feb. 1963, pp.61-67.

11. C.G.Bachman, H.E.King and R.C.Hansen, "Techniques for measurement of reduced radar cross sections - Part II", ibid., Vol.6, March 1963, pp.95-101.

12. C.G.Bachman, H.E.king and R.C.Hansen, "Techniques for measurement of reduced radar cross sections - Part III", ibid., Vol.6, April 1963, pp.80-86.

13. T.B.A.Senior, "A survey of analytical techniques for cross-section estimation", Proc. of IEEE, Vol.53, Aug.1965, pp.822-833.

14. P.Blacksmith JR, R.E.Hiatt and R.B.Mack, "Introduction to radar cross section measurements", Proc. of IEEE, Vol.53, Aug.1965, pp.901-919.

15. R.E.Kell and N.E.Pedersen, "Comparison of experimental radar cross section measurements", Proc. of IEEE, Vol.53, Aug.1965, pp.1092- 1093.

16. R.A.Ross, "Radar cross section of rectangular flat plates as a function of aspect angle", IEEE Trans. Antennas & Propagat., Vol.14, No.3, May 1966, pp.329-335.

17. Armand Wirgin and Roger Deleuil, "Theoretical and experimental investigation of a new type of blazed grating", J.of Opt.Soc.Am., Vol.59, No.10, Oct. 1969, pp.1348-1357.

18. Johanness Jacobsen, "Analytical, numerical and experimental investigation of guided waves on a periodically strip loaded dielectric slab", IEEE Trans. Antennas & Propagat., Vol.18, No.3, May 1970, pp.379-388.

19. Robert B.Green, "Diffraction efficiencies for infinite perfectly conducting gratings of arbitrary profile", IEEE Trans. Microwave Theory Tech., Vol.18, No.6, June 1970, pp. 313-318.

20. Chao- Chun Chen " Transmission through a conducting screen perforated periodically with apertures", ibid., Vol.18, No.9, Sept.1970, pp.627-632.

21. H.A.Kalhor and A.R.Neurether, "Numerical method for the analysis of diffraction gratings", J.of Opt.Soc. Am., Vol.61, Jan.1971, pp.43-48.

22. John A.Desanto, "Scattering from a periodic corrugated structure: Thin comb with soft boundaries", J.Math.Phys., Vol.12, No.9, Sept.1971, pp.1913-1923.

23. John A.Desanto, "Scattering from a periodic corrugated structure II. Thin comb with hard boundaries", ibid., Vol.13, No.3, March 1972, pp.336-341.

24. Hiroyoshi ikuno and kamenosuke yasuura, "Improved point matching method with application to scattering from a periodic surface", IEEE Tran.Antennas & Propagat., Vol.21, No.5, sept.1973, pp.657-662.

25. H.A.Kalhor and A.R.Neurether, "Effects of conductivity, groove shape and physical phenomena on the design of diffraction gratings", J.of Opt.Soc.Am., Vol.63, No.11, Nov.1973, pp.1412-1418.

26. H.A.Kalhor and M.K.Moaveni, "Analysis of diffraction gratings by finite difference coupling technique", ibid., Vol.63, No.12, Dec.1973, pp.1584-1588.

27. William B.Weir, Lloyd A.Robinson and Don Parker, "Broad band automated radar cross section measurements", IEEE Trans.Antennas & Propagat., Vol.22, No.6, Nov. 1974, pp.780-784.

28. James P.Montgomery, "Scattering by an infinite periodic array of thin conductors on a dielectric sheet", ibid., Vol.23, No.1, Jan.1975, pp.70-75.

29. A.Hessel, J.Shmoys and D.Y.Tseng, "Bragg angle blazing of diffraction gratings", J.of Opt.Soc.Am., Vol.65, No.4, April 1975, pp.380-384.

30. D.Maystre and R.Petit, "Brewster incidence for metallic gratings", Opt.Commun. Vol.17, No.2, May 1976, pp.196-199.

31. Joseph T.Mayhan and Leonard L.Tsai, "Reflection and transmission characteristics of thin periodic interface", IEEE Trans.Antennas & Propagat., Vol.24, No.4, July 1976, pp.449-456.

32. J.L.Roumiguieres, D.Maystre and R.Petit, "On the efficiencies of rectangular groove gratings", J.of Opt.Soc.Am., Vol.66, No.8, Aug.1976, pp.772-775.

33. David M.Levine, "The scattering of obliquely incident plane waves from a corrugated conducting surface", IEEE Trans. Antennas & Propagat., Vol.24, No.6, Nov.1976, pp.828-832.

34. E.F.Knott, "Radar cross section reduction using cylindrical segments', IEEE Trans. Antennas & Propagat., Vol.24, No.6, Nov.1976, pp.882-884.

35. H.A.Kalhor, "Numerical evaluation of rayleigh hypothesis for analyzing scattering from corrugated gratings", ibid., Vol.24, No.6, Nov.1976, pp.884-889.

36. Gordon R.Ebbeson, "TM polarized electromagnetic scattering from fin-corrugated periodic surfaces", J.of Opt.Soc.Am., Vol.66, No.12, Dec.1976, pp.1363-1367.

37. John F.Hunka, Robert E.Stovall and D.J.Angelakos, "A technique for the rapid measurement of bistatic radar cross section', IEEE Trans.Antennas & Propagat., Vol.25, No.2, March 1977, pp.243-248.

38. E.V.Jull, J.W.Heath and G.R.Ebbesson, "Gratings that diffract all incident energy", J.of Opt.Soc.Am., Vol.67, No.4, April 1977, pp.557-560.

39. E.V.Jull and G.R.Ebbesson, "The reduction of interference from large reflecting surfaces", IEEE Trans.Antennas & Propagat., Vol.25, July 1977, pp.565-570.

40. Gerald Whitman and Felix Schwering, "Scattering by periodic metal surfaces with sinusoidal height profile- A theoretical approach", ibid., Vol.25, No.6, Nov.1977, pp.869-876.

41. L.S.Cheo, J.Shmoys and A.Hessel,"On simultaneous blazing of triangular groove diffraction gratings", J.of Opt.Soc.Am., Vol.67, No.12, Dec. 1977, pp.1686-1688.

42. H.A.Kalhor, "Diffraction of electromagnetic waves by plane metallic gratings", ibid., Vol.68, No.9, Sept. 1978, pp. 1202-1205.

43. K.Knop, "Rigorous diffraction theory for transmission phase gratings with deep rectangular grooves", ibid., Vol.68, No.9, Sept. 1978, pp.1206-1210.

44. J.W.Heath and E.V.Jull, "Perfectly blazed reflection gratings with rectangular grooves", ibid., Vol.68, No.9, Sept. 1978, pp.1211-1217.

45. James P.Montgomery, "Scattering by an infinite periodic array of microstrip elements", Trans.Antennas & Propagat., Vol.26, No.6, Nov. 1978, pp.850-853.

46. E.V.Jull, Sen and J.W.Heath, "Conducting surface corrugations for multipath interference suppression", Proc.IEE, Vol.125, No.12, Dec. 1978, pp.1321-1326.

47. J.W.Heath and E.V.Jull, "Total backscatter from conducting rectangular corrugations", IEEE Trans.Antennas & Propagat., Vol.27, No.1, Jan. 1979, pp.95-97.

48. Vishwani D.Agrawal and William A imbriale, "Design of a dichroic cassegrain subreflector", ibid., Vol.27, No.4, July 1979, pp.466-473.

49. James P. Montgomery, "Scattering by an infinite array of multiple parallel strips", ibid., Vol.27, No.6, Nov.1979, pp.798-807.

50. H.A.Kalhor, "EM scattering by an array of perfectly conducting strips by a physical optics approximation" ibid., Vol.28, No.2, March 1980, pp.277-278.

51. E.V.Jull and J.W.Heath, "Reflection grating polarizers", ibid., Vol.28, No.4, July 1980, pp.586-588.

52. E.V.Jull and N.C.Beauluei, "An unusual reflection grating behaviour suitable for efficient frequency scanning", Proc.of IEEE AP-S Int.Symp., 1980, pp.189-191.

53. H.A.Kalhor, N.Eshragh and Ch.Muhammad Aslam, "Diffraction of electromagnetic waves by plane metallic gratings using a minimum boundary error approach", J.of Opt.Soc.Am., Vol.71, No.7, July 1981, pp.902-903.

54. Jerome D.Hanfling, Geroge jerinic and Lawrence Lewis, "Twist reflector design using E-type & H-type modes", IEEE Trans. Antennas & Propagat., Vol.29, No.4, July 1981, pp.622-628.

55. Chich-hsing Tsao and Raj Mittra, "A spectral iteration approach for analyzing scattering from frequency selective surfaces", ibid., Vol.30, No.2, March 1982, pp.303-308.

56. P.O.Paul and K.G.Nair, "Rotation of plane of polarisation of a beam of microwaves by corrugated reflection surfaces", Elect.Lett., Vol.18, No.8, April 1982, pp.338-339.

57. Hassan.A.Kalhor and Mohammed Ilyas, "Scattering of plane electromagnetic waves by a grating of conducting cylinders embedded in a dielectric slab over a ground plane", IEEE Trans.Antennas & Propagate., Vol.30, No.4, July 1982, pp.576-579.

58. Shung-Wu Lee and Gino Zarrillo chak-lam law, "Simple formulas for transmission through periodic metal grids or plates", ibid., Vol.30, No.5, Sept.1982, pp.904-909.

59. M.G.Moharam and T.K.Gaylord, "Diffraction analysis of dielectric surface relief gratings", J.Opt.Soc.Am., Vol.72, No.10, Oct.1982, pp.1385-1392.

60. M.J.Archer, "Periodic multielement strip gratings", Ele.Lett., Vol.18, No.22, Oct. 1982, pp.958-959.

61. J.Shmoys and A.Hessel, "Analysis and design of frequency scanned transmission gratings", Rad.Sci., Vol.18, No.4, Aug.1983, pp. 513-518.

62. A.K.Bhattacharyya, S.K.Tandon, Subrata Sanyal and D.R.Sarkar, "A CW radar cross section measurement facility in X-band", IETE Tech.Review, Vol.1, No.5, 1984, pp.59-64.

63. Chich-Hsing Tsao and Raj Mittra, "Spectral-domain analysis of frequency selective surfaces comprised of periodic arrays of cross dipoles and jerusalem cross", IEEE Trans.Antennas & Propagat., Vol.32, No.5, May 1984, pp.478-486.

64. Raj Mittra, Richard C.Hall and Chich-Hsing Tsao, "Spectral domain analysis of circular patch frequency selective surfaces", IEEE Trans.Antennas & Propagat., Vol.32, No.5, May 1984, pp.533-536.

65. R.A.Hurd and E.V.Jull, "Theory of a reflection grating with narrow grooves", Rad.Sci., Vol.16, No.3, May 1984, pp. 271-277.

66. A.K.Bhattacharya and S.K.Tandon, "A corrugated surface with low backscatter", IEEE Trans. Antennas & Propagat., Vol.32, No.8, Aug.1984, pp. 870-872.

67. L.Cai,E.V.Jull and R.Deleuil, "Scattering by pyramidal reflection grating", Proc.of IEEE Ap-S Int.Symp., 1984, pp.45-47.

68. Kazuya kobayashi, "Diffraction of a plane wave by a thick strip grating", ibid., 1985, pp.553-556.

69. E.V.Jull, D.C.W.Hui and P.Facq, "Scattering by dual blazed corrugated conducting strips and small reflection gratings", J.of Opt.Soc.Am., Vol.2, No.7, July 1985, pp.1049-1056.

70. K.A.Jose and K.G.Nair, "Reflector backed perfectly blazed strip gratings simulate corrugated reflector effects", Ele.Lett., Vol.23, No.2, Jan.1987, pp.86-87.

71. Te.Kao.Wu, "Fast convergent integral equation solution of strip gratings on dielectric substrate", IEEE Trans.Antennas & Propagat., Vol.35, No.2, Feb.1987, pp. 205-207.

72. Stefan Johansson, "Periodic arrays of metallic elements as frequency scanning surfaces", Proc.fifth Int.Conf.Antennas Propagat., March 1987, pp.71-74.

73. Robert B.Dybdal, "Radar cross section measurements", Proc.IEEE, April 1987, pp.498-516.

74. A.Matsushima and T.Itakura, "Scattering electromagnetic waves by arrays of conducting strips - Singular integral equation technique", Proc.Sino Jap.Opt.fib.Sci & E.M.Theory, May 1987, pp.447-452.

75. K.A.Jose,C.K.Aanandan and K.G.Nair,"Low backscattered TM polarised strip gratings", Ele.Lett., Vol.23, No.17, Aug.1987, pp.905-906.

76. Hassan A.Kalhor, "Electromagnetic scattering by a dielectric slab loaded with a periodic array of strips over a ground plane", IEEE Trans.Antennas & Propagate., Vol.36, No.1, Jan.1988, pp.147-151.

77. P.S.Kildal, "Definition of artificially soft and hard surfaces for electromagnetic waves", Ele.Lett., Vol.24, No.3, Feb.1988, pp.168-170.

78. Hassan A.Kalhor, "Plane metallic gratings of finite number of strips", IEEE Trans.Antennas & Propagat., Vol.37, No.3, March 1989, pp.406-407.

79. A.Matsushima and T.Itakura, "Electromagnetic scattering from a cascade connection of strip gratings", Proc.of ISAP, Japan, Vol.2, 1989, pp.433-436.

80 F.Stefan Johansson, Lars G.Josefsson and Torlid Lorentzon, " A novel frequency scanned reflector antenna", IEEE Trans.Antennas & Propagate., Vol.37, No.8, March 1989, pp.984-989.

81. F.Stefan Johansson, "Frequency scanned gratings consisting of photoetched arrays", ibid., Vol.37, No.8, Aug.1989, pp.996-1002.

82. Ye.V.Zakharov, Yu, V.Pimenov and M.Yu chervenko " A numerical method ofanalyzing the diffraction of an H-polarised plane wave by a periodic plane wave by a periodic grating", Tele commu. Rad.Engg, Vol.44, No.9, Sept.1989, pp.98-102.

83. S.Sohail, H.Naqvi and N.C.Gallagher, "General solution to the scattering of electromagnetic waves from strip grating", J.of Mod. Opt., Vol.37, No.10, 1990, pp.1629-1643.

84. Jian Ming Jin and John L Volakis, "Electromagnetic scattering by a perfectly conducting patch array on a dielectric slab", IEEE Trans.Antennas & Propagat., Vol.38, No.4, April 1990, pp.556-563.

85. Per Simon Kildal, "Artificially soft and hard surfaces in electromagnetics", ibid., Vol.38, No.10, Oct.1990, pp.1537-1543.

86. T.H.Wu and K.S.Chen, "Analysis of the scattering and guidance of a two dimensionally periodic metal grating structure by spectral domain method", Int.J.Inf.Millimetre waves, Vol.11, No.3, 1990, pp.451-461.

87. Armen Caroglanian and Kevin J.Webb, "Study of curved and planar frequency selective surfaces with non planar illumination", IEEE Trans. Antennas & Propagat., Vol.39, No.2, Feb.1991, pp.211-217.

88. Preston W.Grounds and Kevin J.Webb, "Numerical analysis of finite frequency selective surfaces with rectangular patches of various aspect ratios", ibid., Vol.39, No.5, May 1991, pp.569-579.

89. Jon Anders Aas, "Plane wave reflection properties of two artificially hard surfaces", ibid., Vol.39, No.5, May 1991, pp.651-656.

90. A.Matsushima and T.Itakura, "Singular integral equation approach to electromagnetic scattering from a finite periodic array of conducting strips", J.Electro mag.Appl., Vol.5, No.6, 1991, pp.545-562.

91. F.Stefan Johansson,"Frequency scanned reflection gratings consisting of ring patches", IEE Proc.H, Vol.138, No.4, Aug.1991, pp.273-276.

92. Stephen D.Gedney, Raj Mittra, "Analysis of the electromagnetic scattering by thick gratings using a combined FEM/MM solution", IEEE Trans. Antennas & Propagat., Vol.39, No.11, Nov.1991, pp. 1605-1614.

93. V.G.Borkar, V.M.Pandharipande and R.Ethiraj, "Millimetre wave twist reflector design aspects", ibid., Vol.40, No.11, Nov.1992, pp.1423-1426.

94. Emmanocil E.Kruzis and Demitris P.Chessoutedis, "EM wave scattering by an inclined strip grating", ibid., Vol.41, No.11, Nov.1993, pp.1473-1480.

95. Sonali Chakrabarti, K.Goswami, J.N.Chakravorthy and A.K.Sen, "Reflection echelon and echelette gratings as antennas in quasi-optical millimetre wave bands", Ind.J.Phys., Vol 68 B, No.5, 1994, pp.399-407.

96. Robert A.Kipp and Chi.H.Chan, "A numerically efficient technique for the method of moments solution for planar periodic structures in layered media", IEEE Trans.Microwave Theory.Tech., Vol.42, No.4, April 1994, pp.635-642.

97. David Shively, "Scattering from perfectly conducting and resistive strips on a grounded slab", IEEE Trans.Antennas & Propagate., Vol.42, No.2, April 1994, pp.532-536.

98. B.Gimeno, J.L.Cruz, E.A.Navarro and V.Such, "A polarizer rotator system for three dimensional oblique incidence", ibid., Vol.42, No.7, July 1994, pp.912-919.

99. Wel chen, N.C.Beaulieu, D.G.Michelson and E.V.Jull, "TM blazing of rectangular groove gratings at non bragg incidence", Proc.of URSI Rad.Sci.Int.Symp., 1994, pp.437.

100. E.F.Knott, "RCS reduction of Dihedral corners", IEEE Trans.Antennas & Propagate., Vol.25, 1977, pp.406-409.

101. Ronald D.Javor, Xiao-Dong Wu and Kai Chang, "Design and performance of a microstrip flat reflect array antenna", Microwave & Optical Tech.Lett., Vol.7, No.7, May 1994, pp.321-324.

102. D.C.Chand and M.C.Chang, "Microstrip reflectarray antenna with offset feed", Elect.Lett., July 1992, Vol.28, No.16, pp.1489-1491.

INDEX

LIST OF PUBLICATIONS OF THE AUTHOR

Journal papers

1. "New simulated corrugated scattering surface giving wideband characteristics", *Electronics Letters*, UK, Feb.1993, Vol.29, No.4, pp 329-331.

2. "The performance of a novel simulated corrugated surface for the reduction of radar cross section", *Microwave and Optical Technology Letters*, USA, Aug.1993, Vol.8, No.10, pp 615-617.

3. "A modified strip grating with dual periodicity for RCS reduction", *Microwave and Optical Technology Letters*, USA, May 1994, Vol.7, No.7, pp 315-317.

4. "Wide band trapezoidal strip grating for elimination of specular reflection", *Electronics Letters*, UK, June 1994, Vol.30, No.13, pp 1037-1039.

5. "Analysis of a dual periodic strip grating", *Microwave and Optical Technology Letters*, USA, October 1996.

Symposium papers

1. "The scattering behaviour of a simulated corrugated surface with single periodicity and dual aspect ratio", *Proc. of the National Symp.on Antennas and Propagation*, APSYM-92, pp 64-68, 1992.

2. "A simulated corrugated scattering surface for wide band operation", *Proc. of the National Symp.on Antennas and Propagation*, APSYM-92, pp 69-72, 1992.

3. "The SCS grating : A new electromagnetic scattering technique", *PIERS 1993, Jet propulsion lab*, California Institute of Technology, USA, July 12-16, 1993.

4. "RCS reduction of Trihedral Corner Reflectors using SCS technique", *IEEE Antennas and Propagation symposium*, June 1994, USA.

5. "Backscattering reduction of trihedral corner reflectors using SCS technique", *Proc. of the National Symp.on Antennas and Propagation,* APSYM-94, pp 49-52, 1994.

6. "A dual periodic strip grating for specular reflection suppression", *Proc. of the National Symp.on Antennas and Propagation*, APSYM-94, pp 151-153, 1994.

7. "Development of a blazed reflection grating with enhanced bandwidth and angular range giving polarised backscattering", *IEEE Antennas and Propagation symposium*, June 1995, USA.